Selection of Rac1 Binding Partners
By
Guanine Nucleotide Exchange Factors

A thesis submitted to The University of Manchester for the degree of
Doctor of Philosophy
in the Faculty of Medical and Human Sciences

2014

Hadir Marei

School of Medicine/ Institute of Cancer Sciences

LIST OF CONTENTS

Final word count 69,408

LIST OF FIGURES

LIST OF TABLES

ABSTRACT

University of Manchester

Hadir Marei

For the degree of Doctor of Philosophy (PhD)

Submission date: 30th September 2014

Selection of Rac1 Binding Partners by Guanine Nucleotide Exchange Factors

The small GTPase Rac1 is implicated in various cellular processes that are essential for normal cellular functioning. Rac1 has also been shown to play a major role in tumour initiation, progression and metastasis. Similar to other GTPases, Rac1 cycles between an inactive GDP-bound form and an active GTP-bound form. This cycle is regulated, in part, by Guanine Nucleotide Exchange Factors (GEFs), which act as Rac1 activators. Once active, Rac1 can associate with a variety of other proteins in the cell thereby regulating various cellular functions, including cellular migration. However, it has been shown that Rac1 activation can lead to opposing migratory effects. This complicates our understanding of its role in cancer, particularly during metastasis, and calls for the identification of factors that could influence Rac1-driven cellular motility.

Rac1 differential downstream effects are often attributed to differences in cell type, subcellular localisation of active Rac1, as well as signalling from the extracellular matrix. In addition, there is accumulating evidence implicating GEFs in dictating the downstream specificity of activated GTPases. To address this, the potential role of two Rac1-specific GEFs, Tiam1 and P-Rex1, in dictating Rac1 downstream effects was investigated. Interestingly, under the same cellular conditions, activation of Rac1 by either GEF resulted in distinct morphological and cellular migration abilities in different cell lines. Activation of Rac1 by Tiam1 was associated with enhanced cell-cell adhesions and reduced cellular migration; whereas activation of Rac1 by P-Rex1 resulted in weaker cell-cell contacts accompanied by enhanced cellular migration. Moreover, analyses of Rac1 binding partners upon activation by either GEF suggested a potential GEF-induced differential selection of Rac1 interactors.

Among the proteins showing differential Rac1 binding, the gelsolin protein superfamily member, protein flightless-1 homolog (FLII) showed an increased association with Rac1 under activation by P-Rex1. FLII is an actin-remodelling protein and, similar to Rac1, it has been implicated in cellular migration and gene regulation. Using a variety of techniques the GEF-specific Rac1-FLII interaction was confirmed. Moreover, further biochemical analyses revealed that FLII binds preferentially to P-Rex1 but not Tiam1. Together these results suggest that in addition to serving as a Rac1 GEF, P-Rex1 can also act as a scaffolding protein and thereby influence Rac1 binding to other proteins, such as FLII. Interestingly, the P-Rex1-Rac1 induced cellular migration was mediated through FLII and its role in promoting cellular contraction. These findings highlight a novel P-Rex1-Rac1 signalling cascade that promotes migration in cells, which might help explain the increased metastasis associated with P-Rex1 overexpressing tumours.

DECLARATION

No portion of the wok referred to in the thesis has been submitted in support of an application for another degree or qualification of this or any other university or other institute of learning.

COPYRIGHT STATEMENT

I WOULD LIKE TO DEDICATE THIS THESIS
TO MY LATE GRANDDAD

DR. SABRY AGLAN

You have been an inspiration to all of us
I know deep inside that you, somehow, made sure I end up here!

ACKNOWLEDGEMENTS

It's hard to imagine that four years have passed. I just remember coming to the Cancer Research UK Manchester Institute (Paterson at the time) for my interviews. Doing a PhD has proven quite challenging and without the help of some people I would have not been able to make it.

I guess it is appropriate to start with the people that I spend most of my day with, not to mention my usually grumpy mood =). I have had the honour to meet exceptional people during my PhD in Angeliki's lab. So let's start with you, Angeliki, I want to thank you for giving me a perfect place to work at and an exciting project to keep me occupied for the past four years =). I have learnt a lot working in your lab and this is mainly because of you trusting in me and letting me stumble so that I actually learn. So for that I want to thank you tremendously!!

Another member of the lab that is very dear to my heart is Gavin. Although you might not know this Gavin, but I have always considered you my support throughout my PhD. You have been nothing but helpful, so thank you for all the emotional support you have given me =)

I would also like to thank Helen, Andrew and Lynsey for creating such an exciting scientific environment. I have learnt a lot from you guys and you are always there to help out when I need it. Also Erinn and Anna, I enjoy listening to your crazy stories so please keep it up =)

A special thanks goes to you Zoi for keeping me sane in my last few months…but unfortunately it is too late I am already there =)

A very special thanks goes to Alejandro Carpy for your help with the SILAC mass spectrometry protein identification experiments. You were always patient, even when I drove you crazy with my OCD. Also members of the Bioinformatics group, especially Hui Sun Leong for taking the time to teach me how to use the R project; and Elli for your help making me understand how to operate ingenuity!

I would also like to thank Ivan Ahel and Crispin Miller for providing the necessary guidance and support as my PhD advisors.

Ohhh, moving on to the Mancunian gang, as I like to call you…Elli, Eva, Sharmin, Sara, Marija and Becky…what can I sayyyyy…you guys…you just get me!!! You have been the straw that kept me from flying away all that time =)) I love you girls and can't wait for our second Egyptian trip after graduation.

How can I write an acknowledgement without mentioning my biggest supporters? I have been blessed with the most wonderful family there is.. and it's a BIG one!!!

Lets start with you! Yes you ya mamtiiii….You are the reason I want to succeed in life!! I always want to make you proud! The look in your eye when we achieve something is just priceless!! Ya rab tekoni fa5ora beya 3ashan enti el donia leya!!

Then there is Daddy…whenever I'm feeling down I always remember our conversation on the roof when I had this Biology exam and didn't want to study. You always know how to motivate me and challenge me and sometimes you're just exactly what I need.

Fouad.. You have always been my inspiration. I have always looked up to you. You know that we will always have this bond.. After all I'm your MAMA DOODA =)

MIMIIIIII…Ya agamal el nas fel donya ya set el nas w setii anaaaa…ana bamoooot fikiii ya habibaaa enti sa7betiii w habebtiiii…bahebek awiiii.

Khalooo…no… I really don't know what to say… I have spent time with you growing up more than I have spent with mama and daddy…you were always there for me… You have taught me a lot… And I owe you a lot… Thanks for always making me a priority Bahebak awii.

Zizoooo…Do you remember when you were helping me out with this PhD application?! I still remember like it was yesterday…You are my true best friend. I love you so much and no words can describe how grateful I am for all that you have done for me..REALLY! and OF COURSE your amazing family..Uncle Hamdi with the orzo when I'm craving it; Mazen with our secret hush hush ;) and of course my favourite person of all MALAK!! I love you…That really sums it up =)

Mouly el habibaaaa…I know I haven't always been there for you because of this PhD and I hope you would forgive me!! I always enjoy your company and you give me this warmth that a mother would give..bahebek awiii..I wish I could be with you more enti wel haboob Seif ;) W of course SARAH EL ZARKA.. YOU'RE DEFINITELY MY SISTER from another mister =)

Mostafaaaa… I want to thank you for the amazing time we had this summer (while I was supposed to be writing =)) You tolerated my madness and kept pushing me forward. I want you to know I will always be there for you..ALWAYS! #Masha3er

My lifetime friends!! Rana, Dina M and Dina B =) ana baheboko awii and it was just amazing having spent with you this summer while writing =)

Heba Attia!! I know you are mad at me!! But you still need to wish me luck.. because if I pass I'll make it up for you =)

мама Лена и папа Луша, спасибо за то, что такой удивительный семья , я тебя очень люблю

AND FINALLY

TIMURS MACULINS

I LOVE YOU MORE THAN ANY WORDS CAN DESCRIBE…YOU HAVE BEEN WITH ME ALL THE WAY;

TOLERATED ME WHEN I WAS DOWN; CHEERED ME UP WHEN I NEEDED IT

HUGGED ME WHEN I WAS DOWN; AND LOVED ME NO MATTER WHAT

I WISH THAT I AM TO YOU HALF WHAT YOU ARE TO ME

YOU ARE MY BEST PHD RESULT

LIST OF ABBREVIATIONS

ADP	Adenosine Diphosphate
ALCAM	Activated Leukocyte Cell Adhesion Molecule Receptor
AP-1	Transcription Factor-1
APC	Adenomatous Polyposis Coli
Arf	ADP-ribosylation Factor
Arp2/3	Actin-related protein 2/3
Arp3	Actin-Related Protein 3
Arpc1b	Actin-Related Protein 2/3 Complex, Subunit 1B, 41kDa
Arpc2	Actin-Related Protein 2/3 Complex, Subunit 2, 34kDa
Arpc3	Actin-Related Protein 2/3 Complex, Subunit 3, 21kDa
Arpc4	Actin-Related Protein 2/3 Complex, Subunit 4, 20kDa
Arpc5	Actin-Related Protein 2/3 Complex, Subunit 5, 16kDa
ATP	Adenosine Triphosphate
BR	Biological Replica
Brc/Abl	Breakpoint Cluster Region/Abelson Murine Leukemia
C	Carbon
C-terminus	Carboxyl Terminus
C. elegans	Caenorhabditis elegans
CAMKII	Ca^{2+} /calmodulin-dependent protein kinase II
CAND1	Cullin-associated Nedd8-dissociated Protein 1
CBP	Calmodulin Binding Peptide
CC	Coiled-Coil Domain
Cdc42	Cell Division Control Protein 42 Homolog
CHO	Chinese Hamster Ovary
CML	Chronic Myeloid Leukaemia
Cnt	Control
Cobl	Cordon-bleu Gene
Cos7	CV-1 in Origin and Carrying the SV40
D. melanogaster	Drosophila melanogaster
Daam1	Disheveled-associated Activator of Morphogenesis 1
DAD	Diaphanous Autoinhibitory Domain
DEP	Dishevelled, Egl-10 and Pleckstrin Domain
DH	Dbl Homology Domain
DHR	DOCK-homology Region
DID	Diaphanous Inhibitory Domain

DNA	Deoxyribonucleic Acid
DOCK	Dedicator of Cytokinesis
Dox	Doxycycline
DRF	Diaphanous-related Formin
ECM	Extracellular Matrix
EGF	Epidermal Growth Factor
EGFR	Epidermal Growth Factor Receptor
ELMO	Engulfment and Cell Motility
EMT	Epithelial-to-Mesenchymal Transition
EphA2	Ephrin A2 Receptor
ERK	Extracellular Signal-Regulated Kinase
EV	Empty Vector
EX	Extended Structure
FAK	Focal Adhesion Kinase
FBS	Fetal Bovine Serum
FCS	Fetal Calf Serum
FGF-2	Fibroblast Growth Factor-2
FH	Formin Homology
FLII	Protein Flightless-1 Homolog
FLII FL	Protein Flightless-1 Homolog Full Length
FLII GEL	Protein Flightless-1 Homolog Gelsolin Truncation Mutant
FLII LRR	Protein Flightless-1 Homolog LRR Truncation Mutant
GAP	GTPase Activating Protein
GBD	GTPase Binding Domain
GDI	Guanine Nucleotide Dissociation Inhibitor
GDP	Guanosine Diphosphate
GEF	Guanine Nucleotide Exchange Factor
GEF*	GEF-Dead Mutant
GEL	Gelsolin-like Domain
GFP	Green Fluorescent Protein
GPCR	G-protein Coupled Receptor
GST	Glutathione S-Transferase
GTP	Guanosine Triphosphate
GTPase	Guanosine Triphosphate Phosphohydrolase
H	Hydrogen
H/M	Heavy/Medium
HA	Hemagglutinin
HGF	Hepatocyte Growth Factor

HMEC	Human Microvascular Endothelial Cell
HPRD	Human Protein Reference Database
Hr	Hour
IP4P	Inositol Polyphosphate 4-Phosphatase
IPA	Integrated Pathway Analysis
IQGAP1	Ras GTPase-activating-like Protein 1
IRSp53	Insulin Receptor Tyrosine Kinase Substrate p53
JMY	Junction-mediating and Regulatory Protein
JNK	Jun N-terminal Kinase
K	Lysine
kDa	Kilodaltons
LRR	Leucine Rich Repeats
Lys	Lysine
MAPK	Mitogen-activated Protein Kinase
MAT	Mesenchymal-to-Amoeboid Transition
MCF7	Michigan Cancer Foundation-7
MCS	Multiple Cloning Site
MDCK	Madin-Darby Canine Kidney
MDCK-f3	Fibroblastoid MDCKII cells
mDia1	Diaphanous-related Formin-1
mDia2	Diaphanous-related Formin-2
MET	Mesenchymal-epithelial Transition
Min	Multiple Intestinal Neoplasia
MKK3	Mitogen-activated Protein Kinase Kinase 3
MLC	Myosin Light Chain
MLCK	Myosin Light Chain Kinase
MLK3	Mixed Lineage Kinase 3
MMP	Matrix Metalloproteinase
MT1-MMP	Membrane Type 1 MMP
Mtss1	Metastasis Suppressor-1
MYL6	Myosin Light Polypeptide 6
N	Nitrogen
N-terminus	Amino Terminus
NIH3T3	National Institutes of Health 3-day Transfer, Inoculum 3 x 10^5 cells
NLS	Nuclear Localization Signal
p-paxillin	Phosphorylated Paxillin
P-Rex1	Phosphatidylinositol-3, 4, 5-Trisphosphate-dependent Rac Exchange Factor

PAK1	p21 Activated Kinase-1
PDFRβ	Platelet-Derived Growth Factor Receptor Beta
PDZ	PSD-95/Dlg/ZO-1
PH	Pleckstrin Homology Domain
PHc	C-terminal Pleckstrin Homology Domain
PHn	N-terminal Pleckstrin Homology Domain
PHn-CC-Ex	Pleckstrin Homology Amino Terminal Domain, Coiled-coil, Flanking Region
PIAS3	Protein Inhibitor of Activated STAT3
PIP2	Phosphatidylinositol 4,5-Bisphosphate
PIPs	Protein-Protein Interaction Predictions Database
PLA	Proximity Ligation Assay
PtdIns(3,4,5) P3	Phosphatidylinositol (3,4,5)-Triphosphate
R	Arginine
Rac1	Ras-related C3 botulinum toxin substrate 1
Rac3	Ras-related C3 botulinum toxin substrate 3
Ras	Rat Sarcoma
RBD	Ras Binding Domain
Rho A	Ras homolog gene family member A
RhoG	Ras Homolog Family Member G
RhoGDI	Rho GDP-Dissociation Inhibitor
RhoH	Ras homolog gene family member H
Rif	Rifampicin
RNA	Ribonucleic Acid
ROCK	Rho-associated Serine/Threonine Kinase
S. cerevisiae	Saccharomyces cerevisiae
SDS- PAGE	Sodium Dodecyl Sulfate Polyacrylamide Gel Electrophoresis
SH3	Src-homologous Domain 3
SILAC	Stable Isotope Labelling by Amino Acids in Cell Culture
siRNA	Small Interfering RNA
Src	Sarcoma-family Kinase
SUMO	Small-Ubiquitin Related Modifier
TAM	Tumour-associated Macrophage
TAP	Tandem Affinity Purification
TER	Transepithelial Electrical Resistance
TEV	Tobacco Etch Virus Proteolytic Cleavage Site
Tiam1	T-Cell Lymphoma Invasion and Metastasis-1
TIF	Telomere-Immortalized Human Fibroblast

TIMP	Tissue Inhibitor of Metalloproteinase
TIRF	Total Internal Reflection Fluorescence
TMOD3	Tropomodulin-3
uPA	Urokinase-type Plasminogen Activator
VASP	Vasodilator-stimulated Phosphoprotein
VE	Vascular Endothelial
WASP	Wiskott–Aldrich Syndrome Protein
WAVE	WASP-family Verprolin- Homologous
WH2	WASP Homology 2
WT	Wild Type

Chapter 1 : Introduction

Cancer is a widely spread disease and is currently considered the second leading cause of death worldwide. The word cancer originates from the Greek word *carcinos* (meaning crab), which was used by Hippocrates (460-370 B.C.), a Greek physician to describe the morphology of dissected tumours. Celsus (28-50 B.C.), a Roman physician later translated the term *carcinos* into the Latin version, cancer. The term is now reserved for tumours that have the ability to move from the site of origin to other parts of the body (i.e. malignant tumours). Tumours that lack this ability are commonly referred to as benign tumours. Although the term cancer was not used earlier, the oldest description of what we now refer to as cancer comes from ancient Egyptian manuscripts dating back to 1600 B.C. In these manuscripts, the disease was described as one with no cure (Sudhakar, 2009). Unfortunately, treatment options are still relatively very limited, particularly in the malignant stage. As a result to provide better treatment options, scientific research is aimed at deciphering the different stage of cancer formation and progression, especially how and what triggers the transformation of cancer from benign to malignant tumours.

Work presented in this thesis focuses on understanding the mechanism by which the small GTPase Ras-related C3 botulinum toxin substrate 1 (Rac1), a key player in cellular migration and cancer malignancy, is regulated in an attempt to identify factors responsible for dictating whether Rac1 will inhibit or promote cellular migration. Additionally, this might provide insight into novel mechanisms underlying cancer malignancy. This chapter presents an overview of the literature on cancer, cellular migration, actin dynamics and the Rho family of small GTPases that serves as a backbone for work presented in the following chapters.

1.1 An Overview of Cancer

1.1.1 The Biological Basis of Cancer

Despite the early distinction between benign and malignant tumours, it was not until 1902 that Theodor Boveri, a professor of zoology at Munich unravelled the genetic basis underlying this disease. Through his discovery and subsequent work on centrosomes, structures required for cellular division, he generated sea urchin eggs with additional centrosomes. From his experiments he speculated that malignant tumours form as a result of chromosomal abnormalities that might be instigated by multipolar mitosis in cells. He further postulated that as a result of these chromosomal changes cancer cells acquire the ability to proliferate uncontrollably through becoming less differentiated compared to the normal cells from which they originated (Harris, 2008). Decades of scientific research have now revealed that cancer is a complex progressive disease with both genetic and environmental underlying causes. The

carcinogenesis process is commonly divided into four stages: initiation, promotion, progression and metastases (McKinnell, 2006; Weinberg, 2007).

1.1.1.1 Initiation, Promotion and Progression

Through evolution, cells have developed a variety of mechanisms in order to ensure normal cell homeostasis. These mechanisms include, yet are not limited to, cell cycle checkpoints, DNA proofreading during replication, DNA damage repair pathways, and apoptotic signals. Despite these mechanisms, cells are still constantly being subjected to mutations in their DNA. Some of these mutations are silent, while others, known as missense mutations, have detrimental effects on the cell, often leading to cell death. In other instances, however, these missense mutations, through altering the protein composition in cells, can serve as a selective advantage for cellular viability (Sudhakar, 2009).

In the absence of an underlying genetic cause inherited from parents, cancer initiation is often triggered as a result of an environmental stimulus, known as a carcinogen. In this stage, the carcinogen binds to the DNA within a cell resulting in DNA breaks or mutations. Depending on the location of the alteration, if left unrepaired, this might confer a selective growth advantage. Examples of carcinogens include, but are not limited to tobacco, ultraviolet radiation, chemicals used as food preservatives, and steroidal estrogen found in birth control tablets. Research indicates that alkylating agents, aralkylating agents, and arylhydroxylamines that constitute about 95 % of most carcinogens are the cause of the mutational potential of carcinogens. Under these conditions, if initiated cells are further subjected to additional environmental factors, known as promoters, cellular growth is enhanced even more and cells start forming abnormal growths, known as benign tumours (McKinnell, 2006; Twombly, 2003). Mutations in genes responsible for the regulation of the cell cycle progression and response to DNA damage are of particular danger, as they allow the accumulation of additional genetic alterations with each cellular division, thus leading to uncontrolled cell expansion (Sudhakar, 2009).

As the disease progresses, cells start acquiring additional genetic mutations due to bypassing the normal checkpoints that ensure the accurate replication of DNA during cellular division. As a consequence, cancer cells often undergo additional cellular changes involving actin cytoskeleton rearrangements and disruption of normal cell-cell, cell-extracellular matrix (ECM) adhesions that aid tumour progression to malignancy (McKinnell, 2006; Sudhakar, 2009).

1.1.1.2 Cancer Metastases

Cancer metastasis refers to the process in which cancer cells acquire additional cellular functions that enable them to break off from the original site and invade distal body parts to form secondary tumours. Cancer metastasis is the leading cause of death in cancer patients mainly due to the limited treatment options available at this stage (Geiger and Peeper, 2009;

Yilmaz and Christofori, 2010). As such, understanding the underlying mechanisms behind cancer cellular migration and invasion has been the prime focus of scientific research for decades.

In spite of the extensive efforts and research conducted on the process of cancer metastasis; a detailed insight into how cancer cells invade nearby tissues and form secondary tumours is still lacking (Yilmaz and Christofori, 2010). However, research indicates that the process of cancer metastasis occurs in a series of distinct steps that form an intricate metastatic cascade. This involves morphological and cellular signalling changes to promote increased tumour cellular migration and invasion, blood vessel and lymphatic system intravasation, transport through the blood vessels or lymphatic system and extravasation followed by the outgrowth of a secondary tumour at a distant site (Geiger and Peeper, 2009; Yilmaz and Christofori, 2010).

Under normal conditions, epithelial tissues form highly polarised sheets of cells that are held together with strong cell-cell and cell-ECM adhesions. In solid tumours, the majority of which originate from epithelial tissues, the first step of the metastatic cascade involves tumour cells dissemination, in which cells start breaking off from one another and breaching the basement membrane barrier. Various reports suggest that this process involves extensive changes in cellular morphology and internal cellular signalling that aid in dissolving cell-cell contacts and altering cell-ECM adhesions. These changes facilitate cellular plasticity and result in the loss of the epithelial phenotype and adopting a more motile mesenchymal-like morphology in a process known as epithelial-mesenchymal transition (EMT) (Christofori, 2006; Thiery, 2002; Thiery and Sleeman, 2006). EMT also induces a "cadherin switch" in which E-cadherin, an important component of epithelial adherens junctions, is lost and N-cadherin expression is elevated. Consistent with the morphological changes associated with this process, cells that have undergone EMT also downregulate other epithelial proteins, such as occludin, claudins, and cytokeratins while inducing the expression of mesenchymal proteins, including vimentin, tenascin C, and laminin $\beta 1$ (Christofori, 2006; Jechlinger et al., 2003).

There are various ways by which EMT has been shown to promote cancer metastasis. For example, EMT is associated with an increase in mesenchymal protein expression. Of particular importance is the enhanced expression of N-cadherin. Upregulation of N-cadherin has been reported in a variety of highly metastatic tumours. Additionally, it has been shown to directly regulate cellular migration and invasion in breast cancer cells (Nieman et al., 1999). In a study conducted by Hazan et al. N-cadherin expression in the breast cancer cell line MCF7 was associated with increased cellular migration and Matrigel invasion. Interestingly, N-cadherin expression in MCF7 cells also promoted adhesion to endothelial cells. Moreover, upon stimulation with fibroblast growth factor-2 (FGF-2), there was a sharp upregulation of the matrix metalloproteinase-9 (MMP-9) in N-cadherin expressing cells but not in control transfected cells. These cells also exhibited increased cancer metastasis when injected into nude mice

demonstrating the role of N-cadherin in promoting tumour progression and cancer metastasis even in the presence of E-cadherin (Hazan et al., 2000). EMT also promotes the release of matrix metalloproteinases (MMPs), a class of proteins that digest and remodel the ECM, thus promoting cellular migration in cells (Geiger and Peeper, 2009; Parri and Chiarugi, 2010; Yilmaz and Christofori, 2010).

Additionally, as indicated earlier EMT involves the loss of E-cadherin, which in turn promotes tumour cellular invasion. *In vivo* evidence presented by Derksen et al. demonstrate that the loss of E-cadherin in a p53 null background is associated with an increased number of mammary carcinomas (Derksen et al., 2006). In agreement with these observations, Perl et al. further established the casual effect between E-cadherin loss and enhanced tumour invasion through crossing a pancreatic β-cell carcinogenesis mouse model with transgenic mouse models that either maintain E-cadherin expression in the β-cells or express a dominant negative mutant of E-cadherin. Results from this study revealed that expression of wild type (WT) E-cadherin arrested the tumour development at the adenoma stage; whereas the dominant negative mutant promoted tumour progression and metastasis (Perl et al., 1998).

In addition to its role in disrupting cell-cell contacts, E-cadherin loss has also been shown to enhance cancer metastasis via suppressing anoikis and promoting angiogenesis (Derksen et al., 2006; Onder et al., 2008). Both anoikis and angiogenesis are important determinants of tumour growth and progression. Anoikis is the process in which cells undergo apoptosis as a result of abnormal or absent cell-ECM adhesions (Frisch and Francis, 1994; Meredith et al., 1993). This is of particular relevance at several points during the metastatic cascade in which tumour cells reside in foreign environments that lack the necessary cell-ECM adhesions. This includes invasion of surrounding tissue, transport in blood and lymph vessels, and extravasation at sites of secondary tumour formation (Liotta and Kohn, 2004). It has therefore been proposed that anoikis suppression is important for enhanced cancer metastasis (Geiger and Peeper, 2005; Zhu et al., 2001). In contrast to E-cadherin, N-cadherin loss was shown to promote anoikis in melanoma cells. Given the "cadherin switch" observed in cells that undergo EMT, it therefore follows that EMT can enhance cancer metastasis through regulating anoikis (Geiger and Peeper, 2009). E-cadherin loss also regulates cancer metastasis via promoting angiogenesis (Derksen et al., 2006). The importance of angiogenesis, the formation of new blood vessels from existing ones, in cancer progression was demonstrated in a study conducted by Gimbrone et al. in which inhibition of neovascularisation impeded the metastatic progression of solid tumours and instead promoted tumour dormancy (Gimbrone et al., 1972). Additionally, the increased expression and release of MMPs associated with EMT has been shown to promote angiogenesis. For example, it has been demonstrated that the cleavage of collagen type IV, a component of the ECM, exposes a normally hidden cryptic site that is required for angiogenesis *in vivo* (Xu et al., 2001). Therefore, EMT promotes cancer metastasis also via enhancing angiogenesis. It must be noted, however, that cancer cells can also undergo

metastasis without the occurrence of EMT depending on the mode of migration adopted as outlined later in section 1.2.2 (Friedl et al., 2004; Friedl and Wolf, 2003; Wicki et al., 2006). In fact, due to the variability in the phenotypes associated with EMT, the actual role played by this process in cancer metastasis is yet to be fully understood (Tarin et al., 2005; Thompson et al., 2005).

The second stage of the metastatic cascade involves the invasion of cancer cells into the surrounding tissue. Enhanced cellular migration is crucial for the cancer cell dissemination preceding the formation of secondary tumours (Chambers et al., 2002; Geiger and Peeper, 2009). Increased migration and invasion allow cancer cells to breach the basement membrane and intravasate existing and newly formed blood and lymph vessels (Sahai, 2007). In an *in vivo* imaging study, Wyckoff et al. highlighted the importance of directed cellular migration in the intravasation process. They showed that unlike nonmetastatic tumour cells, which fragment upon interaction with blood vessels, metastatic cells orient themselves towards the blood vessels. Additionally, they demonstrated that there is a direct correlation between the number of cancer cells in the blood stream (i.e. blood burden) and lung metastases indicating that intravasation is a critical step in the metastatic cascade (Wyckoff et al., 2000). Additional studies also revealed that tumour-associated-macrophages (TAMs) play a crucial role in directing cancer cells towards blood vessels (Wyckoff et al., 2004; Wyckoff et al., 2007). As highlighted earlier, it has been proposed that suppression of anoikis is also important for intravasation and the subsequent transport through the bloodstream (Geiger and Peeper, 2005; Zhu et al., 2001).

Once in the bloodstream or the lymphatic system, cancer cells are able to circulate the body and eventually extravasate into a distal organ to form a secondary tumour. The processes involved in tumour cell circulation and extravasation from the blood or lymph vessels are believed to be similar to that required for cancer cell invasion and intravasation. Integrin signalling and platelet interactions have been shown to play a crucial role in circulation and extravasation. In a study by Felding et al. activated integrin $\alpha V\beta 3$ was shown to enhance breast cancer metastases by promoting cancer cell and platelet interaction. Additionally, expression of a constitutively active form of $\alpha V\beta 3$ integrin enhanced the metastatic potential of MDA-MB 435 breast cancer cells in a mouse model (Felding-Habermann et al., 2001). Similar to intravasation and circulation through the blood and lymph vessels, it has been proposed that suppression of anoikis plays a role in extravasation. It has been suggested that enhanced platelet binding might promote the formation of tumour cellular aggregates that in turn can overcome conditions that trigger anoikis (Geiger and Peeper, 2009). Moreover, Khanna et al. identified ezrin, a protein that links the plasma membrane to the actin cytoskeleton, as a key player in the survival of metastasising tumour cells potentially through suppressing anoikis (Khanna et al., 2004).

The final step of the metastatic cascade involves the outgrowth of tumour cells to form secondary tumours following extravasation. This represents the most inefficient step of the cascade due to tumour cell death or dormancy (Aguirre-Ghiso, 2007; Geiger and Peeper, 2009). Additionally, depending on the origin of the primary tumour, cancer cells have been shown to metastasise in a highly selective pattern showing strong preferences to specific organs. This organ selectivity exhibited is referred to as the "seed and soil" hypothesis, which states that both the invading cancer cell (the seed) and the microenvironment of the target organ (the soil) play a role in dictating the site of secondary tumour formation. As a result, secondary tumour formation can only occur if the microenvironment of the target organ can support the growth of the metastasising cancer cell (Geiger and Peeper, 2009; Parri and Chiarugi, 2010). Moreover, it is proposed that for cells that have undergone EMT, the reverse process might be required to establish secondary tumours that resemble the primary one. This involves a reversal from the mesenchymal morphology to an epithelial-like phenotype in a process known as mesenchymal-epithelial transition (MET) (Voulgari and Pintzas, 2009).

Due to the high mortality associated with cancer metastasis considerable effort is being applied in order to fully understand this complex process. A key-defining feature of the metastatic cascade is increased cellular migration. Various cellular processes and proteins have been identified to date to facilitate and regulate cellular migration in normal and cancer cells. The following section outlines some of these processes in more detail.

1.2 Cellular Migration

1.2.1 Molecular Mechanism of Cellular Migration

Cellular migration and invasion of the ECM is a highly complex process with multiple steps that involve alterations in the actin cytoskeleton, cell-cell adhesions, cell-ECM interactions and cellular contractile forces. As outlined in Figure 1.1 migration of cells in 2-dimensional and 3-dimensional environments can be divided into five main steps.

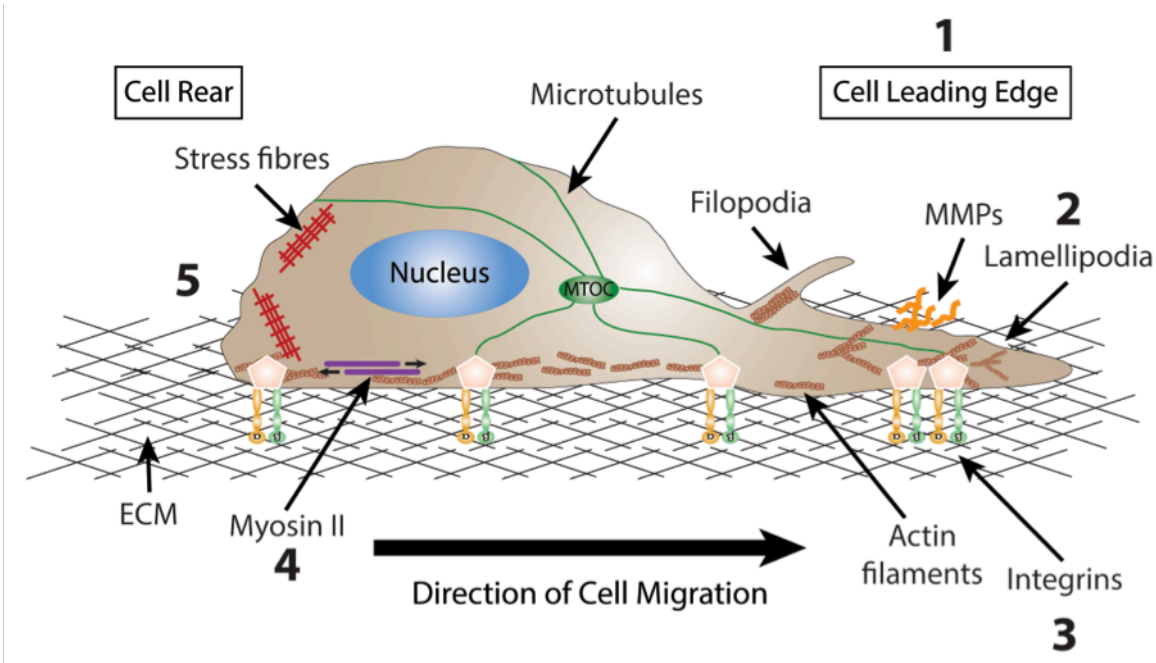

Figure 1.1: Schematic Representation of Steps Required for Cellular Migration
Schematic representation highlighting the five main cellular events that mediate migration in cells: 1) the acquisition of an asymmetrical cellular morphology with enhance front-rear polarisation; 2) the formation of membrane protrusions, including lamellipodia, filopodia and invadopodia; 3) the stimulation of focal complex and focal adhesion assembly at the leading edge of the cell; 4) actomyosin contraction to generate the traction force required for cellular movement; 5) detachment of the cell rear to allow the forward movement of cells. Diagram compiled based on reviews by Lauffenburger et al. and Parri et al.(Lauffenburger and Horwitz, 1996; Parri and Chiarugi, 2010).

1.2.1.1 Front-Rear Cellular Polarisation

To generate the necessary forces for cellular migration, cells need to first acquire an asymmetrical morphology. Depending on environmental cues and the mode of migration utilised by the cell this asymmetry can manifest as a polarised cellular morphology where there is a clear distinction between the front and the rear of the cell. This asymmetry is often the result of spatiotemporal changes in signalling cascades within the cell including receptor-ligand binding kinetic fluctuations. As a consequence of this asymmetrical phenotype, additional molecular arrangements occur to aid the migration process. For example, Sullivan et al. demonstrated that there is an asymmetrical distribution of chemotactic peptide receptors on motile polymorphonuclear leukocytes that is not dependent on receptor stimulation, suggesting a role of the receptor asymmetry in influencing the directionality of migration in the presence of a chemotactic peptide gradient (Sullivan et al., 1984). In a separate study conducted by Lawson et al. an asymmetrical distribution of the adhesion receptor $\alpha V\beta 3$ integrin was also seen in migrating neutrophils with the receptor accumulating at the leading edge (Lawson and Maxfield, 1995). A similar accumulation of $\beta 1$ integrin at the cell leading edge was also observed in motile fibroblast (Schmidt et al., 1993). The asymmetry in these adhesion molecules creates a gradient of cell-ECM interaction, which provides the cells with the necessary traction force required to propel forward (Lauffenburger and Horwitz, 1996).

1.2.1.2 Membrane Extensions

Another important consequence of the asymmetrical cellular phenotype is the formation of membrane extensions, including lamellipodia and filopodia, at the leading edge of the cell. Key to the formation of these extensions is the dynamic regulation of actin filaments (F-actin)(Lauffenburger and Horwitz, 1996).

Under normal cellular conditions, actin exists as monomers (G-actin), which spontaneously come together to form highly unstable actin oligomers in a process known as spontaneous nucleation. Upon stabilisation of these actin oligomers, which can occur naturally, or by the aid of actin-binding proteins, commonly referred to as actin-nucleating proteins, the formation of long stable actin filaments occurs rapidly. Due to the orientation by which G-actin assembles into F-actin, actin filaments are polarised with a slow growing pointed end and fast growing barbed end. Actin filaments are highly dynamic and are constantly undergoing a cycle of polymerisation and depolymerisation in a process known as treadmilling that is regulated via actin binding to ADP and ATP. The actin regulatory protein profilin promotes the exchange of ADP for ATP on actin monomers thus allowing ATP-bound actin monomers incorporation at the barbed end of actin filaments. Upon assembly, actin hydrolyses the bound ATP into ADP releasing the terminal phosphate group, which induces subtle changes in the actin subunit structures that potentiate their disassembly by regulatory actin-binding proteins, such as ADF/cofilin, at the pointed end of F-actin (Pollard et al., 2000; Pollard and Cooper, 2009; Wehrle-Haller and Imhof, 2003). Actin treadmilling is governed by a number of actin-binding proteins that influence polymerisation and depolymerisation through their ability to cap the barbed and pointed ends of F-actin, respectively or through promoting actin nucleation events and severing actin filaments (Goode and Eck, 2007; Pollard and Cooper, 2009). Section 1.3 describes the role of key actin-binding proteins in regulating actin dynamics during cellular migration.

During migration, actin-binding proteins regulate F-actin at the leading edge to allow the formation of membrane protrusions. Both lamellipodia and filopodia are actin-rich structures that are coupled with increased actin polymerisation. Lamellipodia are thin, flat, sheet-like structures that form at the leading edge of migrating cells. Abercrombie et al. first described and named these structures in 1970 (Abercrombie et al., 1970). In a separate study, Abercrombie et al. demonstrated that these structures were rich in microfilaments, such as actin filaments; however contained no microtubules (Abercrombie et al., 1971). Electron microscopy images also indicated that the actin filaments within lamellipodia show extensive branching forming a dendritic bush as described by Svitkina et al. (Svitkina and Borisy, 1999). In addition to the branched actin filaments found in lamellipodia, using electron tomography, Urban et al. revealed that lamellipodia also contains unbranched actin filaments (Urban et al., 2010). The formation of lamellipodia is crucial for directed cellular migration as it allows the tethering of the front of the cell to the ECM thus generating a force to pull the cell forward (Parri and Chiarugi, 2010).

In contrast to lamellipodia, filopodia consist of bundled unbranched actin filaments. As a consequence they form as thin, needle-like projections that undergo cycles of extension and retraction. They function as environmental sensors and thus play a role in dictating the direction of cellular migration in response to environmental cues (Mallavarapu and Mitchison, 1999). In both structures F-actin treadmilling occurs towards the interior of the cell with G-actin incorporation occurring towards the periphery of the membrane protrusion and disassembly toward the cell body. This is essential in defining the polarity of the actin filaments, which in turn dictates both the direction and speed of migration (Wehrle-Haller and Imhof, 2003).

In addition to lamellipodia and filopodia membrane extensions, actin regulation is important for the formation of invadopodia and podosomes. These are actin-rich protrusions that facilitate ECM degradation during cellular invasion (Buccione et al., 2009). Through the crosstalk between microfilaments and microtubules, vesicles containing MMPs, specifically, membrane type 1 MMP (MT1-MMP), are delivered to the tip on invadopodia. This allows the focalised proteolysis of the ECM creating a path for cellular migration (Schoumacher et al., 2010).

1.2.1.3 Cell-ECM Adhesions

Cellular migration requires a highly dynamic regulation of cell-ECM adhesions to generate a cycle of assembly and disassembly that accommodates the movement of cells (Gardel et al., 2010). As indicated earlier, the asymmetrical phenotype promotes molecular rearrangements in the cell that result in an asymmetrical distribution of adhesion molecules at the leading edge in motile cells (Lawson and Maxfield, 1995; Schmidt et al., 1993; Sullivan et al., 1984). This asymmetry in adhesion is crucial for generating the necessary traction forces required for cellular locomotion as protrusions at the leading edge need to be coupled to strong ECM adhesions to propel the cell forward; however this will not be possible if strong adhesions are also present at the cell rear (Gardel et al., 2010; Lauffenburger and Horwitz, 1996; Parri and Chiarugi, 2010).

Cell-ECM adhesions at the leading edge are localised to membrane protrusions, such as lamellipodia and filopodia. They start as small nascent adhesions, which as the leading edge advances, either disassemble or mature to form focal complexes (Choi et al., 2008). Through these complexes the protruding membrane and the ECM form an attachment. This in turn allows $\alpha V\beta 3$ integrins to bind to ECM ligands forming localised clusters of cell-ECM adhesions that also bind to the focal adhesion kinase (FAK) and actin-binding proteins, including phosphorylated paxillin (p-paxillin), α-actinin and talin, thus coupling the focal complexes to the actin cytoskeleton (Gardel et al., 2010). Through fluorescence tracking of GFP-paxillin, GFP-α-actinin and GFP-$\alpha 5$ integrin fusion proteins, Laukaitis et al. demonstrated that paxillin is the first component recruited to the cells' leading edge. As the adhesions mature α-actinin is incorporated into the adhesions as they translocate towards the centre of the cell. The focal

complexes were further stabilised forming focal adhesions upon the recruitment of α5 integrins (Laukaitis et al., 2001). Additional actin-binding proteins, including zyxin, vinculin and VASP are also incorporated into focal adhesions increasing their signalling potential (Gardel et al., 2010; Zamir and Geiger, 2001; Zamir et al., 2000). As cells migrate, cell-ECM adhesions at the different maturation stages undergo disassembly, mainly at the cell rear and at the base of membrane protrusions, to allow the formation of new adhesions at newly formed membrane extensions. Several kinases and adaptor proteins, such as FAK, Src, p130CAS, paxillin, ERK and myosin light chain kinase (MLCK) have been shown to regulate adhesion turnover at the leading edge of cells (Webb et al., 2004). However, under certain conditions, focal adhesions can mature further to form larger more stable fibrillar adhesions that impede migration, instead these adhesions are involved in ECM remodelling (Gardel et al., 2010). The phosphorylation state of paxillin has been shown to regulate the process of focal adhesion maturation into fibrillar adhesions. Live cell imaging using a phosphomimetic form of paxillin demonstrated the importance of paxillin phosphorylation in both the assembly and turnover of cell-ECM adhesions. Additionally, the interaction between FAK and p-paxillin was shown to be important for increased focal complexes turnover and focal adhesion translocation to the cell centre. In contrast, non-phosphorylated paxillin mediated the formation of fibrillar adhesions and was essential for fibronectin fibrillogenesis (Zaidel-Bar et al., 2007).

1.2.1.4 Cellular Contraction

Cellular contraction is crucial for cellular migration as it provides the necessary traction force required for locomotion. In migrating cells, two distinct forces are generated. The first force originates at the leading edge and involves the formation of lamellipodia and filopodia that push against the cell membrane. This force is mainly mediated through actin polymerisation and bundle formation. Unlike the protrusive nature of the first force, the second force is contractile. The motor activity of myosin II is required for this force (Lauffenburger and Horwitz, 1996). It is important to note, however, that coupling of myosin II activity and actin filaments is crucial for contraction to occur. This is mainly mediated via actin-binding proteins, such as tropomyosin, which have the ability to link myosin with actin filaments, thus transforming the myosin motor activity into actomyosin contractility (El-Mezgueldi, 2014). Additionally, actin-capping proteins, including members of the tropomodulin family, a group of pointed end actin-capping proteins, can also facilitate this crosstalk through their ability to bind directly to actin monomers and filaments that are associated with tropomyosin (Weber et al., 1994). Actin-binding proteins associated with focal complexes also play a role in this process by providing an additional link between focal complexes and actomyosin contractility (Gardel et al., 2010). A clear demonstration of such cross talk is the action of the small GTPase Ras homolog gene family, member A (RhoA). Activation of RhoA and its downstream effector the Rho-associated serine/threonine kinase (ROCK) have been shown to stimulate the myosin II

dependent contraction of actin filaments in the cell body. Through the RhoA stimulation, ROCK binds to and phosphorylates myosin phosphatase, which in turn enhances the phosphorylation of the light chain of myosin II (MLC). ROCK has also been shown to directly phosphorylate MLC. As a consequence, pMLC promotes the formation of RhoA-mediated stress fibre formation and focal adhesion assembly at the cell centre, which facilitate actomyosin contractility (Totsukawa et al., 2000). Moreover, increased myosin II activity is associated with actin filament disassembly at the cell rear of migrating cells (Wilson et al., 2010), providing a potential link between actomyosin contractility and the functionality of actin-severing proteins. In addition, there is evidence implicating myosin II motor activity in mediating actin filament contraction at the leading edge and suggesting a role in the extension of lamellipodia. Matsumura et al. demonstrated that phosphorylation of MLC is enhanced both at the leading edge near membrane ruffles as well as at the cell rear towards the nucleus (Matsumura et al., 1998). Consistent with these observations, myosin II activity is also required for contractions at the back of the lamellipodia, in an area known as the lamella. These contractions pull the actin network within the lamellipodia resulting in edge retraction and the formation of new adhesion sites all of which generate the necessary force for forward movement (Giannone et al., 2007). Unlike the ROCK-mediated phosphorylation of MLC at the cell centre, MLC phosphorylation at the leading edge is mediated through the activity of MLCK, suggesting that the two pools of MLC are regulated separately to generate the necessary spatial contraction as well as mediate separate functions (Totsukawa et al., 2000).

Taken together, the above evidence demonstrates the importance of the crosstalk between myosin, actin filaments and focal adhesions. However, it is important to emphasis, that central to cellular contraction is the activation of myosin II. Consistently, inhibition of myosin II hinders cellular migration (Wilson et al., 2010).

1.2.1.5 Detachment of the Cell Rear

As indicated above, an asymmetrical distribution of integrins and cell-ECM adhesions towards the cells' leading edge is essential to ensure efficient cellular migration. This is particularly important in the detachment of the cell rear. The importance of this asymmetry was clearly demonstrated by Palecek et al. where they show that the retraction of the cell rear was limited in Chinese hamster ovary (CHO) cells expressing intermediate and high levels of $\alpha 5$ integrin resulting in reduced cellular migration speeds (Palecek et al., 1998). There are various mechanisms, depending on the cell type, mode of migration, and as indicated above the strength of the cell-ECM adhesions at the cell rear, by which disassembly of cell-ECM adhesions at the cell rear is achieved (Parri and Chiarugi, 2010). For example, in fibroblasts, the major mechanism of tail detachment involves membrane "ripping", in which the majority of integrins released from cell-ECM adhesions remain on the substratum as the cell moves forward (Chen, 1981; Lauffenburger and Horwitz, 1996; Regen and Horwitz, 1992). Calpain, a calcium

dependent protease, has also been shown to mediate focal complex disassembly in slowly moving cells, through its ability to cleave components of the focal complexes, such as talin. Additionally, calpain can promote tail retraction through the cleavage of the cytoplasmic tails of β1 and β3 integrins (Potter et al., 1998). Moreover, cellular contraction is also important for tail detachment. Decreased activation of RhoA and the subsequent reduction in ROCK-mediated MLC phosphorylation and actomyosin contractility can hinder the detachment of the cells' lagging tail (Cox and Huttenlocher, 1998; Parri and Chiarugi, 2010).

1.2.2 Modes of Cellular Migration

The above subsection highlights the keys steps that occur during cellular migration; however, cells have been shown to undergo migration using several modes . As a result the extent by which each step influences the rate of migration can differ from one mode to another.

In general, cellular migration can be classified into single cellular migration, mesenchymal or amoeboid, and collective cellular migration in the form of cell sheets, strands, tubes, or clusters (Friedl and Wolf, 2010; Parri and Chiarugi, 2010). There are various factors that influence the type of migration adopted by the cell, including cytoskeletal rearrangement, the extracellular protease activity, the integrin-mediated cell-ECM interactions, cell-cell cadherin-mediated adhesions, and cellular polarity (Friedl and Wolf, 2003). In addition to the aforementioned factors, it has been shown that stromal cells can also influence this process. For example, stromal fibroblast leader cells tend to promote collective cellular migration, while macrophage pioneer cells play a role in single cellular migration (Yilmaz and Christofori, 2010).

1.2.2.1 Single Cellular Migration

Single cellular migration, as indicated by the name, involves the motility of cells that have completely lost their cell-cell adhesions and migrate as single cells. The gene expression profile associated with EMT has been shown to promote single cellular migration as outlined earlier in section 1.1.1.2 (Geiger and Peeper, 2009). This mode of migration is further divided into mesenchymal motility and amoeboid motility. A hallmark of mesenchymal motility is a morphological change that includes the adoption of a mesenchymal-like morphology with a distinguished cell leading edge and lagging tail that dictate the directionality of migration. Mesenchymal motility also involves the degradation of the ECM by proteolysis through the action of secreted MMPs and urokinase-type plasminogen activator (uPA) (Andreasen et al., 1997; Nabeshima et al., 2002). In this type of cellular motility, which is often stimulated in response to extracellular stimuli, phosphatidylinositol (3,4,5)-triphosphate (PtdIns(3,4,5) P_3) is generated at the leading edge of the cell activating the small GTPase Rac1 (De Wever et al., 2004; Ridley et al., 2003). This in turn, promotes actin nucleation and the formation of branched actin filaments at the leading edge to form lamellipodia (Miki et al., 2000; Takenawa and Miki, 2001). In addition, accumulation of PtdIns(3,4,5) P_3 at the leading edge also results in the

activation of Cell division control protein 42 homolog (Cdc42), another small GTPase, which is involved in maintaining the directionality of cellular motility as well as the polymerisation of actin at the leading edge of the cell (Etienne-Manneville and Hall, 2001; Ridley et al., 2003). The combined action of Rac1 and Cdc42 leads to the formation of actin-rich protrusions that allow the formation of small integrin-dependent focal complexes that attach the protrusions to the ECM. In this type of migration, RhoA and its effector ROCK, which are known to aid in the retraction of the lagging tail, seem to be inhibited by the Rac1 downstream effector WASP-family Verprolin- homologous protein 2 (WAVE2), which has also been implicated in the downregulation of amoeboid motility (Parri and Chiarugi, 2010).

Unlike mesenchymal motility, amoeboid motility does not require the formation of Rac1-mediated membrane protrusions. Instead, RhoA has been shown to play an important role in amoeboid cellular migration. Activation of RhoA and its downstream effector ROCK promotes a rounded cellular morphology that utilises actomyosin contractility to propel cells forward (Sahai and Marshall, 2003). The RhoA/ROCK-mediated rounded morphology also allows cells to squeeze through the ECM instead of releasing MMPs to degrade the ECM. As a consequence, cells adopting the amoeboid mode migrate significantly faster than cells undergoing mesenchymal migration (Friedl and Wolf, 2003; Sahai and Marshall, 2003). Moreover, inhibition of integrin function does not affect the rate of amoeboid migration indicating that cells exhibiting this mode of migration have weaker cell-ECM adhesions (Friedl, 2004). Thus, in contrast to mesenchymal cellular migration, amoeboid migration is dependent on neither cell-ECM adhesions nor ECM proteolytic degradation (Parri and Chiarugi, 2010).

1.2.2.2 Collective Cellular Migration

In contrast to single cellular motility, collective migration of cells, as the name entails, involves retaining cell-cell junctions and migrating as one unit. This could be in the form of sheets, tubes, or clusters (Friedl and Wolf, 2008). Collective motility is similar mechanistically to mesenchymal motility in which asymmetrical enrichment of cell-ECM adhesion at the leading edge and MMP-mediated ECM degradation facilitate cellular migration (Parri and Chiarugi, 2010). For example, localised expression of MT1-MMP and β1 integrin-mediated focal adhesions at the leading edge, are required for the collective migration of HT-1080 fibrosarcoma and MDA-MB-231 breast cancer cells *in vitro* (Wolf et al., 2007).

1.3 Actin-Binding Proteins and Actin Dynamics in Cellular Migration

As described in the previous section, cellular migration is a highly complex process that involves the coupling of the actin cytoskeleton to the cells' motor machines and to adhesion complexes. Despite, the importance of all the steps outlined above, actin cytoskeleton rearrangements seem to govern all steps involved in cellular migrations, starting from inducing a polarised morphology to mediating tail detachment and dictating the direction and speed of

migration. The process of actin cytoskeleton rearrangement is highly dynamic with more than a hundred proteins identified in eukaryotic cells that have been shown to regulate actin nucleation, treadmilling, bundling and cross-linking (Pollard and Cooper, 2009). This section will highlight the role of some of these proteins in regulating actin dynamics at key stages in cellular migration.

1.3.1 Actin Dynamics in Cellular Migration

1.3.1.1 Lamellipodia Formation

As highlighted earlier, under physiological conditions actin monomers can undergo spontaneous nucleation. However, this process is slow due to the highly unstable nature of actin oligomers. As a result, actin-nucleating proteins have been shown to stabilise these oligomers to promote actin filament elongation. It is this localised increase in actin polymerisation that is then able to drive forward membrane protrusion within the lamellipodia (Ridley et al., 2003). The actin-nucleating protein, Actin-Related Protein 2/3 (Arp2/3) complex, is considered as the main regulator of lamellipodia formation (Pollard et al., 2000). The Arp2/3 protein complex was the first direct actin-nucleating protein to be discovered (Goode and Eck, 2007; Mullins et al., 1998). It consists of seven different subunits, Arp2, Arp3, Arpc1, Arpc2, Arpc3, Arpc4 and Arpc5 with Arp2 and Arp3 being the major constituents of the complex (Borths and Welch, 2002). Nucleation promoting factors, such as members of the Wiskott–Aldrich Syndrome Protein (WASP) family, including WASP and WAVE 1–3 play a major role in stimulating the ability of the Arp2/3 protein complex to induce actin nucleation and polymerization (Ridley, 2011; Welch and Mullins, 2002). WASP family members have been shown to bind to the Arp2/3 protein complex and trigger a conformational change in the Arp2/3 protein complex bringing together the Arp2 and Arp3 subunits, which resemble actin monomers, to mimic the barbed end of actin filaments (Kreishman-Deitrick et al., 2005; Rodal et al., 2005). Additionally, members of the WASP family stimulate nucleation by delivering the first actin monomer to the Arp2 and Arp3 subunits (Goley et al., 2004). As indicated earlier, lamellipodia contain an extensive branched network of actin (Svitkina and Borisy, 1999). The Arp2/3 protein complex mediates the formation of branched actin filaments by binding to the side of existing actin filaments. Activation of Arp2/3 protein complex stimulates the formation of new actin filaments at a 70° angle with the complex capping the pointed end of the daughter filament (Goode and Eck, 2007; Lai et al., 2008; Pollard et al., 2000). Once formed additional accessory proteins, such as the scaffolding protein cortactin stabilise the formed actin meshwork thus affecting lamellipodia persistence (Lai et al., 2008; Ren et al., 2009).

Other actin-nucleating proteins have also been found to contribute to actin dynamics leading to lamellipodia extension. An important class of proteins are the formins that promote the formation of unbranched actin filaments. Evidence supporting the role of formins in

regulating lamellipodia formation includes the increased localisation of the Diaphanous-Related Formin-1 (mDia1) at the leading edge (Brandt et al., 2007; Chesarone et al., 2010). Additionally, mDia1 was also shown to cooperate with N-WASP and WAVE2 to generate membrane protrusions in response to epidermal growth factor (EGF) stimulation (Sarmiento et al., 2008). Moreover, Yang et al. demonstrated that mDia2 depletion by siRNA impedes lamellipodia extension due to a reduction in the number of linear actin filaments; whereas expression of constitutively active mDia2 enhanced the persistence of the lamellipodial protrusion (Yang et al., 2007). Formin actin assembly is mediated via the conserved formin domains: formin homology domain 1 and 2 (FH1 and FH2, respectively) (Pruyne et al., 2002; Sagot et al., 2002). The FH1 domain mediates interaction of formins with profilin bound actin monomers (Goode and Eck, 2007). Whereas crystal structure of the *Saccharomyces cerevisiae* (*S. cerevisiae*) formin Bni1p FH2 domain demonstrate that the FH2 domain forms an α-helical dimer with two actin-binding heads at the end allowing formins to bind and protect the barbed end of actin filaments and also to potentially promote actin nucleation via stabilising actin dimers and trimers (Xu et al., 2004). Similar to Arp2/3 protein complex, there is an intricate system for regulating formin activity. For example, the diaphanous-related formins (DRFs), a group of formins that are regulated by small Rho GTPases normally exist in a closed conformation due to an interaction between the N-terminal diaphanous inhibitory domain (DID) and the diaphanous autoinhibitory domain (DAD) located at the C-terminus. As a result, the FH1 and FH2 domains responsible for mediating the DRFs' actin assembly properties are shielded from actin binding (Alberts, 2001; Higashi et al., 2008; Li and Higgs, 2003). Binding of activated small GTPases, including GTP bound RhoA, RhoB and RhoC but not Rac1 or Cdc42, to the GTPase binding domain (GBD) located adjacent to the DID domain present in both Daam1 and mDia1, has been demonstrated to partially disrupt the DID-DAD interaction unleashing the autoinhibition and stimulating DRFs-mediated actin assembly (Higashi et al., 2008).

WASP homology 2 (WH2) actin-nucleating proteins have also been implicated in regulating actin polymerisation at the lamellipodia. For example, increased Cordon-bleu (Cobl) expression in neurons stimulates the formation of membrane protrusions (Ahuja et al., 2007). Similar to formins, members of this family, including Spire and Cobl nucleate linear unbundled actin filaments. WH2 actin-nucleating proteins are characterised by having three or more WH2 domains. Studies suggest that, in addition to capping the pointed end of actin filaments, these proteins function by forming a pre-nucleation actin complex through their ability to bind three or more actin monomers via the WH2 domains (Ahuja et al., 2007; Zuchero et al., 2009).

Actin capping proteins also play an important role in determining the length of lamellipodia. Increased barbed end actin filament capping reduces the length of actin filaments; however it can promote the nucleation of branched filaments by the Arp2/3 protein complex by increasing the number of free G-actin available for nucleation instead of elongation (Akin and Mullins, 2008). Severing proteins, such as ADF/cofilin can also enhance formation of

branched actin filaments via cutting existing filaments and exposing new barbed ends that create new filaments to which Arp2/3 protein complexes can bind to (van Rheenen et al., 2009).

1.3.1.2 Filopodia Formation

As indicated earlier, filopodia are thin membrane protrusions that consist of bundles of parallel linear actin filaments. Actin nucleation in these structures is mainly mediated via formins, particularly the mDia proteins (Mellor, 2010). It has also been proposed that filopodial membrane protrusions can also form from Arp2/3 protein complex-mediated branched actin filaments within the lamellipodia. In fact, in a study conducted by Johnston et al. Arp2/3 protein complex activity was detected in filopodia (Johnston et al., 2008). In addition to actin polymerisation, actin-bundling proteins play an important role in filopdia formation. The major actin-bundling protein found in filopdia is fascin, which has been implicated in maintaining the stability of filopdia and promoting cellular migration (Machesky and Li, 2010).

Anti-capping proteins are also thought to contribute to elongation of actin filaments in filopodia. For example, Ena/VASP proteins localise to the tips of filopodia and are proposed to stabilise filopodial structures through inhibiting actin filament branching, bundling F-actin as well as promoting elongation through their anti-capping functions (Bear and Gertler, 2009). Additionally, the anti-capping protein vasodilator-stimulated phosphoprotein (VASP) has been shown to directly influence filament elongation via delivering profilin-bound actin monomers to the barbed end of F-actin (Breitsprecher et al., 2008).

1.3.1.3 Invadopodia Formation

Similar to lamellipodia, the Arp2/3 protein complex and its activator N-WASP play a major role in invadopodia formation (Buccione et al., 2009). Additionally, the DRFs have also been shown to mediate the formation and invasion of invadopodia indicating that similar to lamellipodia, the Arp2/3 protein complex and formins cooperate to produce these membrane extensions (Lizarraga et al., 2009). Other actin-binding proteins are also known to regulate the assembly and elongation of filaments in invadopodia. For example, cortactin was shown to bind and regulate the severing function of cofilin. Upon cortactin phosphorylation, cofilin is released freeing it to severe actin filaments producing new barbed ends to promoting Arp2/3 protein complex actin nucleation. Subsequent dephosphorylation of cortactin inhibits cofilin-mediated F-actin severing thus stabilising the invadopodia (Oser et al., 2009). The bundling protein fascin is also important for maintaining invadopodia stability (Machesky and Li, 2010).

As highlighted earlier, coordinated regulation of actin filaments and microtubules is crucial for the functionality of invadopodia. This is potentially through microtubule-mediated delivery of MMP-containing vesicles to the tip of invadopodia but also via providing the mechanical support required to stabilise the structure (Schoumacher et al., 2010).

1.3.2 Gelsolin Protein Superfamily

In addition to the above mentioned actin regulatory proteins, the gelsolin protein superfamily represents an interesting group of actin-binding proteins that have actin-capping, severing and polymerisation capabilities and are thus proposed to play a major role in mediating cellular migration. The following subsection gives a brief overview of the superfamily and the role of some of its members in cells.

The gelsolin protein superfamily is a family of highly conserved actin-binding proteins that are present in lower eukaryotic and mammalian cells (Silacci et al., 2004). Gelsolin, the founding member of the family, was first described by Yin et al. in 1979 and is characterised by having two duplicated domains. Each domain consists of three homologues repeats of 125-150 amino acids (S1-S3) known as the gelsolin-like (GEL) domain yielding a total of six GEL domains in the protein (S1-S6). Mammalian gelsolin also contains an additional calcium sensitive segment at the C-terminus, which maintains the protein in a closed conformation in the absence of calcium (Kwiatkowski et al., 1986; Yin and Stossel, 1979). Adseverin, another member of the family, is the closest homologue to gelsolin and similarly consists of six GEL domains. Other members of the family include capG, supervillin, protein flightless-1 homolog (FLII) and the villins: villin, advillin, and the villin-like protein. Similar to gelsolin and adseverin, all members of the gelsolin protein superfamily contain six repeats of the GEL domain with the exception of capG, which only contains three repeats due to a deletion event of the S4-S6 protein encoding region of a gelsolin-like precursor gene (Claudianos and Campbell, 1995; Mishra et al., 1994; Silacci et al., 2004). Evidence from comparative structural and functional analyses of the monomeric GEL domain and destrin, an isoprotein of cofilin, suggest a potential evolutionary link between cofilin and gelsolin protein superfamily members despite the absence of any sequence homology (Hatanaka et al., 1996). Regardless of the expression and cellular localisation differences, all members of this superfamily, through their GEL domains, have been shown to regulate actin dynamics via binding and capping the barbed end of actin filaments. In addition, with the exception of capG, gelsolin protein superfamily members are also able to sever actin filaments in a calcium and pH dependent manner. Moreover, some members of the family have also been reported to contribute to actin filament nucleation via serving as scaffolds that bring actin monomers together (Kwiatkowski, 1999; McGough et al., 2003; Silacci et al., 2004).

In addition to their overlapping functions dictated by the Gel domain, several members contain unique domains, which confer additional functions. For example, villin was found to possess a small headpiece at the C-terminus. Functional analysis of the headpiece revealed its ability to bind to F-actin in a calcium-independent manner. Moreover, it was demonstrated that in the absence of calcium, through the headpiece, villin was capable, not only to bind to actin filaments, but also to form actin bundles while maintaining a uniform filament polarity (Glenney et al., 1981). The actin binding villin headpiece is also found in the closely related proteins,

advillin, the villin-like protein and supervillin (Kwiatkowski, 1999). Supervillin also contains an additional N-terminal domain that facilitates protein-protein interactions and contains a nuclear localisation signal (NLS) (Pestonjamasp et al., 1997; Wulfkuhle et al., 1999). CapG was also found to contain an NLS sequence and localises to both cytoplasm and nucleus (Onoda et al., 1993; Prendergast and Ziff, 1991). Similarly, FLII over its evolution has acquired an additional unrelated N-terminal domain, which consists of 16 Leucine Rich Repeats (LRR) (Campbell et al., 1997; Claudianos and Campbell, 1995). The LRR domain has been previously reported to mediate protein-protein interactions via forming a doughnut- or horseshoe-like conformation that serves as a hydrophobic pocket that acts as a protein interaction recognition site (Kobe and Deisenhofer, 1995; Kobe and Kajava, 2001; Liu and Yin, 1998). Additionally, FLII has also been shown to localise predominantly to the nucleus through an NLS sequence, similar to supervillin and capG (Davy et al., 2001; Lee et al., 2004). Figure 1.2 presents a schematic representation of the different domain structures of gelsolin protein superfamily members.

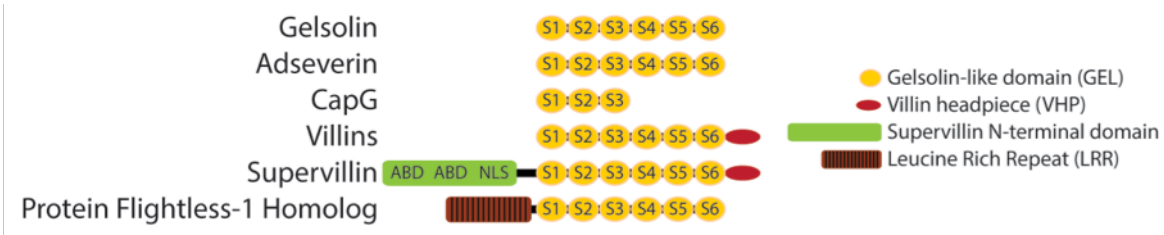

Figure 1.2: Domain Structures of Gelsolin Protein Superfamily Members

Schematic representation of the domain structure of gelsolin protein superfamily members (vertebrates only), modified from Archer et al. and Kwiatkowski et al. (Archer et al., 2005; Kwiatkowski, 1999). The domain structure for villins represents the structure for the villin family including villin, advillin and the villin-like protein. ABD= actin binding domain; NLS= nuclear localisation signal.

1.3.2.1 Gelsolin Protein Superfamily Cellular Functions

As highlighted above, members of the gelsolin protein superfamily are important regulators of actin dynamics. Through F-actin capping, severing and nucleation, gelsolin related proteins influence key cytoskeleton parameters, including the length of actin filaments, the mobility and flexibility of the cytoskeleton, as well as the formation of actin bundles. As a result, members of this superfamily are considered key players in regulating the actin cytoskeleton, which in turn implicates them in a multitude of cellular processes, including cellular migration.

The first indication that members of the gelsolin protein superfamily influence cellular migration was provided through a series of transfection experiments conducted by Cunningham et al. in 1991. Evidence from these experiments revealed a correlation between expression of gelsolin in cultured NIH3T3 cells and the ability of cells to migrate, with increased expression promoting cellular migration (Cunningham et al., 1991). The link between gelsolin superfamily protein members' expression and cellular motility was also reported in hematopoietic cells, where gelsolin and adseverin expression were markedly reduced in the less migratory $Lin^{-}Sca^{+}Kit^{+}$ population compared to the more chemokine responsive $Lin^{-}Sca^{+}Kit^{-}$ population (Evans et al., 2004). *In vivo* experiments also highlighted the importance of gelsolin

in regulating cellular motility. For example, gelsolin null mice were found to have decreased basal and osteopontin induced osteoclast motility as a consequence of their inability to form podosomes (Chellaiah et al., 2000). Moreover, comparison of wild type and gelsolin null mice revealed a role of gelsolin in regulating the growth, formation and retraction of the highly motile neuronal growth cones (Lu et al., 1997). Gelsolin severing activity is also implicated in regulating cellular migration. For example, electroinjection of a gelsolin antibody at a concentration that is sufficient to inhibit its severing function yet not its capping and nucleating functions was shown to reduce cellular migration in human gingival fibroblasts (Arora and McCulloch, 1996). In a separate study conducted by the same group, microinjection of the gelsolin antibody in NIH3T3 cells at the concentration that inhibits gelsolin-mediated actin severing resulted in reduced Mg-ATP induced cellular contraction in 90 % of treated cells compared to cells microinjected with a control antibody. Consistently, depletion of gelsolin by siRNA was associated with a decreased ability of fibroblasts to contract collagen gels in a collagen gel contraction assay (Arora et al., 1999). Together these results implicate gelsolin in regulating cellular contraction in cells, which could also contribute to its role in mediating cellular motility.

Similar to gelsolin and adseverin, capG, despite its inability to sever actin filaments, has also been reported to regulate cellular migration. Overexpression of capG in fibroblasts, similar to gelsolin, was shown to enhance wound healing and the cellular chemotaxis response. Moreover, capG expressing cells were also associated with increased membrane ruffling, increased phosphoinositide turnover, as well as a higher rate of second messenger generation (Sun et al., 1995). Furthermore, it has been documented that capG also plays a role in regulating endothelial cellular motility in response to different mechanical forces dictated by different blood flow patterns in plaque prone and plaque free environments. For example, expression of capG is increased in endothelial cells in response to plaque free environments, which in turn enhances endothelial cellular motility (Pellieux et al., 2003). *In vivo* evidence from capG knockout mice also demonstrated the involvement of capG in macrophage ruffling (Witke et al., 2001). Unlike gelsolin, adseverin and capG, FLII has been identified as a negative regulator of wound healing and cellular migration *in vitro* and *in vivo* (Adams et al., 2008; Cowin et al., 2007; Lin et al., 2011). However, similar to gelsolin, decreased FLII expression is associated with decreased cellular contraction (Kopecki et al., 2011). Given their ability to regulate actin dynamics, gelsolin protein superfamily members are also implicated in other cellular processes that are influenced or require actin cytoskeleton rearrangements, such as phagocytosis, exocytosis, as well as the apoptosis associated membrane blebbing (Silacci et al., 2004).

In addition to their actin binding related cellular processes, gelsolin family members have been shown to localise to the nucleus. This localisation hinted to a potential nuclear function in cells. Indeed, several family members, including gelsolin, supervillin and FLII were found to play a role in regulating transcription (Archer et al., 2004). Supervillin was shown to

associate and mediate the functions of the androgen receptor, a member of the nuclear receptor superfamily that is involved in mediating gene transcription via recruiting co-activator protein complexes to promoters of their target genes (Sampson et al., 2001; Ting et al., 2002). Similar findings were reported for gelsolin in prostate cancer cells where it was found to promote androgen receptor activity in the presences of androgens (Nishimura et al., 2003b). Similar to supervillin and gelsolin, FLII was also reported to regulate gene transcription through acting as a hormone activated nuclear receptor co-activator (Lee et al., 2004).

Given their diverse modes of actin dynamic regulation together with their ability to regulate gene transcription and the evidence supporting their involvement in cellular migration, gelsolin protein superfamily members promise to be key regulators of this process. However, a better understanding of their involvement is still required to decipher their exact functional role in mediating motility.

1.4 Rho Family of Small GTPases

In addition to actin-binding proteins, there are various signalling proteins involved in regulating the actin cytoskeleton and cellular migration. Among these proteins, the Rho family of small GTPases are of particular importance. Through their ability to regulate the actin cytoskeleton, the expression and release of MMPs and cellular plasticity among other cellular processes, research on Rho GTPases presents scientists with an opportunity to understand the complex processes of cellular migration and cancer metastasis. The following section focuses on the Rho family of small GTPases and their role in mediating cellular migration and cancer metastasis, with a particular emphasis on Rac1.

1.4.1 Rho Family of Small GTPases Overview

Members of the Rho family of small GTPases are nucleotide-binding proteins that associate with both guanosine diphosphate and triphosphate (GDP and GTP, respectively). Together with more than 60 other GTPases, the Rho family of small GTPases is part of the larger Ras superfamily of GTPases. In addition to the Rho family there are four additional families constituting this superfamily: Ras, Rab, Arf and Ran GTPases (Etienne-Manneville and Hall, 2002).

In mammals, the Rho family of small GTPases consists of 20 intracellular small (≈21-25 kDa) signalling proteins. Members of this family are structurally homologous and have a characteristic “Rho insert domain”, which is located within the small GTPase domain, between the β strand and α helix (Etienne-Manneville and Hall, 2002; Parri and Chiarugi, 2010; Valencia et al., 1991). As outlined in Figure 1.3 members of this family are further subdivided into five subfamilies that include the Cdc42-like GTPases, Rac-like GTPases, Rho-like GTPases, RhoBTB GTPases and Rnd GTPases. In addition the family also includes RhoD, RhoH/TTF and Rif that do not belong to any subfamilies. The Rho, Cdc42 and Rac GTPases are the best characterised in the family (Burridge and Wennerberg, 2004).

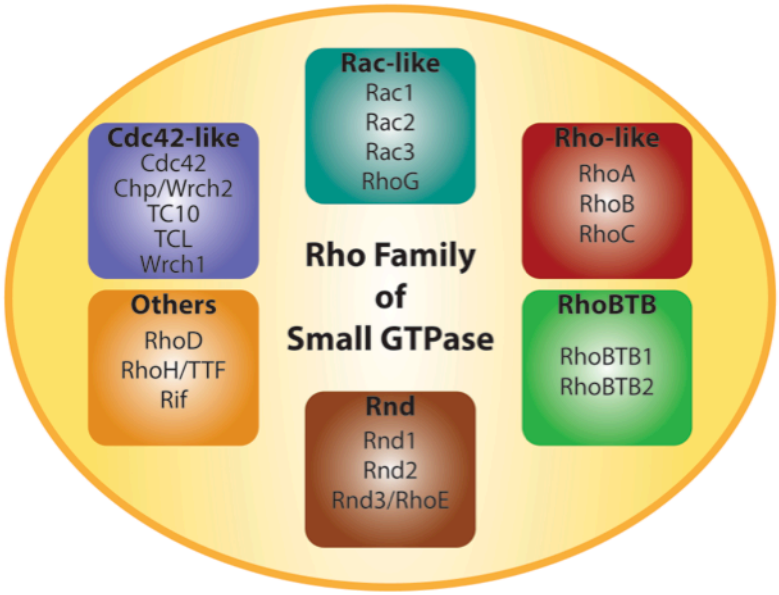

Figure 1.3: Schematic Representation of Rho Family of Small GTPases Subfamilies
Figure formulated based on review by Burridge et al. (Burridge and Wennerberg, 2004).

1.4.1.1 Regulation of Rho Family of Small GTPases

Similar to other GTPases, small Rho GTPases act as molecular switches. They cycle between an inactive GDP-bound state and an active GTP-bound state. Binding of GTP to small GTPases and their subsequent activation induces a conformational change that promotes binding to downstream effectors (Bourne et al., 1991). Regulation of this GDP-GTP activation cycle is mediated mainly by three groups of proteins: Guanine Nucleotide Exchange Factors (GEFs), GTPase Activating Proteins (GAPs) and Guanine nucleotide Dissociation Inhibitors (GDIs) (Jaffe and Hall, 2005; Malliri and Collard, 2003).

GEFs serve as small GTPase activators. They facilitate the exchange of GDP for GTP by promoting the dissociation of GDP from the GTPase, which is then displaced by GTP (Rossman et al., 2005). The GEF family comprises at least 80 members and is further divided into the Dbl family or the DOCK family. Dbl GEFs are characterised by having a Dbl homology domain (DH) that is responsible for its GEF activity. DOCK GEFs, on the other hand, lack the DH domain yet their GEF activity is attributed to two highly conserved regions known as the DOCK-homology region 1 and 2 (DHR1 and DHR2) (Cote and Vuori, 2007; Rossman et al., 2005; Schmidt and Hall, 2002).

In contrast, inactivation of small Rho GTPases is mediated through both GAPs and GDIs. GAPs, as the name implies act via enhancing the intrinsic GTPase activity of the Rho proteins, thus promoting the hydrolysis of the bound GTP into GDP inactivating the protein in the process (Bernards, 2003). Similar to GEFs, more than 70 GAPs have been identified demonstrating the complexity of small GTPases regulation and signalling (Moon and Zheng, 2003). GDIs also act as GTPase inhibitors via stabilising the GDP-inactive form. Their function is mediated through their ability to bind to the C-terminus of the GDP-bound protein thus masking the lipid moieties that are responsible for the plasma membrane translocation that is

required for GTP loading. As a consequence, GDP-bound small GTPases are sequestered in the cytoplasm where GTP loading cannot occur (DerMardirossian and Bokoch, 2005; Olofsson, 1999). Additionally, GDIs have also been shown to bind to the active form of small GTPases, including Rac1 and Cdc42, with an affinity similar to their binding to the GDP-bound form (Chuang et al., 1993; Nomanbhoy and Cerione, 1996). As a result, GDIs can also inhibit small GTPases via hindering their ability to interact with their downstream effectors once in the active form, thereby inhibiting their downstream signalling effects (DerMardirossian and Bokoch, 2005). Only three GDIs have been identified thus far: RhoGDI1-3, with RhoGDI1 being the most well-characterised (Olofsson, 1999). As highlighted above, once activated, Rho proteins can then interact with their downstream effectors activating them. This in turn stimulates and controls a wide variety of cellular processes that influence actin cytoskeleton rearrangements and gene expression, which further enables small Rho GTPases to regulate other downstream effects, including, yet not limited to, cellular morphology, migration, and cell-cell/cell-ECM adhesions (Etienne-Manneville and Hall, 2002).

1.4.1.2 Regulation of Rho Family of Small GTPases Activity through Crosstalk

In addition to the role of GEFs, GAPs and GDIs in regulating the activity of small Rho GTPases, there are several studies highlighting the role of family member crosstalk in mediating the activity of Rho GTPases both spatially and temporally. A key example is the reciprocal inhibition of Rac1 by RhoA activation and vice versa (Leeuwen et al., 1997). Consistently, Sander et al. also demonstrated that both Rac1 and Cdc42 activity induces the downregulation of RhoA activation (Sander et al., 1999). In contrast, under certain cellular conditions, activation of Cdc42 is important for proper Rac1 functioning (Kawakatsu et al., 2002; Nobes and Hall, 1999). RhoG is another example of how crosstalk between family members can regulate activity in cells. Activation of RhoG stimulates its binding to its downstream effector engulfment and cell motility (ELMO). This in turn facilitates the formation of a ternary complex containing RhoG-ELMO-Dock180 that promotes Rac1 activation (Katoh and Negishi, 2003). RhoG has also been suggested to activate Cdc42 in a similar manner (Cote and Vuori, 2007). This crosstalk adds an extra level of regulation that is important for the proper functioning of the family.

Given the focus of this thesis on cellular migration, the next section highlights the role played by small Rho GTPases in cellular migration particularly through regulating actin dynamics in the cell.

1.4.2 The Rho family of Small GTPases and Actin Dynamics in Cellular Migration

Small Rho GTPases are best known for regulating the actin cytoskeleton (Ridley, 2001). They have been documented to cooperate with actin-binding proteins to stimulate the restructuring of the actin filaments required for the morphological changes associated with

cellular migration (Ridley, 2011). Additionally studies have directly implicated small GTPases, including Rac1 and Cdc42 in cellular migration regulation (Nobes and Hall, 1995, 1999).

1.4.2.1 Lamellipodia Formation

There is large body of evidence implicating Rho GTPases in the formation of lamellipodia in migrating cells. For example, active Rac1, RhoA and Cdc42 have been shown to localise to lamellipodial structures during membrane extensions, with RhoA playing a role in the initial protrusion event, and Rac1 and Cdc42 mediating the stabilisation of the formed lamellipodia (Machacek et al., 2009). Consistent with these observations, RhoA has been suggested to regulate lamellipodia formation through stimulating mDia1-mediated actin filament assembly as well as controlling the myosin II-mediated actomyosin contractions at the leading edge (Pertz, 2010; Pertz et al., 2006). Wu et al. further confirmed the requirement of Rac1 for lamellipodia formation via using photoactivatable Rac1. In this study inducing the activation of Rac1 was sufficient to promote migration via stimulating membrane protrusions that helped determine the directionality of cellular movement (Wu et al., 2009). RhoG has also been implicated in lamellipodia formation independent of its ability to activate Rac1 through an unknown mechanism (Meller et al., 2008).

1.4.2.2 Filopodia Formation

Cdc42 is the main Rho GTPase implicated in the formation of filopodia. Its has been proposed that Cdc42 mediates actin assembly within filopodial structures via bringing together three of its downstream effectors, the insulin receptor tyrosine kinase substrate p53 (IRSp53), mDia2 as well as N-WASP (Ahmed et al., 2010). As highlighted earlier in section 1.3.1.2 formins, such as mDia2 nucleate linear actin filaments that are essential for filopodia formation (Mellor, 2010). Cdc42 activation of N-WASP can also promote filopodia formation and elongation since N-WASP serves as a nucleation promoting factor to stimulate the nucleating activity of Arp2/3 protein complex that has also been implicated in filopodia formation (Johnston et al., 2008; Ridley, 2011). Interestingly, IRSp53 can also promote filopodial protrusions and membrane curvature through its I-BAR domain. I-BAR domains are thought to promote membrane extensions via clustering membrane phosphatidylinositol 4,5-bisphosphate (PIP_2), which could then activate PIP-binding proteins, such as N-WASP (Takenawa and Suetsugu, 2007; Zhao et al., 2011). In addition to Cdc42, other Rho GTPases have also been identified as regulators of filopodia formation. For example, the activity of Arp2/3 protein complex in filopodia was shown to be dependent on Rac1 activity (Johnston et al., 2008). Additionally, the small GTPase Rif was found to promote filopodia through mDia2 (Hotulainen et al., 2009).

1.4.2.3 Invadopodia Formation

Similar to filopodia, Cdc42 is the main Rho GTPase associated with invadopodia formation and extension through activating N-WASP and WASP actin nucleation promoters (Ridley, 2011). The Cdc42 specific GEF, Fgd1 is thought to be responsible for activating Cdc42 to form invadopodia (Ayala et al., 2009).

1.4.2.4 Additional Regulation of Cellular Migration

As demonstrated above, Rho GTPases are important regulators of actin dynamics and it is through their ability to restructure the actin cytoskeleton that they are able to regulate cellular migration. In addition to inducing actin cytoskeleton rearrangements, Rho GTPases have been shown to regulate other cellular aspects, such as cellular polarity, cell-cell/cell-ECM adhesions, and expression and release of MMPs that are important for cellular migration. For example, as highlighted earlier, Cdc42 is implicated in maintaining cellular polarity and migration directionality in the mesenchymal mode of migration (Etienne-Manneville and Hall, 2001). Consistent with this, expression of a dominant negative mutant of Cdc42 has been shown to hinder cellular migration due to the failure of cells to polarise correctly. Additionally, inhibition of Cdc42 activity was associated with the formation of lamellipodia all around the cell indicating that the proper activation of Cdc42 is crucial for mediating the asymmetrical morphology that confines Rac1-mediated lamellipodia formation to the front of the cell (Nobes and Hall, 1999). In addition to its role in promoting filopodia and maintaining cellular polarity, Cdc42 is also involved in proteolytic degradation of the ECM through its ability to promote invadopodia formation and the associated dispersal of the MMP-containing vesicles (Ridley, 2011). Moreover, Cdc42, together with Rac1 and RhoA play a role in focal complex assembly (Nobes and Hall, 1999). Various studies also report a role of Cdc42 in cell-cell adhesions. This was illustrated in a study conducted by Du et al. were they showed that activation of Cdc42 is required for maturation of cell-cell contacts (Du et al., 2009). Interestingly, initial formation of cell-cell contacts has been shown to mediate Cdc42 activity suggesting a positive feedback loop between cell-cell contact formation and Cdc42 activation (Fukuhara et al., 2003; Fukuhara et al., 2004). Depending on the mode of migration adopted, regulation of cell-cell contacts by Rho GTPases can also influence cellular migration. Section 1.5.2 provides additional examples for the role of Rac1 in regulating cellular migration.

1.4.3 The Rho Family of Small GTPases and Cancer

Given the magnitude of cellular processes that Rho GTPases regulate, it is not surprising that Rho proteins are implicated in a number of diseases, including cancer. As a consequence of their role in regulating cellular migration, Rho GTPases are also implicated in cancer metastasis. The following section highlights some of the evidence present implicating Rho GTPases in regulating the different stages of cancer.

Unlike the Ras GTPases H-Ras, N-Ras and K-Ras, which have been shown to acquire missense mutations in various human cancers, transforming mutations in small Rho GTPases are rare. In fact, until recently RhoH was the only family member that was found to undergo gene rearrangement and mutation in non-Hodgkin's lymphoma and multiple myeloma (Preudhomme et al., 2000). However, advancement in screening methodologies has enabled the identification of a number of activating mutations in small Rho GTPases. For example, through exome sequencing of 147 melanomas, an activating Rac1 mutation (P29S) was identified in 9.2 % of sun-exposed melanomas. Further analysis of the crystal structure of the $Rac1^{P29S}$ mutant revealed that this mutation enhances Rac1 binding to its downstream effectors thus prolonging Rac1 downstream signalling. As a consequence the Rac1 mutation promotes melanocyte proliferation and migration (Krauthammer et al., 2012). This mutation was also identified in a separate study aimed at mapping driver mutations in melanoma, further corroborating the importance of this mutation in melanoma progression (Hodis et al., 2012). Whole exome sequencing data from 74 tumour and normal sample pairs also identified $Rac1^{P29S}$ as an activating mutation in head and neck squamous cell carcinoma (Stransky et al., 2011). Additionally, Screening of human cancer cell lines also helped identify additional activating mutations in Rac1 and Rac2. For example, the Rac1 activating mutation Rac1 (N92I) was identified in the human sarcoma cell line HT1080. This cell line was also found to harbour an N-Ras (Q61K) activating mutation. Interestingly, functional analysis of both mutants indicated that Rac1 (N92I) might serve as the driving mutation that stimulates the growth of this cell line. Additional transforming mutations identified include RAC1 (P29S) in the breast cancer cell line MDA-MB-157, RAC2 (P29Q) in the chronic myeloid leukaemia (CML) cell line KCL-22, and RAC2 (P29L) in the breast cancer cell line HCC1143. Another transforming Rac1 mutation Rac1 (C157Y) was also identified from this study, which similar to the P29S and N92I results in a rapid GDP-exchange step thus favouring the GTP-bound state of Rac1 (Kawazu et al., 2013). Other mutations recently identified include, the gain-of-function mutations of RhoA in diffuse-type gastric carcinoma (Kakiuchi et al., 2014), as well as the $Cdc42^{G12V}$ activating mutation in melanoma (Hodis et al., 2012).

In contrast to relatively new discovery of transforming mutation, aberrant regulation of Rho GTPases expression levels is well documented in a number of cancers (Aznar et al., 2004; Parri and Chiarugi, 2010). Table 1.1 highlights some examples of Rho GTPases, their mode of deregulation and the associated tumours in which they were reported.

Table 1.1: Aberrant Regulation of Rho GTPases in Cancer

Small GTPase	Mechanism of Deregulation	Tumour Type
Cdc42	Overexpression Mutations*	Breast; Testicular; Melanoma*
RhoA	High protein levels High signalling activity Mutations*	Liver; Skin; Colon; Ovarian; Bladder; Gastric; Esophageal squamous cell carcinoma (SCC); Testicular; Breast; Diffuse-type gastric carcinoma (DGC)
RhoB	Overexpression Downregulation	Breast (overexpression); Lung (downregulation)
RhoC	High protein levels High signalling activity	Melanoma; Squamous cell carcinoma(SCC); Prostate; Breast; Pancreas; Liver; Ovarian; Head and neck; non-small cell lung carcinoma (NSCLC); Gastric
RhoH	Rearrangement Mutations	Non-Hodgkin's lymphomas and multiple myeloma
Rac1	High protein levels High signalling activity Mutations*	Testicular; Gastric; Breast*; Squamous cell carcinoma (SCC); Melanoma*; Head and neck*
Rac1b	High protein expession	Colon; Breast
Rac2	High protein levels	Head and neck; Squamous cell carcinoma (SCC)
Rac3	Hyperactive Overexpression	Breast

Table formulated based on information gathered from reviews by Parri et al. and Alan et al. (Alan and Lundquist, 2013; Parri and Chiarugi, 2010) with minor modifications to introduce evidence for mutations of RhoA (Kakiuchi et al., 2014). Recently identified mutations and their associated tumour type are indicated by asterisks.

In addition to the above there is direct evidence from *in vitro* and *in vivo* studies demonstrating the involvement of Rho GTPases in the various steps of tumour initiation as well as progression. For example, studies have shown that Rho proteins are required for full oncogenic Ras transformation (Benitah et al., 2004; Khosravi-Far et al., 1995). Khosravi et al. showed that co-expression of dominant negative Rac1 and RhoA resulted in inhibition of Ras transformation in NIH3T3 cells. Moreover, expression of active forms of Rac1 and RhoA was associated with increased growth. Additionally, coupling of Rac1/RhoA activation and Raf/MAPK pathway activation was also required for full oncogenic Ras transforming activity (Khosravi-Far et al., 1995). *In vivo* studies also highlighted the requirement of Rac1 for Ras transformation (Kissil et al., 2007; Malliri et al., 2002). Rho GTPases have also been implicated in cell cycle progression, gene transcription and the regulation of pro-angiogenic factors release thus promoting neovascularisation (Benitah et al., 2004; Merajver and Usmani, 2005; Parri and Chiarugi, 2010). In addition, as highlighted earlier, Rho GTPases play a critical role in cellular motility with Rac1 and Cdc42 activation being required for mesenchymal motility and Rho activation required for mediating amoeboid motility. They also dictate cellular invasion through stimulation of invadopodia formation and ECM degradation (Ridley, 2011). Rho proteins are also involved in both EMT and MAT via mediating cellular plasticity, which as outlined earlier are key event in the metastatic cascade of some epithelial tumours (De Wever et al., 2004; Friedl, 2004; Sahai and Marshall, 2003; Wolf et al., 2003).

1.5 Rac-like GTPases

As indicated above the Rho family of small GTPases is further subdivided into five subfamilies with Rac, Rho and Cdc42-like subfamilies being the most studied among small Rho GTPases. The Rac-like subfamily is of particular importance, as its member Rac1 has been shown to play a major role in tumour initiation and progression *in vivo*. It has been implicated in cytoskeleton reorganization, cell-cell adhesions, migration and invasion, as well as the regulation of cell cycle progression and proliferation (Boureux et al., 2007; Jaffe and Hall, 2005; Malliri and Collard, 2003).

1.5.1 Rac-like GTPases Subfamily Overview

Based on sequence homology, the Rac subfamily includes 4 Rho proteins: Rac1, Rac2, Rac3 and RhoG, with RhoG having the least sequence homology (Boureux et al., 2007). Despite their very high sequence similarity, the three Rac isoforms have been shown to have non-redundant functions and varying degrees of expression. Rac1, the most studied member of the subfamily, is ubiquitously expressed. Rac2, on the other hand, is found predominantly in cells of hematopoietic origin and Rac3 is abundant in the brain. Similar to Rac1, RhoG is also widely expressed yet with varying levels depending on the cell type (Bolis et al., 2003; Haataja et al., 1997; Shirsat et al., 1990; Vincent et al., 1992). The non-redundancy of members in this family is clearly demonstrated by the spectrum of defects observed in knockout mice. For example, Rac1 knockout mice in addition to being embryonic lethal show a wide range of germ-layer formation defects. Rac2/Rac3/RhoG knockout mice, on the other hand, do not exhibit clear developmental defects, yet they show a range of functional defects that are cell type specific (Heasman and Ridley, 2008).

1.5.1.1 Rac-like GTPases Regulation

Rac GTPases are members of the Rho family of small GTPases and thus also act as molecular switches cycling between an active GTP-bound state and an inactive GDP-bound state. As mentioned earlier, this cycle is regulated by GEFs, GAPs, and GDIs. Additionally, Rac1 levels and activity are controlled in cells through posttranslational modifications, such as phosphorylation, ubiquitylation and SUMOylation as outlined in Figure 1.4 (Bosco et al., 2009; Bustelo et al., 2007; Castillo-Lluva et al., 2013; Castillo-Lluva et al., 2010; Lynch et al., 2006; Visvikis et al., 2008). For example, Rac1 was shown to undergo phosphorylation by Akt on Ser71, which prevents it from binding to GTP while not affecting its intrinsic GTPase activity (Kwon et al., 2000). Posttranslational modification, in the form of isoprenoid C-terminal modifications on Rac-like GTPases, has also been shown to regulate Rac1 subcellular localisation (Bosco et al., 2009). Moreover, Rac1, but not its splice variant Rac1b, is subjected to ubiquitylation on Lys147 via a Jun N-terminal kinase (JNK)-mediated process creating a negative feedback loop in which increased activation of Rac1 is counteracted by increased Rac1 proteasomal degradation

(Visvikis et al., 2008). Rac1 ubiquitylation is also important for induced cellular scattering in response to external stimuli. For example, Lynch et al. demonstrated that increased Rac1 ubiquitylation and subsequent proteasomal degradation occur in response to hepatocyte growth factor (HGF) treatment (Lynch et al., 2006). Similar observations were also observed in our laboratory in which Rac1 ubiquitylation was mediated through Hace1, a recently identified E3 Ubiquitin ligase in response to HGF treatment to promote cellular scattering (Castillo-Lluva et al., 2013). Rac1 ubiquitylation by Hace1 was also reported by different groups (Mettouchi and Lemichez, 2012; Torrino et al., 2011). In contrast to ubiquitylation, the binding of Rac1 to PIAS3, a SUMO E3-ligase and its subsequent SUMOylation in response to HGF treatment was found to enhance the stability of the GTP-bound state of Rac1 thus stimulating lamellipodia formation, cellular migration as well as cellular invasion (Castillo-Lluva et al., 2010).

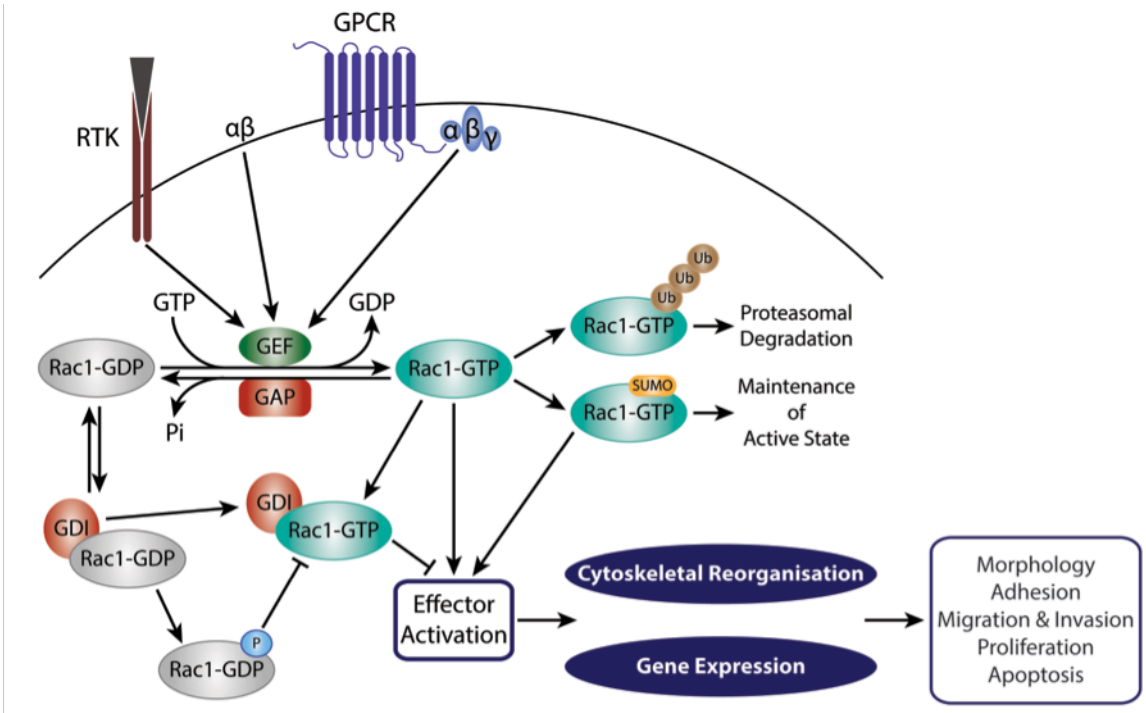

Figure 1.4: Schematic Representation of Rac1 Regulation
Similar to other Rho GTPases, Rac1 cycles between an inactive GDP-bound state and an active GTP-bound state. This cycle is regulated by Guanine Nucleotide Exchange Factors (GEFs), GTPase Activating Proteins (GAPs), and Guanine nucleotide-Dissociation Inhibitors (GDIs). GEFs activate Rac1, in response to upstream signalling, by facilitating the exchange of GDP with GTP. GAPs enhance the intrinsic GTPase activity of Rac1, promoting the hydrolysis of the bound GTP, while GDIs bind to the C-terminus of the GDP-bound protein and prevent its translocation to the membrane where it can be activated by GEFs. GDIs can also bind to the active form of Rac1 and prevent it from binding to downstream effectors. Additionally, Rac1 is regulated by posttranslational modifications. Phosphorylation of Rac1 can impede its ability to bind to GTP; ubiquitylation promotes the degradation of active Rac1, and SUMOylation maintains the activity of Rac1 once bound. Figure was formulated based on literature review outlined in section 1.5.1.1. RTK=Receptor tyrosine kinase; GPCR= G-protein coupled receptor; P=Phosphorylation; Ub=Ubiquitylation; SUMO=SUMOylation.

1.5.2 Rac-like GTPases and Cellular Migration

As described in section 1.2.1, cellular migration can be divided into five main steps: 1) Front-rear cellular polarisation, 2) Membrane extensions, 3) Cell-ECM adhesions, 4) Cellular contraction, 5) Detachment of the cell rear. Evidence from *in vitro* and *in vivo* studies support a role of Rac proteins in a number of these steps. Of particular importance is the role of Rac1 in lamellipodia formation through promoting branched actin polymerisation at the leading edge. Several studies demonstrate that Rac1 regulates the activity of the Arp2/3 protein complex. As a result of Rac1 activation at the leading edge, Rac1 binds to and activates its downstream effector IRSp53. In response, the IRSp53 binds to the WASP-related protein WAVE/Scar through its Src-homologous domain 3 (SH3), which then binds to and activates the Arp2/3 protein complex. Thus Rac1 stimulates the formation of branched actin filaments and lamellipodia formation at the leading edge via activating a signalling cascade that promotes Arp2/3 protein complex nucleating activity (Miki et al., 2000; Takenawa and Miki, 2001). The specificity of Rac1 in regulating this process is clearly demonstrated by Roy et al, where they show that selective inhibition of the Rac1-IRSp53 but not Cdc42-IRSp53 by the ankyrin repeat-containing protein, Kank, hinders lamellipodia formation (Roy et al., 2009). Rac1 activation also regulates cellular migration through mediating cell-ECM adhesions (Price et al., 1998; Rottner et al., 1999). Additionally, Rac1 has also been shown to regulate the expression of various MMPs, which are required for the proteolytic degradation of the ECM. For example, active Rac1 was associated with increased MMP9 expression in chondrocytes and MMP1 in fibroblasts (Jin et al., 2000; Kheradmand et al., 1998). Rac1 can also regulate MMP genes via activating JNK, which via phosphorylation activates the transcription factor Jun, a component of the AP-1 transcription factor complex that is known to regulate the transcription of various genes including the MMP genes (Westermarck and Kahari, 1999).

Other Rac isoforms are also important for regulating cellular migration, including Rac2, which is required for the migration of neutrophils (Roberts et al., 1999). Additionally, both Rac1 and Rac3 are required for promoting invasiveness in fibroblasts (Chan et al., 2005). The role played by each of the Rac isoforms is probably dependant on the cell type as well as their relative expression levels (Parri and Chiarugi, 2010).

Similar to other small Rho GTPases, Rac-like GTPases are also implicated in mediating cell-cell contacts. As discussed earlier, depending on the mode of cellular migration adopted, regulation of cell-cell contacts can be an important determinant for mediating cellular migration. A large number of studies were conducted to determine the exact role played by Rac1 in cell-cell contact regulations. In Madin-Darby canine kidney (MDCK) epithelial cells, time-lapse microscopy revealed a spatiotemporal regulation of Rac1 activity during cadherin-mediated cell-cell contact formation. Rac1 was associated with newer cell-cell contacts and was lost in more mature ones. This implicates Rac1 in the early stages of cell-cell contact assembly (Ehrlich et al., 2002). Additional evidence for the role of Rac-like GTPases in cadherin-mediated

cell-cell contacts stems from colocalisation studies, in which Rac1 was found to colocalise with the calcium dependent adhesion molecule, E-cadherin at adherence junctions in epithelial cells. Interestingly Rac1 cytoplasmic translocation was observed during cell-cell contact disassembly upon depletion of calcium using a chelating agent. Re-addition of calcium to the cells allowed the restoration of E-cadherin-mediated cell-cell contacts while inducing the relocalisation of Rac1 back to cell-cell contacts. Additionally, formation of cell-cell contacts was associated with an increase in levels of active Rac1 that were E-cadherin dependent (Nakagawa et al., 2001). Betson et al. also reported similar observations in keratinocytes, in which Rac1 activation was stimulated upon formation of E-cadherin based cell-cell contacts through epidermal growth factor receptor (EGFR) signalling. More importantly, despite disrupting the actin network associated with antibody-clustered cadherins, Rac1 was still partially activated suggesting that actin polymerisation during cell-cell contact formation is not essential for Rac1 activation at the initial stages (Betson et al., 2002). A more direct involvement of Rac1 in mediating cadherin-dependent cell-cell contacts was demonstrated by Hordijk et al, in which expression of constitutively active Rac1 restored the epithelial morphology of Ras transformed fibroblastoid MDCKII (MDCK-f3) cells via enhancing the formation of E-cadherin based cell junctions (Hordijk et al., 1997). Additionally, the LIM domain protein, Ajuba was found to maintain the stability of E-cadherin-dependent junctions through modulating Rac1 dynamics depending on its p21 activated kinase 1 (PAK)-mediated phosphorylation status (Nola et al., 2011). Interestingly, the metastasis suppressor-1 (Mtss1) was also reported to regulate E-cadherin cell-cell adhesion stability through Rac1. Ectopic expression of Mtss1 resulted in reduced HGF-induced cellular scattering through promoting stronger cell-cell contacts. Additionally, Mtss1 expression was also associated with elevated levels of active Rac1 only in confluent monolayers, suggesting a dependency of cell-cell contact formation for Rac activation to occur (Dawson et al., 2012).

In contrast to the above, a number of studies have suggested that Rac1 can also impede E-cadherin dependent cell junctions. For example, in PANC1 cells ectopic expression of constitutively active Rac1 is associated with reduced levels of E-cadherin. Consistently, expression of dominant negative Rac1 increases E-cadherin levels in the cells (Hage et al., 2009). In support of the negative role of Rac1 in cell-cell contact regulation, Rac1 was reported to promote junction disassembly through its downstream effector Armus that acts as a GAP for the Ras superfamily GTPase Rab7 (Frasa et al., 2010). In a separate study comparing the role of different Rac-like GTPases in regulating cell-cell contacts, both Rac1 and Rac3 were found to induce junction disassembly. In contrast Rac1b, a splice variant of Rac1 was incapable of disrupting cell-cell contacts. Further functional analysis revealed that the downstream effector PAK1 is required for Rac1-mediated junction disassembly, potentially explaining the inability of Rac1b to promote cell-cell disruptions, as it is unable to activate PAK1 (Lozano et al., 2008).

Taken together evidence presented thus far demonstrates that, Rac-like GTPases, mainly Rac1, have been implicated in both the assembly and disassembly of E-cadherin-mediated cell junctions. Depending on the mode of migration, the dual role in regulating cell-cell contacts in addition to their role as regulators of actin structures required for proper cellular migration suggest both an inhibitory and stimulatory function of Rac1 in cellular migration and cancer metastasis. This controversy is particularly evident from experiments conducted by Hordijk et al. and Ridley et al. Using MDCKII cells, Hordijk et al. showed that overexpression of Tiam1, a Rac1-specific GEF, or constitutively active Rac1, inhibited HGF-induced cellular scattering through increased E-cadherin-mediated cell-cell adhesions (Hordijk et al., 1997). In sharp contrast, Ridley et al. demonstrated the requirement of Rac1 for MDCKII cellular motility by using a dominant negative mutant of Rac1. Indeed expression of dominant negative Rac1 impeded cellular migration via reducing the formation of membrane ruffles and lamellipodia normally associated with HGF treatment (Ridley et al., 1995). These two experiments highlight the complexity of cellular migration regulation by Rac1. As a consequence of this dual role, understanding the proper function of Rac1 in cancer progression, particularly in metastasis, is hindered. The next section focuses on the role of Rac-like GTPases in cancer while highlighting examples from the literature supporting both Rac1 migratory roles in cancer cellular migration.

1.5.3 Rac-like GTPases and Cancer

As highlighted in Table 1.1, Rac-like GTPases are deregulated in a variety of tumours (Gomez del Pulgar et al., 2005; Parri and Chiarugi, 2010). For example, Rac1 overexpression has been implicated in the progression of gastric, testicular and breast cancer as well as in tumour initiation (Kamai et al., 2004; Pan et al., 2004; Schnelzer et al., 2000). Khosravi et al. demonstrated the requirement of Rac1 for full oncogenic Ras transformation in NIH3T3 cells using *in vitro* transforming assays (Khosravi-Far et al., 1995). Additionally, Kissil et al. showed the requirement of Rac1 for K-Ras-mediated proliferation and transformation in a conditional lung cancer mouse model (Kissil et al., 2007). Similar findings were outlined, where mice lacking Tiam1 had fewer, yet more aggressive tumours upon the application of a two-stage skin carcinogenesis protocol. This study not only implicated Rac1 in Ras transformation, but also highlighted that Tiam1 activation of Rac1, while promoting proliferation, inhibits tumour cell spreading (Malliri et al., 2002). Consistent with the pro-migratory role of Rac1, expression of constitutively active Rac1 has been shown to stimulate cellular migration in T47D mammary carcinoma cells as well as mediating the loss of cell junctions thus promoting cellular invasiveness (Keely et al., 1997; Sander et al., 1998). Another mode by which Rac1 can promote cellular invasiveness is via regulating MMPs and their inhibitors (TIMPs) production (Lozano et al., 2003). In contrast, as indicated earlier, Mtss1 stabilises E-cadherin-dependent cell-cell adhesions in a Rac1-dependent manner. Mtss1 is commonly lost in a number of cancers and it

has been proposed that its loss might contribute to increased cancer metastasis through the loss of the Rac1-mediated stabilisation of cell-cell contacts (Dawson et al., 2012).

Overexpression of the other Rac-like GTPases Rac2 and Rac3 has also been reported in various tumours. For example, *in vivo* studies utilising Rac3 knockout mice demonstrated that Rac3 is required for the development of Bcr/Abl-induced lymphomas (Cho et al., 2005). In addition, Rac1b is upregulated in colon cancer (Jordan et al., 1999).

1.5.4 Rac-like GTPases Downstream Specificity

As can be seen from the previous sections, Rac proteins are involved in a variety of cellular processes and in some cases the same protein can stimulate opposing cellular responses. There are various factors that might influence Rac protein downstream specificity. The first and most obvious factor is the activation profile of the GTPase, which is mediated via the actions of GEFs and GAPs as discussed earlier. Also, subcellular localisation plays a major role in downstream specificity of Rac proteins. Differential localisation of Rac proteins is mainly mediated via C-terminus lipid modifications. In addition, GDIs play a role in cellular localisation by sequestering Rac proteins in the cytoplasm through C-terminus binding (Bosco et al., 2009; Etienne-Manneville and Hall, 2002; Pechlivanis and Kuhlmann, 2006). Additionally, factors, such as tissue type, cellular substrate and external stimuli have been shown to differentially regulate the outcome downstream of Rac-like GTPases (Etienne-Manneville and Hall, 2002; Sander et al., 1998).

1.5.4.1 Role of GEFs in Rac-like GTPases Downstream Specificity

As highlighted earlier a large number of GEFs have been identified and shown to regulate the activity of small Rho GTPases. Various Rac GEFs have been identified to date and include the Dbl GEFs Asef, α-PIX, β-PIX, STEF, Tiam1, P-Rex1, P-Rex2, Vav1 and Vav2. Among these GEFs only STEF, Tiam1, P-Rex1 and P-Rex2 are Rac specific (Rossman et al., 2005).

In addition to their role as Rac activators, GEFs are thought to influence signalling events downstream of GTPases. For example, Zhou et al. demonstrated that co-expression of Tiam1 with Rac1 or Cdc42 results in increased activation of PAK1, while inducing a modest activation of JNK. In contrast, expression of another GEF, GFKG1 together with Rac1 or Cdc42 was associated with activation of JNK without enhancing PAK1 activation (Zhou et al., 1998). This was also shown in *Saccharomyces cerevisiae* (*S. cerevisiae)*, where Rom2 and Tus1 activation of the RhoA orthologue, Rho1, resulted in stimulation of selectively different pathways (Krause et al., 2012). Taken together, this suggests that GEFs can influence GTPase cellular effects via selective activation of signalling cascades.

Despite the evidence supporting the involvement of GEFs in regulating GTPase downstream signalling, little is known about the underlying mechanism. However, there is accumulating evidence from the literature suggesting that GEFs can serve as scaffolding

proteins and thereby modulate the binding of GTPases to different effectors, influencing differential downstream effects as a consequence. For example, Buchsbaum et al. demonstrate the ability of the Rac1 GEFs, Tiam1 and Ras-GRF1, to influence Rac1 signalling through serving as scaffolding proteins. They show that both GEFs through binding to the scaffolding protein IB2/JIP2 facilitate the interaction between Rac1 and its downstream effector MLK3, which also associates with IB2/JIP2. Thus through this scaffolding complex Tiam1 and Ras-GRF1 are able to selectively drive Rac1-mediated activation of MLK3, which triggers the MKK3 and P38 signalling cascade over the JNK signalling cascade (Buchsbaum et al., 2002). In another study, Buchsbaum et al. also show that Tiam1, through its PHn-CC-Ex domain, can bind to another scaffolding protein, Spinophilin. Interestingly, Tiam1 binding to Spinophilin helps localise Tiam1 at the cell membrane. Additionally, through the ability of Spinophilin to bind to the Rac1 effector p70 S6 kinase, Tiam1 binding to Spinophilin stimulates the Rac1 induced activation of p70 S6 kinase. They also found that expression of Spinophilin in Cos7 cells suppresses the Tiam1-Rac1-driven activation of PAK1 while stimulating the activation of p70 S6 kinase (Buchsbaum et al., 2003). These studies highlight the ability of GEFs to bind to scaffolding proteins to allow the formation of protein complexes that involve the activated GTPase and thus influence the outcome downstream of this GTPase.

In addition to binding to scaffolding proteins, GEFs have also been reported to associate directly with GTPase effectors. For example, Tiam1 was shown to bind directly to the Rac1 downstream effector IRSp53 and enhancing the interaction between Rac1 and IRSp53 and WAVE2-IRSp53 (Connolly et al., 2005). IRSp53 has previously been reported to provide a link between Rac1 and WAVE2 thus allowing the polymerisation of actin and the formation of lamellipodia (Miki et al., 2000; Takenawa and Miki, 2001). Interestingly, Tiam1 expression stimulates the localisation of IRSp53 at Rac1-mediated lamellipodia suggesting that Tiam1 modulates Rac1 binding to IRSp53 and WAVE2 thereby directly influencing Rac1-driven actin polymerisation and the formation of lamellipodia (Connolly et al., 2005). It has also been demonstrated that GEFs can bind to different GTPase effectors in response to different upstream signalling. This was clearly demonstrated by Rajagopal et al. where they show that activation of Tiam1 by pervanadate or PDGF results in an increased association between Tiam1 and IRSp53. As outlined earlier, this interaction is important in promoting Rac1-IRSp53-WAVE2 actin polymerisation. In contrast, stimulation of cells with forskolin or epinephrine enhanced the Tiam1-Spinophilin interaction (Rajagopal et al., 2010). This highlights the ability of GEFs to translate extracellular signals to activate specific GTPase downstream cascades. Examples of other GEFs that have been reported to bind to Rac1 downstream effectors include members of the PIX family of GEFs, which through their SH3 domain, bind to PAKs (Manser et al., 1998).

Together these reports suggest that GEFs, via serving as scaffolding proteins, can modulate Rac1 downstream signalling. It is important to note, however, that in spite of this evidence it is hard to assess the extent by which GEFs actually influence the downstream

specificity of Rac proteins. A study directly comparing the Rac1-mediated cellular response upon activation with different GEFs under the same cellular conditions is required to determine the significance of GEFs in dictating Rac downstream specificity. The next section highlights some evidence from the literature shedding light on the role played by Tiam1 and P-Rex1 in influencing Rac1 downstream specificity.

1.6 Role of Tiam1 and P-Rex1 in Dictating Rac1 Downstream Signalling Effects

Among the GEFs that are specific to members of the Rac subfamily, various reports show that depending on the cellular context activation of Rac1 by Tiam1 or P-Rex1 can lead to opposing Rac1 downstream effects. The next section highlights evidence from the literature shedding light on the role played by Tiam1 and P-Rex1 in influencing Rac1 downstream cellular outcomes, particularly cellular migration and invasion.

1.6.1 T-Cell Lymphoma Invasion and Metastasis 1 (Tiam1)

Tiam1 was first identified through a retroviral mutagenesis screen identifying proteins associated with an increased invasive phenotype in murine T-lymphoma cells. Tiam1 is a widely expressed highly conserved multi-domain protein that consists of 1591 amino acids and a molecular weight of ≈200kDa (Habets et al., 1995). Similar to other Dbl-like GEF family members, Tiam1 contains the DH domain and a pleckstrin homology domain (PHc) that mediate Rac1 binding and its subsequent activation (Worthylake et al., 2000). Tolias et al. demonstrated the importance of the DH-PH of Tiam1 for Rac1 activation through introducing two point mutations in the DH domain (Q1191A and K1195A), which were sufficient to abolish the activation of Rac1 in dendritic cells (Tolias et al., 2005). In addition to the DH-PH domain, Tiam1 contains another PH domain at the N-terminus (PHn) followed by a coiled coil region (CC). Functional analysis of the different domains of Tiam1 showed that the PHn domain together with the adjacent CC domain and its flanking region (Ex), known collectively as the PHn-CC-Ex domain, are responsible for localising Tiam1 to the plasma membrane and thus allowing it to activate Rac1 and induce membrane ruffles in fibroblasts (Stam et al., 1997). Tiam1 has also been shown to act downstream of Ras, where a direct interaction between Tiam1 and Ras through the Ras binding domain (RBD) allows Tiam1 to activate Rac1 in response to Ras upstream signalling (Lambert et al., 2002). Other domains identified in Tiam1, include a myristoylation site, a PDZ domain and two N-terminal PEST domains that are believed to regulate the turnover of Tiam1 by targeting it for degradation (Mertens et al., 2003; Rechsteiner, 1990).

1.6.1.1 Tiam1-Rac1 Signalling and Cellular Migration and Invasion

The role of Tiam1-Rac1 signalling in cellular migration and cancer cell invasion is highly controversial with some reports suggesting an inhibitory role, while others implicating Tiam1 in promotion of migration.

As mentioned earlier, the initial discovery of Tiam1 was through a mutagenesis screen, in which Tiam1 was identified as an inducer of murine T-lymphoma cellular invasion. It was thus named T-cell lymphoma invasion and metastasis 1 (Tiam1) as an indication of its pro-invasion properties (Habets et al., 1995). Following its discovery, there were various reports implicating Tiam1 in promoting cellular migration and invasion in both normal and cancer cells. For example, Tiam1 expression was found to induce both the migration and the neurite outgrowth in neuronal cells (Ehler et al., 1997). Moreover, Minard et al. showed that there was a four to five-fold increase in the levels of Tiam1 in a highly migratory SW480 human colorectal carcinoma subline derived from the parental cell line. The importance of Tiam1 in promoting the migratory potential in these cells was further confirmed by expressing Tiam1 in the parental SW480 cell line, which resulted in increased migration similar to that seen in the highly migratory derived subline (Minard et al., 2005). The pro-migration and pro-invasion properties of Tiam1 were also observed in the human colon adenocarcinoma cell lines Caco-2 and HCT116, where Tiam1 was implicated in the Syndecan-2-mediated cellular migration and invasion in these cells (Choi et al., 2010). Similarly, increased expression of Tiam1 in breast cancer cell lines, including SP-1 cells, induced their migratory and invasive potential (Bourguignon et al., 2000; Minard et al., 2004). On the other hand, downregulation of Tiam1 in human giant-cell lung carcinoma cells has been associated with decreased levels of *in vitro* invasion (Hou et al., 2004). These pro-migration and pro-invasion Tiam1 properties are believed to be through its ability to activate Rac1. Tiam1-Rac1 signalling has been directly shown to play a role in the invasion of T-lymphoma cells, where the expression of Tiam1 or a constitutively active form of Rac1 increase invasion in these cells (Michiels et al., 1995).

In contrast to the above, a number of reports clearly demonstrate the role of Tiam1-Rac1 signalling in suppressing the migration and invasion of normal and cancer cells. For example, Hordijk et al. demonstrated that the ectopic expression of C1199 Tiam1, a more active truncated form of Tiam1, in MDCKII cells enhanced and maintained E-cadherin-mediated cell-cell adhesion thus reducing cellular motility in response to HGF treatment (Hordijk et al., 1997). Similar effects were also reported in the renal cell carcinoma cell line ClearCa-28, where expression of Tiam1 or constitutively active Rac1 inhibited cellular migration via enhancing E-cadherin-mediated cell-cell contacts. Moreover, invasion of these cells through a matrigel layer, although not influenced by the E-cadherin-mediated cell-cell contacts, was reduced due to a Tiam1-Rac1-mediated upregulation of the tissue inhibitor of metalloproteinases-1 (TIMP-1) and -2 (TIMP-2) whilst not affecting the secreted levels or activity of MMP-9 or MMP-2 (Engers et al., 2001). Consistent with the above, Tiam1 overexpression in metastatic melanoma cells reverted

their mesenchymal phenotype into an epithelial-like morphology through promoting the formation of activated leukocyte cell adhesion molecule (ALCAM) receptor-mediated cell-cell contacts (Uhlenbrock et al., 2004). Work from our laboratory also highlights the antagonising role of Tiam1-Rac1 signalling in HGF-mediated cell scattering in various cell lines where proteasomal degradation of Tiam1 is essential in order for efficient cellular scattering (Vaughan et al., 2015). The loss of Tiam1 *in vitro* and *in vivo* has also been shown to increase cellular migration and invasion. Malliri et al. demonstrated that Tiam1 knockdown in MDCKII cells correlates with an increased rate of cellular migration. Moreover, further analysis revealed that E1A acts through Tiam1 and Rac1 signalling cascades to promote an epithelial-like morphology in primary mouse embryonic fibroblasts via enhancing cadherin-mediated cell-cell contacts (Malliri et al., 2004). Additional evidence from studies conducted on Tiam1 deficient mice show that although Tiam1 is required for the initiation of Ras-induced skin tumours, the few tumours formed in the Tiam1 deficient mice were more malignant indicating that Tiam1, while promoting tumour cell proliferation, inhibit migration and metastasis (Malliri et al., 2002). Similarly, Tiam1 deficiency in APC mutant multiple intestinal neoplasia (Min) mice reduced the polyp growth while enhancing the migration and invasion of the intestinal tumours formed when compared to mice expressing Tiam1 (Malliri et al., 2006).

As outlined above, there are conflicting reports regarding the role of Tiam1-Rac1 signalling in cellular migration and invasion. This is mainly due to the fact that Tiam1 activation of Rac1 regulates both actin cytoskeleton rearrangements as well as cell-cell and cell-matrix adhesions. It is has thus been proposed that these controversial roles of Tiam1-Rac1 signalling are cell type and substrate specific (Etienne-Manneville and Hall, 2002; Sander et al., 1998) .A clear example of such discrepancy in Tiam1-Rac1 signalling downstream outcomes is evident in the ability of Tiam1, through Rac1, to enhance E-cadherin-mediated cell-cell contacts when Ras transformed MDCK-f3 cells were plated on fibronectin or laminin. On the other hand, expression of Tiam1 or constitutively active Rac1 in MDCK-f3 cells plated on different types of collagen induced membrane ruffling and the formation of lamellipodia thus promoting migration (Sander et al., 1998). The role of Tiam1-Rac1 signalling in regulating cellular migration and invasion is therefore context dependent (Etienne-Manneville and Hall, 2002; Sander et al., 1998).

1.6.2 Phosphatidylinositol-3, 4, 5-Trisphosphate-dependent Rac Exchange Factor 1 (P-Rex1)

Relative to Tiam1, the discovery of P-Rex1 is fairly recent. It was isolated from the cytosol of neutrophils as a 1659 amino acid long protein with a molecular weight of ≈185kDa. Similar to other Dbl-like GEF family members, P-Rex1 was shown to possess the characteristic DH-PH domain at its N-terminus (Welch et al., 2002). Like Tiam1, two point mutations in the DH domain of P-Rex1 (E56A; N238A) are sufficient to abolish Rac1 activation (Nie et al., 2010).

Moreover, through *in vitro* analysis of its GEF activity, P-Rex1 was identified as a PtdIns(3,4,5)P-sensitive Rac-GEF. *In vitro,* P-Rex1 exhibited specificity towards Rac1, Rac2, Cdc42 and to a lesser extent RhoA in their lipid modified state; however Rac1 activation was not dependent on Rac1 being modified. *In vivo* analysis of P-Rex1 GEF activity, however, demonstrated that expression of P-Rex1 results in increased levels of active Rac1 but not Cdc42 conferring Rac1 specificity (Welch et al., 2002). More recently, P-Rex1 has also been shown to activate RhoG, another member of the Rac subfamily of small GTPases; however the induced downstream effects are still mediated through the indirect activation of Rac1 by RhoG, highlighting the importance of Rac1 in P-Rex1 signalling (Damoulakis et al., 2014). In addition to the DH-PH domain, P-Rex1 has two DEP domains. These domains facilitate the activation of P-Rex1 by the Gβγ subunits of heterotrimeric G-proteins thereby linking Rac1 signalling to G-protein coupled receptors (GPCRs) signalling. Other P-Rex1 domains are outlined in Figure 3.1 B and include two PDZ domains and a C-terminal region with high sequence homology to inositol polyphosphate 4-phosphatase; however no activity has been associated with this domain (Welch et al., 2002).

1.6.2.1 P-Rex1-Rac1 Signalling and Cellular Migration and Invasion

Unlike Tiam1, the role of P-Rex1-Rac1 signalling in cellular migration and invasion is highly consistent, with the majority of reports implicating P-Rex1 in increased cellular migration. Amongst the first indications of the involvement of P-Rex1 in promoting cellular migration was the finding that expression of dominant negative P-Rex1 impedes neuronal migration in mouse foetal cerebral cortex (Dong et al., 2005; Welch et al., 2005; Yoshizawa et al., 2005). It has also been shown that P-Rex1 is upregulated in cell lines derived from invasive tumours, including human melanoma-derived cell lines as well as invasive telomere-immortalised human fibroblasts (Scott et al., 2004). Together, these observations highlight a role of P-Rex1 in regulating cellular migration and cancer metastases. Further studies also support the pro-migratory and pro-metastases role of P-Rex1 *in vitro* and *in vivo*. For example, Campbell et al. clearly demonstrate the role of P-Rex1-Rac1 signalling in driving cellular migration in an immortalised primary human fibroblast cell line. They also highlight that the migration potential induced by P-Rex1 expression is enhanced upon co-expression of functional PDGF receptor beta (PDFRβ). Consistent with these observations, knockdown of P-Rex1 or PDGFRβ in the melanoma cell line WM852 impedes invasion in these cells (Campbell et al., 2013). Moreover, *in vivo* studies show that mice deficient in P-Rex1 have a decreased rate of melanoblast migration. Consistently, these mice when crossed to a murine model of melanoma exhibit reduced metastasis implicating P-Rex1-Rac1 signalling in promoting cellular migration and cancer cell invasion (Lindsay et al., 2011). Additional evidence supporting the positive role of P-Rex1-Rac1 signalling in cancer cell invasion includes a study by Qin et al. highlighting that increased levels of activated P-Rex1 downstream of receptor tyrosine kinase or G-protein coupled receptor signalling correlates with increased metastatic potential in a panel of

prostate cancer cell lines and in specimens of human prostate cancer. Additionally Qin et al. show that knockdown of endogenous P-Rex1 in the prostate cancer cell line PC-3 is associated with a reduction in the migration and invasion potential in these cells. On the other hand, expression of P-Rex1 wild type (WT) but not P-Rex1 GEF-dead mutant (GEF*) in the prostate cancer cell line, CWR22RV1, promotes prostate cancer migration and invasion both *in vitro* and in a mouse xenograft model (Qin et al., 2009). P-Rex1 is also implicated in promoting Rac1-driven cellular proliferation and migration mediated by the ErbB receptor (Sosa et al., 2010). Taken together, the above evidence demonstrates that P-Rex1-Rac1 signalling is predominantly associated with increased migration and invasion and relies to a lesser extent on the cellular context.

1.6.3 Limitations in Understanding Differential Rac1 Signalling

As evident from the role of Tiam1-Rac1 signalling in cellular migration and invasion, cellular context plays a crucial role in determining Rac1 downstream effects. However, despite the controversial role of Tiam1-Rac1 signalling in cellular migration and invasion, it is intriguing that Tiam1 and P-Rex1, two Rac1 specific GEFs that belong to the same GEF family, are capable of influencing Rac1 to promote distinct cellular outcomes. It could be, therefore argued that under the same cellular conditions, the role of GEFs in mediating differential Rac1 downstream effects could be more significant. If true, understanding this extra level of regulation is crucial as it could mark an additional checkpoint by which Rac1 downstream signalling pathways are selectively directed depending on its activating GEF. Additionally it will help pinpoint signalling cascades that are directly downstream of Rac1, rather than a collective signalling network instigated by extracellular signalling.

As highlighted earlier there is accumulating evidence from the literature supporting an additional GEF regulatory role in GTPase signalling. However, in the studies conducted other cellular factors that contribute to differential Rac1 signalling have not been controlled and thus it is hard to accurately determine the exact role played by GEFs in these settings. For example changes in the activation signals upstream of GEFs can have a huge influence on how they will regulate the signalling downstream of a given GTPase. This is clearly demonstrated in the previously described study conducted by Rajagopal et al. in which Tiam1 was shown to associate with two different Rac1 effectors upon activation with different upstream signals, suggesting that upstream activation of GEFs can influence their scaffolding role and thus any potential differentially regulated GTPase downstream effects (Rajagopal et al., 2010). Therefore, while these studies provide evidence of the scaffolding role of GEFs they fail to address the exact role played by GEFs in mediating GTPase signalling. Given that the focus of this work was to understand and identify factors involved in regulating Rac1 downstream signalling with an emphasis on cellular migration, exploring the potential role of GEFs in regulating Rac1 signalling, thus presents an opportunity that might shed light at the complex role of Rac1 in

modulating cellular migration and cancer metastasis. The next section will give an overview of the project, its description, objectives and working framework or hypothesis.

1.7 Project Description

As highlighted from the literature review presented above, Rho GTPases play a central role in regulating cellular migration in normal and cancer cells. Rac1 is of particular importance as it has been shown to be involved in all stages of carcinogenesis and is deregulated in a number of cancers. Of particular interest is its role in mediating cellular migration and invasion. As outlined, through its ability to promote lamellipodia formation, mediate focal complex assembly and enhance the expression and release of MMPs, Rac1 is considered a potent stimulator of cellular migration and invasion. On the other hand, Rac1 has been shown to contribute to both the assembly and disassembly of cadherin-mediated cell-cell adhesions and thus has also been implicated in reduced cellular motility in both normal and cancer cells. Given this complexity, understanding how Rac1 is regulated is key to deciphering the exact role it plays in tumour progression, which in turn might shed light onto novel ways to tackling cancer metastasis.

Evidence from the literature also supports a role of GEFs in mediating GTPase activity. Interestingly, Tiam1 and P-Rex1 have been demonstrated to inhibit and induce cellular migration through Rac1, respectively. Despite the controversial role of Tiam1-Rac1 signalling reported under certain cellular conditions, the contradictory Rac1-mediated cellular migration patterns seen with Tiam1 and P-Rex1 together with the reported role of GEFs in influencing GTPase downstream signalling suggest that under the same cellular conditions Tiam1 and P-Rex1 could potentially specifically dictate Rac1 downstream signalling thus adding an extra level of Rac1 regulation, which could explain its dual role in cellular migration and invasion. Given the above a project was designed to gain a better understanding of the role played by GEFs, namely Tiam1 and P-Rex1 in influencing Rac1 downstream signalling under the same cellular conditions.

1.8 Project Hypothesis:

Evidence from the literature regarding the role of Rac1 and its GEFs, Tiam1 and P-Rex1 in cellular migration together with the proposed scaffolding role of GEFs served as a backbone for the working hypothesis governing this work stating the following:

"Activation of Rac1 by a particular GEF influences its downstream biological outcome."

1.9 Project Aims:

The first aim of the project was to examine whether activation of Rac1 by Tiam1 or P-Rex1 could influence the cellular outcome downstream of Rac1. In order to control for other cellular factors, such as cell type and signalling from the ECM, an inducible GEF expression system was designed to selectively activate Tiam1-Rac1 or P-Rex1-Rac1 signalling cascades. Additionally, to exclude effects that are due to GEF overexpression and not Rac1 activation, GEF-dead mutants (GEF*) were also utilised.

Following the analysis of the GEF-induced phenotypes, the second aim entailed understanding the mechanism by which Tiam1 and P-Rex1 might be influencing Rac1 signalling. This was addressed by performing a quantitative proteomic screen of Rac1 binding partners upon activation by either GEF in order to determine whether Tiam1/P-Rex1 can influence the Rac1 interactome.

Finally, the screen was followed by further validation of identified Rac1 binding partners under the different activating conditions to decipher Tiam1 and P-Rex1-driven signalling cascades downstream of Rac1 that might be involved in regulating cellular migration. This was conducted through the use of a number of biochemical, molecular and cell biology techniques to further study the interactions between Rac1 and its GEF-induced binding partners.

Chapter 2 : Materials and Methods

2.1 Buffers and Solutions

1X MOPS SDS running buffer	1X MOPS SDS running buffer (Life Technologies, NP0001) in dH_2O
1X NuPAGE® transfer buffer	5% 20X NuPAGE® transfer buffer, 10 % methanol in dH_2O
1X Tris-Acetate SDS running buffer	5% 20X Tris-Acetate SDS running buffer (Life Technologies, LA0041) in dH_2O
1X Tris-acetate-EDTA (TAE) buffer	40 mM Tris, 20 mM acetic acid, 1 mM EDTA
2X SDS-PAGE sample buffer	50 % NuPAGE® LDS sample buffer 4X (Life Technologies, NP0008) (v/v), 20 % NuPAGE® sample reducing agent 10X (Life Technologies, NP0004) (v/v) in dH_2O
Cell fixing buffer	4 % formaldehyde in PBS -/-
Cell freezing media	50 % FBS (v/v), 10 % DMSO (v/v), 40 % culture media (v/v)[1]
Cell permeabilisation buffer	0.5 % Triton-X (v/v) in PBS-/-
GST-FISH buffer	10 % glycerol (v/v), 50 mM Tris-HCl pH 7.4, 100 mM NaCl, 1% Nonidet P40 (v/v), 2 mM $MgCl_2$, 1 EDTA-free protease inhibitors tablet (Roche, 11873580001)[2] in dH_2O
Immunofluorescence blocking buffer	1 % BSA (w/v) in PBS-/-
Immunofluorescence fixing buffer	4 % formaldehyde (v/v) in PBS -/-
Immunoprecipitation (IP) lysis buffer	50 mM Tris-HCL pH 7.5, 150 mM NaCl, 1 % Triton-X-100 (v/v), 10 % glycerol (v/v), 2 mM EDTA, 25 mM NaF, 2 mM NaH_2PO_4, 1 % protease inhibitor cocktail (Sigma-Aldrich, P8340) (v/v), 1 % phosphatase inhibitor cocktails 1 and 2 (Sigma-Aldrich, P5726, P0044) (v/v)[3] in dH_2O
IP binding buffer	10 mM Na_3PO_4, 150 mM NaCl, 10 mM EDTA pH 7.0
NativePAGE™ anode buffer	5 % 20X NativePAGE™ running buffer (Life Technologies, BN2001) in dH_2O
NativePAGE™ dark blue cathode buffer	5 % 20X NativePAGE™ running buffer, 5 % 20X NativePAGE™ cathode additive (Life

	Technologies, BN2002) in dH_2O
NativePAGE™ light blue cathode buffer	5 % 20X NativePAGE™ running buffer, 0.5 % 20X NativePAGE™ cathode additive in dH_2O
Non-denaturing lysis buffer	50 mM Bis-Tris pH 7.4, 50 mM NaCl, 1mM EDTA in dH_2O
PBS +/+	0.5 mM $MgCl_2$, 1 mM $CaCl_2$ in PBS -/-
PBS-Tween (PBST)	0.1% Tween (v/v) in PBS -/-
Phosphate-buffered saline (PBS) -/-	137 mM NaCl, 2.7 mM KCl, 10 mM Na_2PO_4, 2 mM KH_2PO_4 in dH_2O
SF-TAP FLAG® elution buffer	4 % FLAG® peptide stock solution (v/v) in TBS
SF-TAP FLAG® peptide stock solution	4 mg 3x FLAG® peptide (Sigma-Aldrich, F4799) in 800 µl TBS
SF-TAP lysis buffer[4]	0.5 % Nonidet P40 (v/v), 1 % protease inhibitor cocktail (v/v), 1 % phosphatase inhibitor cocktails 1 and 2 (v/v) in TBS
SF-TAP *Strep*-Tactin® elution buffer	2.5 mM d-desthiobiotin (Sigma-Aldrich, D1411) in dH_2O
SF-TAP wash buffer[4]	0.5 % Nonidet P40 (v/v), 1 % phosphatase inhibitor cocktails 1 and 2 (v/v) in TBS
TBS-Tween (TBST)	0.1 % Tween (v/v) in TBS
Tris-buffered saline (TBS)	30 mM Tris pH 7.4[5], 150mM NaCl in dH_2O
Western blot blocking buffer 1	5 % non-fat milk powder (w/v) in PBST or TBST
Western blot blocking buffer 2	5 % BSA (w/v) in TBST
Western blot stripping buffer	0.2 M Glycine, 1 % SDS (v/v), pH 2.5[5] in dH_2O

[1] The culture media added was adjusted according to the cell line used (see section 2.2.1)
[2] EDTA-free protease inhibitor tablet was added fresh before use
[3] Protease and phosphatase inhibitors were added fresh before use
[4] Buffers prepared fresh before use
[5] pH adjusted using HCl

2.2 Cell Culture Techniques

2.2.1 Cell Maintenance

All cell lines were cultured at 37 ˚C and 5 % CO2. A431, MCF7 and NIH3T3 cell lines were cultured in Dulbecco's Modified Eagle Medium (DMEM 4.5 g/L glucose, Life Technologies, 61965-026) supplemented with tetracycline-free fetal bovine serum (FBS v/v) and 10 µg/ml penicillin-streptomycin (Life Technologies, 15140-122). Primary human fibroblasts were cultured in the same media supplemented with 1% sodium pyruvate (v/v). Low glucose DMEM (1 g/L, Life Technologies, 10567-014) was used for MDCKII and HEK293T cells.

For antibiotic selection, cells harbouring the pRetroX- Tet-On Advanced plasmid only were grown in tetracycline-free DMEM media with 1 mg/ml G418 selection (Sigma-Aldrich, A1720). Cells with both the pRetroX-Tet-On Advanced and pRetroX-Tight-Pur (empty or with indicated inserts) were subjected to selection by addition 1 mg/ml G418+ 2 μg/ml Puromycin (Sigma-Aldrich, P8833).

Upon thawing, cells were subcultured every 2-3 days and seeded at 2.5-5 x 10^5 cells in T-75 flasks depending on cell line. Subculturing was performed by washing cells once with PBS-/- followed by trypsin (Life Technologies, 25200-056)-induced cell detachment. Trypsin was inhibited by addition of equal volume of culturing media. For cell density measurements, 100 μl of trypsinsed cells was added to 10 ml isoton solution and used for cell counting using the Beckman Coulter cell counter. Cells were spun down at 1200 rpm for 5 minutes and resuspended in the appropriate amount of media to obtain required cellular density. No more than ten passages were used for experiments.

2.2.2 Cell Freezing

Cells were frozen down at various stages of cell culture to maintain different passages. For thawing cells were spun down by centrifugation at 1200 rpm for 5 min. Cell pellets were then resuspended in 3 ml cell freezing media and stored at -80 ˚C in three Nalgene® cryogenic vials. Cell vials were transferred to liquid nitrogen tanks if storage exceeded 3 months.

2.2.3 Cell Transfection

2.2.3.1 Expression plasmids

Cells were plated at appropriate density (depending on experimental setup) 24 hours prior to transfection. Using the *Trans*IT®-LT1 reagent (Mirus, MIR 2305) the desired constructs were prepared according to manufacturer's instructions.

2.2.3.2 Small Interfering RNA (siRNA) Reverse Transfection

For the knockdown of mouse protein flightless-1 homolog (FLII) in NIH3T3 cells prior to ORIS™ migration assay, the two FLII siRNA oligonucleotides (Sigma-Aldrich; 20 μM stock) outlined below were prepared using the DharmaFECT™ 1 transfection reagent (GE Healthcare, T-2001-01) according to manufacturers instructions. A total of 2 x 10^5 cells were seeded/ well in a 6-well plate together with appropriate siRNA/transfection reagent mixture. Cells were retransfected after 48 hours in the presence of ethanol or 1 μg/ml dox for an additional 24 hours. DharmaFECT™ 1 reagent alone or together with Dharmacon non-targeting siRNA#4 (GE Healthcare, D-001210-04-20), were also used as additional controls.

FLII siRNA 1 (Mm01_00187916) 5'-CAGAUCAACUACAAGCUCU[dT][dT]-3'

FLII siRNA 2 (Mm01_00187920) 5'-GACUUUGAUGGGCUGCCUU[dT][dT]-3'

Transient silencing of human FLII in primary human fibroblast cells was achieved by reverse transfection (as outlined above) of the siRNA oligonucleotide from Eurofins MWG operon detailed below using Lipofectamine RNAiMAX™ (Life Technologies, 137781) according to manufacturer's instructions.

FLII A siRNA 5'-GCUGGAACACUUGUCUGUG[dT][dT]-3'

2.2.4 Two-Step Retroviral Transduction

2.2.4.1 Retrovirus Production

Phoenix A packaging cells were used for viral production. Cells were seeded at a density of 1 x 10^6 cells/10 cm plate. Cells were left for 24 hours after which 3 µg of the desired retroviral construct was mixed with 3 µg VSVG plasmid and used for transfection using *Trans*IT®-LTI reagent according to manufacturer's instructions. Transfected Phoenix A cells were cultured for 24 hours, after which the supernatant from the respective cells was collected and replaced with new media. The collected supernatant was spun at 1200 rpm for 5 minutes then passed through a 0.45 µm pore size to remove floating cells. Polybrene (Sigma-Aldrich, 107689) was added to the cleared supernatant (10 µg/ml final concentration) used for retrovirus transduction. Following the collection of three supernatant batches, Phoenix A cells were lysed and subjected to Western Blot analysis to assess transfection efficiency.

2.2.4.2 Retrovirus Transduction

Indicated cells were seeded at a density of 3 x 10^5 cells per T-75 culturing flask 24 hours prior to transduction. Cleared supernatant collected from Phoenix A as outlined in section 2.2.4.1 was added to cultured cells following a PBS wash. Transduction was repeated three times with 24 hours intervals using fresh supernatant each time. Upon completion of transduction, a small batch of cells was used for Western blot analysis to check protein expression, while the remainder were maintained in the appropriate selection containing media.

2.3 Molecular Biology Techniques

2.3.1 Restriction digests

Restriction digests were performed using 1 µg of relevant plasmid DNA together 1 µl of indicated restriction enzymes in a total volume of 20 µl using supplied restriction enzyme buffer. Reactions were performed at 37 °C for 60-90 minutes, unless alternative incubation

conditions were required. Alkaline phosphatase (Promega, M1821) (1 µl of a 1:50 dilution) was added for the last 30 minutes of restriction digest of vector backbones.

2.3.2 Polymerase Chain Reaction (PCR) DNA Amplification

PCR amplification was used to amplify unmodified target genes as well as to introduce restriction sites that can then be used for DNA cloning. The required oligonucleotides were designed depending on cloning strategy and were synthesised by Eurofins MWG operon. The PCR amplification was conducted using the *Pfu* DNA polymerase (Thermo Scientific, EP0501) according to manufacturer's instructions. The PCR amplification cycle conditions are outlined in Table 2.1. Run conditions highlighted in red represent the conditions used for DNA fragments around 0.5 kb.

Table 2.1 PCR Running Conditions

Stage	Temperature (°C)	Duration (Minutes)	Number of Cycles
Initial denaturation	95 °C	2 minutes	1 cycle
Denaturation	95 °C	30 seconds/1 minute	25/30 cycles
Annealing	58/60°C	30 seconds	
Extension	74 °C	2 minutes/10 minutes	
Final Extension	74 °C	5 minutes/30 minutes	1 cycle
Soak	12 °C	Forever	N/A

2.3.3 Agarose gel electrophoresis and DNA Extraction

Following restriction digest or PCR amplification, DNA samples were prepared using the 6X Blue/Orange loading dye (Promega, G1881) according to manufacturer's instructions. Samples were resolved using 0.8-1.2 % agarose/TAE gels containing Gel Red nucleic acid stain (1:50000, v/v) to allow visualisation of the DNA by UV at an absorbance of 205 nm. DNA ladders were also run alongside the samples for DNA fragment size evaluation (Promega 100 bp DNA ladder G2101, 1 kb DNA ladder G5711). Gels were run at 100 V for the time required per experiment. Desired DNA bands were cut from agarose gels using a sterilised scalpel. DNA was extracted from each cut band using the QIAquick® gel extraction kit (Qiagen, 28704) following instructions in provided protocol.

2.3.4 Molecular Cloning

For the subcloning of digested DNA fragments or PCR amplification products the pGEM®-T-Easy vector system (Promega, A1360) was used according to manufacturer's instructions as an intermediate vector prior to cloning into the final desired expression vector.

For *Pfu* DNA polymerase blunt-ended PCR amplification products this step was preceded with A-tailing using Go*Taq®* DNA polymerase (Promega, M3001). For A-tailing 5 μl of purified PCR DNA fragment were mixed with 2 μl dATP (1mM stock), 2 μl 5X supplied polymerase buffer and 1 μl of Go*Taq®* DNA polymerase in a final volume of 10 μl. A-tailing was achieved by incubating the mixture for 30 minutes at 70 °C.

2.3.5 DNA Ligation

The T4 DNA ligase (Roche, 10799009001) was used for required vector and insert DNA fragment ligation reactions following manufacture's instructions. Ligation reactions were conducted in a total volume of 10 μl containing 1 μl ligase and left incubating for 3 hours at room temperature or overnight at 16 °C.

2.3.6 Bacterial Transformation and Plasmid DNA Preparation

NEB 10-beta competent *E. coli* (High Efficiency) (50 μl) (Life Technologies, C3019H) were mixed with 3 μl of respective ligation reactions or 0.5 μl plasmid DNA for 30 minutes on ice. Cells were then subjected to a heat shocked by incubating at 42 °C for 40 seconds followed by incubation on ice for 2 minutes. Following heat shock treatment 250 μl of SOC media supplied with competent cells was added to transformed bacterial cells and incubated for 1 hour at 37 °C with agitation. Samples were then split into 50 μl and 200 μl samples that were plated on the appropriate antibiotic-containing agar plates. After 12-18 hours bacterial colonies were selected and placed in 5 ml antibiotic-containing LB, cultured overnight and the plasmid DNA using the mini-prep service at the Molecular Biology Core Facility (MBCF) at CRUKMI. For maxi-prep DNA preparations, the QIAquick® plasmid maxi kit (Qiagen, 12162) was used according to the manufacturer's instructions.

2.3.7 Glycerol Stock Preparation

For long-term storage glycerol stocks of transformed bacteria were generated through spinning down 5 ml of cultured transformed competent cells by centrifugation at 3460 rpm for 5 minutes. Cells were then resuspended in 800 μl 15% glycerol/LB solution (v/v) and stored at -80 °C.

2.3.8 DNA sequencing

The respective plasmid DNA (500 ng) was sequenced using 1 μl of designed or purchased primers in a total volume of 12 μl in dH_2O. Samples were submitted to the in house Molecular Biology Core Facility for analysis.

2.3.9 Determination of DNA concentration

For DNA concentration determination, 1 µl of DNA solution was analysed using the NanoDrop fluorospectrometer (Thermo Scientific, 3300).

2.3.10 Expression Plasmids

Table 2.2 provides a list of all constructs used in this project either directly or as an intermediate plasmid that was used to generate another construct. Additionally the table provides information, if applicable, on how the construct was generated

Table 2.2 List of Expression Plasmids

Construct Label	Vector Backbone	Insert	Supplier/Cloning Strategy
FLAG-FLII-FL	pcDNA3.1	FLAG-FLII full length	Kind gift from the Stallcup group, University of Southern California, USA. Previously described by Lee et al. (Lee et al., 2004)
FLAG-FLII-GEL	pSG5	FLAG-FLII GEL domain	Kind gift from the Stallcup group, University of Southern California, USA. Previously described by Lee et al. (Lee et al., 2004)
FLAG-FLII-LRR	pSG5	FLAG-FLII LRR domain	Kind gift from the Stallcup group, University of Southern California, USA. Previously described by Lee et al. (Lee et al., 2004)
pRetroX-Tiam1 GEF*	pRetroX-Tight-Pur	HA-Tiam1 GEF*	The Malliri group, CRUKMI
pRetroX-Tiam1 WT	pRetroX-Tight-Pur	HA-Tiam1 WT	The Malliri group, CRUKMI
pLHCX-P-Rex1 GEF*	pLHCX	Myc-P-Rex1 GEF*	The Malliri group, CRUKMI, UK
pRetroX-P-Rex1 GEF*	pRetroX-Tight-Pur	Myc-P-Rex1 GEF*	- The nucleotide region encoding the first 3.5 kb of Myc-P-Rex1 GEF* was amplified by PCR while introducing XbaI restriction site using the following primers: Forward primer: Xba1 sequence in bold 5'-acct**tctaga**accatggagcagaagctgatc-3' Reverse primer: 5'-gagtggggataactcatggt-3' - The PCR product was inserted into pGEM®-T-Easy vector after A-tailing - pGEM®-T-Easy-P-Rex1 and pRetroX-P-Rex1

			WT were digested using XbaI and NruI. - Restriction digests were resolved on 0.8 % agarose gel and relevant fragments were extracted and purified prior to ligation - Minipreps were generated and P-Rex1 GEF* mutations were screened by sequencing using the P_{Tight} primer: 5′-ATCTGAGGCCCTTTCGTCTTCACT-3′ - Positive minipreps were used for maxiprep generation followed by HEK293T transfection for protein expression confirmation using Western blot analysis
PLHCX-P-REX1 WT	PLHCX	MYC-P-REX1 WT	The Malliri group, CRUMI, UK
pRetroX-P-Rex1 WT	pRetroX-Tight-Pur	Myc-P-Rex1 WT	- The nucleotide region encoding Myc-P-Rex1 WT was amplified by PCR while introducing XbaI and MluI restriction sites using the following primers: <u>Forward primer</u>: Xba1 sequence in bold 5′-acct**tctaga**accatggagcagaagctgatc-3′ <u>Reverse primer</u>: Mlu1 sequence in bold 5′-acct**acgcgtt**Tcagaggtccccatccsccgg-3′ - The PCR product was inserted into pGEM®-T-Easy vector after A-tailing - pGEM®-T-Easy-P-Rex1 and pRetroX-Tight-Pur were digested using XbaI (introduced) and NruI (internal P-Rex1 site). - Restriction digests were resolved on 0.8 % agarose gel and relevant fragments were extracted and purified prior to ligation - Minipreps were generated and screened by sequencing using the P_{Tight} primer: 5′-ATCTGAGGCCCTTTCGTCTTCACT-3′ - Positive minipreps were used for maxiprep generation - pGEM®-T-Easy-P-Rex1 and pRetroX-P-Rex1 (3.5 kb) were digested using NruI and MluI

			restriction enzymes to introduce the remaining 1.5 kb P-Rex1 C-terminal fragment - Restriction digests were resolved on 0.8 % agarose gel and relevant fragments were extracted and purified prior to ligation - Minipreps were generated and screened by sequencing using the following primers: Forward primers: P_{Tight} 5'-ATCTGAGGCCCTTTCGTCTTCACT-3' P_{MCS} 5'-TCAGATCGCCTGGAGAAGGA-3' Reverse primers: $P_{Rev\ \#12}$ 5'-TCATGTGTGGCACAGGCATG-3' - Positive minipreps were used for maxiprep generation followed by HEK293T transfection for protein expression confirmation using Western blot analysis
pcDNA3-Myc-Rac1 WT	pcDNA3.0	Myc-SF-Rac1 WT	The Malliri goup, CRUKMI, UK
pcDNA4-Myc Tiam1	pcDNA4.0	Myc-Tiam1 WT	The Malliri group, CRUKMI, UK
N-SF-TAP-pcDNA3	pcDNA3.0	N-terminal SF-tag	Kind gift from the Ueffing group, University of Tuebingen, Germany. Previously described in by Gloeckner et al. (Gloeckner et al., 2007).
pRetroX-Tet-On Advanced	N/A	N/A	Clontech, PT3968-5; 632104
pRetroX-Tight-Pur	N/A	N/A	Clontech, PT3960-5; 632104/632105
pcDNA3-SF-Rac1 WT	pcDNA3.0	SF-Rac1 WT	- The nucleotide region encoding Rac1 WT (without the Myc tag) was amplified by PCR while introducing NheI and XbaI restriction sites using the following primers: <u>Forward primer:</u> NheI sequence in bold 5'-T**GCTAGC**CTGCAGGCCATCAA-3' <u>Reverse primer:</u> XbaI sequence in bold 5'-ACTG**TCTAGA**GGATCCTTACAACACAGGCA-3' - The PCR product was inserted into pGEM®-T-

			Easy vector after A-tailing - pGEM®-T-Easy-Rac1 and pRetroX-Tight-Pur were digested using BamHI. - Restriction digests were resolved on 1.2 % agarose gel and relevant fragments were extracted and purified prior to ligation - Minipreps were generated and screened by sequencing using T7 and CMV forward primers and SP6 reverse primer. - Positive minipreps were used for maxiprep generation followed by HEK293T transfection for protein expression confirmation using Western blot analysis
pRetroX-SF-Rac1	pRetroX-Tight-Pur	SF-Rac1 WT	- pcDNA3-SF-Rac1 WT was digested using BamHI restriction enzyme - Restriction digest product was run on 1.2 % agarose gel to separate digested fragments and isolate SF-Rac1 WT - The PCR product was inserted into pGEM®-T-Easy vector after A-tailing - pGEM®-T-Easy–SF-Rac1 and N-SF-TAP pcDNA3 were digested using NheI and XbaI. - Restriction digests were resolved on 1.2 % agarose gel and relevant fragments were extracted and purified prior to ligation - Minipreps were generated and screened by sequencing using the P_{Tight} primer: 5′-ATCTGAGGCCCTTTCGTCTTCACT-3′ - Positive minipreps were used for maxiprep generation followed by HEK293T transfection for protein expression confirmation using Western blot analysis

2.4 Protein Detection Techniques

2.4.1 Protein Sample Preparation

Proteins were prepared from cells by washing once with ice-cold PBS-/- followed by the addition of 200-500 µl IP lysis buffer while scrapping. Scrapped cells + lysis buffer were

collected in an eppendorf tube and incubated on ice for 5 minutes followed by centrifugation at 13 K rpm for 10 minutes. Depending on the experiment, protein concentrations were determined (described below) and the required amount was diluted in 2x SDS-PAGE sample buffer in an equal ratio. Samples were then either processed immediately or stored at -80 ˚C for later use.

2.4.2 Protein Concentration Determination

The concentration of proteins in samples was determined using the Precision Red Advanced Protein Assay Reagent (Cytoskeleton, Inc., ADV02-A) following manufacturer's instructions, and measuring using on an UV/Visible spectrophotometer (absorbance 600 nm).

2.4.3 PolyAcrylamide Gel Electrophoresis (PAGE)

2.4.3.1 SDS-PAGE

For SDS-PAGE, protein samples were prepared as described above. Lysates were then incubated for 10 minutes at 70 ˚C. Samples were resolved using NuPAGE®Novex® Tris-Acetate pre-cast gels (Life Technologies, 3-8 % 10-well EA0375BOX, 3-8 % 12-well EA03752BOX) or NuPAGE®Novex® Bis-Tris pre-cast gels (Life Technologies, 12 % 10-well NP0341BOX, 12% 12-well NP0342BOX, 4-12% 10-well NP0321BOX, 12-well NP0321BOX). A Rainbow full range molecular weight marker (GE Healthcare RPN800E) was run alongside the samples for protein size reference. Gels were run using the XCell *SureLock*® Mini-Cell electrophoresis system (Life Technologies, EI0001). The Tris-Acetate gels were run at 150 V for 70 minutes using 1X Tris-Acetate SDS running buffer and the Bis-Tris gels were run at 200-220 V for 45-50 minutes using 1X MOPS SDS running buffer.

2.4.3.2 NativePAGE™

For the analysis of protein complexes, the NativePAGE™ Bis-Tris gel system was utilised. First, cells were lysed in the non-denaturing lysis buffer. Lysates were prepared following instructions in the NativePAGE™ Sample Prep kit (Life Technologies, BN2008) and were resolved using NativePAGE™ Novex® 3–12% Bis-Tris gels (LIFE Technologies, BN1001BOX). The NativeMark™ Unstained Protein Standard (Life Technologies, LC0725) was run alongside the samples for protein complex size reference. Gels were resolved using the XCell *SureLock*® Mini-Cell electrophoresis system with the dark blue cathode buffer loaded in the upper cathode chamber and the anode buffer into the lower chamber. Gels were run at 150 V for 30 minutes (or until the dye front migrated to one third of the gel) then the dark blue cathode buffer was replaced by the light blue cathode buffer and the run was resumed for an additional hour. Upon completion of sample resolution, the gel was rinsed using the transfer buffer and analysed as outlined below.

2.4.3.3 Western Blot Analysis

For Western blot analysis, proteins were transferred from gels onto Immobolin® PVDF membranes (Millipore, IPFL00010,) using the XCell II™ blot module (Life Technologies, EI0002) at 32 V for 100 minutes. Following transfer, membranes were incubated with Western blocking buffer 1 or 2, depending on the antibody in use for 1 hour at room temperature with agitation. This was followed by incubation with primary antibody solution (prepared with Western blocking buffer) for 1 hour at room temperature or overnight at 4 ˚C with agitation. Membranes were then washed three times (10 minutes/wash) with PBST or TBST and then incubated with the required HRP-conjugated secondary antibody for 30 minutes to 1 hour at room temperature with agitation, after which membranes were re-washed for 30 minutes in PBST or TBST. Western blots were visualised on Hyperfilm ECL (GE Healthcare, 28-9068) using the ECL Western Blotting Analysis System (GE Healthcare, RPN2109). Table 2.3 lists the antibodies used in this project.

Table 2.3 List of Antibodies Used for Western Blot Analysis

Antibody	Species	Manufacturer	Dilution/Remarks
Anti-HA	Rabbit	Abcam, ab13834	1:5000 of 1 mg/ml
Anti-Mouse-HRP	N/A	GE Healthcare, RPN4201	1:5000
Anti-Rabbit-HRP	N/A	GE Healthcare, RPN4301	1:5000
c-Myc (9E10)	Mouse	Santa Cruz, sc-40	1:1000 of 200 μg/ml
Cdc42 (P1)	Rabbit	Santa Cruz, Sc-87	1:1000 of 200 μg/ml
FLAG® M2	Mouse	Sigma-Aldrich, F1804	1:5000 of 1mg/ml
Flightless I (116.40)	Mouse	Santa Cruz, sc-21716	1:1000 of 200 μg/ml
FLII	Rabbit	Sigma-Aldrich, HPA007084	1:1000 of 100 μg/ml
IQGAP1 (24)	Mouse	BD Biosciences, 610611	1:1000 of 250 μg/ml
P-Rex1	Rabbit	Sigma-Aldrich, HPA001927	1:1000 of 200 μg/ml
P-Rex1	Goat	Sigma-Aldrich, SAB2501302	1:1000 of 500 μg/ml
Phospho-Myosin Light Chain 2 (Ser19)	Rabbit	Cell Signalling, 3671	1:1000 overnight Blocking buffer 2, TBST
Rac1 (102)	Mouse	BD Biosciences, 610650	1:1000 of 250 μg/ml
Rac1 (23A8)	Mouse	Millipore, 05-389	1:1000 of 1 mg/ml
RhoGDI (FL-204)	Rabbit	Santa Cruz, sc-33201	1:1000 of 200 μg/ml
Tiam1 (C16)	Rabbit	Santa Cruz, sc-872	1:1000 of 200 μg/ml
Tiam1	Rabbit	Bethyl, A300-099A	1:1000 of 1 mg/ml
TMOD3	Rabbit	Sigma-Aldrich, HPA001849	1:1000 of 200 μg/ml
α-Tubulin (DM1A)	Mouse	Sigma-Aldrich, T9026	1:5000 of 1 mg/ml

2.4.4 PVDF Membrane Stripping and Reprobing

For repossessing of PVDF membranes using antibodies from the same species origin, PVDF membranes were incubated with Western stripping buffer for 20 minutes. Membranes were then washed and processed as outlined in section 2.4.3.3.

2.4.5 Western Blot Densitometric Analysis

Western blots were scanned using the EPSON PERFECTION 3200 PHOTO scanner at a 300 dpi resolution. Scanned images were saved as JPEG files that were imported into the image-processing program Image J. Bands corresponding to proteins under investigation were quantified using the Gel tab to determine the respective integrated density associated for each band. The raw values were imported to Excel for further normalisations according to the experimental design.

2.5 Identification and Validation of Rac1 Binding Partners

2.5.1 *Strep*-FLAG Tandem Affinity Purification (SF-TAP)

The SF-TAP technique was performed in accordance with the protocol outlined by Gloeckner et al. (Gloeckner et al., 2007) with minor modification to optimise it for SF-Rac1 pulldown as described in section 4.2.1.3. In brief, NIH3T3 cells harbouring the dox inducible system for expressing SF-Rac1 alone or together with the different GEF constructs as indicated were plated at a density of 1.25 x 10^7 cells/500 cm^2 plate (two plates per sample). After 48 hours cells were treated with either ethanol (- dox) or 1 μg/ml dox (+ dox) and incubated for an additional 48 hours. Cells were then harvested and incubated SF-TAP lysis buffer for 15 minutes to lyse cells followed by centrifugation at 10,000 x g at 4 °C, followed by supernatant clearing through a 0.22 μm syringe filter. The protein concentration for each sample was then determined as outlined in section 2.4.2. Equal protein levels were taken from each sample for the first step of SF-TAP, in which each sample was incubated with 200 μl *Strep*-Tactin® superflow resin (IBA GmbH, 2-1206-10), that were prewashed twice with TBS and once with SF-TAP lysis buffer, for 90 minutes at 4 °C while rotating. Lysates were then washed three times using TBS to remove proteins and contaminants that bound non-specifically to the resin. The specific resin-bound proteins were then eluted via incubating with 500 μl 2.5 mM desthiobiotin elution buffer for 30 minutes at 4°C while rotating. Eluates from the first step were then incubated with TBT pre-washed anti-FLAG® M2 affinity gel (Sigma-Aldrich, A2220) (100 μl settled resin/sample) for 75 minutes at 4 °C, while rotating. Samples were washed three times using TBS to remove any residual non-specific proteins bound to the beads. Bound proteins were then eluted by incubating with FLAG® peptide elution buffer for 30 minutes at 4 °C, while rotating. Eluates were then concentrated down to the required volume using Amicon filter units with a 3 KDa protein cut off (EMD Millipore, UFC500396) to concentrate the FLAG® eluates. Concentrated

protein samples were then mixed with 20 µl 2X SDS-PAGE sample buffer and stored at -80 °C for later use. All intermediate steps and washes were performed on ice to prevent protein complex dissociations.

2.5.2 Conventional Mass Spectrometry Protein Identification

2.5.2.1 Sample Preparation

For the conventional mass spectrometry experiments cells were plated at different densities to obtain the varying protein starting materials indicated for each biological replicas. Concentrated samples were resolved using 12 % NuPAGE®Novex® Bis-Tris pre-cast gels as outlined in section 2.4.3. Following the SDS-PAGE run, gels were rinsed with dH_2O for 5 minutes while agitating (x3) at room temperature. Proteins were then visualised by staining with SimplyBlue™ Safestain (Life Technologies, LC6060) for 1 hour while agitating at room temperature followed by distaining in dH_2O for an additional 1 hour. Each Lane was then laddered into 27 equal sections and placed into a well of a 96-well plate (Genomic Solutions, PRO10003). The samples were submitted to the Cancer Research UK Manchester Institute (CRUKMI) mass spectrometry facility for protein identification and were analysed by Duncan L Smith, PhD as detailed below.

2.5.2.2 Gel band destaining and washing

Bands were destained with three 20 minutes changes of 1 ml 200 mM ammonium bicorbante, 40 % (V/V) acetonitrile. Gel bands were then dehydrated by the addition of 500 µl acetonitrile for fifteen minutes followed by rehydration in 500 µl of water for a further fifteen minutes. This dehydration-rehydration procedure was performed a total of three times followed by a final dehydration in acetonitrile.

2.5.2.3 In-Gel Digestion

Gel bands were rehydrated in 25 µl of 50 mM ammonium bicarbonate, 9 % (v/v) acetonitrile, 20 ng/µl sequencing grade trypsin (Sigma-Aldrich) for twenty minutes. The bands were then covered in 100 µl of 50 mM ammonium bicarbonate, 9 % (v/v) acetonitrile and incubated at 37C for 18 hours. Following digestion, samples were acidified by the addition on 10 µl of 10 % (v/v) formic acid. The digest supernatant was then transferred to a fresh eppendorf tube and the digest was dried in a vacuum centrifuge at 40C for 30 minutes. The dried peptides were then resuspended in 20 µl of water, 0.1 % trifluoroacetic acid (Sigma-Aldrich) prior to LCMS analysis.

2.5.2.4 Nano-LC-MS/MS Analysis

Peptides were separated utilising a Nano-Acquity UPLC system (Waters) as detailed below. Sample was loaded onto a Waters C18 Symmetry trap column (180 µm ID, 5 µm 5 cm) in water, 0.1 % (v/v) acetonitrile, 0.1 % (v/v) formic acid at a flow rate of 7 µl per minute for 5 minutes. Peptides were then separated using a Waters NanoAcquity BEH C18 column (75 um ID, 1.7 um, 25 cm) with a gradient of 1 to 40% (v/v) of acetonitrile, 0.1% formic acid over 30 minutes at a flow rate of 400 nl per minute. The nLC effluent was sprayed directly into the LTQ-Orbitrap XL mass spectrometer aided by the Proxeon nano source at a voltage offset of 2.5 KV. The mass spectrometer was operated in parallel data dependent mode where the MS survey scan was performed at a nominal resolution of 60, 000 (at m/z 400) resolution in the Orbitrap analyser between m/z range of 400-2000. The top 6 multiply charged precursors were selected for CID in the LTQ at normalised collision energy of 35 %. Dynamic exclusion was enabled to prevent the selection of a formally targeted ion for a total of 20 seconds.

2.5.2.5 Data Processing and Analysis

MGF peak list files were generated with the use of Mascot Distiller (Matrix Science, London UK) prior to a database searching using Mascot (Matrix Science, London). The database search was restricted to the *Mus musculus* taxonomy, precursor mass accuracy of 10 parts per million, fragment mass accuracy of 0.6 Da and variable modifications of oxidation (M) and deamidation (N/Q)

2.5.3 Stable Isotope Labelling by Amino Acid in Cell Culture (SILAC):

2.5.3.1 SILAC Labelling

Three different SILAC culturing media were used for SILAC labelling of NIH3T3 cells containing the dox inducible system for expressing SF-Rac1 alone or together with the different GEF constructs. All SILAC media was prepared using high glucose DMEM without Lysine (K) or Arginine (R) (PAA) supplemented with 10 % dialysed FBS (Life Technologies, 26400-044), 1% L-Glutamine (Sigma-Aldrich, G7513) and 10 µg/ml penicillin-streptomycin. To minimise contamination, amino acids stock solutions, outlined in Table 2.4, as well as all prepared media were filter sterilised before use on cells. Additionally, all labelling steps were performed in tissue cabinet hoods. Details of the amino acid combinations used for SILAC media preparation are outlined in Table 2.5.

For labelling, NIH3T3 cells were cultured for six doubling rounds. Cells were washed, trypsinsed and counted every 24-48 hours depending on their confluency to determine the number of doublings completed while labelling. Table 2.5 outlines which SILAC media was used for each GEF expressing NIH3T3 cells in the different experiments.

Table 2.4 SILAC Amino Acid Isotope Stock Solutions

SILAC Stock Solution Label	Amino Acid Isotope
K0 stock solution [1]	L-Lysine monohydrochloride (Sigma-Aldrich, L5626)
K4 stock solution [1]	4.4.5.5-D4-L-Lysine HCL (Silantes, 211104112)
K8 stock solution [1]	L-Lysine HCL ^{13}C, ^{15}N (Silantes, 211604102)
R0 stock solution [2]	L-Arginine monohydrochloride (Sigma-Aldrich, A5131)
R6 stock solution [2]	L-Arginine HCL ^{13}C (Silantes, 201204102)
R10 stock solution [2]	L-Arginine HCL ^{13}C, ^{15}N (Silantes, 201604102)

[1] Lysine final concentration of 146 mg/ml in PBS
[2] Arginine final concentration of 84 mg/ml in PBS
[3] Stock solutions were stored in 1 ml aliquots at 4 °C

Table 2.5 NIH3T3 SILAC Labelling

SILAC Experiment	SILAC Media	Isotope Composition	NIH3T3 GEF Expression
SILAC	LIGHT	K0+R0	Control (SF-Rac1 only)
	MEDIUM	K4+R6	Tiam1 WT; Tiam1 GEF*
	HEAVY	K8+R10	P-Rex1 WT; P-Rex1 GEF*
Reverse SILAC	LIGHT	K0+R0	Control (SF-Rac1 only)
	MEDIUM	K4+R6	P-Rex1 WT; P-Rex1 GEF*
	HEAVY	K8+R10	Tiam1 WT; Tiam1 GEF*

2.5.3.2 *Amino Acid Incorporation Check*

After six doubling rounds a small batch of cells were lysed and sent for mass spectrometry analysis to the Proteome Center at the University of Tuebingen, Germany, headed by Professor Boris Macek to check for amino acid incorporation. Alejandro Carpy, a PhD student in the Macek laboratory, performed the amino acid incorporation check by looking at the ratio of lysine and arginine labelled protein peptides versus the unlabelled portion using mass spectrometry. An amino acid incorporation rate was then calculated using the equation outlined below:

$$1 - \left[\frac{1}{(\text{Ratio H/L}) + 1} \right]$$

H= Labelled protein peptides
L= unlabelled protein peptides

2.5.3.3 *Sample Preparation*

Upon confirming amino acid incorporation and completion of SILAC labelling, cells were expanded to obtain the required cell densities needed for SF-TAP as outlined in section 2.5.1. For SILAC labelled cells, the same SF-TAP protocol outlined above was adopted with the exception that the different FLAG® eluates within a set were mixed together prior to protein concentration. To accommodate for the increase in sample volume 4 ml Amicon filter units

were used (EMD Millipore, UFC800308). Concentrated mixed eluates were then stored overnight at -80 °C and sent the following day on dry ice for mass spectrometry analysis by Alejandro Carpy. Small aliquots were also taken at each step of the SF-TAP and were analysed by Western blot analysis to assess efficiency of dox induction as well as of SF-Rac1 pulldown.

Once received the samples were prepared by Alejandro Carpy and a third of each sample was resolved on 12 % NuPAGE®Novex® Bis-Tris pre-cast gels for 9 minutes. Gels were then stained with Coomassie Blue to visualise bands and cut as one section for processing.

2.5.3.4 In-Gel Digestion

In-gel digestion was performed as described by Krug et al. with minor modifications (Krug et al., 2013). In brief, 10 mM ammonium bicarbonate and acetonitrile (1:1 v/v) were used to destain gel pieces by washing three times while agitating. Proteins reduction was then achieved by incubating with 10 mM dithiothreitol (DTT) in 20 mM ammonium bicarbonate for 45 minutes at 56 °C. This was followed by incubation with 55 mM iodoacetamide in 20 mM ammonium bicarbonate for 30 minutes at room temperature in the dark to alkylate the protein samples. Proteins were then washed twice with 5 mM ammonium bicarbonate followed by one acetonitrile wash and dehydrated using a vacuum centrifuge. Proteins were then pre-digested with Lys-C (Wako) (12.5 ng/μl in 20 mM ammonium bicarbonate) and digested with trypsin (Promega). Resultant peptides were then extracted first in three consecutive steps using the following solutions in the stated order: 1) 3 % TFA in 30% acetonitrile; 2) 0.5 % acetic acid in 80 % acetonitrile; 3) 100% acetonitrile. Upon evaporation, the peptide fractions were desalted using StageTips.

2.5.3.5 Nano-LC-MS/MS Analysis

The Nano-LC-MS/MS analysis was performed as described by Krug et al. with a few adjustments (Krug et al., 2013). In brief, all peptide fractions were measured using the EASY-nLC II nano-LC coupled to an Orbitrab Velos mass spectrometer. Chromatographic separation was conducted on a 15 cm PicoTip fused silica emitter with an inner diameter of 75 μM and 8 μM Tip inner diameter. With recered-phase ReproSil-Pur C18-AQ 3 μM resin. Together with 0.5 % acetic acid, peptides were injected into the column at 700 nL/minute using a maximum pressure of 280 Bar. Elution of peptides was then achieved by using a 121 minute or a 51 minutes segmented gradient of 5-50 % solvent B (80 % acetonitrile in 0.5 % acetic acid) at a flow rate of 200 nL/min. The mass spectrometer was operated on a data-dependent mode. Using a resolution of 60,000 and a target value of 1E6 charges, survey full-scans for the MS spectra were recorded between 300-2000 Thompson. The upper most intense 15 peaks from the sans were selected for fragmentation using collision induced dissociation at a target value of 5000

charges. The resultant spectra were then recorded in the linear ion trap. Selected masses were included in a dynamic exclusion list for 90 seconds.

2.5.3.6 Data Processing and Analysis

MS raw files were processed using MaxQuant software (v.1.2.2.9) se described by Carpy et al. (Carpy et al., 2014). Multiplicity was set as three to match the number of SILAC labels used (i.e. LIGHT, MEDIUM, HEAVY) with K4+R6 set as medium and K8+R10 set as heavy. Following peptide quantification, a database search was performed using the Andromeda search engine. For proteome measurements trypsin was set as the enzyme used. Data was searched against the Uniprot mouse reference proteome downloaded on January 12, 2012. For statistical significance between detected SILAC ratios, the MaxQuant software was used to determine the significance B value associated with each identified proteins with p-value ≤ 0.05 considered significant.

2.5.3.7 Ingenuity® Analysis and Data Presentation

Generated protein lists provided by Alejandro Carpy were further classified using a cut off of ± 1.3 SILAC ratio fold change to identify proteins that show differential Rac1 binding compared to control cells expressing SF-Rac1 only. Generated protein lists for each GEF were used for further analysis using the Ingenuity® integrated pathway analysis (IPA). This allowed the clustering of proteins according to their functional role in cells. The IPA software was also used to generate protein networks to facilitate the identification of proteins that are known to interact or to cooperate to induce a certain signalling event.

Information from the IPA software was also utilised to generate heat maps corresponding to functional protein groups of interest. Hui Sun Leong from the Bioinformatics group at the CRUKMI generated the heat map presented in this thesis using the R Project software.

2.5.4 Bioinformatics

Protein lists generated from both conventional mass spectrometry and SILAC experiments were analysed using available protein databases, such as the Human Protein Reference Database (HPRD) (Prasad et al., 2009), NetPath (Kandasamy et al., 2010) and the Human Protein-Protein Interaction Predictions (PIPs) database (McDowall et al., 2009; Scott and Barton, 2007). These databases coupled with an extensive literature search were used to determine the efficiency of the screens in identifying Rac1 binding partners, through classifying identified proteins into known Rac1 binding partners, predicted Rac1 binding partners and proteins involved in Rac1 signalling. Remaining proteins were considered as novel Rac1 binding partners that require additional validation as outlined in the next section.

2.5.5 Validation of Rac1 Binding Partners

2.5.5.1 Immunoprecipitation and Pulldowns

For immunoprecipitation, 2.5 μg of the relevant antibody were bound to 25 μl of GammaBind G Sepharose beads (GE Healthcare, 17-0885-01) per sample for 75 minutes at room temperature while rotating. Beads with the same antibodies were handled together to ensure similar antibody binding efficiency between samples. Following antibody binding, beads were pelleted by centrifugation at 5,000 x g for 30 seconds. Antibody-bound beads were washed three times with SF-TAP lysis buffer to remove any unbound antibody. Beads were pelleted and resuspended in required SF-TAP lysis buffer volume to facilitate equal aliquoting for each sample. Protein lysates were prepared as described in section 2.4.1 and 2.4.2; however for SF-TAP lysis buffer was used instead of IP lysis buffer for these experiments. Following protein concentration determination, equal protein levels were incubated with the respective antibody-bound beads for 2 hours at 4 °C. Beads were then pelleted by centrifugation, and washed three times with SF-TAP lysis buffer. Beads were then resuspended in 20-25 μl 2X SDS-PAGE sample buffer and were either subjected to SDS-PAGE immediately or stored at -80 °C for later use. For FLAG immunoprecipitations anti-FLAG® M2 affinity gel were used followed by elusion using the FLAG® peptide elution buffer. Table 2.6 lists the antibodies used for immunoprecipitations in this study.

SF-TAP and *Strep* pulldown experiments were also used to validate Rac1 binding partners. For SF-TAP experiments the protocol outlined in section 2.5.1 was scaled down to one 15 cm plate per sample (1 x10^7 cells per plate). The *Strep* pulldown experiments were also set up in 15 cm plates and were performed as outlined in the first step of the SF-TAP technique.

Table 2.6 List of Antibodies/Conjugated beads Used for Immunoprecipitation

Antibody	Species	Manufacturer
Anti-FLAG® M2 affinity gel	N/A	Sigma-Aldrich, A2220
c-Myc (9E10)	Mouse	Santa Cruz, sc-40
Flightless I (116.40)	Rabbit	Santa Cruz, sc-21716
FLII	Mouse	Sigma-Aldrich, HPA007084
P-Rex1	Rabbit	Sigma-Aldrich, HPA001927
P-Rex1	Goat	Sigma-Aldrich, SAB2501302

2.5.5.2 Duolink® In Situ Proximity Ligation Assay (PLA)

Cells were seeded on glass coverslips at a density of 2.5 x 10^5 cells per well in a 6-well plate. Upon plating, cells were treated with either ethanol or 1 μg/ml dox for 24 hours. Cells were washed three times in PBS -/- and then fixed by incubating with cell fixing buffer for 15 minutes at room temperature with agitating. Upon fixing cells were washed four times in PBS -/-

and followed by cell permeabilisation via incubating with permeabilisation buffer for 5 minutes at room temperature. Coverslips were then washed and blocked in immunofluorescence blocking buffer for 1 hour at room temperature with agitation. This was followed by incubated with the relevant antibodies raised in different species for an additional hour at room temperature. Coverslips were then washed twice in PBS -/-. Duolink® In Situ PLA® probes (Olink Bioscience, anti-mouse 92004-0100, anti-rabbit 92002-0100) were prepared according to manufactures instructions and added to the washed coverslips for 1 hour at 37 °C. coverslips were then washed twice in 1X TBS and PLA probes ligation was stimulated using the provided ligase and incubating for 30 minutes at 37 °C. Following ligation coverslips were rinsed twice using 1X TBS then subjected to amplification reaction following instructions outlined in the Duolink® In Situ detection reagent kit (Olink Bioscience, 92014-0100). Coverslips were washed twice in 1X TBS followed by incubation with Alexa Fluor® 568 Phalloidin (Life Technologies, A12380) for 1 hour at room temperature in the dark. The coverslips were rinsed twice (10 minute each) using 1X TBS followed by one short wash in 0.01X TBS. Coverslips were left to dry at room temperature in the dark followed by mounting using ProLong® Gold antifade reagent with DAPI staining (Life Technologies, P36935). Coverslips were left overnight at room temperature in the dark to ensure proper mounting prior to visualising using the Low light microscope system. Antibody combinations used are outlined in Table 2.7.

Table 2.7 List of Antibodies Used for Duolink® In Situ PLA® Assay

Interaction Investigated	Antibody Combination	Manufacturer
Rac1-FLII	Mouse anti-Rac1	BD Biosciences, 610650
	Rabbit anti-FLII	Sigma-Aldrich, HPA007084
Rac1-TMOD3	Mouse anti-Rac1	BD Biosciences, 610650
	Rabbit anti-TMOD3	Sigma-Aldrich, HPA001849

For quantification of the duolink® signal, images were imported into the CellProfiler software to count the number of dot or speckles per image, which was then normalised to the number of nuclei in the field to obtain the number of speckles per cell. The average speckle count per cell was calculated by adding the dots obtained from indicated number of cells. To account for background, extra control samples were prepared for each experiment in which cells were only incubated with one primary antibody followed by the normal duolink® In Situ PLA protocol. Speckle/dot counts per cell from these samples were subtracted from the average speckle count per cell identified for each condition. The obtained numbers were then normalised to the control cells within each experiment to determine fold-changes in average speckle per cell upon expression of the different GEF constructs.

2.6 Cell Imaging Techniques

2.6.1 Cell Fixation

Cells were washed once with PBS -/- followed by 15-40 minutes incubation with 4 % Formaldehyde (v/v) in PBS -/- at room temperature. This was followed by six washes with PBS -/- with each wash approximately 2 minutes long. Fixed cells were either processed immediately as required or were stored in PBS -/- at 4 °C for later use.

2.6.2 Immunofluorescence

Cells were seeded on glass coverslips at a density of 2.5 x 10^5 cells/well in a 6-well plate. Upon plating, cells were treated with either ethanol or 1 μg/ml dox for 24 hours. Cells were fixed as outlined above and then incubated for 3 minutes with cell permeabilisation buffer followed by incubation with immunofluorescence blocking solution for 30 minutes at room temperature with agitation. Coverslips were then incubated with relevant primary antibody solution for 1 hour at room temperature. Cells were then washed six times with PBS -/- followed by secondary antibody solution incubations for an additional hour at room temperature and in the dark. Coverslips were rinsed six times with PBS -/- to remove any non-bound antibodies. The ProLong® Gold antifade reagent with DAPI staining was then used to mount coverslips onto microscope slides. Mounted slides were left overnight at room temperature in the dark before processing the following day. Table 2.8 lists the antibodies used for immunofluorescence.

Table 2.8 List of Antibodies Used for Immunofluorescence

Antibody	Species	Manufacture	Dilution
Alexa Fluor® 568 Phalloidin	N/A	Life Technologies, A12380	1:100
Anti-HA	Rabbit	Abcam, ab13834	1:500
E-cadherin, DECMA-1	Rat	Abcam, ab11512	1:100
Myc-488 conjugated	N/A	Life Technologies, 13-2511	1:100
Secondary Alexa Flour® conjugated antibodies (488 & 568)	N/A	Life Technologies	1:500

2.6.3 Microscope Systems

Phase-contrast images were taken on a Ziess Inverted microscope (Axiovert 2.5) using the 10x magnification lens and the Axiovision software. Immunofluorescence images were taken on the Low light microscope system using the Metamorph (Molecular Devices) software.

Low Light Microscope system: The low light microscope system is based on a Ziess Axiovert 200M enclosed in a full environmental chamber (Solent Scientific). The system utilises Metamorph software and a -80 °C cooled Roper Cascade EMCCD 512B back illuminated camera.

For fluorescence illumination a 300 W Xenon light source was used. Additionally, wavelength switching was automated using shutters and filter wheels with the ET-Sedat filter set (406/488/568/647 nm excitation). Data was imaged with Ziess alpha plan flour 10x objective lens or 100x 1.45 NA oil immersion objective lens.

2.7 Functional Cell-Based Assays

2.7.1 Rac1/Cdc42 Activity Assay

Cells were plated at a concentration of 1 x 10^6 cells per well in a 6-well plate in the presence of ethanol (- dox) or 1 μg/ml dox (+ dox) for 24 hours prior to the assay. On the day of the assay, cells were washed once with ice-cold PBS +/+ then 200 µl GST-FISH buffer + 2 µl biotinylated or GST-tagged Cdc42/Rac1 Interactive Binding peptide from their downstream effector PAK (PAK-CRIB) was added to each well. Cells were scraped quickly and placed in eppendorfs to allow the CRIB peptide to bind active Rac1/Cdc42 while rotating for 30 minutes at 4 °C. Lysates were then cleared by centrifugation at 10,000 x g for 5 minutes at 4 °C and 120-140 µl were incubated with 20 µl pre-washed *Strep*-Tactin® superflow resin (for biotinylated PAK-CRIB) or GST agarose beads (Pierce, 20211 for GST PAK-CRIB) while rotating for 15 minutes at 4 °C. Beads were then spun down at 6,000 x g and washed three times using the GST-FISH buffer. The beads were then resuspended in 20 µl 2X SDS-PAGE sample buffer. To assess equal protein loading, 20-40 µl were taken upon clearing of lysates, and 10 µl were mixed with an equal volume of 2X SDS-PAGE sample buffer. Samples were either processed immediately by SDS-PAGE and Western blot analysis or were stored at -80 °C for later use. Levels of active Rac1 and Cdc42 were detected using anti-Rac1 and anti-Cdc42 antibodies, respectively.

2.7.2 Cellular Morphology Analysis

Cells were seeded at various concentrations and phase-contrast images were taken. Cells were classified into three groups based on their morphology, which differed between different cell types. For example, given the mesenchymal phenotype associated with NIH3T3 cells, the three groups used for assessing GEF-induced changes in cellular morphology were as following: 1) Mesenchymal, 2) Ruffling Epithelial-like and 3) Protrusive Mesenchymal-like. In brief, NIH3T3 cells with the normal triangular fibroblast morphology were considered to be mesenchymal. Cells exhibiting increased cellular aggregation accompanied by membrane ruffling were assigned the epithelial-like category. While cells with increased numbers of thin membrane protrusions were considered as protrusive.

In contrast, MDCKII and A431 cell lines have a characteristic epithelial morphology, thus the three groups used for morphological classification were as follows: 1) Epithelial, 2) Ruffling

Epithelial-like and 3) Protrusive Mesenchymal-like. Given that both the first and second groups entailed an epithelial phenotype, to distinguish between the two morphologies, more emphasis was put on how flat the colonies where and whether membrane ruffling was observed. Cells with a flattened morphology and membrane ruffling with or without increased cellular aggregation were considered as the ruffling epithelial-like group. Whereas, as indicated by the name, cells with a mesenchymal-like phenotype and increased numbers of membrane protrusions were assigned the protrusive mesenchymal-like morphology.

For all cell lines investigated phase-contrast images were captured from different experiments and in total 150 cells were analysed per cell line. Graphs represent number of cells within each category as a percentage of the total number of cells analysed.

2.7.3 ORIS™ Migration Assay

Cells were plated at a concentration of 5 x10^5 cells per well in a 6-well plate in the presence of ethanol (- dox) or 1μg/ml of dox (+ dox) 24 hours prior to assay. Cells were then trypsinised, counted and spun down at 1200 rpm for 5 minutes. Pellets were resuspended in the appropriate amount of media for a final concentration of 1 x 10^6 cell/ml. Cells (≈ 5 x1 0^5 cells) were then taken and made up to 1 ml with Dic16 dye at a final concentration of 2.5 μM and incubated at 37 °C and 5 % CO_2 for 30 minutes. In the meantime, stoppers (supplied with plate) were fitted in the appropriate number of wells in 96-well plate (Platypus Technologies, CMA1.101). Prior to stopper fitting, the required number of, 96-well plates were coated with fibronectin at a final concentration of 5 μg/ml for 1 hour at 37 °C. After Dic16 cell labelling, cells were spun down at 1200 rpm for 5 minutes and were then resuspended in 1 ml DMEM (-/+ dox). Cells were then seeded (100 μl per well) in the stopper fitted fibronectin coated 96-well plate (3-8 wells per condition depending on the experiment). Cells were left incubating overnight in humidity chamber set at 37 °C and 5 % CO_2 prior to the removal of the stoppers. Fluorescence images were taken at 0 and 24 hours upon removal of stoppers. The percentage of migration was calculated using the following equation:

$$\frac{(\text{24 hours migration})_{\text{Area}} - (\text{0 hour migration})_{\text{Area}}}{(\text{0 hour migration})_{\text{Area}}} \text{ X } 100$$

Percent migration values obtained for each sample were normalised to the parental – dox treated control within each experiment. Graphs represent normalised average percent migration from three independent experiments.

2.7.4 Cellular Scattering Assays

Cells were seeded at a concentration of 2 x 10^3 cells per well in a 6-well plate for 24 hours in normal DMEM media. Cells were then washed twice with PBS -/- to remove any traces of

serum followed by culturing in serum-free media (DMEM+ 0.01 % FBS) for 18-24 hours prior to the addition of hepatocyte growth factor (HGF; 10 ng/ml) or epidermal growth factor (EGF; 100 ng/ml). Phase-contrast images of individual colonies were captured at 0, 6 and 24 hours following addition of growth factor.

To quantify cellular scattering, 50 colonies per condition were examined and classified into unscattered or scattered depending on the number of cells within each colony that are still in contact. Colonies with less than 3 cells remaining in complete contact were considered scattered colonies, where complete contact refers to when two adjacent cells within a colony are sharing the same cell-cell junction while maintaining contact at every position along the junction. It is important to note that single cells were not included for this assay and that only colonies with ≥ 4 cells were analysed. Graphs represent number of colonies identified in each group as a percentage of total number of colonies analysed from three independent experiments.

2.7.5 Transepithelial Electrical Resistance (TER) Cell-Cell Adhesion Assay

MDCKII cells were plated onto 12 mm Transwell® with 0.4 μ pore polyester membrane inserts (Corning, 3460) at a cellular density of 5 x 10^5 cells per membrane in the presence of ethanol (- dox) or 1 μg/ml dox (+ dox). MDCKII culturing media (1.5 ml -/+ dox) was also placed in the surrounding well and cells were left to settle in a humidity chamber set at 37 °C and 5 % CO_2. After 24 hours, the media was replaced (-/+ dox) to remove unattached cells and cells were left incubating for an additional 48 hours. The TER associated with the different GEF expressing MDCKII cells was then measured to detect the basal resistance across the contacts of the plated cells in media containing normal calcium levels. The media was then replaced with low calcium media (LCM, 0.02 mM $CaCl_2$) for 18 hours to disrupt tight junctions after which, calcium was re-added by changing the LCM to high calcium media (LCM + 1.8 mM $CaCl_2$). This was performed very gently so as to not disturb the monolayers. Calcium switch TER readings were taken at hourly intervals until the TER peak is reached and starts to go back to basal TER readings. TER readings were also taken at 24 hours to monitor the ability of tight junctions to reform upon expression of the different GEFs. Cells were then lysed using IP lysis buffer and expression of the respective GEFs was examined.

2.7.6 Collagen Gel Contraction Assay

Primary human fibroblasts were transiently co-transduced with respective pRetroX-EV/GEF together with pRetroX-Tet-On Advanced to generate a transient dox inducible system for expression of EV or different GEF constructs. After 48 hours from the final viral transduction cells were trypsinsed (with no preceding PBS -/- wash). For 25 ml collagen I (prepared by Gavin White in our laboratory at 2 mg/ml) 1 x10^6 cells were needed. The cells were mixed with the collagen together with 3 ml 10x MEM and approximately 3 ml 0.22 M NaOH that was added drop wise while stirring to avoid increasing the mixture's alkalinity as this affects the ability of the cells to contract the collagen gels (the mixture colour should turn orange and not pink). Once the required mixture is achieved, 500 μl of collagen-fibroblast mix was added gently yet quickly to a well in a 24-well plate. The number of well replicas per experiment varied depending on the amount of collagen-fibroblast mix available. All steps required for collagen-fibroblast gel preparations were performed on ice and in pre-chilled bottles to prevent collagen solidification.

Once placed in the wells, the collagen was left to solidify for 10 minutes in a humidity chamber set at 37 °C and 5 % CO_2 after which the primary human fibroblast culturing media was added containing ethanol or 1μg/ml of dox to stimulate GEF expression in the respective collagen gels. The sides of the gels were gently detached from the well walls to ensure efficient fibroblast-mediated disc contraction and discs were incubated at 37 °C and 5 % CO_2 for 24 hours. Collagen gels were scanned using an EPSON PERFECTION 3200 PHOTO scanner at 0 and 24 hours post -/+ dox treatment and the percent of collagen gel contraction was calculated using the following equation:

$$\frac{\text{(Gel surface area at 24 hours) - (Gel surface area at 0 hours)}}{\text{(Gel surface area at 0 hours)}} \text{ X 100}$$

Percent collagen gel contraction values obtained for each sample were normalised to the parental – dox treated control within each experiment. Graphs represent normalised average percent collagen gel contraction from three independent experiments.

2.8 Quantifications and Statistical Significance

As highlighted above, each assay contained its own quantification method. For assessing statistical significance paired student's t-test was conducted with p-value ≤ 0.05 considered significant and p-value ≤ 0.01 considered highly significant.

Chapter 3 : The Role of Tiam1 and P-Rex1 in Dictating Rac1 Downstream Effects

3.1 Introduction:

The first aim of this project was to examine the potential role of Tiam1 and P-Rex1 in dictating Rac1 signalling under the same cellular conditions. The choice of the GEFs examined was based on their reported roles in determining whether Rac1 will inhibit or promote cellular migration and invasion. However, the discrepancy in the literature regarding the role of Tiam1 in cellular migration and invasion complicates the comparison of Rac1 effects on migration upon activation by either Tiam1 or P-Rex1. Despite the presence of evidence suggesting that these controversial effects could be attributed to factors, such as cell type and ECM signalling (Etienne-Manneville and Hall, 2002; Sander et al., 1998) it was important to first establish whether Tiam1 and P-Rex1 have the potential to induce different cellular effects downstream of Rac1 before endeavouring to decipher their Rac1 regulatory potential. Thus, to address this a preliminary experiment was conducted in our laboratory in which either Tiam1 WT or P-Rex1 were ectopically expressed, in distinct NIH3T3 pools that originated from the same source, to eliminate any cellular variability. The morphological changes induced upon expression of either GEF were assessed and revealed an opposing role of each GEF on NIH3T3 cellular morphology. Tiam1 expression was found to promote cellular aggregation inducing an epithelial-like morphology. On the other hand, P-Rex1 expression resulted in an enhanced mesenchymal phenotype.

The preliminary observations supported the premise that under the same cellular conditions, the role of GEFs in dictating GTPase signalling would be more evident. Thus together with the reported roles of Tiam1 and P-Rex1 in regulating cellular migration, these observations called for a more thorough investigation of the role of Tiam1 and P-Rex1 in regulating Rac1 downstream signalling events to illicit differential downstream outcomes. This chapter focuses on a series of experiments that were designed and conducted to further investigate the extent by which Tiam1 and P-Rex1 dictate Rac1 signalling

3.2 Results

3.2.1 Activation of Rac1 by Tiam1 and P-Rex1, under the Same Cellular Conditions, Induces Differential Rac1 downstream Cellular Effects

3.2.1.1 *Generation of Retroviral Doxycycline Inducible GEF Expression System in NIH3T3 Cells*

In order to accurately assess the extent by which GEFs, particularly Tiam1 and P-Rex1, can influence outcomes downstream of a Rac1, an experimental system was needed in which all other factors that could contribute to Rac1 downstream signalling are controlled. Therefore, the first objective of the project was to setup a doxycycline (dox) inducible system to express Tiam1 and P-Rex1 in different cell lines to allow the selective activation of Tiam1-Rac1 and P-Rex1-Rac1 signalling cascades irrespective of upstream signalling.

This system is based on two retroviral plasmids. The first plasmid, pRetroX-Tet-On Advanced, is responsible for the expression of the rtTA-Advanced protein, which has two dox docking sites and in the presence of dox is able to bind to the P_{Tight} promoter present in the second plasmid, pRetroX-Tight-Pur. The second plasmid also contains a multiple cloning site (MCS), in which a protein of interest can be inserted and expressed only upon dox addition as demonstrated in Figure 3.1 A. The two plasmids can then be introduced into a cell line by viral transduction as described in section 2.2.4 to assess the cellular effects induced by the expressed protein.

Given the preliminary evidence outlined earlier, the retroviral dox inducible GEF expression system was first tested in NIH3T3 cells. Plasmids containing wild type (WT) human HA-Tiam1 or Myc-P-Rex1 WT were introduced into NIH3T3 cells by transduction. Additionally, GEF-dead mutants (GEF*) for both proteins were also introduced in cells. Figure 3.1 B shows a schematic representation of the domain structures and the differences between the WT and GEF* mutants of the inserted proteins. As with the preliminary experiments, the same batch of NIH3T3 parental cells was used to generate cells with the different plasmids.

Following antibiotic selection, expression of each GEF upon the addition of 1 μg/ml dox was assessed using immunofluorescence (Figure 3.1 C-F) and Western blot analysis (Figure 3.1 G). As shown in Figure 3.1 C-F, expression of the respective GEFs can be detected by immunofluorescence using anti-HA or anti-Myc antibodies for Tiam1 and P-Rex1 constructs, respectively, only upon dox induction. In addition, DAPI staining was used to determine the percentage of GEF expressing cells relative to the total number of cells analysed. As can be seen the majority of cells are expressing the respective GEFs. Western blot analysis also confirmed that GEF expression was restricted to dox induction. Moreover, through the use of anti-Tiam1 and anti-P-Rex1 antibodies, the integrity of the plasmids was validated. Interestingly, the P-Rex1 antibody was only able to detect the exogenous levels of P-Rex1 demonstrating the absent or very low levels of endogenous P-Rex1 in NIH3T3 cells.

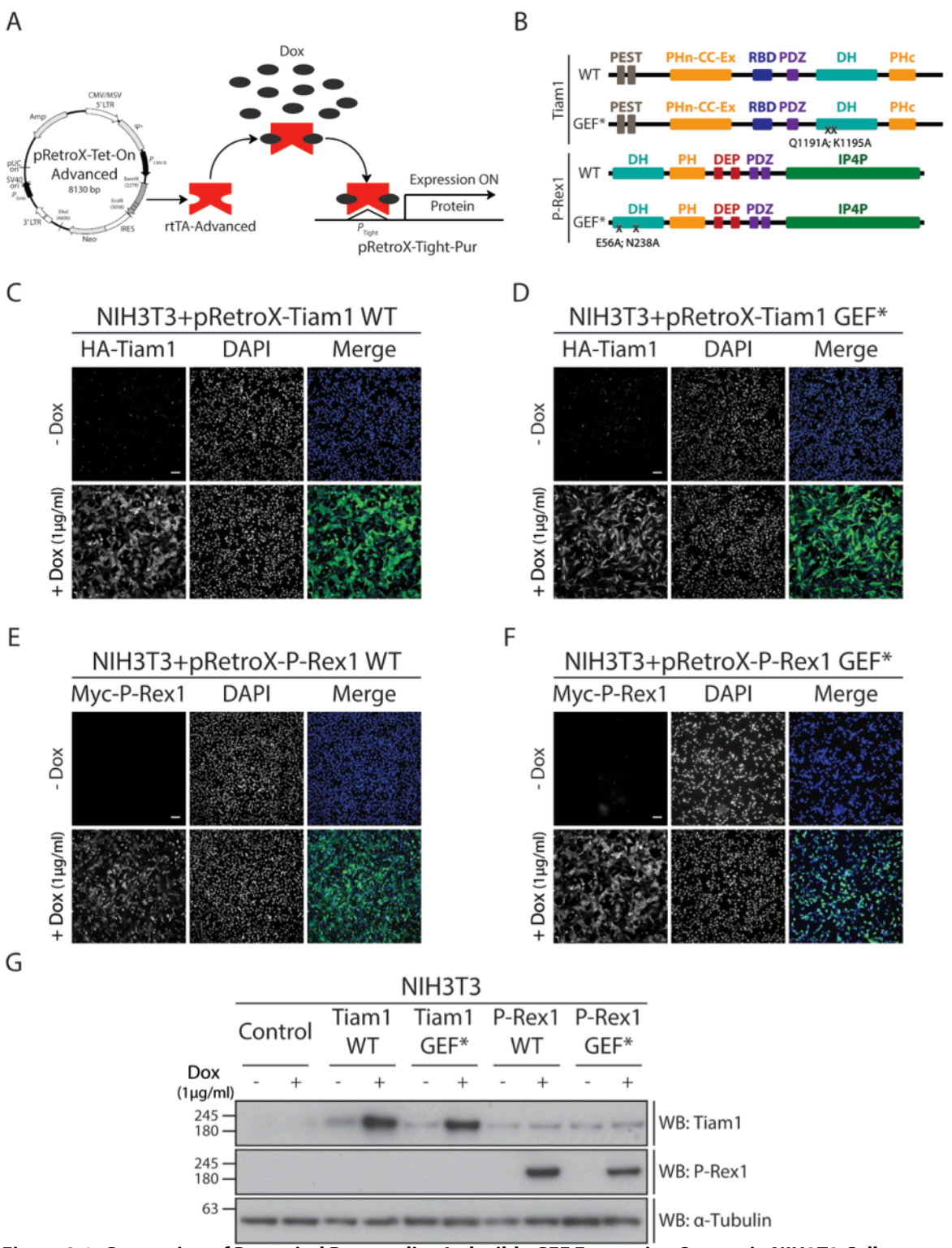

Figure 3.1: Generation of Retroviral Doxycycline Inducible GEF Expression System in NIH3T3 Cells

(A) Schematic representation of pRetroX-Tet-On Advanced and pRetroX-Tight-Pur doxycycline (dox) inducible system. Upon addition of 1 µg/ml dox to cells harbouring the inducible system, the expression of proteins under the P_{Tight} promoter in the pRetroX-Tight-Pur vector is induced. (B) Schematic representation of the domain structures of Tiam1 wild type (WT), Tiam1 GEF-dead mutant (GEF*) as described by Tolias et al.(Tolias et al., 2005) and P-Rex1 WT, P-Rex1 GEF* as described by Nie et al (Nie et al., 2010). PH=Pleckstrin homology domain; PHn=N-terminal PH domain; PHc=C-terminal PH domain; CC=Coiled-coil domain; EX=Extended structure; RBD=Ras binding domain; PDZ=PSD-95/Dlg/ZO-1 domain; DH=Dbl homology domain; DEP=Dishevelled, Egl-10 and Pleckstrin domain; IP4P=Inositol polyphosphate 4-phosphatase. (C, D, E, F) NIH3T3 cells treated with ethanol (- dox) or 1 µg/ml dox (+ dox) for 24 hours, fixed in 4 % formaldehyde and markers against HA-tagged Tiam1 WT/GEF* or Myc-tagged P-Rex1 WT/GEF* were used for immunofluorescence. Images of – dox and + dox treated cells were taken using the low light microscope system (10x magnification), showing Tiam1 WT (C), Tiam1 GEF* (D), P-Rex1 WT (E) P-Rex1 GEF* (F) expression. Scale bar=100 µM. (G) NIH3T3 cells harbouring the dox inducible system were treated with - dox or + dox for 24 hours. Cells were harvested and expression levels of Tiam1 WT/GEF* and P-Rex1 WT/P-Rex1 GEF* were detected by Western blot analysis using anti-Tiam1 and anti-P-Rex1 antibodies, respectively. α-Tubulin was used as a loading control.

Together this demonstrates the high efficiency of the viral transduction, which resulted in the uniform expression of the GEFs, as well as the dox selectivity, since minimal expression was detected in the ethanol (- dox) treated cells.

3.2.1.2 Ectopic Expression of Tiam1 and P-Rex1 Wild Type but not GEF-Dead Mutant Proteins Results in Elevated Levels of Active Rac1 in NIH3T3 Cells

Following the confirmation of the efficiency of the dox inducible GEF expression system in NIH3T3 cells it was important to verify the integrity and activity of the GEFs being expressed. A way to assess this is to compare the ability of Tiam1 WT or P-Rex1 WT to activate Rac1 in cells relative to their GEF* mutants. To determine levels of active Rac1, NIH3T3 cells harbouring the different GEF expression vectors were treated with ethanol (- dox) or 1 μg/ml dox (+ dox) to induce protein expression. Cells were then collected and subjected to a PAK-CRIB pulldown. Levels of active Rac1 were then detected by Western blot analysis using anti-Rac1 antibody.

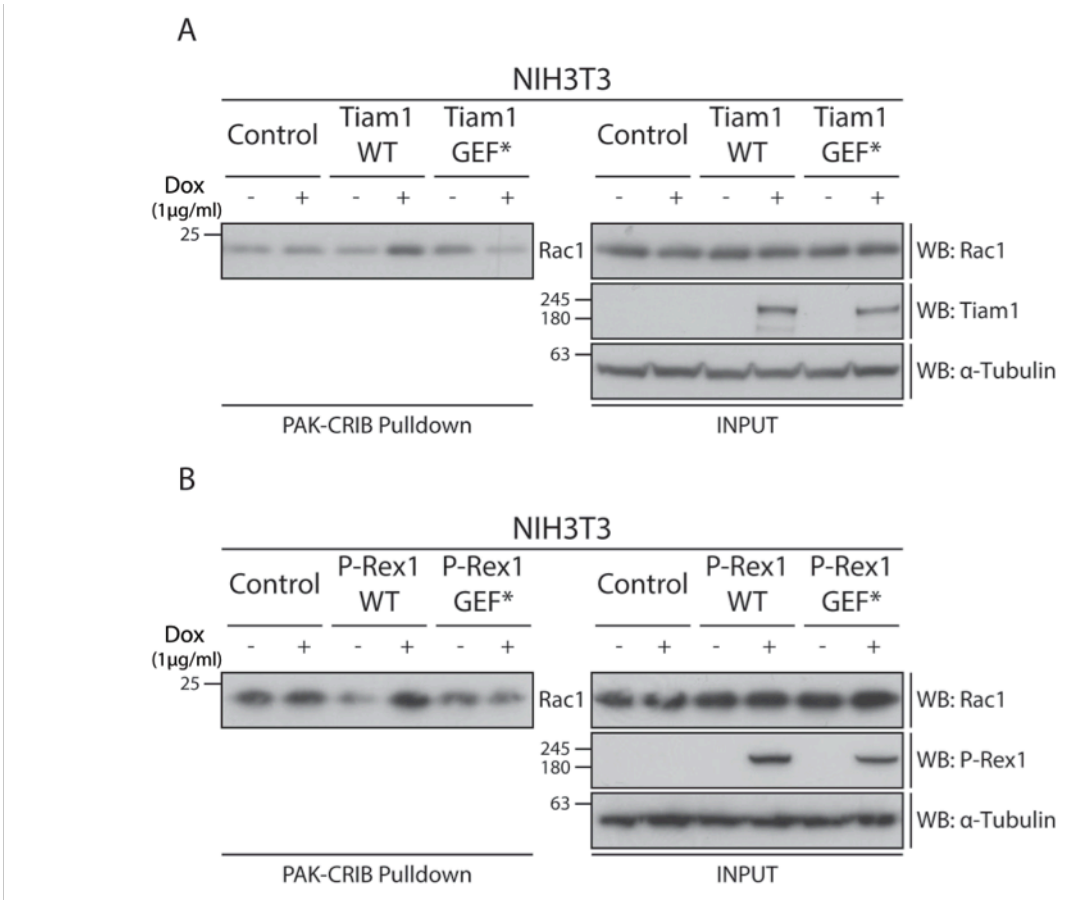

Figure 3.2: Ectopic expression of Tiam1 and P-Rex1 Wild Type but not GEF-dead Mutant Proteins Results in Elevated Levels of Active Rac1 in NIH3T3 cells

(A) NIH3T3 cells harbouring the doxycycline (dox) inducible system for the expression of wild type Tiam1 (Tiam1 WT) or Tiam1 GEF-dead mutant (Tiam1 GEF*) were treated with ethanol (- dox) or 1μg/ml dox (+ dox) for 24 hours. Cells were then harvested and subjected to a PAK-CRIB pulldown of active Rac1. Levels of active Rac1 were detected by Western blot analysis using anti-Rac1 antibody. α-Tubulin was used as a loading control. Representative Western blot from three independent experiments. (B) NIH3T3 cells harbouring the dox inducible system for the expression of wild type P-Rex1 (P-Rex1 WT) or P-Rex1 GEF-dead mutant (P-Rex1 GEF*) were treated with dox for 24 hours. Cells were then harvested and subjected to a PAK-CRIB pulldown of active Rac1. Levels of active Rac1 were detected by Western blot analysis using anti-Rac1 antibody. α-Tubulin was used as a loading control. Representative Western blot from three independent experiments.

As can be seen from Figure 3.2 A, levels of active Rac1 in the – dox and + dox treated parental NIH3T3 cells (control) were equal indicating that dox treatment does not stimulate Rac1 activation. Similar basal active Rac1 levels were also observed in Tiam1 WT and Tiam1 GEF* - dox treated cells. In contrast, upon dox induction and expression of Tiam1 WT, increased levels of active Rac1 were detected by Western blot analysis. However, as expected this increase was not observed upon the expression of Tiam1 GEF*. Interestingly, expression of Tiam1 GEF* resulted in even lower levels of active Rac1 when compared to control cells as well as the Tiam1 GEF* – dox counterparts. Importantly, these changes in Rac1 levels were confined to the active form and not to total Rac1 levels as indicated by the accompanying input Western blots.

Similar to Tiam1 WT, P-Rex1 WT expression in NIH3T3 cells also resulted in increased levels of active Rac1, while not affecting the levels of total Rac1. This increase was not detected between control – dox and + dox treated cells. Additionally, expression of P-Rex1 GEF* failed to induce increased levels of active Rac1, and similar to Tiam1 GEF* was associated with lower levels of active Rac1 when compared to the control and P-Rex1 GEF* – dox treated cells.

Together these results demonstrate that Rac1 activation is restricted to expression of Tiam1 WT or P-Rex1 WT and not their GEF* mutants. This further validates the functionality of the proteins expressed and suggests that comparison of the cellular effects induced upon expression of the WT GEFs versus the GEF* mutants could help pinpoint the effects that are specifically dependent on Rac1 activation.

3.2.1.3 Ectopic Expression of Tiam1 and P-Rex1 Wild Type Proteins Results in elevated Levels of Active Rac1 but not Active Cdc42

Rho GTPases have been shown to influence the activity of one another through a crosstalk system as detailed in section 1.4.1.2. Given the reported interplay between Rac1 and Cdc42 it was interesting to examine whether expression of Tiam1 WT or P-Rex1 WT would also increase the levels of active Cdc42 in NIH3T3 cells.

Similar to Rac1, levels of active Cdc42 can be detected using the PAK-CRIB peptide. The PAK-CRIB pulldown was therefore conducted on NIH3T3 cells containing the dox inducible system for Tiam1 WT or P-Rex1 WT expression. Active levels of Rac1 and Cdc42 were evaluated by Western blot analysis using anti-Rac1 and anti-Cdc42 antibodies, respectively. As demonstrated from Figure 3.3, expression of both Tiam1 WT and P-Rex1 WT resulted in a significant increase in the levels of active Rac1 ($p=0.013$ and $p=0.002$, respectively) when compared to parental NIH3T3 cells (Cnt.). Additionally, although P-Rex1 WT expression was associated with lower levels of active Rac1 compared to Tiam1 WT, the difference was found to be statistically insignificant ($p=0.147$), suggesting that these differences could be due to experimental variations.

Interestingly, expression of Tiam1 WT or P-Rex1 WT did not result in elevated levels of active Cdc42 when compared to Cnt. cells. Quantification from three independent experiments

illustrated that there was no significant increase between the levels of active Cdc42 in Tiam1 WT (p=0.939) or P-Rex1 WT (p=0.266) expressing cells verses Cnt. cells. Moreover, there was no significant difference between cells expressing Tiam1 WT or P-Rex1 WT (p=0.384).

These results indicate that expression of Tiam1 WT and P-Rex1 WT activated Rac1 in a specific and selective manner, suggesting that the majority of the cellular effects induced upon expression of either GEF, if dependent on their GEF function, would be mediated through Rac1 and not Cdc42. Given this specificity, the system was utilised to investigate the role that Tiam1 and P-Rex1 play in dictating Rac1 downstream cellular outcomes.

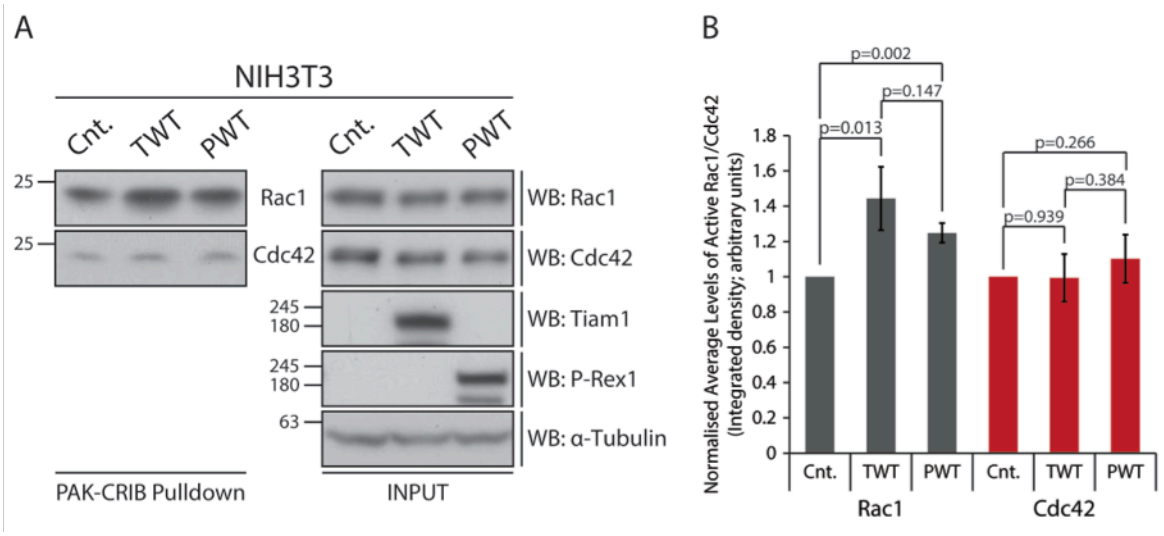

Figure 3.3: Ectopic expression of Tiam1 and P-Rex1 Wild Type Proteins Results in Elevated Levels of Active Rac1 but not Cdc42 in NIH3T3 cells
(A) NIH3T3 cells harbouring the doxycycline (dox) inducible system for the expression of wild type Tiam1 (TWT) or P-Rex1 (PWT) were treated with 1μg/ml dox (+ dox) for 24 hours. Cells were then harvested and subjected to a PAK-CRIB pulldown of active Rac1 and Cdc42. Levels of active Rac1 and Cdc42 were detected by Western blot analysis using anti-Rac1 and anti-Cdc42 antibodies, respectively. α-Tubulin was used as a loading control. Representative Western blot from three independent experiments. (B) Levels of active Rac1 and Cdc42 were quantified using Image J software to calculate the integrated density of bands in each sample. Active levels were then normalised to the total levels of Rac1/Cdc42 and to the α-Tubulin loading control. Graph shows the average levels of active Rac1/Cdc42 ± standard error from three independent experiments normalised to the levels in parental NIH3T3 cells (Cnt.). Student's t-test was used to assess significance between levels of active Rac1/Cdc42 within the different samples and p-values are indicated on the graph. p-values ≤ 0.05 are considered significant; ≤0.01 are considered highly significant.

3.2.1.4 Activation of Rac1 by Tiam1 and P-Rex1 Induces Distinct Morphological Phenotypes in NIH3T3 Cells

Preliminary observations, highlighted earlier, demonstrated the role of Tiam1 and P-Rex1 in differentially regulating cellular morphology in NIH3T3 cells. It was thus important to confirm these results using the newly generated dox inducible GEF expression system and to further investigate the dependency of these phenotypes on Rac1 activity via utilising Tiam1 GEF* and P-Rex1 GEF*.

Figure 3.4 A shows representative phase-contrast images of – dox and + dox treated NIH3T3 cells harbouring the dox inducible GEF expression system. As shown, all – dox treated cells exhibited a mesenchymal morphology that is characteristic of parental NIH3T3 cells (control). Similarly, the treatment of control cells with dox did not alter the normal NIH3T3

morphology. On the other hand, ectopic expression of Tiam1 WT resulted in increased cellular aggregation and membrane ruffling. This was accompanied by reverting of the mesenchymal morphology into an epithelial-like phenotype. In contrast, expression of P-Rex1 WT in NIH3T3 cells was associated with a highly polarised cellular structure and increased formation of thin membrane protrusions. In addition, P-Rex1 WT expressing cells showed reduced ability to adhere to one another. Interestingly, these distinct Tiam1 WT and P-Rex1 WT induced cellular morphologies were not observed in cells expressing Tiam1 GEF* or P-Rex1 GEF* indicating a

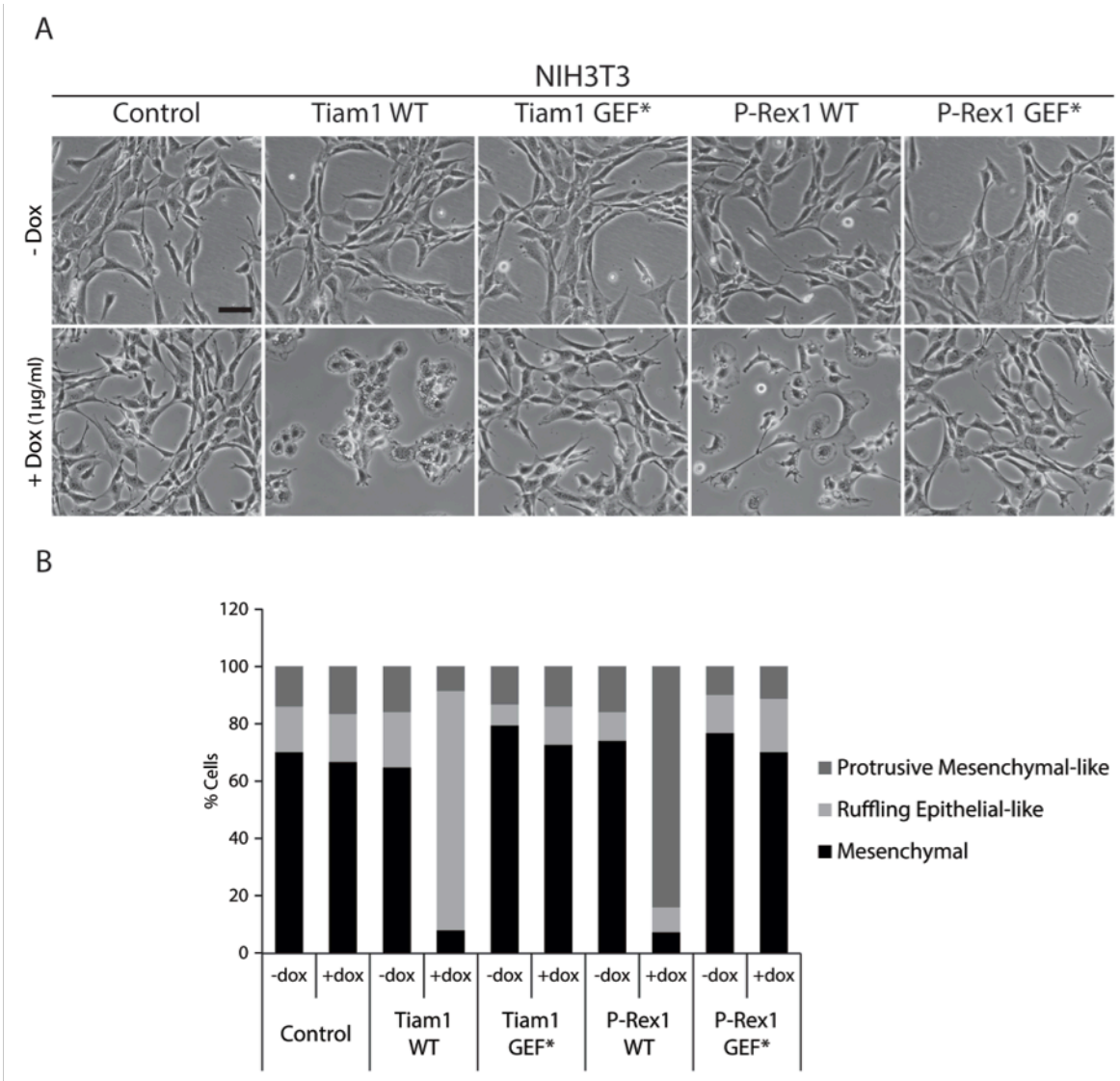

Figure 3.4: Ectopic Expression of Tiam1 and P-Rex1 Wild Type but not GEF-dead Mutant Proteins Induces Distinct Morphological Phenotypes in NIH3T3 Cells

(A) NIH3T3 cells harbouring the doxycycline (dox) inducible GEF expression system for wild type (WT) Tiam1 or P-Rex1 or their GEF-dead mutants (GEF*) were treated with ethanol (- dox) or 1µg/ml dox (+ dox) and phase-contrast images (10x) were taken using the Zeiss inverted microscope (Axiovert 2.5). Scale bar= 100µM. (B) To quantify the GEF induced cellular phenotypes, cells were classified into three groups based on their morphology as follows:
1) Mesenchymal, 2) Ruffling Epithelial-like and 3) Protrusive Mesenchymal-like. Graph represents % cells in each subset from a total of 150 cells/condition from various cell passages.

dependency on Rac1 activation for induction of these phenotypes.

To quantify the morphological phenotypes induced upon activation of Rac1 by the different GEFs, 150 cells per GEF were examined and categorised into one of three categories: 1) Mesenchymal, 2) Ruffling Epithelial-like and 3) Protrusive Mesenchymal-like based on the

criteria outlined in section 2.7.2. As illustrated in Figure 3.4 B, although all three categories were identified in parental NIH3T3 cells, with the majority of cells exhibited a mesenchymal morphology, which is consistent with NIH3T3 being a mouse embryonic fibroblast cell line. This phenotype was not altered upon addition of dox with 66.7 % of cells exhibiting the mesenchymal morphology as opposed to 70 % of cells in the – dox treated control. Similar percentages for mesenchymal cells were also observed for both Tiam1 GEF* and P-Rex1 GEF* - dox (79.3 % and 76.7 %, respectively) and + dox treated cells (72.7 % and 70 %, respectively). On the contrary, expression of Tiam1 WT resulted in 83.3 % of cells exhibiting the ruffling epithelial-like morphology as opposed to 19.3 % in Tiam1 WT – dox treated cells. P-Rex1 WT expression, on the other hand, was associated with 84 % of cells fitting the criteria outlined for the protrusive mesenchymal-like group compared to the 16 % observed in the – dox counterpart.

Taken together, these results confirm the preliminary observations outlined earlier. Additionally, they demonstrate that not only do Tiam1 and P-Rex1 induce distinct morphological changes in NIH3T3 cells, but that their ability to activate Rac1 is crucial for such phenotypes to occur.

3.2.1.5 Activation of Rac1 by Tiam1 and P-Rex1 Induces Distinct Actin Cytoskeleton Rearrangements in NIH3T3 Cells

Similar to other Rho GTPases, Rac1 is known to induce morphological changes in the cells as a result of its ability to regulate actin cytoskeleton rearrangements. Given the role of Tiam1 and P-Rex1 in dictating differential cellular morphologies downstream of Rac1, their ability to influence Rac1-driven actin cytoskeleton rearrangements was examined.

NIH3T3 cells harbouring the different dox inducible GEF expression systems were treated with ethanol (- dox) or 1 μg/ml dox (+ dox). After 24 hours, changes in the actin cytoskeleton were visualised using phalloidin immunofluorescence staining. In addition, to ensure that the expression of the respective GEFs was observed only in + dox treated cells and not in their – dox counterparts, Tiam1 and P-Rex1 expression was assessed using anti-HA and anti-Myc primary antibodies, respectively, followed by AlexaFlour® secondary antibodies. DAPI was used to visualise the nuclei of cells.

Consistent with the distinct morphological changes induced upon activation of Rac1 by Tiam1 or P-Rex1, expression of Tiam1 WT and P-Rex1 WT but not their GEF* mutants was associated with changes in the actin cytoskeleton. Tiam1 WT expression resulted in accumulation of actin at cell-cell contacts when compared to parental NIH3T3 cells (control) or Tiam1 WT – dox cells. However, these results were not induced upon expression of Tiam1 GEF*. Expression of P-Rex1 WT, on the other hand, was associated with actin cytoskeleton rearrangements that explain the elongated morphology highlighted in the previous section.

Unlike P-Rex1 WT expression, the expression of P-Rex1 GEF* did not induce any changes in the actin cytoskeleton (Figure 3.5).

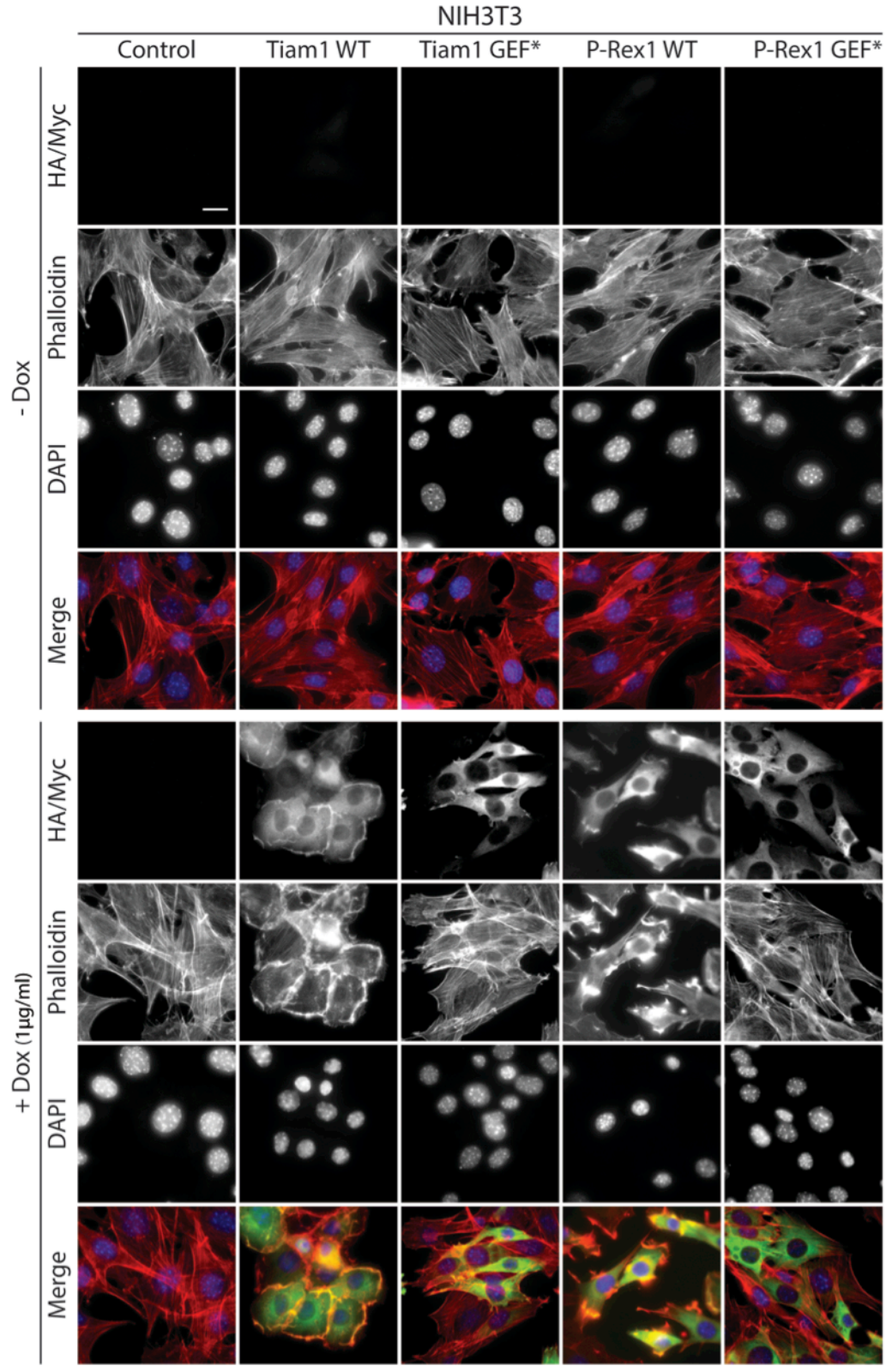

Figure 3.5: Ectopic Expression of Tiam1 and P-Rex1 Wild Type but not GEF-dead Mutant Proteins Induces Distinct Actin Cytoskeleton Rearrangements in NIH3T3 Cells

NIH3T3 cells harbouring the doxycycline (dox) inducible GEF expression system for wild type (WT) Tiam1 or P-Rex1 or their GEF-dead mutants (GEF*) were treated with ethanol (- dox) or 1µg/ml dox (+ dox) for 24 hours. Cells were then fixed in 4 % formaldehyde and stained with phalloidin to detect the actin cytoskeleton by immunofluorescence. Images were taken using the low light microscope system (100x magnification). Fluorescence markers against HA-tagged Tiam1 WT/GEF* or Myc-tagged P-Rex1 WT/GEF* were used to detect the expression of the respective GEFs upon dox induction. DAPI was used to stain the nuclei. Scale bar=20µM.

These observations validate the results from the previous section and indicate that Tiam1 and P-Rex1 induce differential morphological changes in NIH3T3 cells via influencing the actin cytoskeleton. Moreover, the inability of Tiam1 GEF* and P-Rex1 GEF* to induce actin cytoskeleton rearrangements compared to parental NIH3T3 cells stress the importance of Rac1 activation in mediating Tiam1 and P-Rex1- driven changes in the actin cytoskeleton.

3.2.1.6 Activation of Rac1 by Tiam1 and P-Rex1 Induces Differential Cellular Migration Rates in NIH3T3 Cells

Results outlined thus far supported the hypothesis that under the same cellular conditions, GEFs could influence GTPase signalling. It was therefore speculated that Tiam1 and P-Rex1 expression in this controlled cellular setting would induce distinct effects on the ability of Rac1 to regulate cellular migration.

To test this, the migration of ethanol (- dox) or 1 μg/ml dox (+ dox) treated NIH3T3 cells with the dox inducible GEF expression system was assessed using the Oris™ migration assay. Figure 3.6 A outlines the experimental setup for this assay. Migration of cells expressing the different GEF constructs was assessed by looking at migration of cells into the cell-free region created by the stoppers at 0 and 24 hours post stopper removal.

As can be seen from the representative fluorescence images shown in Figure 3.6 B, there is a similar migration rate after 24 hours of stopper removal in all – dox treated cells. Similarly, + dox treated parental NIH3T3 cells (control), Tiam1 GEF* and P-Rex1 GEF* expressing cells, all exhibited migration rates that were comparable to their – dox counterparts and to one another. In contrast, expression of Tiam1 WT in NIH3T3 cells, as predicted, was associated with a reduced migration ability when compared to parental NIH3T3 cells, the – dox treated cells, and other GEF expressing cells. In sharp contrast, the expression of P-Rex1 resulted in increased migratory potential of NIH3T3 cells.

The fluorescence images were also used to quantify the percent migration upon expression of the different GEFs using the equation outlined in section 2.7.3 and Figure 3.6 A. as demonstrated from the graph in Figure 3.6 C, there was no significant difference between the percent migration observed in all – dox treated cells as well as the control, Tiam1 GEF* and P-Rex1 GEF* + dox treated cells. Conversely, Tiam1 WT expression resulted in a significant ($p=0.01$) decrease in cellular migration by 32 % when compared to the – dox treated control cells and by 30 % when compared to the Tiam1 WT – dox treated cells. P-Rex1 WT expression, however, induced a significant ($p=0.004$) increase in the migration of cells by 22 % when compared to both the –dox control cells and the P-Rex1 WT – dox treated cells.

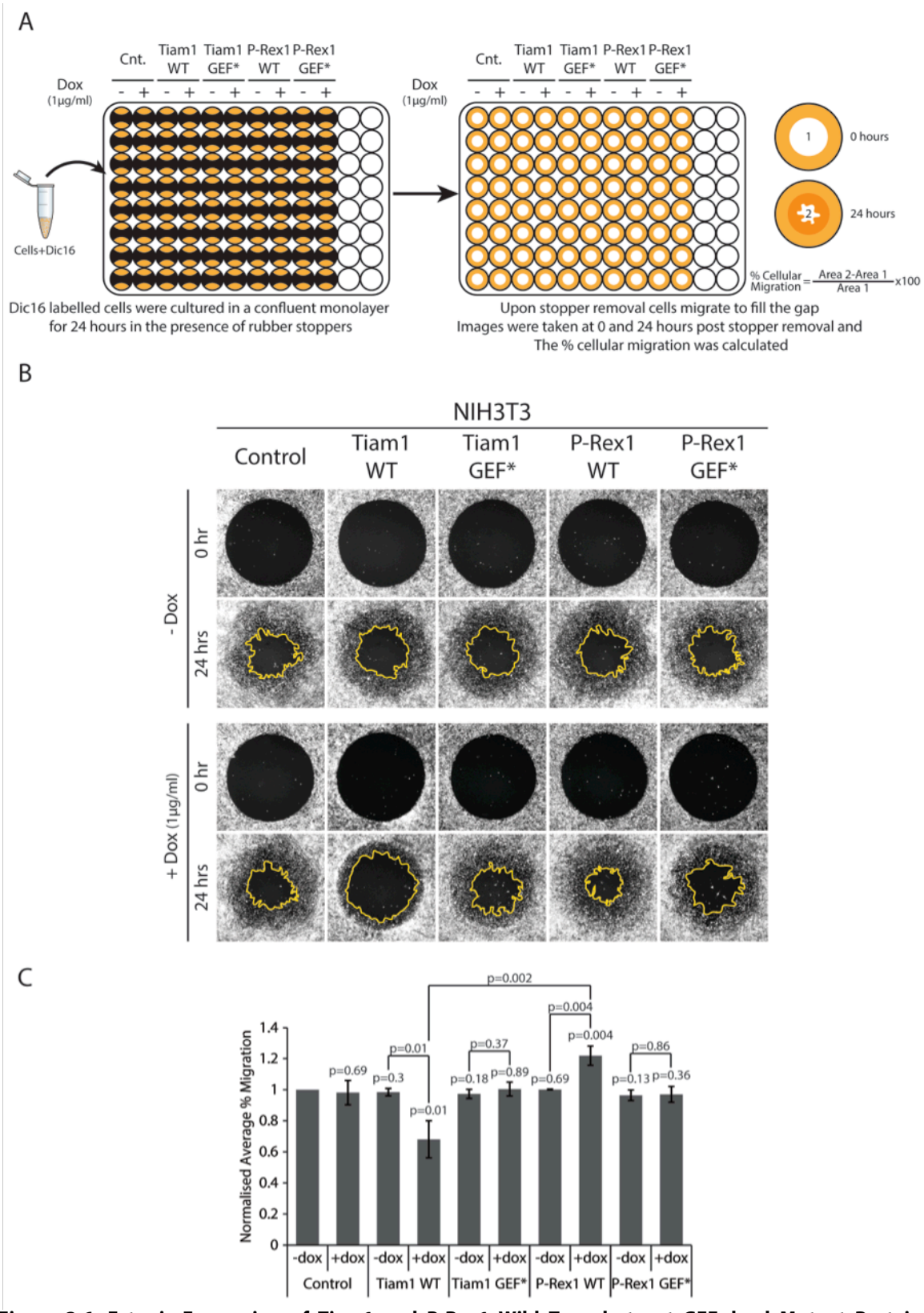

Figure 3.6: Ectopic Expression of Tiam1 and P-Rex1 Wild Type but not GEF-dead Mutant Proteins Induces Differential Migration rates in NIH3T3 Cells

(A) Schematic representation of the Oris™ Migration Assay experimental setup. (B) Parental and doxycycline (dox) inducible GEF expressing NIH3T3 cells were treated with ethanol (- dox) or 1µg/ml dox (+ dox) for 24 hours. The migration potential of - dox and + dox treated cells was then assessed using the Oris™ Migration Assay. Fluorescence images were taken using the low light microscopy system (5x magnification) at 0 hours and 24 hours post stopper removal. Representative images from three independent experiments. (C) Quantification of cellular migration of – dox and + dox treated cells normalised to parental - dox treated cells. Graphs represent the normalised average % migration ± standard error from three independent experiments. Student's t-test was used to assess significance between migration abilities within the different cells as indicated on the graph. p-values above each bar refer to significance values relative to the parental - dox treated cells. Other values shown refer to significance values between indicated pairs. p-values ≤ 0.05 are considered significant; ≤0.01 are considered highly significant.

3.2.1.7 Section Summary

Results outlined in this section highlight the efficiency of the generated dox inducible system by demonstrating that the system is tightly regulated with expression only occurring upon dox induction. Moreover, utilizing the PAK-CRIB pulldown assays, it was established that only Tiam1 WT and P-Rex1 WT activate Rac1 and that this activation is not extended to Cdc42. More importantly, via utilising this system, it was shown that under the same cellular conditions, Tiam1 WT and P-Rex1 WT induce distinct morphological phenotypes, cytoskeletal rearrangements, as well as differential migratory rates in NIH3T3 cells. Moreover, through using Tiam1 GEF* and P-Rex1 GEF* it was confirmed that these differential effects are mediated specifically through the ability of Tiam1 and P-Rex1 to activate Rac1, and thus suggest that they are Rac1 downstream effects. In conclusion, this section highlights the role of Tiam1 and P-Rex1 in dictating Rac1 downstream effects under the same cellular conditions in NIH3T3 cells.

3.2.2 Activation of Rac1 by Tiam1 and P-Rex1 Induces Differential Cellular Effects in a Cell-Type Independent Manner

As mentioned above, the cell type in which Rac1 is activated has been shown to contribute to the specificity of Rac1 downstream signalling. Therefore, it was important to evaluate whether the observed role of Tiam1 and P-Rex1 in dictating the Rac1 downstream cellular effects was restricted to the NIH3T3 cell line. To investigate this, the dox inducible GEF expression system was transduced in two additional cell lines, the MDCKII cell line and the epithelial squamous cell carcinoma A431 cell line.

This section highlights findings obtained from utilising the dox inducible GEF expression system in these two cell lines to evaluate the role of Tiam1 and P-Rex1 in influencing Rac1 effects in different cellular contexts.

3.2.2.1 Generation of Retroviral Doxycycline Inducible GEF Expression System in MDCKII Cells

Using a similar approach to the one described in section 2.2.4, the retroviral dox inducible system was transduced into MDCKII cells. In order to ensure a similar efficiency to that seen in NIH3T3 cells, the expression of the respective GEFs was evaluated using immunofluorescence and Western blot analysis, as described in Materials and Methods.

Using anti-HA and anti-Myc antibodies to detect the expression of Tiam1 and P-Rex1 constructs, respectively, the immunofluorescence images shown in Figure 3.7 A-D demonstrated that similar to the system in NIH3T3 cells, expression of the respective GEFs in the MDCKII cell line was also uniform across the selected pool and that it was restricted only to the + dox treated cells. This was further confirmed by Western blot analysis (Figure 3.7 E), which showed increased expression of the different GEF constructs upon addition of dox. Unlike, NIH3T3 cells, a modest increase in the levels of Tiam1 WT and P-Rex1 WT were observed in the respective – dox treated MDCKII cells suggesting that there is some basal protein expression

induction even in the absence of dox. However, it is important to note that the basal expression varied between batches of cells analysed and thus this background expression was not consistently observed. Additionally, the basal expression was not detectable by immunofluorescence, thus it was assumed that protein expression in the absence of dox is minimal particularly when compared to the expression induced in + dox treated cells.

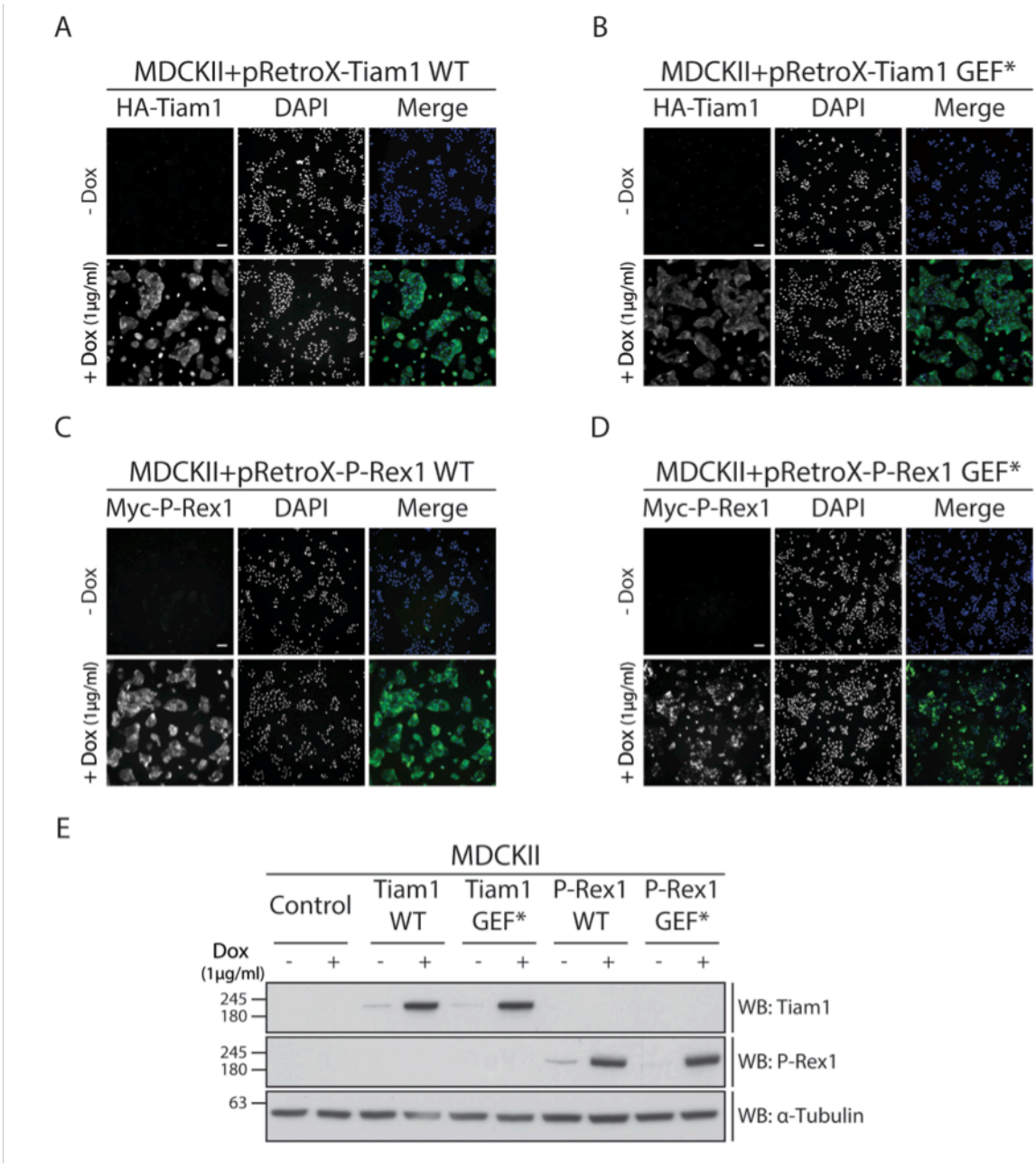

Figure 3.7: Generation of Retroviral Doxycycline Inducible GEF Expression System in MDCKII Cells
(A, B, C, D) MDCKII cells harbouring the doxycycline (dox) inducible system for the expression of wild type Tiam1 (pRetroX-Tiam1 WT), GEF-dead mutant Tiam1 (pRetroX-Tiam1 GEF*), wild type P-Rex1 (pRetroX-P-Rex1 WT) or GEF-dead mutant P-Rex1 (pRetroX-P-Rex1 GEF*) were treated with ethanol (- dox) or 1µg/ml dox (+ dox) for 24 hours, fixed in 4 % formaldehyde and markers against HA-tagged Tiam1 WT/GEF* or Myc-tagged P-Rex1 WT/GEF* were used for immunofluorescence. Images of – dox and + dox treated cells were taken using the low light microscope system (10x magnification), showing Tiam1 WT (A), Tiam1 GEF* (B), P-Rex1 WT (C) P-Rex1 GEF* (D) expression. Scale bar=100 µM. (E) MDCKII cells harbouring the dox inducible system were treated with - dox or + dox for 24 hours. Cells were harvested and expression levels of Tiam1 WT/GEF* and P-Rex1 WT/P-Rex1 GEF* were detected by Western blot using anti-Tiam1 and anti-P-Rex1 antibodies, respectively. α-Tubulin was used as a loading control.

3.2.2.2 *Ectopic Expression of Tiam1 and P-Rex1 Wild Type but not GEF-Dead Mutant Proteins Results in Elevated Levels of Active Rac1 in MDCKII Cells*

Upon generating the dox inducible GEF expression system in MDCKII cells, it was important to establish that upon expression, the different GEF constructs are also able to influence Rac1 activation in a similar way to that observed in NIH3T3 cells.

To evaluate the ability of each of the different GEF constructs to activate Rac1, MDCKII cells were treated with 1 μg/ml dox for 24 hours. Upon dox induction and the expression of the respective GEFs, cells were harvested and subjected to the PAK-CRIB pulldown of active Rac1. Levels of active Rac1 were detected by Western blot analysis.

As expected, Figure 3.8 demonstrates that activation of Rac1 was only observed upon expression of Tiam1 WT and P-Rex1 WT but not their GEF* mutants.

These results indicate that the GEF expression system functions in a similar way to that observed in NIH3T3 cells and can thus be used to investigate the role played by either GEF in dictating Rac1-specific downstream effects.

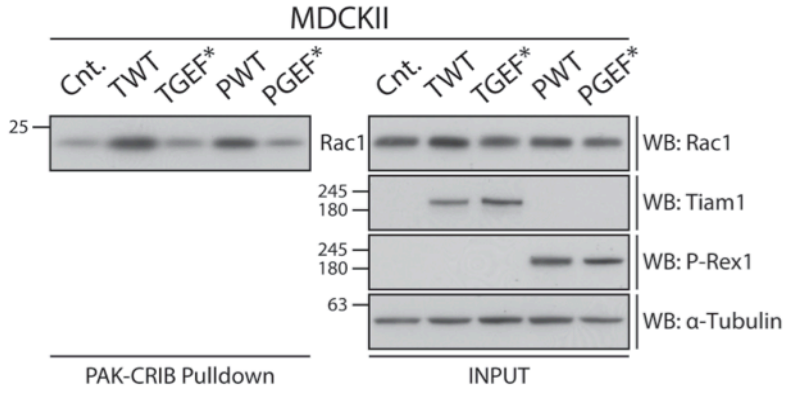

Figure 3.8: Ectopic Expression of Tiam1 and P-Rex1 Wild Type but not GEF-dead Mutant Proteins Results in Elevated Levels of Active Rac1 in MDCKII cells
MDCKII cells harbouring the doxycycline (dox) inducible system for the expression of wild type Tiam1 and P-Rex1 (TWT and PWT, respectively) or Tiam1 and P-Rex1 GEF-dead mutant (TGEF* and PGEF*, respectively) were treated with 1μg/ml dox for 24 hours. Cells were then harvested and subjected to a PAK-CRIB pulldown of active Rac1. Levels of active Rac1 were detected by Western blot analysis using anti-Rac1 antibody. Parental MDCKII cells (Cnt.) were used to evaluate basal levels of active Rac1 in MDCKII cells. α-Tubulin was used as a loading control. Representative Western blot from three independent experiments.

3.2.2.3 *Activation of Rac1 by Tiam1 and P-Rex1 Results in Distinct Morphological Phenotypes in MDCKII Cells*

Unlike the mesenchymal nature of NIH3T3 cells, MDCKII cells have a distinct epithelial morphology, growing in compact colonies under sub-confluent conditions. These cells, therefore, provided an alternative cellular system in which the role of Tiam1 and P-Rex1 in influencing Rac1 downstream functions could be assessed while still maintaining other factors that might contribute to differences in Rac1 downstream signalling.

MDCKII cells harbouring the dox inducible GEF expression system were plated at different densities and treated with ethanol (- dox) or dox (+ dox) for 24 hours. Changes in cellular morphologies were then observed upon expression of the different GEF constructs.

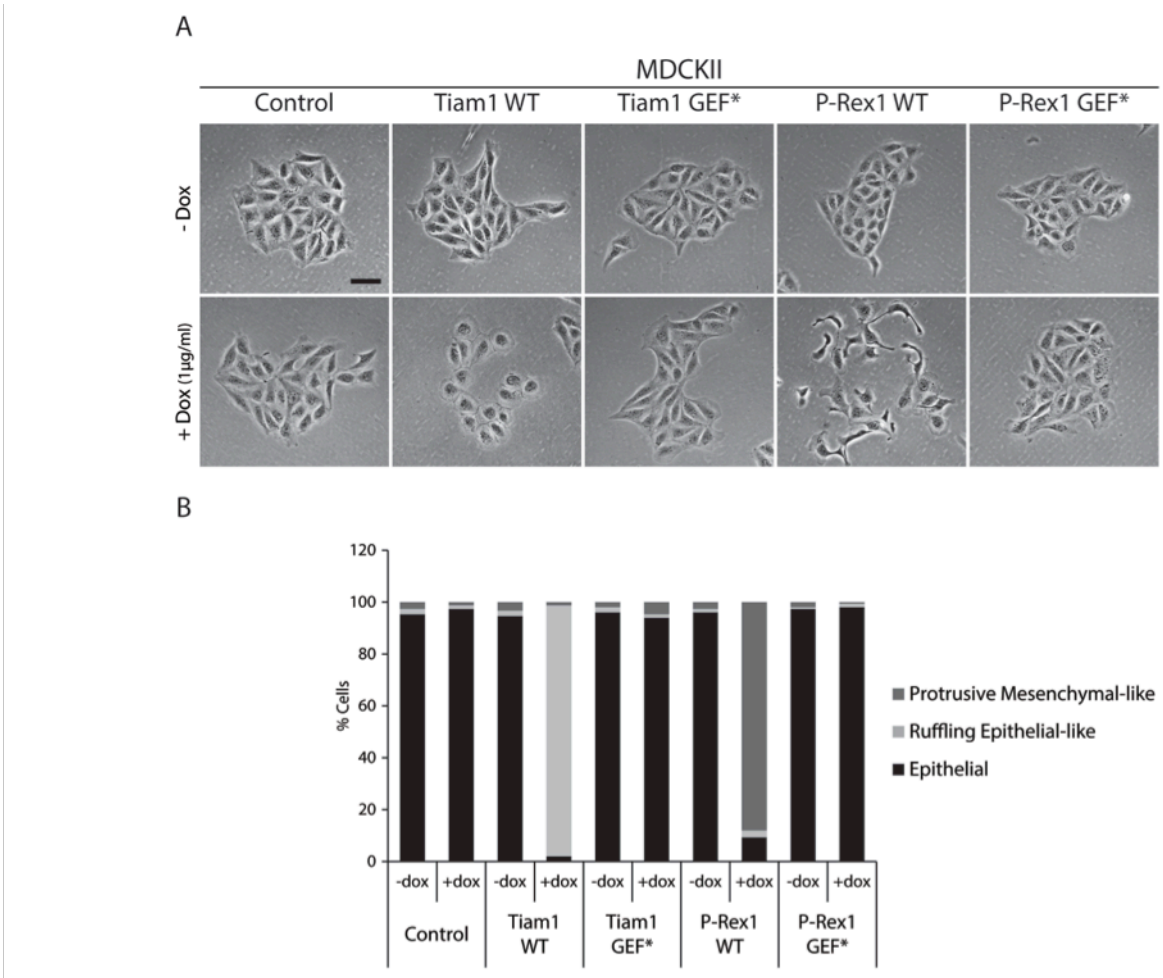

Figure 3.9: Ectopic Expression of Tiam1 and P-Rex1 Wild Type but not GEF-dead Mutant Proteins Induces Distinct Morphological Phenotypes in MDCKII Cells

(A) MDCKII cells harbouring the doxycycline (dox) inducible GEF expression system for wild type (WT) Tiam1 or P-Rex1 or their GEF-dead mutants (GEF*) were treated with ethanol (- dox) or 1µg/ml dox (+ dox) and phase-contrast images (10x) were taken using the Zeiss inverted microscope (Axiovert 2.5). Scale bar= 100µM. (B) To quantify the GEF induced cellular phenotypes, cells were classified into three groups based on their morphology as follows:
1) Epithelial, 2) Ruffling Epithelial-like and 3) Protrusive Mesenchymal-like Graph represents % cells in each subset from a total of 150 cells/condition from various cell passages.

As can be seen from the representative phase-contrast images shown in Figure 3.9 A, similar to NIH3T3 cells, expression of Tiam1 WT and P-Rex1 WT induced distinct morphological changes when compared to parental MDCKII cells (control) and to one another. Control cells as well as the – dox treated cells exhibited the characteristic MDCKII epithelial morphology. In contrast, ectopic expression of Tiam1 WT in MDCKII cells was associated with increased cellular ruffling and more defined cell-cell contacts. In addition, cells had a flattened morphology. Expression of P-Rex1 WT, on the other hand, resulted in the dissolution of cell-cell contacts and the promotion of a highly mesenchymal phenotype. Unlike cells expressing Tiam1 WT and P-Rex1 WT, cells with Tiam1 GEF* and P-Rex1 GEF* expression failed to induce any changes in the cellular morphology when compared to both parental MDCKII cells and their own – dox treated counterparts.

Using the criteria outlined in section 2.7.2 and classifying 150 cells/GEF into three groups based on their morphology as follows: 1) Epithelial, 2) Ruffling Epithelial-like and 3) Protrusive Mesenchymal-like confirmed that as expected, the majority of cells in parental MDCKII cells, both – dox (95.3 %) and + dox treated cells (97.3 %), exhibited the epithelial morphology. Similarly, expression of Tiam1 GEF* and P-Rex1 GEF* was associated with 94 % and 98 %, respectively, of cells under the epithelial category. This was consistent with their – dox treated counterparts with 96 % and 97.3 % of cells exhibiting the epithelial morphology for Tiam1 GEF* and P-Rex1 GEF* - dox treated cells, respectively. Although, Tiam1 WT expression in MDCKII cells was also associated with an epithelial phenotype, cells had a characteristic fattened morphology and membrane ruffling. As a result, Tiam1 WT expression was associated with a shift from the 94.7 % normal epithelial morphology observed in the – dox treated cells, to a 96.7 % ruffling epithelial-like phenotype. In contrast, P-Rex1 WT expression was associated with a shift from 96 % epithelial morphology in the – dox treated control to an 88 % of cells with a mesenchymal-like morphology with extending protrusions (Figure 3.9 B).

These results are in agreement with the observed role of Tiam1 and P-Rex1 in influencing the Rac1-driven cellular morphologies in NIH3T3 cells, indicating an ability of GEFs to influence morphology in a cell type independent manner.

3.2.2.4 Activation of Rac1 by Tiam1 and P-Rex1 Induces Distinct Actin Cytoskeleton Rearrangements in MDCKII Cells

Having demonstrated that similar to NIH3T3 cell, activation of Rac1 by Tiam1 and P-Rex1 in MDCKII cells was also associated with differential cellular morphologies, it was interesting to see if these changes were accompanied by distinct actin cytoskeleton rearrangements. Given the absence of a phenotype in Tiam1 GEF* and P-Rex1 GEF* expressing cells changes in the Rac1 downstream effects were only investigated in Tiam1 WT and P-Rex1 WT expressing cells in comparison with parental MDCKII cells.

MDCKII cells harbouring the dox inducible system for expressing Tiam1 WT and P-Rex1 WT were treated with ethanol (- dox) or 1 μg/ml dox (+ dox). After 24 hours of dox induction, cells were fixed in 4 % formaldehyde and phalloidin staining was used to visualise changes in the actin cytoskeleton. As illustrated in Figure 3.10 the phalloidin staining observed in – dox treated Tiam1 WT and P-Rex1 WT cells was similar to that seen in parental MDCKII – dox and + dox treated cells. In these cells, the actin structures supported the epithelial nature of the MDCKII colonies with a modest actin localisation at cell-cell contacts. In contrast, expression of Tiam1 WT resulted in increased localisation of actin at cell-cell contacts. This is in agreement with the phase-contrast images shown in Figure 3.9 A where cell-cell contacts appeared more established when compared to parental MDCKII cells. In order to accurately assess the effect of P-Rex1 WT expression on actin cytoskeleton rearrangement and actin localisation, colonies with varying P-Rex1 WT expression were examined.

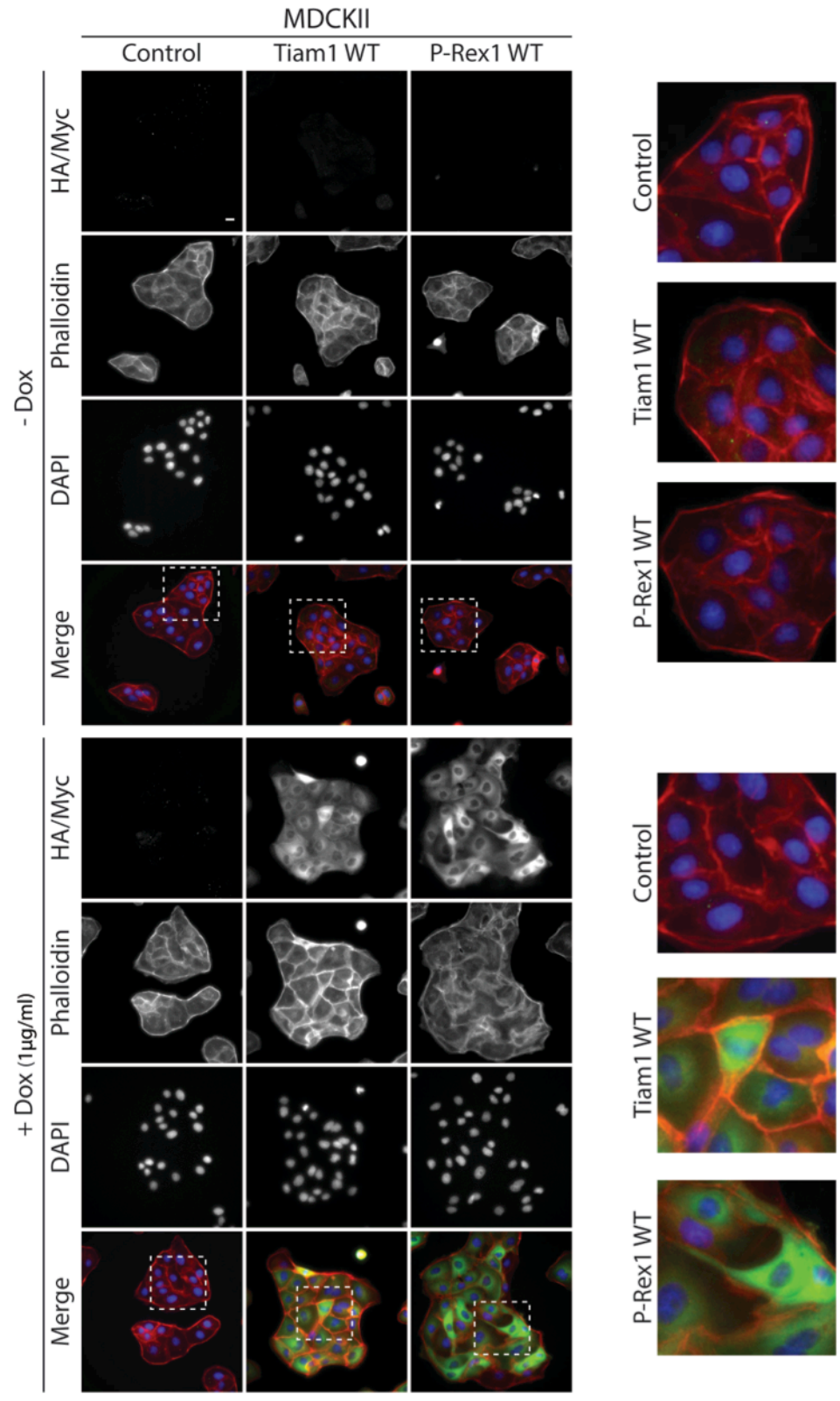

Figure 3.10: Ectopic Expression of Tiam1 and P-Rex1 Wild Type but not GEF-dead Mutant Proteins Induces Distinct Actin Cytoskeleton Rearrangements in MDCKII Cells

Parental MDCKII cells, or cells harbouring the doxycycline (dox) inducible system for wild type (WT) expression of Tiam1 and P-Rex1, were treated with ethanol (- dox) or 1µg/ml dox (+ dox) for 24 hours. Cells were then fixed in 4 % formaldehyde and stained with phalloidin to detect the actin cytoskeleton by immunofluorescence. Images were taken using the low light microscope system (40x magnification). Fluorescence markers against HA-tagged Tiam1 WT or Myc-tagged P-Rex1 WT were used to detect the expression of the respective GEFs upon dox induction. DAPI was used to stain the nuclei. Scale bar=20µM. Enlarged images are from the sections enclosed within the white dashed boxes.

As shown in Figure 3.10 in cells in which anti-Myc staining is higher, the actin cytoskeleton is reorganised forming elongated membrane protrusions at the extremities of cells. Whereas cells with lower P-Rex1 WT expression, although still exhibiting distorted actin staining, possessed actin structures that are more similar to the parental MDCKII cells. The enlarged images in Figure 3.10 highlight these differential actin cytoskeleton rearrangements, with Tiam1 WT increasing the localisation of actin at cell-cell contacts, further enhancing the epithelial morphology of MDCKII cells; whereas P-Rex1 WT expression inducing the formation of membrane extensions while reducing cell-cell contact associated actin when compared to –dox treated cells and parental MDCKII cells. These results show that the Tiam1 WT and P-Rex1 WT induced morphological changes are associated with their ability to influence cytoskeleton changes.

3.2.2.5 Activation of Rac1 by Tiam1 and P-Rex1 Induces Differential Effects on Cell-Cell Contacts in MDCKII Cells

Adherens junctions and tight junctions are known to associate with the actin cytoskeleton to establish cell-cell contacts in epithelial cells (Matter and Balda, 2003). Thus following the observation that Tiam1 WT and P-Rex1 WT induced distinct morphological changes that were associated with altered actin localisation, the integrity of cell-cell contacts was assessed upon expression of either GEF.

To evaluate the role of Tiam1 and P-Rex1 on adherens junctions, the scattering ability of MDCKII cells upon stimulation with HGF was examined. HGF is a potent inducer of cell scattering and was shown to function through binding to its receptor cMet inducing a multitude of downstream signalling cascades, which ultimately promote EMT (Park et al., 1986; Stoker et al., 1987). For example, Fujita et al. has shown that HGF promotes the dissolution of cell-cell contacts via targeting E-cadherin for ubiquitylation and endocytosis (Fujita et al., 2006).

HGF can also stimulate cellular scattering by remodelling the ECM through promoting the expression of uPA(Moriyama et al., 1999; Nishimura et al., 2003a). Additionally, HGF can act through Stat3 (Syed et al., 2011), which is known to regulate the expression and release of MMP, allowing HGF to modulate ECM remodelling (Dechow et al., 2004; Itoh et al., 2006; Xie et al., 2004). Interestingly, HGF has also been shown to regulate cellular migration and invasion directly and indirectly, through Stat3, via activating Rac1 and Cdc42 to induce rearrangements in the actin cytoskeleton, thus promoting the formation of lamellipodia and filopodia, respectively (Ridley et al., 1995; Royal et al., 2000; Teng et al., 2009). Figure 3.11 A highlights the signalling pathways downstream of HGF that stimulate cellular scattering. The effect of HGF on MDCKII parental cells is also demonstrated experimentally in Figure 3.11 B via phase-contrast images at 0, 3 and 24 hours post HGF treatment. As illustrated by these images, MDCKII colonies respond to HGF treatment with initial cellular spreading (between 0 and 3 hours) that precedes cellular scattering. It must be noted that cellular scattering is observed at time points

as early as 6 hours post HGF treatment; however after 24 hours the majority of cells are expected to have undergone the transformations necessary for full cellular scattering.

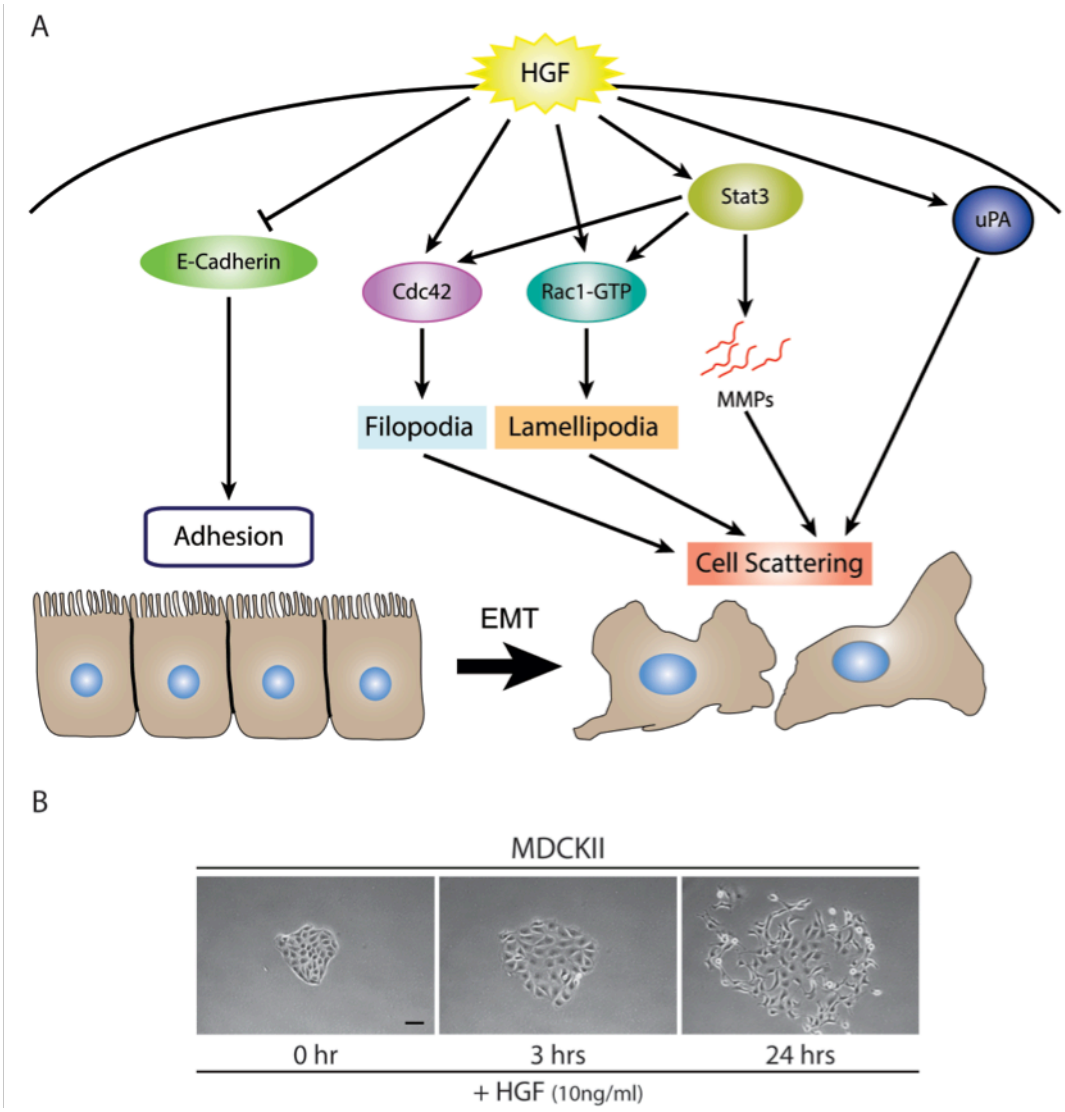

Figure 3.11: Schematic Representation of HGF Signalling in Cells
(A) Schematic representation of Hepatocyte Growth Factor (HGF) signalling cascade in cells. Upon binding of HGF to its receptor cMet, several signalling cascades are induced in the cell leading to weaker cell-cell contacts, through inhibiting E-cadherin, and actin cytoskeleton rearrangements, through activating Rac1 and Cdc42. This ultimately causes the cells to undergo epithelial mesenchymal transition (EMT). This together with the increased release of metalloproteinases (MMPs) increases the scattering, migratory and invasive potential of the cells. (B) Parental MDCKII cells were used to demonstrate the effect of HGF treatment on cell scattering. Phase contrast images were taken at 0 hour, 3 hours and 24 hours post HGF treatment using the Zeiss inverted microscope (Axiovert 2.5). Scale bar= 100µM. Figure formulated based on literature review presented in section 3.2.2.5.

Given the established response of MDCKII cells to HGF treatment, MDCKII cells harbouring the dox inducible GEF expression system were used to investigate the role of Tiam1 and P-Rex1 in influencing HGF-induced cellular scattering. Scattering was evaluated in untreated (- HGF) or 10 ng/ml HGF (+ HGF) treated cells by taking phase-contrast images at 0, 3 and 24 hours post HGF treatment.

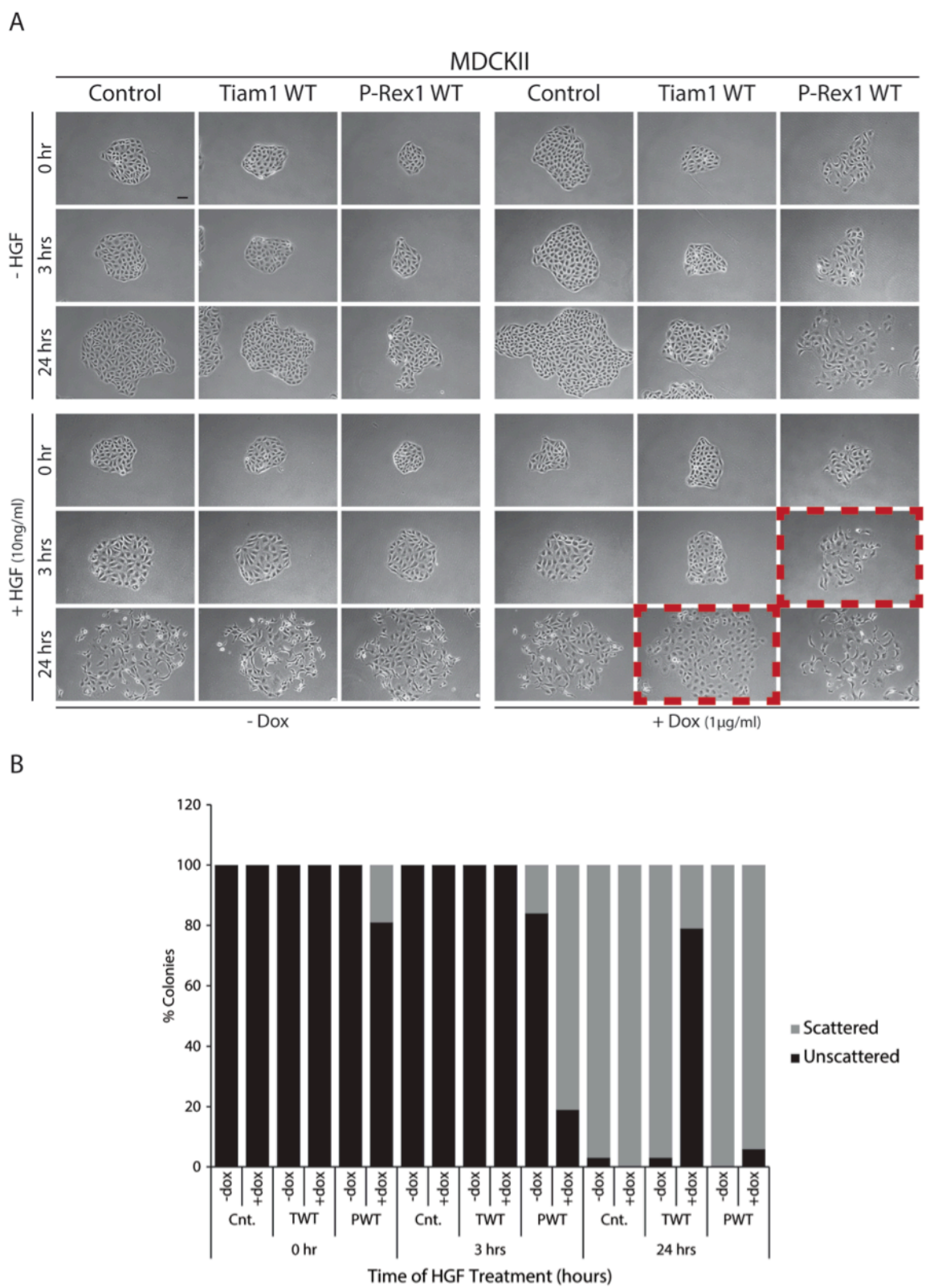

Figure 3.12: Ectopic Expression of Tiam1 and P-Rex1 Wild Type but not GEF-dead Mutant Proteins Induces Differential Scattering Abilities in MDCKII Cells

(A) MDCKII cells harbouring the doxycycline (dox) inducible system for expressing wild type (WT) Tiam1 and P-Rex1 were used to assess the role of either GEF on Rac1-driven cellular scattering upon treatment with Hepatocyte Growth Factor (HGF) in cells treated with ethanol (- dox) or 1µg/ml dox (+ dox). Phase contrast images were taken at 0 hour, 3 hours and 24 hours post HGF treatment using the Zeiss inverted microscope (Axiovert 2.5). Scale bar= 100µM. (B) Quantification of HGF-induced cell scattering (n=50 colonies/condition). MDCKII colonies were examined and classified depending the number of cells within each colony that are still in contact. Colonies with ≤ 3 cells in contact were considered scattered colonies. Graphs represent averages of % colonies from three independent experiments.

As expected, parental MDCKII - dox and + dox treated cells, responded similarly to cells shown in Figure 3.11 B, with cells spreading by 3 hours and complete cellular scattering observed by 24 hours. Similarly the – dox treated cells for Tiam1 WT and P-Rex1 WT showed a similar HGF response to parental MDCKII cells. Unlike the – dox treated counterparts, MDCKII cells expressing Tiam1 WT showed minimal cellular scattering even by 24 hours post HGF treatment; however the ability of cells to spread was not affected. This suggests that Tiam1 impedes HGF-induced cell scattering via enhancing cell-cell contacts. In contrast, ectopic expression of P-Rex1 WT led to a striking increase in the HGF-induced cellular scattering, where colonies were completely scattered after only 3 hours of HGF treatment. To ensure that this was not solely due to the previously highlighted role of P-Rex1 WT in promoting a mesenchymal phenotype in MDCKII cells as shown in section 3.2.2.3, colonies with lower P-Rex1 WT expression, reflected in their ability to form cell-cell contacts, were selected for this assay (Figure 3.12 A).

The HGF-induced cellular scattering mediated by Tiam1 WT and P-Rex1 WT was quantified as outlined in section 2.7.4. As shown in Figure 3.12 B, at 0 hours post HGF treatment, all – dox treated cells as well as cells expressing Tiam1 WT had no scattered colonies. Expression of P-Rex1 WT, on the other hand, even at 0 hour results in 19 % of colonies to scatter, which increased to 81 % at 3 hour, whereas no cellular scattering was observed in parental MDCKII cells, P-Rex1 WT- dox treated cells and cells expressing Tiam1 WT. At 24 hours post HGF treatment, parental MDCKII cells, - dox treated cell and cells expressing P-Rex1 WT had minimal unscattered colonies. Tiam1 WT expression, in contrast, was associated with 79 % colonies in the unscattered category. These results are consistent with the actin localisation observations highlighted earlier and both suggest that Tiam1 WT and P-Rex1 WT can differentially regulate adherens junctions, thereby affecting the HGF-induced cellular scattering ability in these cells.

In addition to adherens junctions, tight junction are also linked to the actin cytoskeleton. It has recently been shown by our laboratory that Tiam1 WT expression impedes the proper formation of tight junctions due to a disruption in the apical-basal gradient of active Rac1 in the cell (Mack et al., 2012). It was therefore intriguing to examine whether ectopic expression of P-Rex1 WT also resulted in disruptions of tight junction assembly.

The Transepithelial Electrical Resistance (TER) cell-cell adhesion assay described in section 2.7.5 and outlined in Figure 3.13 A was used to assess the ability of Tiam1 WT and P-Rex1 WT to regulate tight junction formation in MDCKII cells. As demonstrated from the graphs presented in Figure 3.13 B there was minimal variation between the TER readings associated with all – dox treated cells. In contrast, tight junction formation in Tiam1 WT expressing cells was greatly hindered as indicated by the lower resistance across the contacts of cells. In addition there was a delay in the characteristic surge of resistance upon re-addition of calcium suggesting a delay in the formation of the junctions. Similarly, P-Rex1 WT expression was also associated with a reduction and delay in TER peak upon the re-addition of calcium; however

unlike, Tiam1 WT, cells expressing P-Rex1 WT had an even lower peak that barely exceeded the initial basal reading. These results suggest that, similar to Tiam1 WT, P-Rex1 WT is also associated with disruptions in tight junction formation; however the lower TER readings might indicate that this occurs through a different mechanism than the disruption of active Rac1 across the apical-basal membrane. Instead this could highlight a different role played by P-Rex1 in regulating tight junctions. It would also be important to couple TER readings with experiments aimed at understanding the role of Tiam1 and P-Rex1 in regulating E-cadherin meditated cell junctions in MDCKII cells, as differential regulation of E-cadherin localisation, might also contribute to differences in TER readings.

Taken together, results from this subsection show a differential role of Tiam1 and P-Rex1 in regulating cell-cell contacts, specifically adherens junctions, in MDCKII cells. This, as a result, can then affect other Rac1-driven cellular effects, such as cellular scattering.

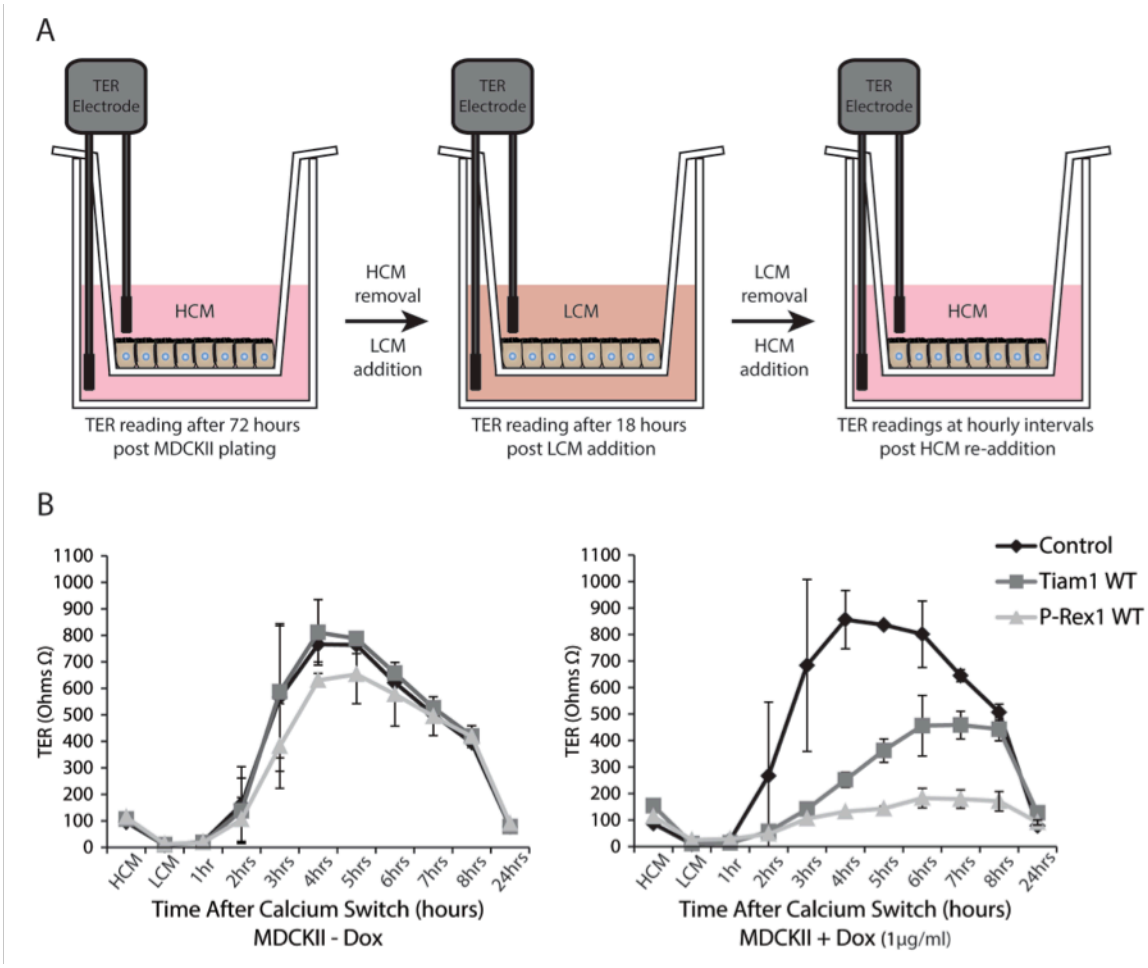

Figure 3.13: Ectopic Expression of Tiam1 and P-Rex1 Wild Type Proteins Results in Disruption of Tight Junction Formation in MDCKII cells

(A) Schematic representation of experimental setup for measuring the Transepithelial Electrical Resistance (TER) across a monolayer of MDCKII cells (B) parental MDCKII cells and harbouring the doxycycline (dox) inducible system for expressing wild type (WT) Tiam1 and P-Rex1 were plated in a confluent monolayer onto Transwell® permeable supports (12 mm, 0.4 μM pore size). Media was changed the following day and cells were left incubating for 72 hours with ethanol (- dox) or 1μg/ml dox (+ dox). TER was then measured in ohms using an EVOM2 epithelial volthometer with STX-2 electrodes to give the basal reading in media containing high calcium (HCM). The cell monolayer in the different wells was then washed and low calcium medium (LCM) was added to the filters and wells overnight to disassemble cell-cell junctions. TER was measured after 18 hours in LCM. The LCM was then removed and replaced with HCM. TER readings were subsequently taken at hourly intervals to monitor the reformation of cellular tight junctions and at 24 hours after calcium re-addition. Graphs represent average TER readings minus the basal TER reading (calculated from an empty filter containing media) from three independent experiments ± standard error.

3.2.2.6 *Activation of Rac1 by Tiam1 and P-Rex1 Induces Differential Cellular Migration Rates in MDCKII Cells*

Given that MDCKII and NIH3T3 cells represent two distinct cell types with different cellular architectures, the migration ability of MDCKII cells upon expression of either Tiam1 WT or P-Rex1 WT was assessed to evaluate their role in dictating differential migration patterns in a different cellular context.

As can be seen from Figure 3.14, using the Oris™ migration assay, all – dox treated cells together with the + dox treated parental MDCKII cells exhibited similar migration rates with no significant differences as indicated by Student's t-test and the associated p-value shown on the graph in Figure 3.14 B. In contrast, expression of Tiam1 WT in MDCKII cells resulted in a significant reduction (p=0.001) in the ability of cells to migrate by 20 % when compared to parental MDCKII cells and 15 % when compared to the Tiam1 WT – dox treated cells. Conversely, P-Rex1 WT expression in MDCKII cells, similar to NIH3T3 cells, was associated with a significant increase (p=0.001) in cellular migration by 27 % when compared to the parental – dox treated cells, or 20 % when compared to P-Rex1 WT – dox treated.

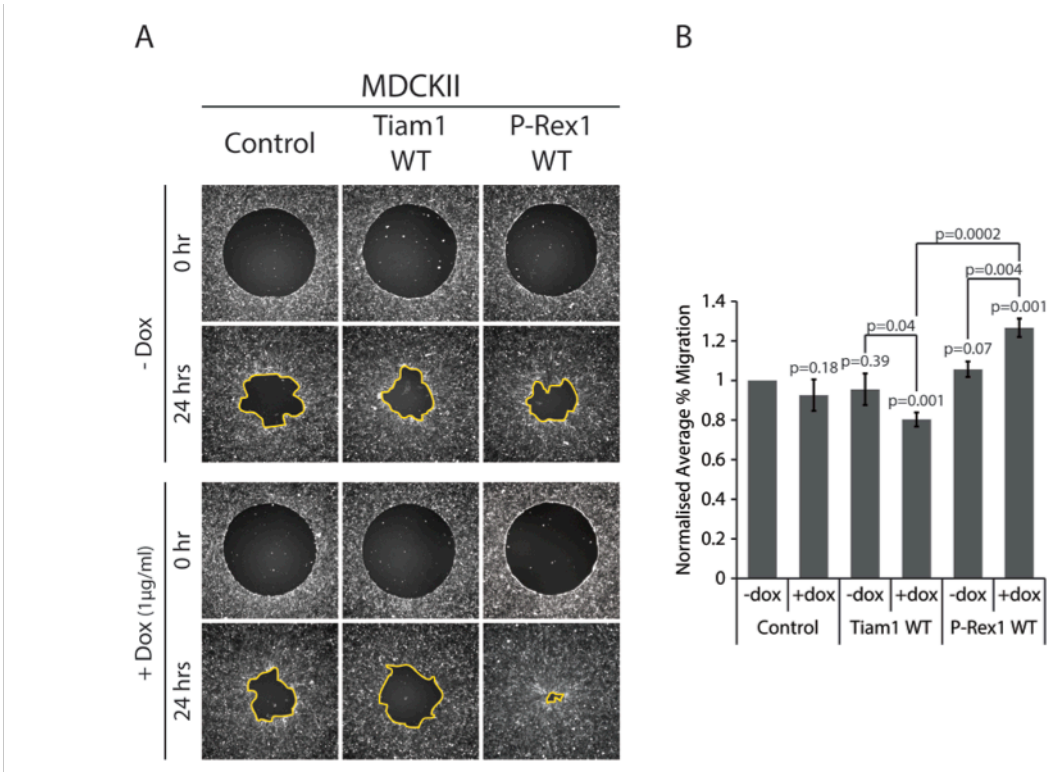

Figure 3.14: Ectopic Expression of Tiam1 and P-Rex1 Wild Type Proteins Induces Differential Cellular Migration rates in MDCKII Cells

(A) Parental MDCKII cells and cells harbouring the doxycycline (dox) inducible system for expressing wild type (WT) Tiam1 and P-Rex1 were treated with ethanol (- dox) or 1µg/ml dox (+ dox) for 24 hours. The migration potential of - dox and + dox treated cells was then assessed using the Oris™ Migration Assay. Fluorescence images were taken using the low light microscopy system (5x magnification) at 0 hour and 24 hours post stopper removal. (B) Quantification of cellular migration of – dox and + dox treated cells normalised to parental - dox treated cells. Graphs represent the normalised average % migration ± standard error from three independent experiments. Student's t-test was used to assess significance between migration abilities within the different cells as indicated on the graph. p-values above each bar refer to significance values relative to the parental - dox treated cells. Other values shown refer to significance values between indicated pairs. p-values ≤ 0.05 are considered significant; ≤0.01 are considered highly significant.

These results suggest that despite differences in the cellular architecture between NIH3T3 cells and MDCKII cells, expression of Tiam1 and P-Rex1, and the subsequent activation of Rac1, can drive similar cellular processes that govern the Rac1 anti- or pro-migratory effects in different cell types.

3.2.2.7 Generation of Retroviral Doxycycline Inducible GEF Expression System in A431 Cells

Upon confirming that activation of Rac1 by Tiam1 and P-Rex1 results in distinct cellular effects downstream of Rac1 and that these effects can be mediated in different cellular type settings, it was important to establish whether these GEF-induced differential effects are also observed in cancer cell lines.

The epithelial squamous-cell carcinoma A431 cell line provided a good system for such analysis. Firstly, A431 cells are epithelial in nature forming colonies under normal conditions. Therefore, the integrity of cell-cell contacts upon expression of either GEF can be readily examined in A43 cells. Secondly, A431 cells have been reported to have elevated levels of EGFR and therefore utilized to study signalling pathways initiated in response to the EGF-EGFR binding (Buss et al., 1982). This is particularly useful in understanding the role of Tiam1 and P-Rex1, in EGF-induced cellular responses that stimulate cellular migration and invasion. Lastly, through routine cancer cell line screening conducted in our laboratory, A431 cells were found to express minimal levels of endogenous Tiam1 and P-Rex1; however they contained moderate levels of Rac1. It was thus hypothesised that ectopic expression of either GEF in A431 cells could mimic the overexpression observed in some cancers and thus could be used to investigate the potential regulation of Rac1 in a cancer-like setting.

To determine this, the retroviral dox inducible systems for expressing the WT and GEF* mutant forms of Tiam1 and P-Rex1 were introduced into A431 cells. After antibiotic selection to generate a pool with the required plasmids, expression of the respective GEFs was evaluated using immunofluorescence and Western blot analysis. As shown in Figure 3.15, expression of the respective GEFs was uniform across the selected pool only observed upon dox induction. Similarly, the GEF expression was only detected in + dox treated cells using Western blot analysis. Moreover, as can be seen in Figure 3.15 E, despite using anti-Tiam1 and anti-P-Rex1 antibodies, which can normally detect both endogenous and exogenous proteins, no signal was observed in parental A431 cells or in – dox treated control cells. These results demonstrate that the dox inducible GEF expression system is highly efficient and selective only to dox induction, allowing the use of the system to further investigate the role of Tiam1 and P-Rex1 in dictating the downstream effects of Rac1 in a cancer cell line.

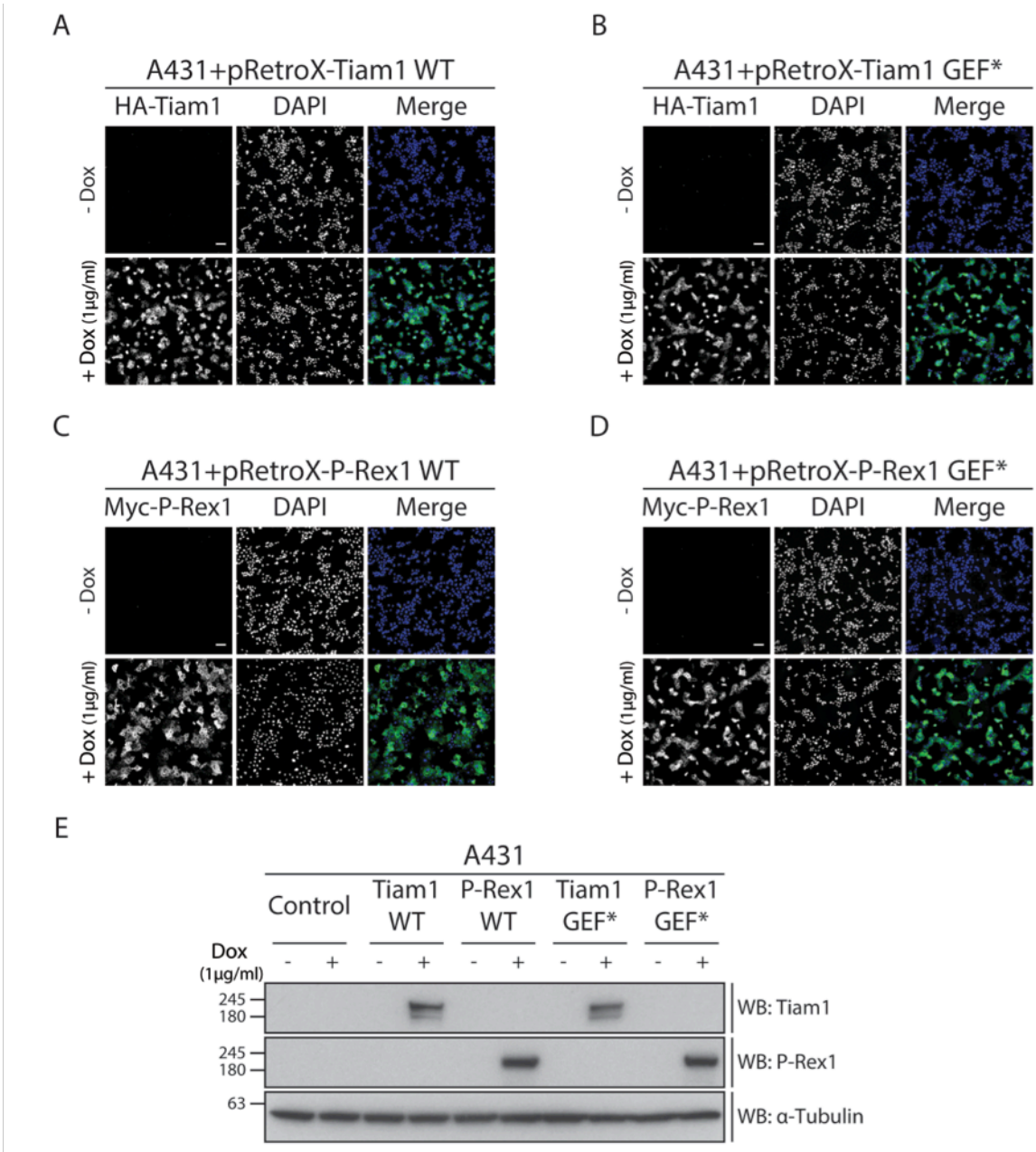

Figure 3.15: Generation of Retroviral Doxycycline Inducible GEF Expression System in A431 Cells
(A, B, C, D) A431 cells harbouring the doxycycline (dox) inducible system for expressing wild type (WT) Tiam1 and P-Rex1 or their GEF-dead mutants (GEF*) were treated with ethanol (- dox) or 1µg/ml dox (+ dox) for 24 hours. Cells were then fixed in 4 % formaldehyde and fluorescence markers against HA-tagged Tiam1 WT/GEF* or Myc-tagged P-Rex1 WT/GEF* were used. Immunofluorescence images of – dox (upper panel) and + dox treated cells (lower panel) were taken using the low light microscope system (10x magnification), showing Tiam1 WT (A), Tiam1 GEF* (B), P-Rex1 WT (C) P-Rex1 GEF* (D) expression. Scale bar=100 µM. (E) Parental A431 cells and cells harbouring the dox inducible GEF expression system were treated with - dox or + dox for 24 hours. Cells were harvested and expression levels of Tiam1 WT/GEF* and P-Rex1 WT/P-Rex1 GEF* were detected by Western blot analysis using anti-Tiam1 and anti-P-Rex1 antibodies, respectively. α-Tubulin was used as a loading control.

3.2.2.8 Ectopic Expression of Tiam1 and P-Rex1 Wild Type but not GEF-Dead Mutant Proteins Results in Elevated Levels of Active Rac1 in A431 Cells

As demonstrated in Figure 3.15 E, Tiam1 and P-Rex1 are not expressed on an endogenous level in A431 cells. It was, therefore, essential to confirm that ectopic expression of the WT GEFs but not their GEF* mutants would result in increased levels of active Rac1.

To assess the effect of expressing the respective GEFs on the levels of active Rac1, A431 cells harbouring the dox inducible GEF expression system were treated with 1 µg/ml dox for 24

hours. Cells were then harvested and subjected to the PAK-CRIB peptide to pulldown active Rac1. As illustrated in Figure 3.16 expression of both Tiam1 WT and P-Rex1 WT was associated with increased levels of active Rac1 when compared to parental A431 cells (Cnt.). On the other hand, expression of Tiam1 GEF* and P-Rex1 GEF* failed to induce Rac1 activation, consistent with findings observed in NIH3T3 and MDCKII cells.

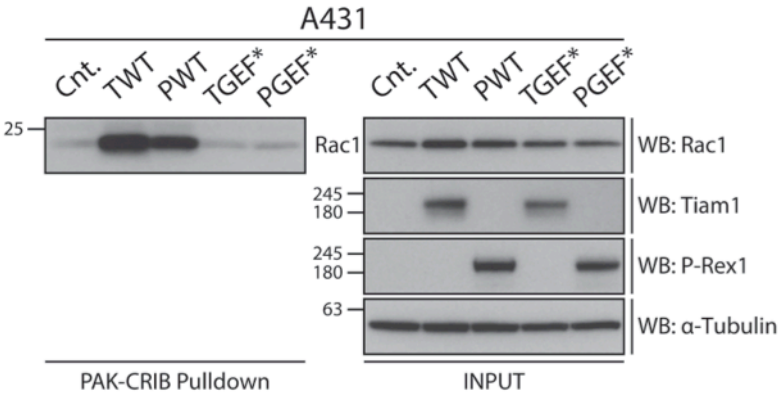

Figure 3.16: Ectopic expression of Tiam1 and P-Rex1 Wild Type but not GEF-dead Mutant Proteins Results in Elevated Levels of Active Rac1 in A431 cells
Parental A431 cells and cells harbouring the doxycycline (dox) inducible system for the expression of wild type Tiam1 and P-Rex1 (TWT and PWT, respectively) or Tiam1 and P-Rex1 GEF-dead mutant (TGEF* and PGEF*, respectively) were treated with 1μg/ml dox for 24 hours. Cells were then harvested and subjected to a PAK-CRIB pulldown of active Rac1. Levels of active Rac1 were detected by Western blot analysis using anti-Rac1 antibody. Basal levels of active Rac1 in parental MDCKII cells (Cnt.) were used as a reference for active Rac1 levels induced upon GEF overexpression. α-Tubulin was used as a loading control. Representative Western blot from three independent experiments.

Together these results indicate, that despite the lack of endogenous Tiam1 and P-Rex1, activation of Rac1 is stimulated upon ectopic expression of the WT form of either protein. Also given their inability to activate Rac1, the use of GEF* mutants can help eliminate any effects that might be due to the increased expression of proteins that A431 cells normally lack.

3.2.2.9 Activation of Rac1 by Tiam1 and P-Rex1 Induces Distinct Morphological Phenotypes in A431 Cells

Given the increase in levels of active Rac1 upon expression of Tiam1 WT and P-Rex1 WT in A431 cells, the system was used to evaluate the role of either GEF in dictating Rac1-driven cellular morphologies as conducted for NIH3T3 and MDCKII cells.

As shown in Figure 3.17 A, similar to MDCKII cells, parental A431 cells together with the – dox treated cells exhibited a characteristic epithelial morphology. Moreover, expression of Tiam1 GEF* and P-Rex1 GEF* did not induce any changes in this epithelial morphology. In contrast, Tiam1 WT expression in A431 cells was associated with increased membrane ruffling and a flattened cell surface. P-Rex1 WT ectopic expression, on the other hand, despite not completely disrupting cell-cell contacts, it stimulated the formation of thin membrane protrusions even in cells within the main body of the colony. These morphological changes were quantified as described in section 2.7.2. As illustrated in Figure 3.17 B, Tiam1 WT expression resulted in as shift from the characteristic epithelial morphology associated with

parental A431 cells to 98.7 % of cells exhibiting the epithelial-like, yet ruffling and flattened morphology. This shift was not observed in the Tiam1 WT – dox treated cells in which 94.7 % of cells had a normal epithelial morphology. In contrast, P-Rex1 WT expression was associated with 90 % of cells falling under the protrusive mesenchymal-like category, which was not seen in P-Rex1 WT – dox treated cells with 98 % of cells with epithelial morphology. Unlike, Tiam1 WT and P-Rex1 WT expression, the majority of cells expressing Tiam1 GEF* (98 %) or P-Rex1 GEF* (97.3 %) exhibited the normal morphology. This was similar to their – dox counterparts with 92.7 % and 95.3 % of cells under the normal category in – dox treated Tiam1 GEF* and P-Rex1 GEF*, respectively. These results demonstrate that activation of Rac1 is required in order for Tiam1 and P-Rex1 to induce distinct morphological changes in A431 cells.

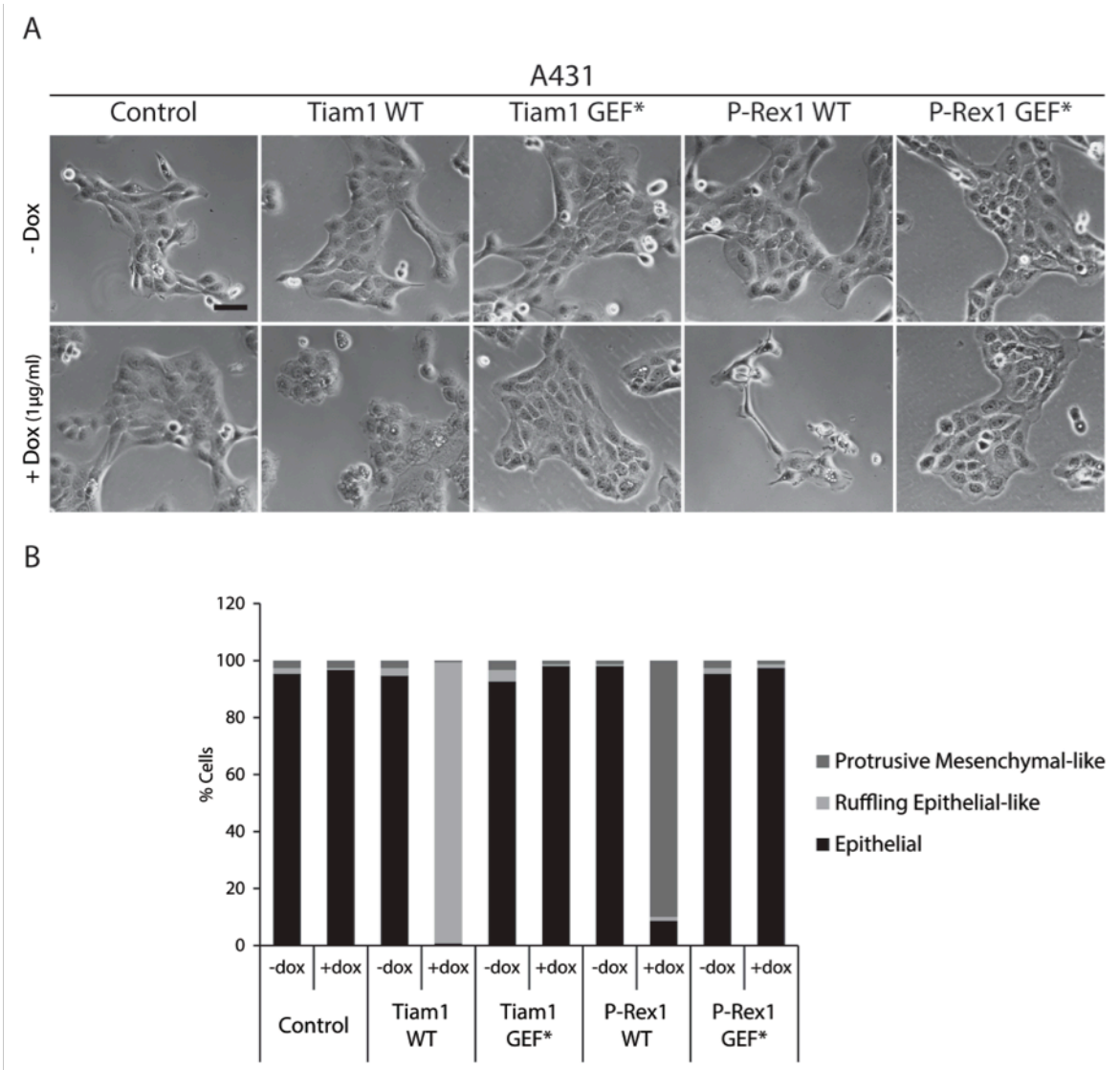

Figure 3.17: Ectopic Expression of Tiam1 and P-Rex1 Wild Type but not GEF-dead Mutant Proteins Induces Distinct Morphological Phenotypes in A431 Cells

(A) A431 cells harbouring the doxycycline (dox) inducible system for expressing wild type (WT) Tiam1 and P-Rex1 or their GEF-dead mutants (GEF*) were treated with ethanol (- dox) or 1µg/ml dox (+ dox) and phase-contrast images (10x) were taken using the Zeiss inverted microscope (Axiovert 2.5). Scale bar= 100µM. (B) To quantify the GEF induced cellular phenotypes, cells were classified into three groups based on their morphology as follows:
1) Epithelial, 2) Ruffling Epithelial-like and 3) Protrusive Mesenchymal-like Graph represents % cells in each subset from a total of 150 cells/condition from various cell passages.

3.2.2.10 Activation of Rac1 by Tiam1 and P-Rex1 Induces Distinct Actin Cytoskeleton Rearrangements in A431 Cells

Given the results outlined earlier from the NIH3T3 and MDCKII cells together with the distinct morphological changes observed in A431 cells upon expression of Tiam1 WT and P-Rex1 WT, it was hypothesized that expression of either GEF will also induce differential actin cytoskeleton rearrangements in A431 cells. Therefore, the actin cytoskeleton was visualised by immunofluorescence with representative images illustrated in Figure 3.18. As expected, parental A431 cells as well as the – dox treated cells exhibited very similar actin localisation, with actin staining present in both the cytoplasm and also localised at cell-cell contacts. Expression of Tiam1 WT resulted in a greater increase in the actin staining at cell-cell contacts, suggesting stronger cellular adhesions. Unlike Tiam1 WT, expression of Tiam1 GEF* did not induce the localisation of actin at cell-cell contacts. Similarly, P-Rex1 WT expression was not associated with increased actin staining at cell-cell contacts. Instead, P-Rex1 WT expression resulted in actin cytoskeleton rearrangements that induced the formation of membrane protrusions, even in cells expressing low levels of P-Rex1 WT. P-Rex1 GEF* expression, on the other hand, did not stimulate changes in the actin cytoskeleton when compared to parental A431 cells and to the – dox treated cells. These results further corroborate the importance of upstream Rac1 activation in determining how Rac1 regulates actin cytoskeleton rearrangements.

3.2.2.11 Activation of Rac1 by Tiam1 and P-Rex1 Induces Differential Effects on Adherens Junctions in A431 Cells

As mentioned earlier, E-cadherin is a component of adherens junctions and its internalisation and removal from cell-cell contacts has been associated with increased cellular movement (Fujita et al., 2002). Changes in E-cadherin localisation upon expression of Tiam1 and P-Rex1 can thus give an indication regarding the stability of adherence junctions in the presence of either GEF.

To examine E-cadherin localisation in parental A431 cells and cells with the dox inducible GEF expression system, cells were treated with ethanol (- dox) or 1 μg/ml (+ dox) for 24 hours. Cells were then fixed in 4 % formaldehyde and an anti-E-cadherin antibody was used to detect endogenous E-cadherin in the cells upon ectopic expression of the different GEFs using immunofluorescence.

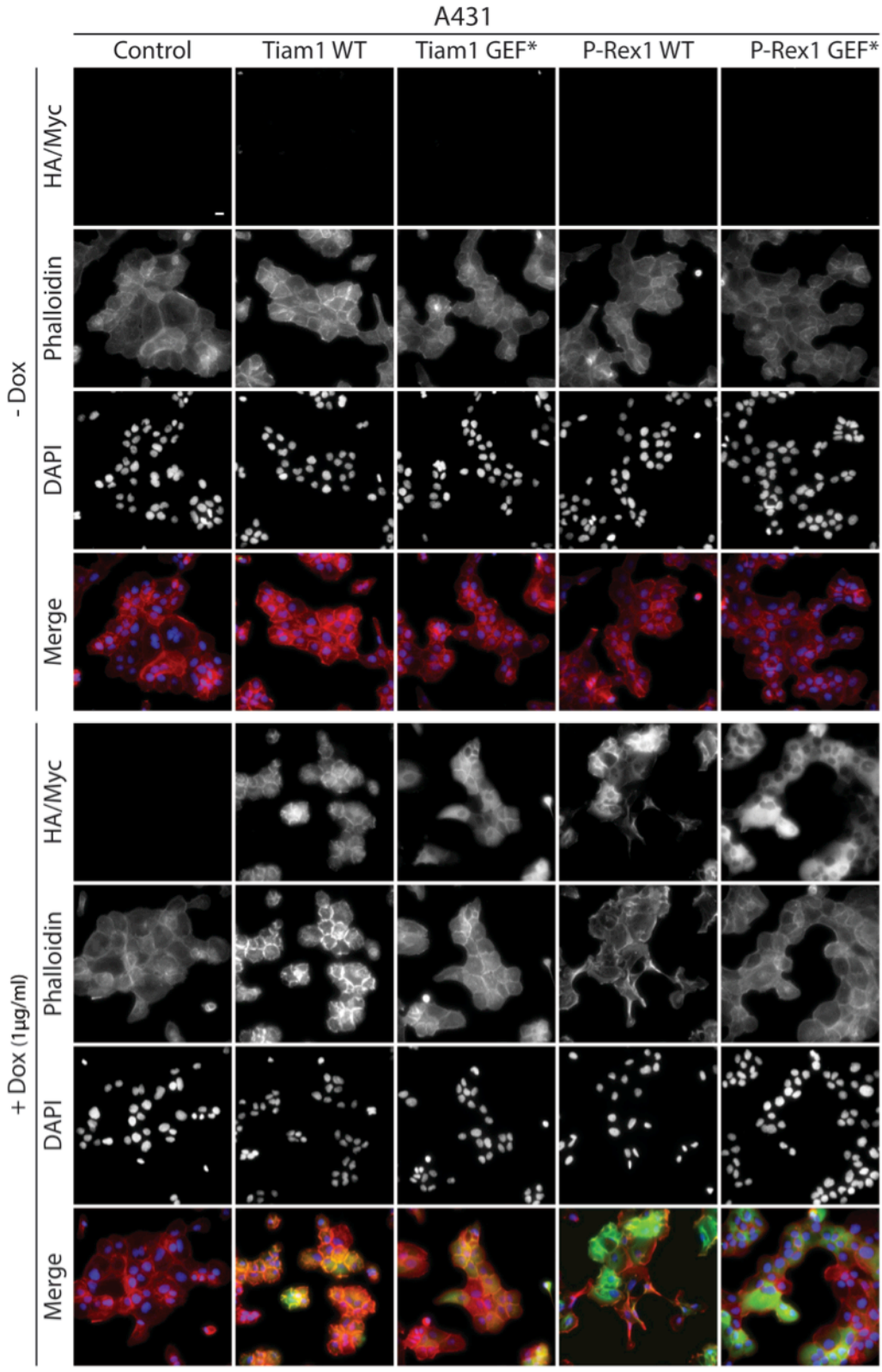

Figure 3.18: Ectopic Expression of Tiam1 and P-Rex1 Wild Type but not GEF-dead Mutant Proteins Induces Distinct Actin Cytoskeleton Rearrangements in A431 Cells

A431 cells harbouring the doxycycline (dox) inducible system for expressing wild type (WT) Tiam1 and P-Rex1 or their GEF-dead mutants (GEF*) were treated with ethanol (- dox) or 1µg/ml dox (+ dox) for 24 hours. Cells were then fixed in 4 % formaldehyde and stained with phalloidin to detect the actin cytoskeleton by immunofluorescence. Images were taken using the low light microscope system (40x magnification). Fluorescence markers against HA-tagged Tiam1 WT/GEF* or Myc-tagged P-Rex1 WT/GEF* were used to detect the expression of the respective GEFs upon dox induction. DAPI was used to stain the nuclei. Scale bar=20µM.

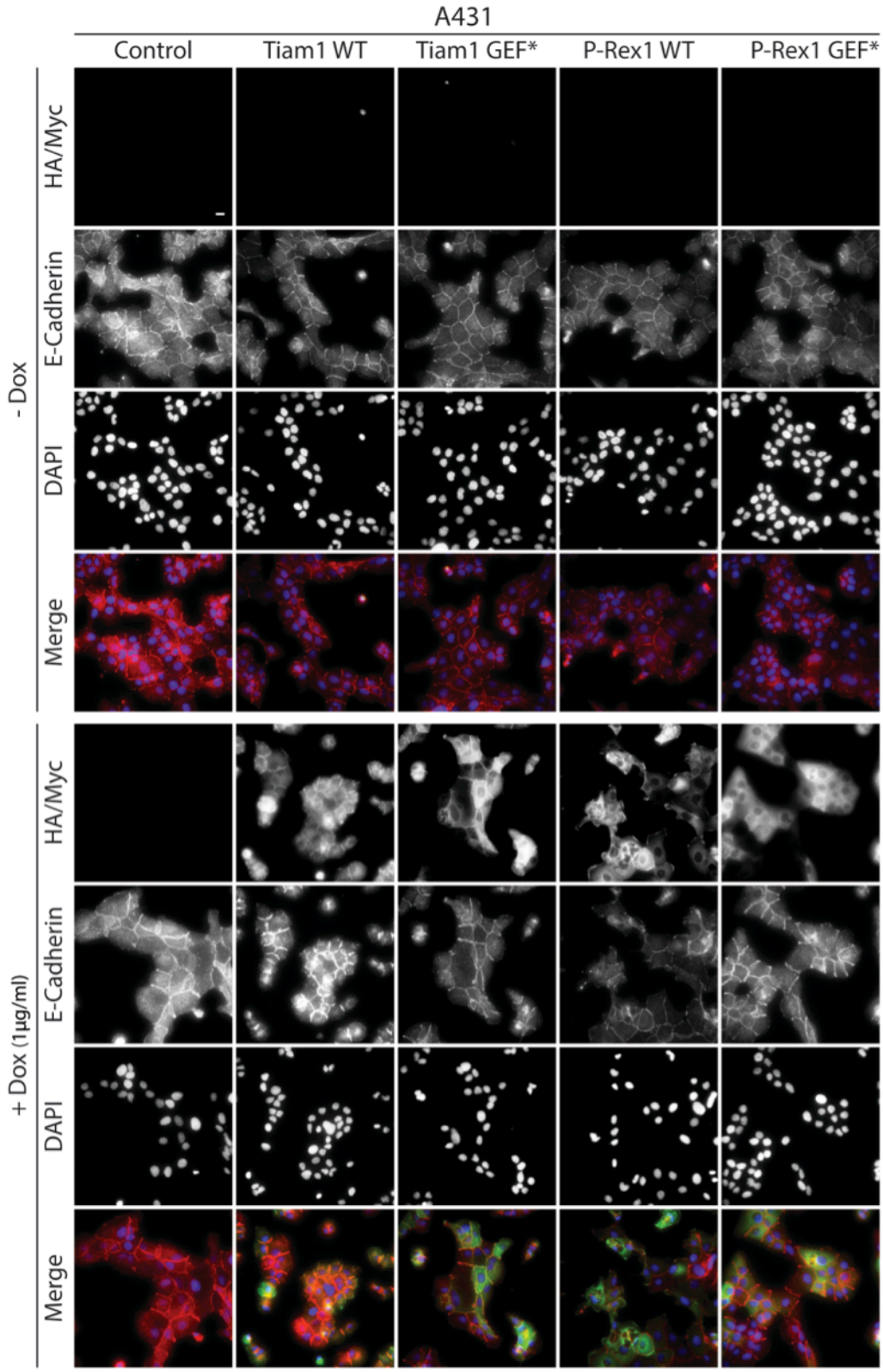

Figure 3.19: Ectopic Expression of Tiam1 and P-Rex1 Wild Type but not GEF-dead Mutant Proteins Induces Differential Effects on E-Cadherin Localisation in A431 Cells

A431 cells harbouring the doxycycline (dox) inducible GEF expression system were treated with ethanol (- dox) or 1µg/ml dox (+ dox) for 24 hours. Cells were then fixed in 4 % formaldehyde and stained with anti-E cadherin antibody to detect the localisation of E-cadherin and adherens junctions by immunofluorescence. Images were taken using the low light microscope system (40x magnification). Fluorescence markers against HA-tagged Tiam1 WT/GEF* or Myc-tagged P-Rex1 WT/GEF* were used to detect the expression of the respective GEFs upon dox induction. DAPI was used to stain the nuclei. Scale bar=20µM.

As expected, Figure 3.19 demonstrates that parental A431 as well as – dox treated cells showed a distinct localisation of E-cadherin at cell-cell contacts. This is characteristic of epithelial cells. However, expression of Tiam1 WT enhanced E-cadherin localisation specifically at cell-cell junctions. Conversely, P-Rex1 WT expression in A431 cells was associated with reduced E-cadherin staining at cell-cell contacts when compared to the parental A431 cells or the – dox treated cells. Moreover, these distinct changes in E-cadherin localisation upon expression of Tiam1 WT and P-Rex1 WT were not observed upon expression of Tiam1 GEF* and P-Rex1 GEF*. This indicates that these changes are also dependent on the ability of both Tiam1 and P-Rex1 to activate Rac1.

Given the established role of HGF in dissolving cell-cell contacts to promote cellular scattering, results outlined above are, therefore, consistent with observations demonstrated in section 3.2.2.5, in which Tiam1 WT and P-Rex1 WT induced differential cellular scattering upon HGF treatment of MDCKII cells. This indicates that Tiam1 and P-Rex1 activation of Rac1 results in distinct regulation of adherens junction via controlling the localisation of E-cadherin.

3.2.2.12 Activation of Rac1 by Tiam1 and P-Rex1 Induces Differential Cellular Scattering in A431 Cells

As mentioned earlier, A431 cells have a well documented upregulation in EGFR expression (Buss et al., 1982). Through increased EGF signalling, upregulation of EGFR has been shown to increase cancer cellular migration and invasion (McCawley et al., 1997). Additionally it has been shown by Chinkers et al. and Rijken et al. that EGF signalling in A431 cells is associated with changes in cellular morphology as well as actin cytoskeleton rearrangements (Chinkers et al., 1979; Rijken et al., 1991). Given the well-documented role of EGF signalling in A431 cells, EGF stimulation of A431 cells upon expression of either GEF could shed light on the role played by Tiam1 and P-Rex1, through Rac1 activation, in regulating actin cytoskeleton rearrangements as well as the integrity of cell-cell contacts to mediate cellular movement.

To investigate the effect of ectopic expression of WT and GEF* Tiam1 or P-Rex1 in A431 on EGF-induced cellular scattering, cells were plated as described in section 2.7.4 and phase-contrast images were taken at 0, 3 and 24 hours post EGF treatment.

As illustrated in Figure 3.20 unlike the untreated cells (- EGF), parental and – dox treated A431 cells responded to EGF stimulation by rounding up by 3 hours. This was followed by changes in the cellular morphology allowing the formation of thin membrane protrusions that stimulate cellular scattering. A similar response was also seen in cells expressing Tiam1 GEF* and P-Rex1 GEF* showing that expression of GEFs that are unable to activate Rac1 do not interfere with the normal EGF-induced response in A431 cells. Interestingly, expression of Tiam1 WT, on the other hand, greatly hindered the normal EGF-induced response in A431 cells. Even at 24 hours post EGF treatment cells did not undergo cellular scattering and a minimal number of cells were found to possess the characteristic EGF-mediated cellular phenotypic changes. Cell rounding, however, was not affected by the expression of Tiam1 WT. In contrast,

expression of P-Rex1 WT resulted in an increased stimulation of cellular scattering in response to EGF treatment even at 3 hours. It must be noted however, that it was difficult to find compact colonies for P-Rex1 WT expressing cells even in the absence of EGF.

These effects were quantified as detailed in section 2.7.4 and as shown in Figure 3.20 B the majority of cells were unscattered at 0 hour post EGF treatment. This was also observed at 3 hours where cells were mainly rounded. In cells expressing P-Rex1 WT, however, 96.2 % of colonies were considered as scattered. This was in contrast to 5.2 % scattered colonies upon expression of P-Rex1 GEF*. At 24 hours post EGF treatment, similar to the response seen in parental A431 cells, the majority of GEF expressing cells, with the exception of Tiam1 WT, were scattered. Tiam1 WT expression, as mentioned above impeded the EGF-induced cellular scattering with 97.4 % exhibiting only the rounded morphology 24 hours post EGF treatment. Tiam1 GEF*, on the other hand, failed to induce such a response with 87 % of colonies showing cellular scattering at 24 hours.

These results indicate that Tiam1 and P-Rex1 are able to modulate the cellular response downstream of EGF signalling. Moreover, given the GEF* results, these effects appear to be dependent on the ability of either GEF to activate Rac1.

3.2.2.13 Section Summary

Results from this section highlight an important aspect of Tiam1 and P-Rex1 regulation of Rac1 signalling. As demonstrated in this section, despite the different epithelial nature of MDCKII and A431 cells when compared to NIH3T3 cells, Tiam1 and P-Rex1 were still able to induce distinct cellular outcomes. It is important to highlight that, similar to results obtained from the NIH3T3 expression system, the ability to activate Rac1, was crucial in the GEF induced differential cellular outcomes.

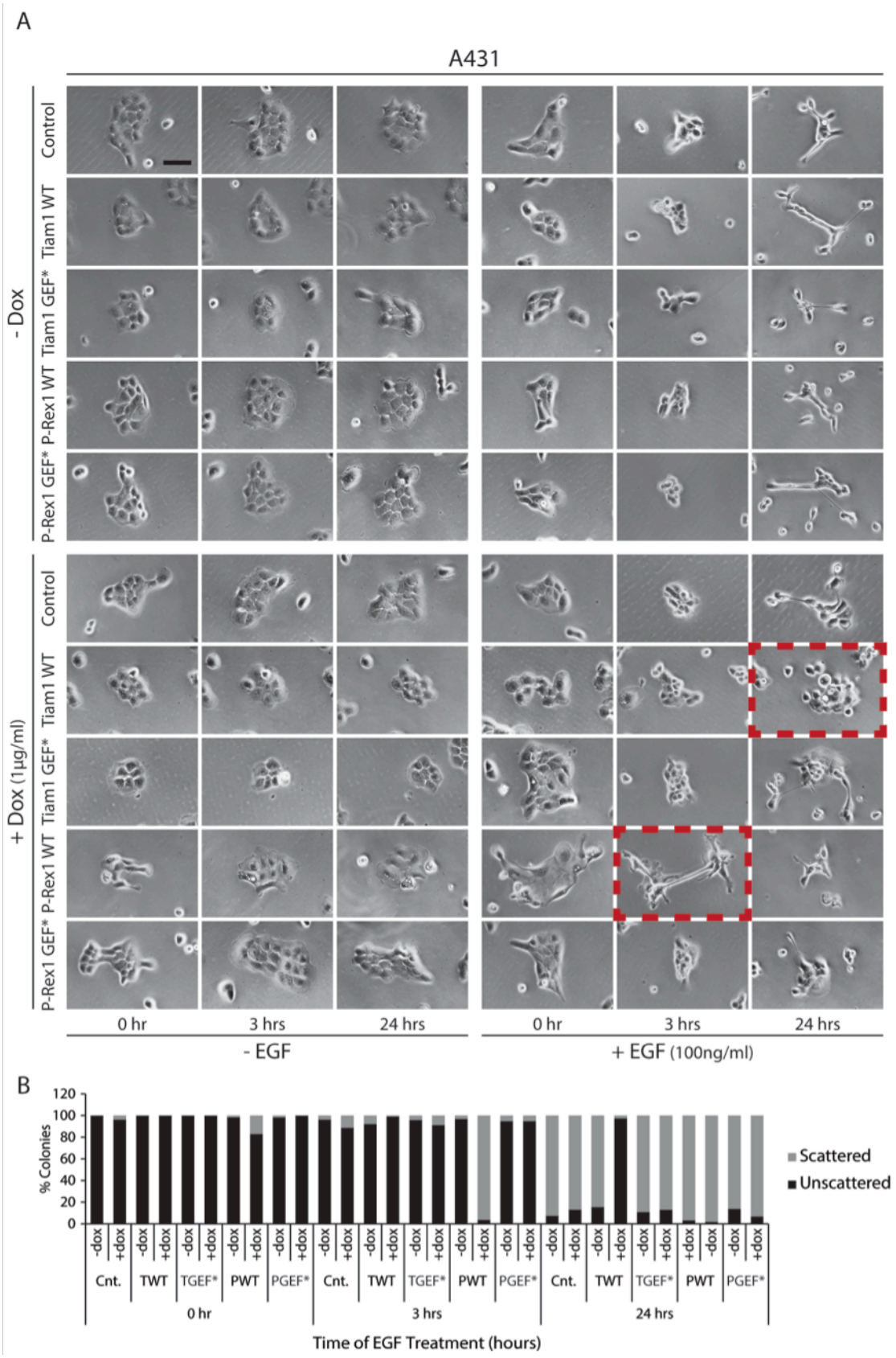

Figure 3.20: Ectopic Expression of Tiam1 and P-Rex1 Wild Type but not GEF-dead Mutant Proteins Induces Differential Cellular Scattering in A431 Cells

(A) A431 cells harbouring the doxycycline (dox) inducible GEF expression system were used to assess the role of wild type Tiam1 or P-Rex1 (TWT or PWT respectively) or GEF-dead mutant Tiam1 or P-Rex1 (TGEF* and PGEF*, respectively) on Rac1-driven cellular scattering following Epidermal Growth Factor (EGF) treatment in the presence of ethanol (- dox) or 1µg/ml dox (+ dox). Phase-contrast images were taken at 0 hour, 3 hours and 24 hours post EGF treatment using the Zeiss inverted microscope (Axiovert 2.5). Scale bar= 100µM. (B) Quantification of EGF induced cell scattering (n=50 colonies/condition). A431 colonies were examined and classified depending on the number of cells within each colony that exhibited a scattered morphology. Colonies with ≤ 3 cells in contact were considered scattered colonies. Graphs represent averages of % colonies from three independent experiments.

3.3 Discussion

Rac1 plays an important role in various cellular processes that are important for normal cellular functioning. Moreover, Rac1 has also been implicated in the initiation and progression of cancer; however due to its controversial role in regulating cellular migration and invasion, the exact role of Rac1 in promoting cancer metastasis is unclear. As a result, understanding Rac1 regulation and how its downstream specificity is dictated is of utmost importance. In addition to factors that have been shown to regulate Rac1 downstream signalling, such as cell type and ECM signalling, there is growing evidence suggesting that depending on the cellular context GEFs can also contribute to the specificity of Rac1 signalling. As outlined in section 1.6 evidence from the literature implicates Tiam1 and P-Rex1 in differentially regulating Rac1-driven cellular migration and invasion in both normal and cancer cells; however, there are contradictory evidence suggesting that both GEFs can stimulate migration, further emphasizing the effect of cellular context on Rac1 signalling. The role of Tiam1 and P-Rex1 in dictating Rac1 downstream signalling was therefore investigated further.

3.3.1 Generation and Validation of Retroviral Doxycycline Inducible GEF Expression Systems

As outlined earlier, in order to accurately assess the role of GEFs in dictating the downstream specificity of its target GTPase, it was important to establish a system in which the cellular conditions are controlled yet the system can accommodate different signalling pathways to be stimulated specifically. This was accomplished through the use of the dox inducible GEF expression system allowing the ectopic expression of different GEFs, namely Tiam1 and P-Rex1, in a highly regulated manner. Utilising the system allowed the manipulation of GEF protein levels without affecting any other cellular conditions that might contribute to differential Rac1 signalling.

3.3.2 GEF Protein Constructs Functionality

Upon generation of the dox inducible GEF expression system, it was important to establish that the GEF constructs introduced in the different cell lines are functional and are capable of binding to Rac1 and activating it. This was particularly evident from the PAK-CRIB pulldown experiments conducted demonstrating that only expression of Tiam1 WT and P-Rex1 WT but not their GEF* mutants was associated with elevated levels of active Rac1 when compared to parental cells. This observation was consistent across the different cell lines tested and highlight that the GEF* constructs were a suitable control for eliminating any non-Rac1-driven downstream effects. The use of such constructs also helped overcome the inherent limitations of ectopic expression studies, as they eliminated effects that were solely due to increased expression of the respective proteins in the tested cell lines.

3.3.3 GEF-Induced Rac1-Driven Downstream Cellular Effects

The main aim of experiments outlined in this chapter was to identify the role, if any, played by GEFs in influencing Rac1 downstream effects, specifically regarding cellular migration. Changes in cellular morphologies and actin cytoskeleton rearrangements are known to precede cellular movement (Lauffenburger and Horwitz, 1996). As a result, changes in these cellular processes were examined in all cell lines utilised. Interestingly, results outlined in this chapter highlight that despite the inherent differences between the cell lines used, expression of Tiam1 WT was associated with increased cellular aggregation and membrane ruffling. This is consistent with reports indicating that Tiam1 promotes the formation of an epithelial-like morphology in Ras transformed MDCK-f3 and metastatic melanoma cells (Sander et al., 1998; Uhlenbrock et al., 2004). Tiam1 expression has also been shown to enhance E-cadherin mediated cell-cell contacts in epithelial cells, including MDCKII cells (Engers et al., 2001; Hordijk et al., 1997). This is in agreement with results observed from the HGF and EGF induced cell scattering in MDCKII and A431 cells respectively, where Tiam1 expression resulted in a reduced cellular scattering ability. Of course, caution must be taken when interpreting the results from these scattering assays due to the strict criteria used to define scattered colonies, which might have reduced the number of identified scattered colonies upon Tiam1 WT expression. Instead, these assays were used as a reference to determine the ability of Tiam1, relative to P-Rex1 to regulate cellular scattering. However, despite such strict criteria, these findings together with the observed E-cadherin staining in A431 implicate Tiam1 in enhancing adherens junctions' stability via increasing the localisation of E-cadherin at cell-cell contacts, which could help explain its role in reducing cellular scattering. Moreover, consistent with Tiam1 enhancing cell-cell contacts, phalloidin staining observed in the three cell lines, indicates that there is an increased localisation of actin at cell junctions. In agreement, Uhlenborck et al. previously reported a similar increased actin localisation at cell junctions upon Tiam1 expression in metastatic melanoma cells (Uhlenbrock et al., 2004). These morphological changes were also accompanied with reduced cellular migration in NIH3T3 and MDCKII cells as well as reduced scattering induced by HGF and EGF in MDCKII and A431 cells respectively. These results have also been reported in various cell lines, normal and cancerous, in which Tiam1-Rac1 signalling impedes cellular migration and invasion (Engers et al., 2001; Malliri et al., 2006; Malliri et al., 2002; Malliri et al., 2004). It is important to note, however, that more experiments are needed in order to determine whether the role of Tiam1 in reducing cellular migration is a direct one, or perhaps through other cellular processes, such as its role in regulating E-cadherin-mediated cell junctions.

In striking contrast to the above, expression of P-Rex1 WT was predominantly associated with a mesenchymal morphology and the formation of thin membrane protrusions. This was particularly evident in the epithelial cell lines used, MDCKII and A431, given their otherwise epithelial morphology. In these cells, P-Rex1 WT expression was associated with disrupted cell-

cell attachments as illustrated by the reduced localisation of actin at cell-cell contacts in all three cell lines and reduced E-cadherin staining at cellular junctions in A431 cells. Consistent with these observations, P-Rex1 WT expression also resulted in an increased ability of cells to scatter in response to HGF and EGF stimulation in MDCKII and A431 cells, respectively. Moreover, results from the Oris^{TM} migration assay in NIH3T3 and MDCKII cells highlight the pro-migratory properties associated with P-Rex1-Rac1 signalling. These results are in agreement with various reports implicating P-Rex1-Rac1 signalling in promoting cellular migration and invasion in both normal and cancer cells as detailed in 1.6.2.1.

Taken together these results clearly demonstrate that under the tested cellular conditions, Tiam1 and P-Rex1, through their ability to activate Rac1, are able to induce distinct cellular phenotypes. This provides direct evidence implicating GEFs in dictating GTPase downstream signalling. In addition, given the different cell types depicted by NIH3T3, MDCKII and A431 cells, these results illustrate that, under the same cellular conditions, Tiam1 and P-Rex1 are capable of regulating similar cellular processes in both mesenchymal and epithelial cell types. In order to extend this statement to involve other cell types, the dox inducible GEF expression system needs to be introduced in more cell lines representing different cell types.

3.3.4 GEF-Induced Cellular Effects and Rac1 Dependency

As stated earlier, via using Tiam1 GEF* and P-Rex1 GEF* constructs, cellular effects that are not through the ability of either GEF to activate Rac1 could be eliminated. This allowed the identification of cellular phenotypes induced upon expression of Tiam1 or P-Rex1, which depended on downstream Rac1 activation.

Results obtained from the dox inducible GEF expression system introduced into NIH3T3, MDCKII and A431 cells show that expression of Tiam1 GEF* and P-Rex1 GEF* is firstly unable to activate Rac1. The inability of Tiam1 GEF* to activate Rac1 is consistent with results from a previous study in which the mutations have been described (Tolias et al., 2005). Similarly, P-Rex1 GEF* GEF-dead properties were demonstrated by Nie et al., thus PAK-CRIB pulldowns are in agreement with this report (Nie et al., 2010). Importantly through the use of these constructs and the lack of any distinct phenotypic changes when compared to parental cells or the respective – dox treated cells demonstrates the importance of Rac1 activation in the differential GEF-induced cellular effects. This clearly highlights that Tiam1 and P-Rex1 function through Rac1 to regulate cellular processes, including cellular migration and invasion.

In addition to the above the ability of Tiam1 and P-Rex1 to activate other small Rho GTPases was assessed. Cdc42 is another member of the Rho family of small GTPases and has been reported to play a role in promoting cellular movement (Parri and Chiarugi, 2010). Moreover, as reported by Kawakatsu et al. and Nobes et al. Cdc42 has been shown to regulate Rac1 activity (Kawakatsu et al., 2002; Nobes and Hall, 1999). It was therefore important to identify whether Tiam1 and P-Rex1 induce distinct cellular effects through Cdc42 activation as well. However,

PAK-CRIB pulldown assays in NIH3T3 cells demonstrate that expression of Tiam1 WT and P-Rex1 WT, although increase levels of active Rac1, do not influence levels of active Cdc42. This indicates that in these cells Tiam1 and P-Rex1 do not induce these cellular effects as a response to Cdc42 activation. However, it must be noted that these experiments were not performed in MDCKII and A431 cells and thus activation of Cdc42 by Tiam1 and P-Rex1 needs to be evaluated in these cells.

In order to fully establish that these distinct cellular effects are mainly through Rac1 activation, it would also be interesting to examine the effect of expressing Tiam1 and P-Rex1 in a Rac1 null background. However, given the importance of Rac1 in normal cellular functioning, this might present a challenge, particularly when interpreting the GEF-driven cellular effects. Another caveat of this method is the potential functional overlap between Rac1 and other small GTPases, which might not be activated by Tiam1 and P-Rex1 under normal conditions, but in the absence of Rac1 become the primary GTPase downstream of the ectopically expressed GEFs. These issues can be addressed through the use of a Rac1 inhibitor and evaluating its effect on the GEF-induced cellular effects. Moreover, screening of other small Rho GTPases and their activation profiles could shed more light on the extent to which Tiam1 and P-Rex1 depend on Rac1 activation to elicit these cellular functions. Furthermore, given the recent role of P-Rex1 in directly activating RhoG (Damoulakis et al., 2014), it would be interesting to investigate whether Tiam1 can also influence RhoG in cells and thus induce differential downstream effects.

3.4 Conclusions

As demonstrated from this chapter, expression of Tiam1 WT and P-Rex1 WT in NIH3T3, MDCKII and A431 cells was associated with distinct cellular outcomes that were dependent on the ability of either GEF to activate Rac1. Taken together these results provide clear evidence supporting the role of GEFs, not only in activating Rac1, but also in dictating its downstream cellular functions. Figure 3.22 provides a schematic representation of a working model by which Tiam1 and P-Rex1 regulate Rac1 signalling. Both Tiam1 and P-Rex1 are Rac1 activators; however based on evidence presented in this chapter, Tiam1 and P-Rex1 seem to influence Rac1 downstream signalling through an unknown mechanism. As a result of this regulation, Tiam1 and P-Rex1 are able to induce a series of Tiam1-Rac1-driven and P-Rex1-Rac1-driven cellular outcomes, respectively. Consequently, upon activation of Rac1 by Tiam1, Rac1 reduces cellular migration, whereas activation by P-Rex1 enhances cellular migration. For simplicity the model was designed assuming that Tiam1 and P-Rex1 regulate two separate pools of Rac1 in cells. However, in order to accurately represent the situation that actually occurs in cells, it would be important to investigate whether Tiam1 and P-Rex1 manipulate separate pools of Rac1, or act on a common pool.

This model helps tackle the controversial role of Rac1 in cellular migration and invasion and provides a potential explanation for discrepancies in reported Rac1 downstream functions. However, it also calls of an even better understanding of the underlying mechanism by which Tiam1 and P-Rex1 are inducing these distinct effects. The following results chapters were aimed at addressing this question.

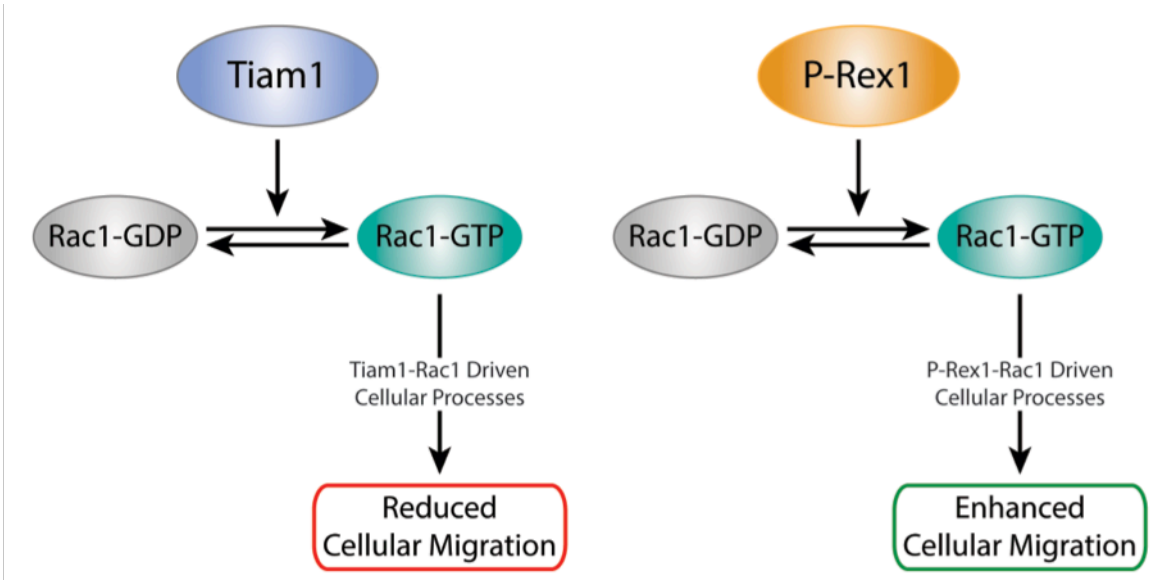

Figure 3.21: Schematic Representation of GEF-Induced Rac1 Downstream Effects Working Model
Tiam1 and P-Rex1 activate Rac1 by facilitating the exchange of GDP with GTP. Active Rac1 is then able to bind to downstream effectors and thereby elicit various downstream cellular functions. In addition to their role as Rac1 activators, Tiam1 and P-Rex1 can dictate GEF-specific Rac1 downstream functions, thus inducing distinct Rac1-driven cellular phenotypes that can help explain their deferential role in regulating cellular migration.

Chapter 4 : Mechanism of GEF Induced Rac1 Downstream Specificity

4.1 Introduction

Rac1 activation in cells is associated with a wide variety of cellular processes, which are mediated via its ability to bind to a multitude of downstream effectors (Buchsbaum et al., 2002). Despite the identification of a vast number of these effectors, mechanisms influencing Rac1 downstream signalling specificity, through effector binding, are poorly understood. There is accumulating evidence implicating GEFs in regulating Rac1 downstream signalling via modulating Rac1 binding to different effectors; however their exact function in GTPase regulation remains poorly defined. Results outlined in chapter 3 provide strong evidence to support this role of GEFs in mediating GTPase signalling and clearly demonstrate that Tiam1 and P-Rex1 influence distinct Rac1-driven cellular phenotypes. However, the mechanism by which Tiam1 and P-Rex1 confer such selectivity is yet to be elucidated. Given the evidence outlined thus far it was hypothesised that Tiam1 and P-Rex1 induce distinct Rac1 downstream effects via differentially affecting the Rac1 interactome, thus influencing effector binding to Rac1 to elicit the observed cellular outcomes.

This study focused on the role of GEFs in regulating Rac1 binding to other proteins, under the same cellular conditions. Hence, the main aim of this part of the PhD was to evaluate whether Tiam1 and P-Rex1 have the ability to influence the pool of effectors that bind to Rac1 upon activation by either GEF through conducting a proteomic screen of Rac1 binding partners under the different activating conditions.

Multiple purification techniques have been described and used to identify the interactome of proteins. Among these methods, tandem affinity purification (TAP) has proven to be an efficient and specific system for purifying proteins and their associated complexes in mammalian cells (Angrand et al., 2006; Benzinger et al., 2005; Bouwmeester et al., 2004). Developed by Rigaut et al. the TAP method is a two-step purification technique separated by a cleavage step of a TAP-tagged protein and its associated protein complexes. The conventional TAP-tag consists of two IgG binding domains from Protein A followed by a tobacco etch virus (TEV) proteolytic cleavage site and a calmodulin binding peptide (CBP). The first step involves the immunoprecipitation of the bait protein using an IgG matrix. Due to the high binding affinity of Protein A to the IgG matrix, release from the matrix can only be achieved under denaturing conditions and at low pH. This, however, can disrupt protein complexes and thus reduce the efficiency of the technique. As a result the TEV proteolytic cleavage site was introduced. Upon addition of TEV protease, the IgG matrix bound proteins can be released. The eluates are then subjected to the second purification step, which involves incubation with beads coated with calmodulin in the presence of calcium. In addition to decreasing unspecific background binding, this step also helps remove the TEV protease and other contaminants

following the first step. The bound proteins can then be released using EGTA (Rigaut et al., 1999).

Despite the efficiency of TAP in identifying protein-protein interactions there are associated limitations to the technique that can be summarised in three key points: i) size; ii) duration; and iii) signalling interference. Regarding the size of the TAP-tag, the conventional tag is 21 KDa, making the tag a relatively large. As a result there is an increased chance of functional interference when the tag is fused to a protein (Gloeckner et al., 2007). This was particularly important for this project since untagged Rac1 is ≈21 KDa, thus doubling the size of the protein might interfere with either the functional side of Rac1 or its ability to interact with other protein complexes.

Another limitation of the conventional TAP technique is the length of the purification. Due to the TEV proteolytic cleavage step, the duration of the TAP procedure is considerably increased. As a consequence the purification efficiency is greatly reduced especially for transient interactions (Gloeckner et al., 2007). This also presented a challenge for this project, since Rac1 interactions are often transient and thus a large amount of binding partners might be missed using this long purification technique.

As highlighted above, signal interference due to the use of the calmodulin binding peptide and its ability to bind to calmodulin, an important regulator of cellular signalling has been reported to influence the reliability of the conventional TAP method. For example, it has been shown that both calmodulin and calcium can regulate the Ras/Raf/MEK/ERK pathway (Agell et al., 2002). A more relevant illustration of potential interference with Rac1 signalling is that calmodulin binding to Rac1 was shown to be important for modulating Rac1-mediated ARF-6 dependent endocytosis (Vidal-Quadras et al., 2011). Therefore there is a possibility that the binding of CBP to calmodulin and the addition of calcium in the second purification step might influence Rac1-mediated signalling networks inside the cells and thus complicate the interpretation of the data (Gloeckner et al., 2007). It may also interfere with the ability of Tiam1 and P-Rex1 to induce distinct cellular phenotypes downstream of Rac1.

Fortunately, the limitations highlighted above inspired the generation of a new set of TAP tags that address these issues. Among the indentified tags, the *Strep-Flag*-tag (SF-tag) was identified as a highly efficient tag. It was first described by Gloeckner et al. as a novel TAP technique used to identify the interactomes of B-Raf, MEK1 and 14-3-3ε (Gloeckner et al., 2007; Gloeckner et al., 2009a). Unlike the conventional TAP-tag, the SF-tag consists of two *Strep*-Tag® II components and one FLAG® component and is only 4.6 KDa thus eliminating the size problem associated with the original TAP. Additionally, given the domain composition of the SF-tag, the TEV cleavage step in the original TAP technique is no longer required, thus reducing the purification time, which in turn increases the chances of identifying an increased number of transient interactors. Additionally, the substitution of Protein A and CBP with *Strep*-Tag® II and FLAG® tag also meant that any potential interference from CBP-calmodulin binding would be

eliminated (Gloeckner et al., 2007). Therefore, the improved design of the SF-tag helped overcome the limitations associated with the conventional TAP method. The technique was thus researched further prior to employing it.

Similar to other TAP techniques, SF-TAP is a two-step purification technique. Cells expressing the SF-tagged bait protein are harvested and lysed using a mild lysis buffer at pH 7.4 to maintain the integrity of protein complexes isolated. The first step involves the incubation of lysates with a *Strep*-Tactin® superflow to pulldown the protein of interest using the *Strep*-Tag® II component of the SF-tag. This is followed by washes to remove proteins and contaminants that bind non-specifically to the *Strep*-Tactin® superflow. Due to the intrinsic nature of the *Strep*-Tag® II i.e. medium affinity binding, bound proteins are then removed by adding d-desthiobiotin, a derivative of the *Strep*-Tag® II binding protein, biotin. D-desthiobiotin competes with bound proteins through binding to the biotin-binding pocket of the *Strep*-Tactin® superflow thus allowing the release of such proteins. Eluates from the first step are then incubated with anti-FLAG® M2 agarose beads that precipitate the protein of interest and the associated protein complexes through the FLAG® component of the SF-tag. This is followed by washes to remove any residual non-specific proteins bound to the beads. The second FLAG® immunoprecipitation step together with the washes allows the enrichment of proteins that bind specifically to the bait protein. Similar to the first step, bound proteins are then eluted by competition from the beads by incubating with FLAG® peptide elution buffer. Eluates can then be concentrated down to the required volume using various methods. For example, in the original paper describing the SF-TAP technique, Gloeckner et al., utilise Amicon filter units with a 3 KDa protein cut off to concentrate the FLAG® eluates (Gloeckner et al., 2007). Given the practicality of the SF-tag and the associated reduction in potential Rac1 signalling interference the SF-tag presented a good system for the required analysis of the potential GEF-induced changes in the Rac1 interactome.

In addition, to advancements in purification techniques, the field of proteomics has flourished over the past few years due to advances in mass spectrometry based technologies (Aebersold and Mann, 2003; Gingras et al., 2005). Thus to address the inherent limitation of mass spectrometry, such as its non quantitative nature, several approaches have been developed that involve the use of stable isotopes to label different proteomes either chemically or metabolically (Ong and Mann, 2005). Among these techniques is the Stable Isotope Labelling by Amino Acids in Cell Culture (SILAC). SILAC was first described by Ong et al. and is an example of a metabolic labelling process. In SILAC, live cells are labelled using a heavy amino acid that contains hydrogen (^{2}H instead of ^{1}H), carbon (^{13}C instead of ^{12}C) or nitrogen (^{15}N instead of ^{14}N) isotopes. The SILAC labelling process is fairly straightforward with the majority of proteins incorporating the labelled amino acid in five to six cell doubling rounds. Upon labelling, proteins that incorporate the heavy amino acid will have a different, yet known, mass shift when compared to unlabelled proteins. This mass shift can be detected by mass spectrometry and

results in distinct isotope specific intensity peaks for the same proteins that correspond to the relative peptide abundance. Thus using the intensities of these peaks a ratio can be calculated allowing the quantification of the relative abundance of proteins in two or more differentially labelled cell populations (Ong et al., 2002).

A major advantage of SILAC is that, unlike labelling by chemical modifications, SILAC does not involve a derivative step. This overcomes the problem of incomplete chemical reactions as well as unwanted by products that might interfere with the quantification process. Another key advantage of using SILAC over conventional mass spectrometry is the reduced number of false positives identified in the screen since only proteins that show fold change differences in their SILAC ratios will be considered. Furthermore, given the relatively easy SILAC labelling procedure, switching the amino acid labelling and repeating the mass spectrometry identification should yield the reciprocal ratios for proteins that are specifically regulated in a given condition thus allowing further validation of screen results (Schulze and Mann, 2004).

However, as with other technique, there are potential limitations that need to be taken into consideration if SILAC is to be employed. The first limitation that SILAC presents is the efficiency by which the amino acid isotopes are incorporated. This varies between different cell lines, and as such, several cell lines might have to be tested. Another potential limitation is the use of media containing 10 % dialysed FBS for efficient labelling and to avoid contamination with naturally occurring amino acids that might be present in the normal FBS. This in turn might affect the normal growth of cells and thus have to be assessed experimentally prior to data interpretation (Ong et al., 2002).

Given the above, the specificity of the SF-TAP technique combined with the quantitative power of SILAC promised to be a good system to analyse changes in Rac1 binding partners, including transient interactors, in response to activation by either Tiam1 or P-Rex1. As a result, SF-TAP combined with SILAC and mass spectrometry protein identification was used as a tool to better understand the mechanism behind the observed differential GEF-induced cellular effects. This chapter highlights results from the proteomic analysis conducted together with follow-up experiments designed to validate the screen.

4.2 Results

4.2.1 Validation and Optimisation of *Strep*-FLAG Tandem Affinity Purification

4.2.1.1 Generation of Retroviral Doxycycline Inducible SF-Rac1/GEF Expression System in NIH3T3 Cells

Given the benefits of the SF-tag over the original TAP-tag, while maintaining the low unspecific background, the SF-tag was fused to the N-terminus of Rac1 and inserted into the MCS of the pRetroX-Tight-Pur plasmid. Transduction of this plasmid in NIH3T3 cells harbouring the dox inducible GEF expression system allowed the generation of a protein co-expression system, which is outlined in Figure 4.1 A. Upon addition of dox and the binding of the rtA-Advanced protein to the P_{Tight} promoter, the expression of the different GEF together with SF-Rac1 is induced. The domain structure of SF-Rac1 is highlighted in Figure 4.1 B.

Upon generation of the NIH3T3 cells harbouring the dox inducible system for the expression of SF-Rac1 alone (NIH3T3+pRetroX-SF-Rac1 control) or together with the different GEF constructs, the expression levels of the respective proteins was assessed using Western blot analysis. Due to the size difference between endogenous Rac1 (≈ 21KDa) and SF-Rac1 (≈ 26 KDa) both endogenous and exogenous Rac1 could be detected using the same anti-Rac1 antibody. SF-Rac1 expression could also be detected using an anti-FLAG® M2 antibody that recognises the FLAG® epitope of the SF-tag.

As indicated in Figure 4.1 C addition of dox to cells induced the expression of relatively equal levels of SF-Rac1 across the different generated cell pools as detected by both the anti-Rac1 and the anti-FLAG® M2 antibodies. Additionally, dox treatment was successful in the induction of both GEF and SF-Rac1 expression simultaneously in cells. It must be noted, however, that expression of Tiam1 GEF* and P-Rex1 GEF* when compared to the WT expression levels was affected by the co-expression of SF-Rac1. To remedy this, cells were re-transduced with vectors encoding Tiam1 GEF* and P-Rex1 GEF*, yet this failed to enhance the expression to levels comparable to the WT proteins. This suggested that in addition of dox, expression of SF-Rac1 might also influence Tiam1 GEF* and P-Rex1 GEF* expression as part of a negative feedback loop to suppress the dominant negative effects associated with these mutants. As a result of this differential expression, information regarding Rac1 binding partners obtained from the GEF* expressing cells were used only as an additional filtering control for the WT Rac1-effector profiles. Interestingly, though, expression of SF-Rac1 in NIH3T3 cells was associated with a reduction in the levels of endogenous Rac1. This was particularly promising for the SF-TAP experiment, as it suggested that SF-Rac1 is capable of competing with endogenous Rac1 for binding partners.

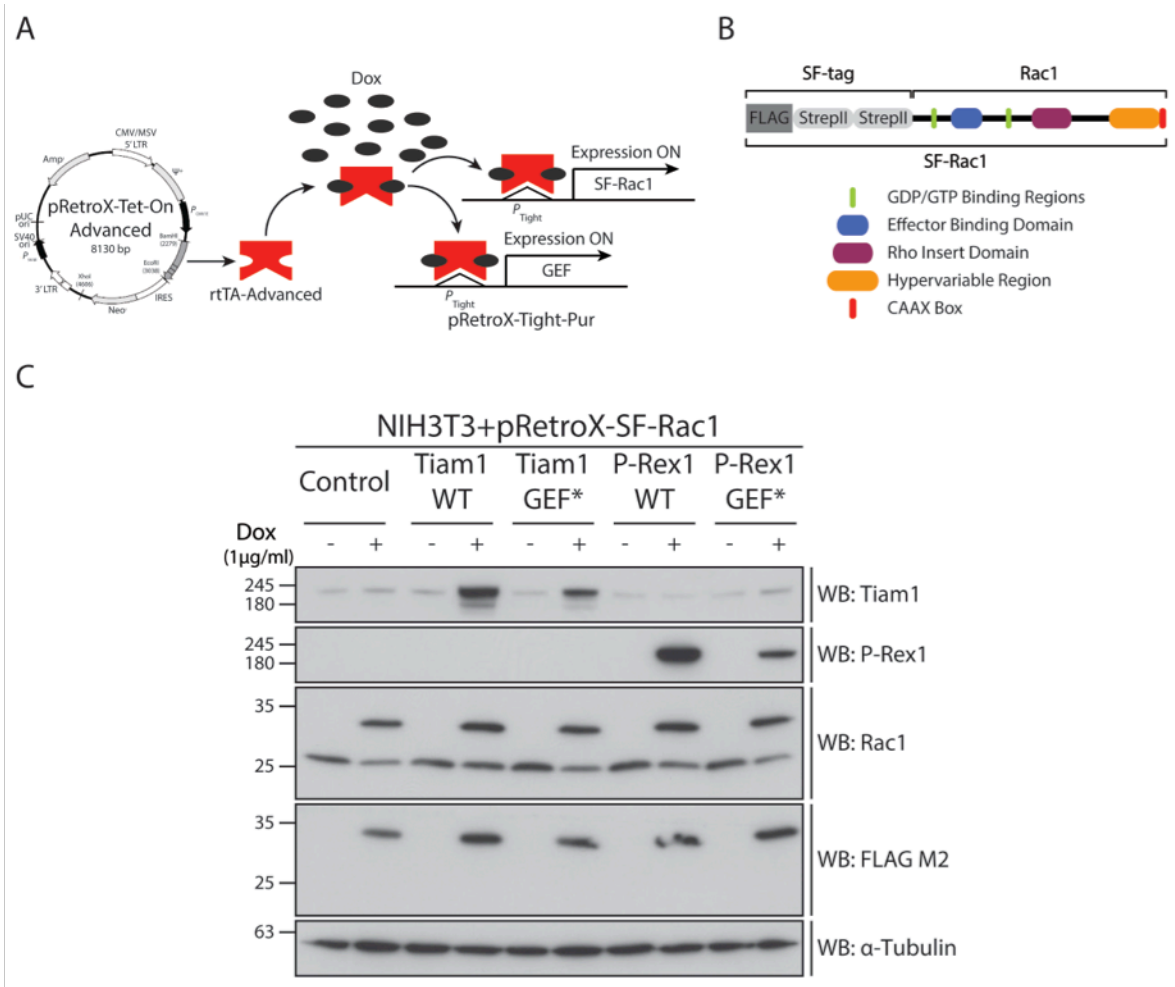

Figure 4.1: Generation of Retroviral Doxycycline Inducible SF-Rac1/GEF Expression System in NIH3T3 Cells

(A) Schematic representation of pRetroX-Tet-On Advanced and pRetroX-Tight-Pur doxycycline (dox) inducible system. Upon addition of 1µg/ml dox to cells harbouring the inducible system, the expression of SF-Rac1 alone or together with one of the GEF constructs under the P_{Tight} promoter in the pRetroX-Tight-Pur vectors is induced. (B) Schematic representation of Rac1 domains fused at the N-terminus to the *Strep*-FLAG tag (SF-tag). (C) NIH3T3 cells harbouring the dox inducible system for expression of SF-Rac1 alone (NIH3T3+pRetroX-SF-Rac1 control) or together with one of the different GEF constructs were treated with ethanol (- dox) or 1µg/ml dox (+ dox) for 24 hours. Cells were harvested and expression levels of wild type (WT) Tiam1 or P-Rex1 or their GEF-dead mutants (GEF*) was detected by Western blot analysis using anti-Tiam1 and anti-P-Rex1 antibodies. The expression of SF-Rac1 was detected using anti-Rac1 antibody, which detects both endogenous Rac1 and SF-Rac1 and anti-FLAG M2 antibody that detects only exogenous SF-Rac1. α-Tubulin was used as a loading control.

4.2.1.2 Activation of SF-Rac1 by Tiam1 and P-Rex1 Induces Differential Cellular Phenotypes in NIH3T3 cells

As outlined in section 4.2.1.1, expression of SF-Rac1 in NIH3T3 cells was associated with a reduction in endogenous Rac1 levels. This suggested that the cell recognises the exogenous SF-Rac1 in a similar way to the endogenous protein. However, it was important prior to analysing the Rac1 interactome, to confirm that similar to the endogenous protein, SF-Rac1 can be activated and that ectopic expression of Tiam1 and P-Rex1 can elevate the levels of active SF-Rac1 in cells. To evaluate this, NIH3T3 cells with the dox inducible SF-Rac1/GEF expression system were treated with ethanol (- dox) or 1 µg/ml dox (+ dox) for 24 hours. The cells were then harvested and subjected to a GST PAK-CRIB pulldown of active Rac1 as outlined in section 2.7.1. Using this technique the levels of both active endogenous and SF-Rac1 upon expression of the different GEF constructs were assessed by Western blot analysis using an anti-Rac1 antibody.

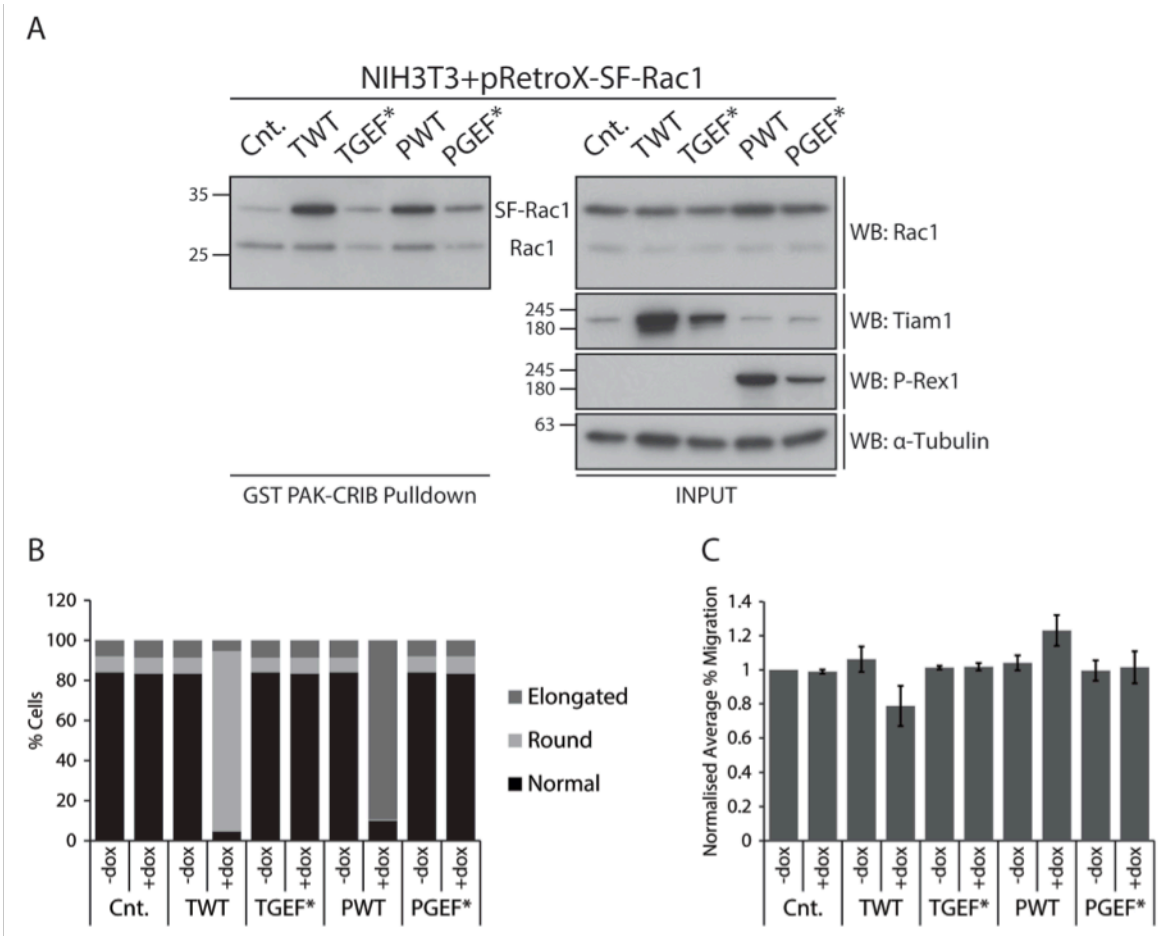

Figure 4.2: Activation of SF-Rac1 by Tiam1 and P-Rex1 Induces Differential Cellular Phenotypes in NIH3T3 Cells

(A) NIH3T3 cells harbouring the doxycycline (dox) inducible system for the expression of SF-Rac1 alone (NIH3T3+pRetroX-SF-Rac1 control) or together with wild type Tiam1 and P-Rex1 (TWT and PWT, respectively) or Tiam1 and P-Rex1 GEF-dead mutant (TGEF* and PGEF*, respectively) were treated with dox for 24 hours. Cells were then harvested and subjected to GST PAK-CRIB pulldown of active Rac1. Levels of active endogenous and SF-Rac1 were detected by Western blot analysis using anti-Rac1 antibody. Basal levels of active SF-Rac1 in cells expressing SF-Rac1 alone (Cnt.) were used as a reference for active SF-Rac1 levels induced specifically upon GEF expression. α-Tubulin was used as a loading control. Representative Western blot from three independent experiments. (B) To quantify the GEF induced cellular phenotypes, cells were classified into three groups based on their morphology: normal, round and elongated. Graph represents % cells in each subset from a total of 150 cells/condition from various cell passages and seeding densities. (C) Quantification of cellular migration from one representative experiment of – dox and + dox treated cells normalised to – dox control treated cells. Graphs represent the normalised average % migration ± standard deviation.

As demonstrated in Figure 4.2 A, co-expression of Tiam1 WT or P-Rex1 WT with SF-Rac1 resulted in an increase in the levels of active SF-Rac1 when compared to cells expressing SF-Rac1 alone (Cnt.). Interestingly, there was only a modest increase in the levels of endogenous active Rac1 in these cells. In contrast and as expected, expression of Tiam1 GEF* and P-Rex1 GEF* did not influence the levels of active Rac1 both on the endogenous and exogenous levels.

These results provided evidence for the functionality of the SF-Rac1 construct and the ability of SF-Rac1 to compete with endogenous Rac1 for GEF-mediated activation. However it was crucial to further examine whether co-expression of SF-Rac1 with the different GEF constructs would interfere with the ability of Tiam1 and P-Rex1 to dictate differential Rac1 downstream effects. Therefore, the morphology and migration potential of the NIH3T3 cells harbouring the dox inducible SF-Rac1/GEF expression system was assessed.

Using the same classification criteria outlined in section 2.7.2, NIH3T3 cells were classified into three categories based on their morphology: normal, round and elongated. As shown in Figure 4.2 B, even in the presence of SF-Rac1, expression of Tiam1 WT and P-Rex1 WT resulted in a morphological shift in NIH3T3 cells. Tiam1 WT expression was associated with 80 % of cells falling under the round morphology as opposed to 6.7 % in the Tiam1 WT – dox treated cells, 8.7 % in control – dox treated cells and 7.3 % in + dox treated control cells expressing SF-Rac1 alone. This shift was not observed in Tiam1 GEF* – dox and + dox treated cells with 86 % and 86.7 % of cells exhibiting the normal morphology, respectively. P-Rex1 ectopic expression, on the other hand, induced an elongated morphology in 86.7 % of cells compared to only 6.7 % in P-Rex1 WT – dox treated cells. Additionally, P-Rex1 GEF* expression did not affect the normal morphology of NIH3T3 cells with 83.3 % of cells showing a normal phenotype in + dox treated cells, which was comparable to the 89.3 % in P-Rex1 GEF* – dox treated cells. These results together with the PAK-CRIB assay indicate that activation of SF-Rac1 in NIH3T3 cells is also associated with differential downstream cellular morphologies, similar to that described in section 3.2.1.4 with endogenous Rac1.

Given the focus of this project on the dual role of Rac1 in cellular migration and its implications in cancer progression, it was important to ensure that SF-Rac1 activation by Tiam1 and P-Rex1 would also induce differential migration potential in cells. Therefore, the Oris^{TM} migration assay was used to assess the migration of cells expressing SF-Rac1 alone or together with the different GEF constructs. Normalised average percent migration rates outlined in Figure 4.2 C. were consistent with previous observations seen with endogenous Rac1. Tiam1 WT expression resulted in a reduction in cellular migration by 21 % compared to – dox treated control cells, 20 % when compared to cells expressing SF-Rac1 alone and 27 % when compared to Tiam1 WT – dox treated cells. Similar to cellular morphology, expression of Tiam1 GEF* did not affect the migration potential in the cells when compared to its – dox treated counterpart or to the control – dox and + dox treated cells. Conversely, P-Rex1 WT but not GEF* expression resulted in a 23 % increase in cellular migration when compared to – dox treated control cells, 24 % when compared to cells expressing SF-Rac1 alone and 19 % when compared to its – dox counterpart.

Taken together, the above observations highlight that the differential regulation of Rac1-driven cellular morphology and migration observed upon activation of SF-Rac1 by Tiam1 and P-Rex1 is comparable and consistent with the effects observed with endogenous Rac1, thus demonstrating the functionality of SF-Rac1 and the ability of Tiam1 and P-Rex1 to influence cellular effects through the activation of SF-Rac1 in a similar manner to the activation of endogenous Rac1. This highlights the suitability of this co-expression system in identifying potential differential regulation of Rac1-effector binding induced by Tiam1 and P-Rex1.

4.2.1.3 Optimisation of Strep-FLAG Tandem Affinity Purification

As highlighted earlier, the SF-tag was identified as a novel tag used for the TAP purification of bait proteins and their associated protein complexes. Using the SF-TAP framework described by Gloeckner et al. (Gloeckner et al., 2009b) different incubation times and elution buffer concentrations were tested to optimise the SF-TAP technique for the pulldown of SF-Rac1. Moreover, given the transient nature of Rac1 activation and binding to downstream proteins various experiments were designed to test different eluates' concentration methods to try and optimise the yield of SF-Rac1 obtained following the SF-TAP from HEK293T cells transiently expressing SF-Rac1. Equal protein levels were used to test three different methods as demonstrated by the schematic representation in Figure 4.3 A. The first method tested involved boiling of the FLAG® M2 agarose beads in 2X SDS-PAGE sample buffer to release the bound proteins. For the second and third methods, bound proteins were first eluted using the FLAG® peptide followed by either concentration using 3K Amicon filter units or acetone and methanol protein precipitation and resuspension in 2X SDS-PAGE sample buffer, respectively. Lysates and concentrated SF-TAP proteins obtained from all three methods were then resolved on 12 % NuPAGE®Novex® Bis-Tris pre-cast gels and stained using SimplyBlue™ SafeStain.

As shown in Figure 4.3 B a specific band corresponding to the size of SF-Rac1 was observed only in cells expressing SF-Rac1 and not in parental HEK293T cells in all three techniques tested. Analysis of the stained gel revealed that the release of SF-Rac1 by boiling, although yielded a sufficient amount of SF-Rac1, also released the light and heavy IgG chains bound to the FLAG® M2 agarose beads. Thus, this method introduces extra contaminants that might complicate the identification of Rac1 and low abundant Rac 1 binding partners. In contrast, using the second and third techniques the protein pools obtained were relatively clean when compared to the parental HEK293T lanes. However, the acetone and methanol precipitation technique resulted in a very low protein yield when compared to the Amicon filter units concentration despite the relatively equal levels of protein inputs used. Using the third method, therefore, requires a larger starting material, which will increase the time required to lyse the cells and thus might influence the levels of active SF-Rac1 in the protein mix leading to the identification of fewer Rac1 binding partners. Additionally, despite the relatively low starting material of ≈ 4 mg/ml proteins per sample, specific bands of SF-Rac1-associated proteins were observed only after the use of the Amicon filter units. As a result, it was determined from these experiments that concentration of FLAG® peptide eluates using the Amicon filter units is the most appropriate method for the subsequent identification of SF-Rac1 binding proteins using mass spectrometry. Figure 4.3 C illustrates the optimised SF-TAP steps used for subsequent experiments outlined in this chapter.

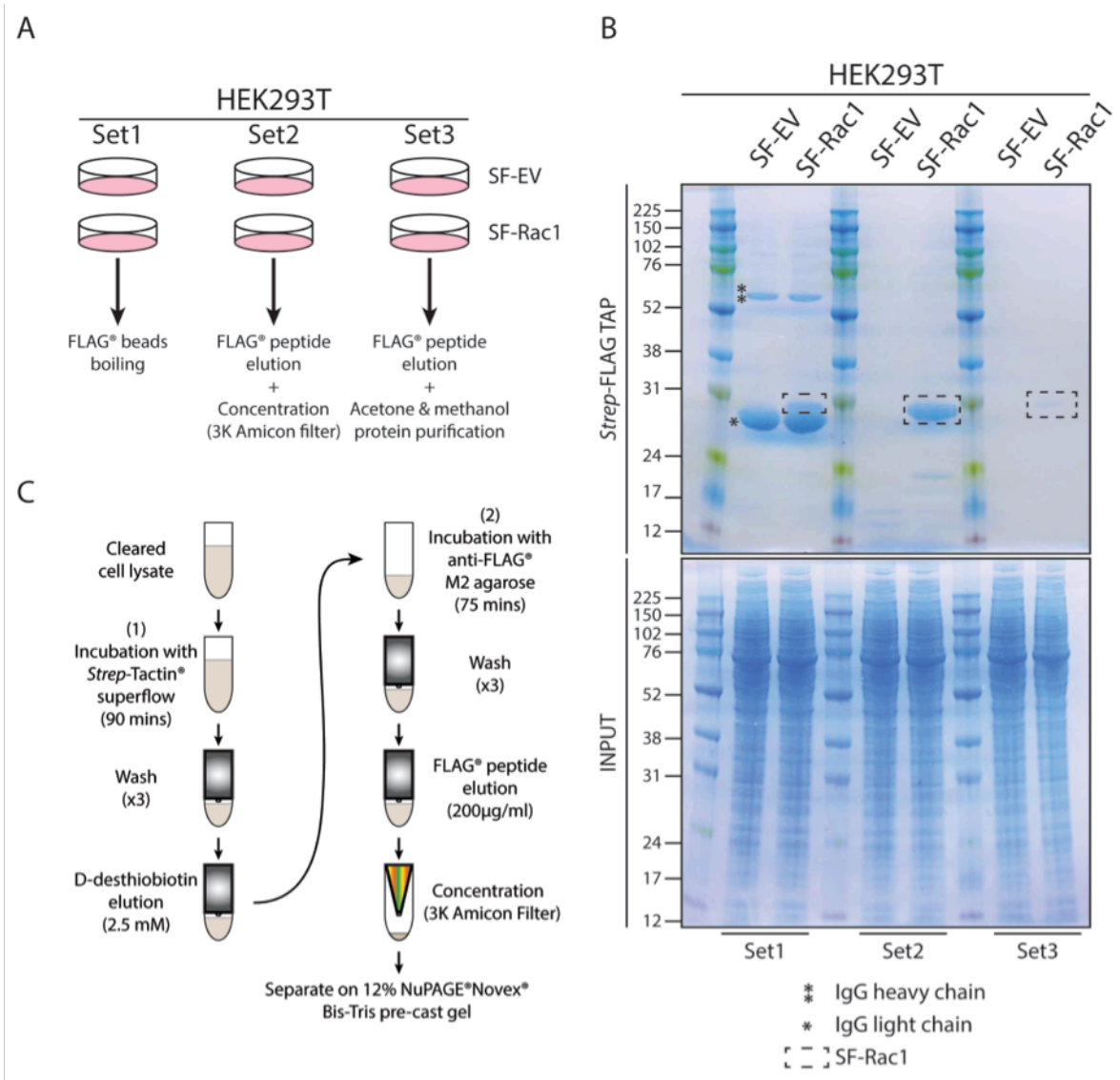

Figure 4.3: Optimisation of *Strep*-FLAG Tandem Affinity Purification

(A) Schematic representation of experimental setup for *Strep*-FLAG Tandem Affinity Purification (SF-TAP) optimisation in HEK293T cells. Three sets of HEK293T cells were plated in a confluent monolayer ($1x10^7$cells/15cm plate; 2 plates/set) and after 24 hours were transfected with either pRetroX-*Strep*-FLAG (SF-EV) or pRetroX-*Strep*-FLAG-Rac1 (SF-Rac1). After 48 hours the cells were harvested and subjected to the SF-TAP purification. Following FLAG® M2 agarose beads incubation, lysates from set1 were mixed with 2x sample buffer and boiled at 70°C; proteins in set2 and set3 were eluted from the FLAG® beads using 3x FLAG® peptide and either concentrated down with a 3K Amicon filter unit (set2) or purified using acetone and methanol (set3). (B) HEK293T lysates from set1, set2 and set3 were run and separated on 12 % NuPAGE®Novex® Bis-Tris pre-cast gels using SDS-PAGE and stained with SimplyBlue™ SafeStain. (C) Schematic representation of optimised SF-TAP procedure.

4.2.1.4 Section Summary

Experiments outlined in this section were aimed at establishing a system that would allow the pulldown of Rac1 and its associated protein complexes upon expression of the different GEF constructs. Therefore SF-Rac1 was introduced to cells using the dox inducible system outlined in subsection 4.2.1.1. Results from this section demonstrate that expression of SF-Rac1 alone or together with the respective GEF constructs is induced in a dox dependent manner. In addition, further analysis of the cellular outcome upon expression of SF-Rac1 revealed that, similar to endogenous Rac1, SF-Rac1 is activated only by Tiam1 WT and P-Rex1 WT and not their GEF* mutants. Moreover, Tiam1 WT and P-Rex1 WT activation of SF-Rac1 was associated with distinct morphological and migration phenotypes in NIH3T3 cells that are

comparable to that observed upon activation of endogenous Rac1. Interestingly, expression of SF-Rac1 in NIH3T3 cells was also accompanied with a reduction in the endogenous Rac1 levels, suggesting that despite the addition of the SF-tag, the cellular machinery recognises both proteins as one. Taken together this indicates that SF-Rac1 is capable of functioning and is regulated in a similar fashion to the endogenous protein. Given these results, as outlined in this section, the SF-TAP technique was optimised for the pulldown of SF-Rac1 and Figure 4.3 C outlines the outcome of this optimisation in the form of a schematic representation of the SF-TAP procedure that was used for subsequent SF-Rac1 pulldown experiments outlined below.

4.2.2 Identification of Rac1 Binding Partners by Mass Spectrometry

Following the optimisation of the SF-TAP technique, it was crucial to ensure that the generated system is suitable for identifying SF-Rac1 binding partners by mass spectrometry and also to identify experimental parameters that increase the protein identification rate. Therefore, NIH3T3 cells containing the dox inducible SF-Rac1/GEF expression system were prepared for mass spectrometry as outlined in section 2.5.2.1.

Prior to sample submission, small aliquots of protein inputs and SF-TAP eluates were analysed by Western blot analysis to evaluate the efficiency of dox induction and SF-Rac1 pulldown. As shown in Figure 4.4 A, dox treatment induced the expression of relatively equal levels of SF-Rac1 in the different samples and was absent in the – dox treated control. However, similar to previous observations, the level of Tiam1 GEF* and P-Rex1 GEF* expression was affected by SF-Rac1 co-expression when compared to WT proteins. Therefore, as mentioned earlier, conclusions, based on the identified Rac1 interactomes under GEF* expression, were to be taken with caution. For example, if a protein was identified with WT proteins but not the GEF* mutants, given the differences in expression, this did not conclusively indicate that this Rac1-effector interaction is only modulated by the WT activation of Rac1. The efficiency of SF-TAP was also assessed by Western blot analysis using 1 % of concentrated SF-TAP eluates. Similar to SF-Rac1 expression levels, the SF-TAP yielded relatively equal amounts of SF-Rac1 in the different samples analysed, and was restricted only to + dox treated cells.

Having confirmed the efficiency of dox induction and SF-Rac1 pulldown, the reminder of the concentrated SF-TAP eluates were separated on 12 % NuPAGE®Novex® Bis-Tris pre-cast gels and stained with SimplyBlue™ SafeStain as demonstrated in Figure 4.4 B. The different lanes were then laddered and cut into 27 gel slices and sent separately to identify the composition of Rac1 binding proteins in each sample using mass spectrometry.

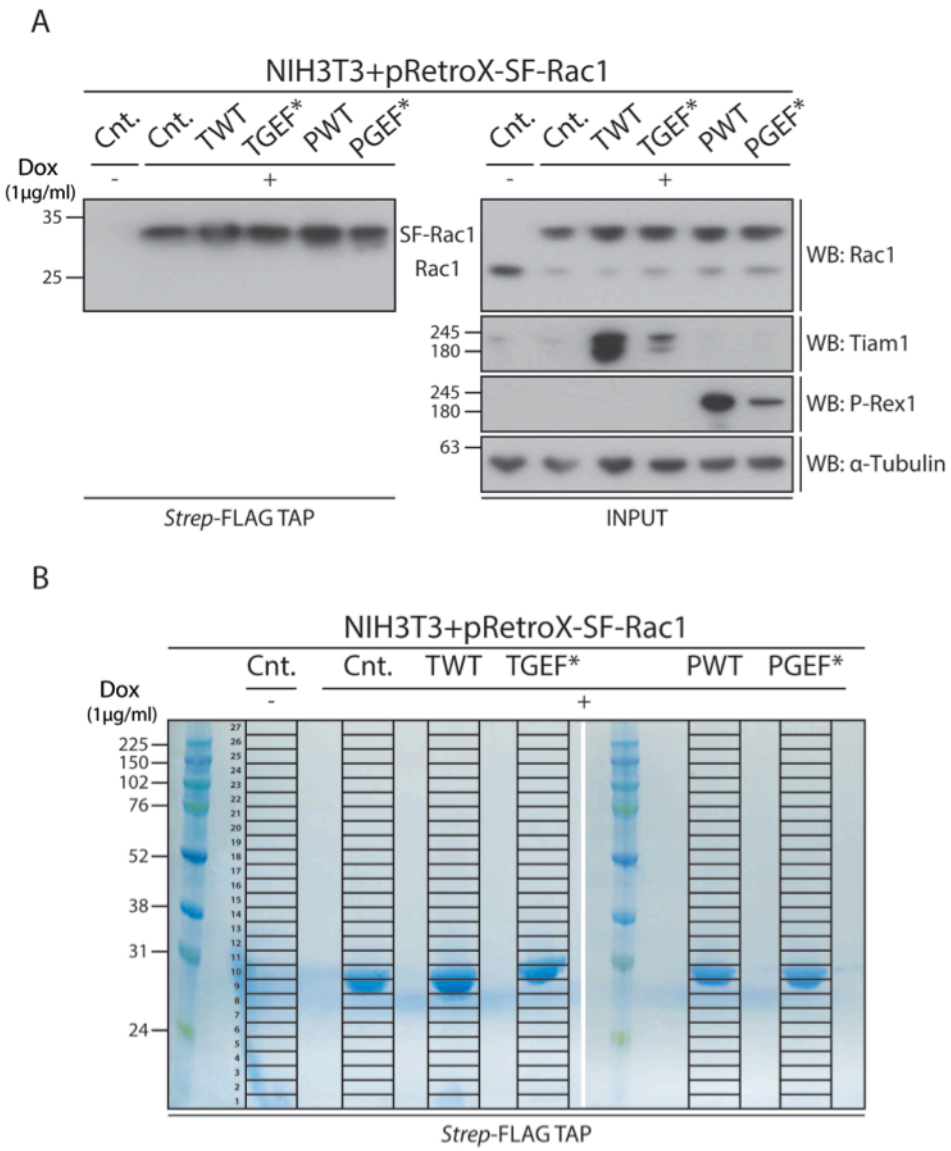

Figure 4.4: Identification of Rac1 Binding Partners By Mass Spectrometry
NIH3T3 cells harbouring the pRetroX doxycycline (dox) inducible system for expression of SF-Rac1 alone (NIH3T3+pRetroX-SF-Rac1 Cnt.) or together with one of the different GEF constructs were treated with ethanol (- dox) or 1µg/ml dox (+ dox) for 48 hours. Cells were harvested and subjected to *Strep*-FLAG Tandem Affinity Purification (TAP) to pulldown SF-Rac1 and its binding partners. (A) The efficiency of the SF-TAP and the dox induced protein expression was assessed by Western blot analysis using 1% of SF-TAP eluates and 0.1% input lysate material. (B) Concentrated SF-TAP lysates were run and separated on 12 % NuPAGE®Novex® Bis-Tris pre-cast gels using SDS-PAGE and stained using SimplyBlue™ SafeStain. The different lanes were then laddered and cut into 27 pieces and sent for mass spectrometry to identify proteins that bind to Rac1 under the different activating conditions.

4.2.2.1 Optimisation of Mass Spectrometry for Efficient Identification of Rac1 Binding Partners

The SF-TAP technique followed by mass spectrometry proteomic analysis was conducted three times, each time using different protein concentrations as the starting material (6.88 mg/ml, 11.298 mg/ml and 13.5 mg/ml) to identify an optimal protein concentration for the detection of Rac1 and its associated protein complexes. As expected, increasing the protein starting material also increased the number of identified Rac1 binding partners in each lane. Figure 4.5 highlights such relationship by looking at the number of identified Rac1-associated proteins, after eliminating contaminants, such as keratin, uncharacterised proteins as well as proteins that were identified in control – dox treated cells for each independent biological replica (BR1-3). With the exception of proteins identified upon

expression of Tiam1 GEF* in BR3, the increase in protein concentration results in an increase in the number of Rac1 specific binding partners.

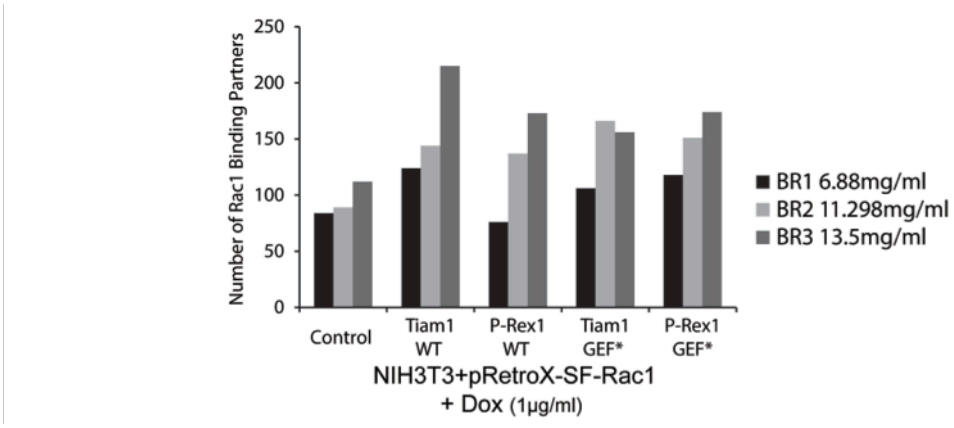

Figure 4.5: The Effect of Protein Concentration Input on the Number of Rac1 Binding Partners Identified by Mass Spectrometry

The number of Rac1 binding partners identified in three different biological replicas (BR1-3) was compared to assess the influence of increasing the protein concentration used as starting material on the mass spectrometry identification rate. Graph represents the number of Rac1 binding partners in NIH3T3 cells harbouring the doxycycline (dox) inducible system for expressing SF-Rac1 alone (control) or together with wild type (WT) Tiam1 and P-Rex1 of their GEF-dead mutants (GEF*). Ethanol (- dox) treated control cells were used to filter proteins that bind non-specifically following the SF-TAP procedure. Contaminants, such as keratin, as well as uncharacterised proteins identified were also removed. The graph represents the filtered number of Rac1 binding partners for each cellular condition in the three different mass spectrometry experiments. The protein starting material for each BR is indicated in the legend.

4.2.2.2 Mass Spectrometry Screen Analysis

Experiments described above were designed to test the specificity and sensitivity of SF-TAP followed by mass spectrometry in identifying Rac1 binding partners. Therefore, the combined list of proteins identified upon expression of the different GEFs after filtering non-specific interactors identified in the – dox treated control cells were analysed using available protein databases, such as the Human Protein Reference Database (HPRD) (Prasad et al., 2009), NetPath (Kandasamy et al., 2010) and the Human Protein-Protein Interaction Predictions (PIPs) database (McDowall et al., 2009; Scott and Barton, 2007). These databases provided an opportunity to assess the robustness of the SF-TAP in identifying Rac1 binding partners. For example, the HPRD provides a centralised platform that integrates information that was manually extracted from the literature regarding domain composition, PTMs, and protein-protein interaction networks for all the proteins identified thus far in the human proteome. It therefore, provides a powerful tool for determining whether protein lists generated from the mass spectrometry screen contain known Rac1 interactors (Prasad et al., 2009). Similarly, the NetPath database, a joint collaboration between the Pandey lab at John Hopkins University and the Institute of Bioinformatics, is a manually generated database that provides information on previously described signal transduction pathways, and thus is also useful in identifying known Rac1 interactors from the generated lists (Kandasamy et al., 2010). Unlike the HPRD and NetPath, the PIPs database was created by the University of Dundee as a resource to predict potential protein-protein interactions by intercalating information from gene co-expression

studies, protein orthology, domain co-occurrence, colocalisation experiments, PTMs and protein network analysis (McDowall et al., 2009; Scott and Barton, 2007). Therefore, the PIPs database was utilised to determine the power of the performed screen in identifying predicted Rac1 binding partners. Together these databases in combination with evidence from the literature manually extracted, were used to classify the identified proteins into known Rac1 binding partners, predicted partners and proteins that are involved in Rac1 signalling. Unclassified proteins were considered to be novel Rac1 binding partners. The full list of identified specific Rac1 associated proteins can be found for each BR in Tables S.1-S.3 on the supplementary CD accompanying the appendix section.

Table 4.1 List of Known Rac1 Binding Partners Identified From Mass Spectrometry Experiments

Protein Name	Evidence*
Alpha-tubulin	HPRD
Annexin A2	Ref.1
Calmodulin	Ref.2
Dedicator of cytokinesis 7	Ref.3
Dedicator of cytokinesis protein 1	NetPath
Engulfment and cell motility protein 1	Ref.4
Filamin-A	HPRD
Filamin-B	Ref.5
Phosphatidylinositol-3, 4, 5-trisphosphate-dependent Rac exchange Factor 1	Ref.6
Ras GTPase-activating-like protein IQGAP1	NetPath
Ras GTPase-activating-like protein IQGAP2	HPRD
Ras GTPase-activating-like protein IQGAP3	Ref.7
Ras-related C3 botulinum toxin substrate 1	-
Rho GDP-dissociation inhibitor 1	HPRD
Rho GDP-dissociation inhibitor 2	HPRD
Small ubiquitin-related modifier 2	Ref.8
Tubulin alpha-1A chain	HRPD
Tubulin alpha-1B chain	HRPD
Ubiquitin	Ref.9; 10; 11; 12; 13
Vang-like protein 2	Ref.14

** Data gathered from indicated Pubmed references; the Human Protein Reference Database (HPRD) or the NetPath Database*

Ref.1 (Hansen et al., 2002); Ref.2 (Vidal-Quadras et al., 2011); Ref.3 (Watabe-Uchida et al., 2006); Ref.4 (Wang et al., 2014); Ref.5 (Jeon et al., 2008); Ref.6 (Welch et al., 2002); Ref.7 (Alan and Lundquist, 2013; Wang et al., 2007); Ref.8 (Castillo-Lluva et al., 2010); Ref.9 (Lynch et al., 2006); Ref.10 (Visvikis et al., 2008); Ref.11 (Torrino et al., 2011); Ref.12 (Mettouchi and Lemichez, 2012); Ref. 13 (Castillo-Lluva et al., 2013); Ref.14 (Lindqvist et al., 2010).

Following the above analysis, Table 4.1 presents a list of known Rac1 binding partners identified from BR1-3. As demonstrated, Rac1 (highlighted in bold) together with a number of known Rac1 associated proteins were identified from the mass spectrometry experiments. As expected, a number of the identified known Rac1 binding partners are involved in the GDP-GTP cycle and include various GEFs and GDIs that have been reported to activate and inactivate Rac1, respectively (highlighted in green).

Additionally, the screen was also able to identify previously reported posttranslational modifications such as ubiquitylation and SUMOylation as indicated by the binding of ubiquitin and Small-Ubiquitin Related Modifier 2 (SUMO-2). Importantly, among the known Rac1 binding proteins are previously described Rac1 effectors (highlighted in red) that bind to Rac1 once in

the active form. In addition to the known Rac1 interactors, predicted Rac1 binding partners were also identified from the mass spectrometry experiments based on evidence gathered from the PIPs database. Table 4.2 highlights the list of predicted Rac1 binding partners and their interaction scores. Moreover, through an extensive literature search conducted a list of Rac1 binding partners that are implicated in Rac1 signalling was also generated and is outlined in Table 4.3.

Taken together this analysis clearly demonstrates the efficiency of SF-TAP followed by mass spectrometry in identifying Rac1 binding partners that have been previously shown, either by direct interaction or indirectly through various mechanisms, to cooperate with Rac1 and induce specific downstream signalling cascades. Given the above, it can be argued that a large number of the remaining unclassified Rac1 associated proteins identified from the screen are, in fact, specific novel Rac1 binding partners.

Table 4.2 List of Predicted Rac1 Binding Partners Identified From Mass Spectrometry Experiments

Protein Name	Interaction Score*
26S proteasome non-ATPase regulatory subunit 1	0.051
40S ribosomal protein SA	0.032
Alpha-actinin-4	0.025
AP-2 complex subunit alpha-1	0.027
AP-2 complex subunit mu	0.025
Bifunctional aminoacyl-tRNA synthetase	0.025
Breast cancer type 2 susceptibility protein homolog	0.028
Coatomer subunit alpha	0.025
Coatomer subunit epsilon	0.041
Disabled homolog 2	0.051
Dynactin subunit 1	0.025
E3 ubiquitin-protein ligase HUWE1	0.028
Early endosome antigen 1	0.0416
Gelsolin	3.47
Golgin subfamily A member 3	0.028
Golgin subfamily A member 4	0.028
Hsp90aa1 protein	0.025
Integrin-linked protein kinase	0.025
IQ motif and SEC7 domain-containing protein 2	0.104
KH domain-containing, RNA-binding, signal transduction-associated protein 1	0.137
LIM domain only 7	0.028
M-phase inducer phosphatase 1	0.025
Microtubule-associated protein RP/EB family member 1	0.025
Myosin-9	0.082
Probable E3 ubiquitin-protein ligase MYCBP2	0.025
Rho-associated protein kinase 1	0.085
Rho-associated protein kinase 2	0.037
RNA polymerase-associated protein CTR9 homolog	0.028
S-methyl-5'-thioadenosine phosphorylase	0.025
Spectrin alpha chain, erythrocyte	0.028
T-complex protein 1 subunit delta	0.025
T-complex protein 1 subunit zeta	0.025
Thiosulfate sulfurtransferase	0.025
Transitional endoplasmic reticulum ATPase	0.025
Vigilin	0.025

** Data gathered from the Human Protein-Protein Interaction Prediction (PIPs) Database*

Table 4.3 List of Rac1 Binding Partners Involved in Rac1 Signalling Identified From Mass Spectrometry Experiments

Protein Name	Evidence*
Alpha-actinin 1	Ref.1
Alpha-1-syntrophin	Ref.2
Aurora kinase A	Ref.3
Calpastatin	Ref.4
Dock10 protein	Ref.5
Dystrophin	Ref.6
Engulfment and cell motility 2, ced-12 homolog (C. elegans)	Ref.7
Fibronectin	Ref.8
Gamma-aminobutyric acid (GABA-A) receptor, subunit alpha 3	Ref.9
Integrin alpha-2	Ref.10
Integrin beta-1	Ref.11
Kinesin-1 heavy chain	Ref.12
Matrix metalloproteinase-15	Ref.13
Myh11 protein	Ref.14
Myosin heavy chain	Ref.14
Myosin light chain 1, skeletal muscle isoform	Ref.14
Myosin light polypeptide 6	Ref.14
Myosin-10	Ref.14
Myosin-3	Ref.14
Myosin-4	Ref.14
Myosin-7B	Ref.14
Myosin-Ic	Ref.14
Myosin-Id	Ref.14
Myosin-XV	Ref.14
Myosin, heavy polypeptide 10, non-muscle	Ref.14
Myosin, heavy polypeptide 13, skeletal muscle	Ref.14
Myosin, heavy polypeptide 7, cardiac muscle, beta	Ref.14
Nestin	Ref.15
Nitric oxide synthase, inducible	Ref.16
Nuclear factor NF-kappa-B p100 subunit	Ref.17
Nucleolin	Ref.18
Protein disulfide-isomerase	Ref.19
Protein flightless-1 homolog	Ref.20
Rab21	Ref.21
Stathmin	Ref.22
Vascular cell adhesion protein 1	Ref.23
Zyxin	Ref.24

** Data gathered from indicated Pubmed references*

Ref.1 (Kovac et al., 2013); Ref.2 (Bhat et al., 2014); Ref.3 (Braun et al., 2014); Ref.4 (Shan et al., 2010); Ref.5 (Gadea et al., 2008); Ref.6 (Oak et al., 2003); Ref.7 (Gumienny et al., 2001); Ref.8 (Kimura et al., 2006); Ref.9 (Meyer et al., 2000); Ref.10 (Keely et al., 1997); Ref.11 (Yu et al., 2005); Ref.12 (Takahashi and Suzuki, 2008); Ref.13 (Yukinaga et al., 2014); Ref.14 (van Leeuwen et al., 1999) ; Ref.15 (Yoon et al., 2011); Ref.16 (Wang et al., 2011); Ref.17 (Matos and Jordan, 2006); Ref.18 (Villace et al., 2004); Ref. 19 (Pescatore et al., 2012); Ref.20 (Kopecki et al., 2011); Ref.21 (Fujii et al., 2013); Ref.22 (Morimura and Takahashi, 2011); Ref.23 (Cook-Mills et al., 2004); Ref.24 (Sun et al., 2012).

4.2.2.3 Unique Rac1 Binding Partners Upon Tiam1 and P-Rex1 Rac1 Activation

As mentioned earlier, the aim of this screen was to assess the role played by Tiam1 and P-Rex1 in mediating differential Rac1-effector binding profiles as an underlying mechanism to their ability to influence distinct Rac1-driven cellular effects. Given the outcome of the analysis outlined above highlighting the strength of the screens performed, the proteins identified upon expression of Tiam1 WT and P-Rex1 WT were subjected to a series of filtering steps to identify unique Rac1 binding partners induced by either GEF. This was conducted by comparing the proteins identified in the Tiam1 WT or P-Rex1 WT lanes and eliminating any that were identified in control (- dox and + dox treated cells), Tiam1 GEF* and P-Rex1 GEF* cells. These lists were then compared to one another and common proteins, contaminants and uncharacterised

proteins were disregarded, thereby creating a list of proteins that associate with Rac1 only in the presence of Tiam1 WT and P-Rex1 WT. In addition, to assess reproducibility, each biological replica was analysed separately. Unique Rac1 binding partners identified in each experiment upon activation of SF-Rac1 by Tiam1 WT and P-Rex1 WT are outlined in Tables A.1-A.3 in the appendix section. As can be seen from these tables, despite the identification of unique partners in each experiment the overlap between the lists was minimal, with only one protein for Tiam1 [Cullin-associated Nedd8-dissociated protein 1 (CAND1)] and P-Rex1 [Protein flightless-1 homolog (FLII)] identified in more than one experiment.

4.2.2.4 Section Summary

As demonstrated from this section, SF-TAP followed by mass spectrometry was efficient in identifying SF-Rac1 and its associated protein complexes. Through an extensive literature review combined with information gathered from databases, such as HPRD, NetPath and PIP it was shown that a number of known Rac1 interactors were identified. Among this list are proteins involved in regulating the GDP-GTP Rac1 cycle, Rac1 effectors as well as posttranslational modifications' modifiers, all adding to the validity of the screen. Moreover, a number of predicted Rac1 binding partners, as indicated by the PIPs database, were also detected. The screen also identified a number of proteins that have not been reported to bind to Rac1, yet contribute to Rac1 signalling. Taken together this indicates that SF-TAP followed by mass spectrometry is an efficient way to identify Rac1 associated protein complexes. However, despite this success, conventional mass spectrometry was unable to capture a large number of unique Rac1-effector complexes upon expression of Tiam1 WT and P-Rex1 WT consistently across the biological replicas, thus questioning the robustness of the technique employed. Yet, given that the prime focus of the experiments described in this section was to optimise conditions necessary for identifying Rac1 binding partners using SF-TAP followed by mass spectrometry, direct comparison between the replicas might be misleading as different conditions, such as the protein input starting material, were used. The lack of reproducibility in these experiments might also indicate that Tiam1 and P-Rex1 induce differential Rac1 signalling, not only by promoting the formation of unique Rac1-protein complexes, but also by modulating the binding level of commonly bound Rac1 interactors identified under both GEFs, calling for the use of a more sensitive quantitative protein identification approach, such as SILAC.

4.2.3 Quantitative Mass Spectrometry: Stable Isotope Labelling by Amino Acids in Cell Culture (SILAC)

4.2.3.1 SILAC Experimental Setup

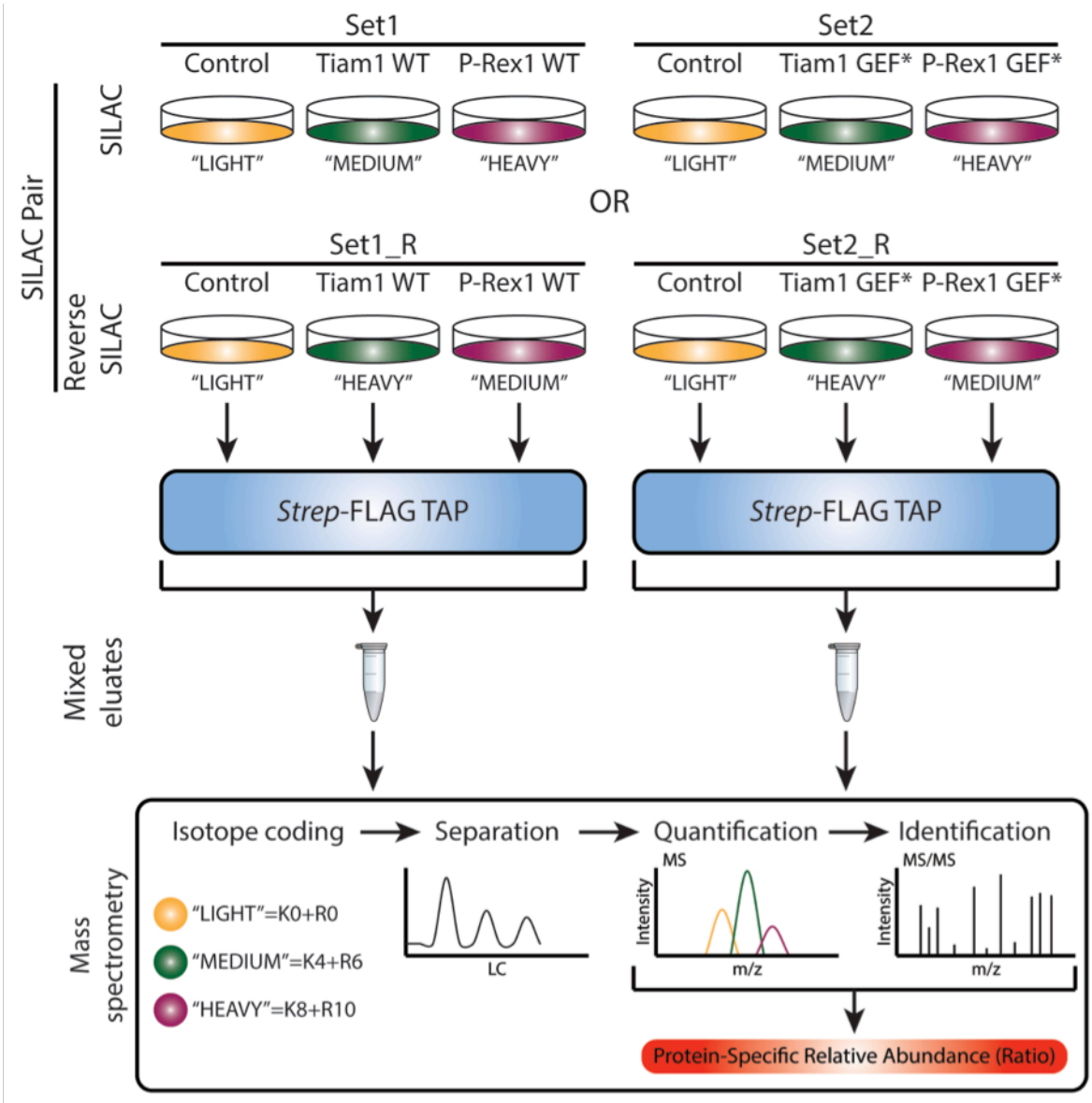

Figure 4.6: Schematic Representation of Five-Way SILAC Experimental Setup
Schematic representation of five-way Stable Isotope Labelling by Amino Acid in Cell Culture (SILAC) experimental setup in conjunction with the *Strep*-FLAG Tandem Affinity Purification (SF-TAP) technique. NIH3T3 cells harbouring the doxycycline (dox) inducible expression system for SF-Rac1 alone (NIH3T3+pRetroX-SF-Rac1 control) or together with Tiam1/P-Rex1 wild type (WT; Set1/Set1_R) or GEF-dead mutants (GEF*; Set2/Set2_R) were cultured in different isotopically labelled SILAC media ("LIGHT"= Lysine 0 (K0)+Arginine 0 (R0); "MEDIUM" = K4+R6; "HEAVY" = K8+R10) as indicated. Cell extracts from all three cell types were purified using the SF-TAP technique. Eluates from each set were then mixed. Rac1 together with any binding partners that came down in the SF-TAP experiment were subjected to mass spectrometry analysis. As a result of SILAC labelling, proteins from the different culturing conditions have different yet known mass shifts allowing a quantitative comparative proteomic analysis of Rac1 interactors upon expression of the different GEF constructs. The reciprocal experiment was also conducted with the reverse labelling of Tiam1 and P-Rex1 (reverse SILAC). The SILAC and Reverse SILAC samples were considered a SILAC pair and were processed together to eliminate background proteins identified from the screen. Two SILAC pairs were performed to assess reproducibility.

Figure 4.6 outlines the experimental design of the identification of Rac1 binding partners using SILAC and SF-TAP. In brief, NIH3T3 cells harbouring the dox inducible system for expressing SF-Rac1 alone (control) or together with different GEF constructs were labelled

using three different SILAC labelling media that were prepared as outlined in section 2.5.3.1. Due to the limited number of isotopes available for labelling cells were divided into two sets. The first set included the control cells together with Tiam1 WT and P-Rex1 WT expressing cells. Using the same control, the second set included the Tiam1 GEF* and P-Rex1 GEF* expressing cells. This five-way SILAC setup allowed the comparison of the proteomes within each set directly with one another but also indirectly with the proteomes identified in the other set relative to the common control. As illustrated in the schematic representation, control cells in both sets were cultured in LIGHT SILAC media, and no alerted protein masses were expected and the cells were considered as unlabelled cells. In the forward SILAC setup Tiam1 WT/GEF* expressing cells were cultured in MEDIUM SILAC media, while P-Rex1 WT/GEF* were cultured in HEAVY SILAC media. The culturing conditions for Tiam1 and P-Rex1 expressing cells were reversed between the SILAC and reverse SILAC experiments to enhance the robustness of the screen. Thus in reverse SILAC Tiam1 WT/GEF* expressing cells were cultured in HEAVY SILAC media and P-Rex1 WT/GEF* expressing cells in MEDIUM SILAC media. After six doubling rounds and confirmation of the amino acid incorporation into the proteome, cells were expanded in their respective culturing media and subjected to the SF-TAP technique. SF-TAP eluates from each set were then mixed in equal ratios and proteins were analysed as one sample per set using mass spectrometry. The SILAC and reverse SILAC samples were considered a SILAC pair and were processed together to eliminate background proteins identified from the screen. Two SILAC pairs were performed to assess reproducibility. The relative abundance of Rac1 binding partners in each sample was enabled due to the associated mass shifts induced by the amino acid isotope labelling of proteins.

4.2.3.2 NIH3T3 Isotope Labelling

Using the experimental setup described in the above subsection, NIH3T3 cells harbouring the dox inducible SF-Rac1/GEF expression system were labelled in the respective media as outlined in Figure 4.6. To calculate the normal doubling cycle of unlabelled NIH3T3 cells, - dox treated cells were plated at equal densities and the cells were counted every 24 hours for 6 days. Results from this experiment suggested a 24-36 hours doubling time. Therefore, using this information, cells were plated at relatively equal densities and were expanded when 80 % confluent for 6 days in the respective SILAC media. Figure 4.7 A outlines the actual cellular densities of SILAC labelled cells after 3 days and 6 days of labelling relative to expected cellular densities. As can be seen, at Day 6 cells exceeded the expected cell count indicating that more than 6 doubling rounds were achieved in the labelling media. This was also seen with reverse SILAC labelled cells. A small batch of labelled cells were treated with ethanol (- dox) or 1 μg/ml dox (+ dox) for 48 hours and used to check that culturing cells does not affect the ability of dox to induce protein expression.

A

Cell density ($1x10^5$)	Day1	Day3	Day6
Control	0.746	4.2 (2.984)	66 (47.744)
Tiam1 WT	0.886	3.744 (3.544)	73 (56.704)
Tiam1 GEF*	0.756	4.222 (3.024)	82 (48.384)
P-Rex1 WT	0.884	4.554 (3.536)	81.45 (56.576)
P-Rex1 GEF*	0.504	2.184 (2.016)	32 (32.256)

B

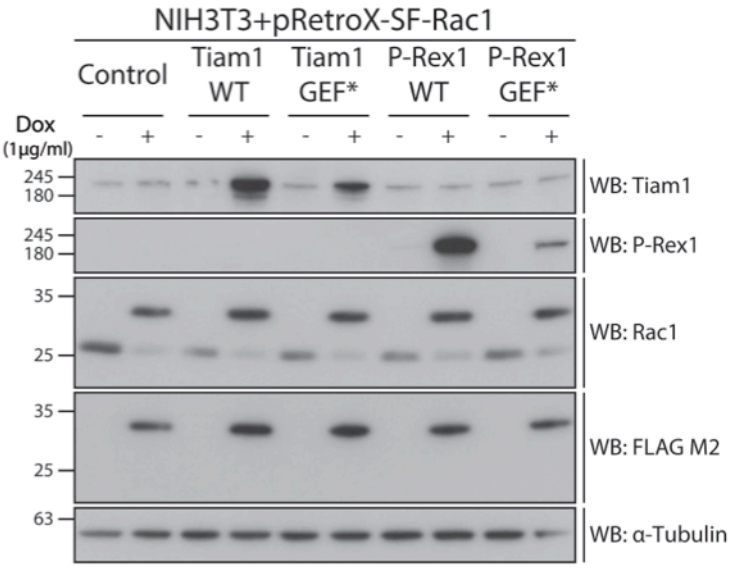

C

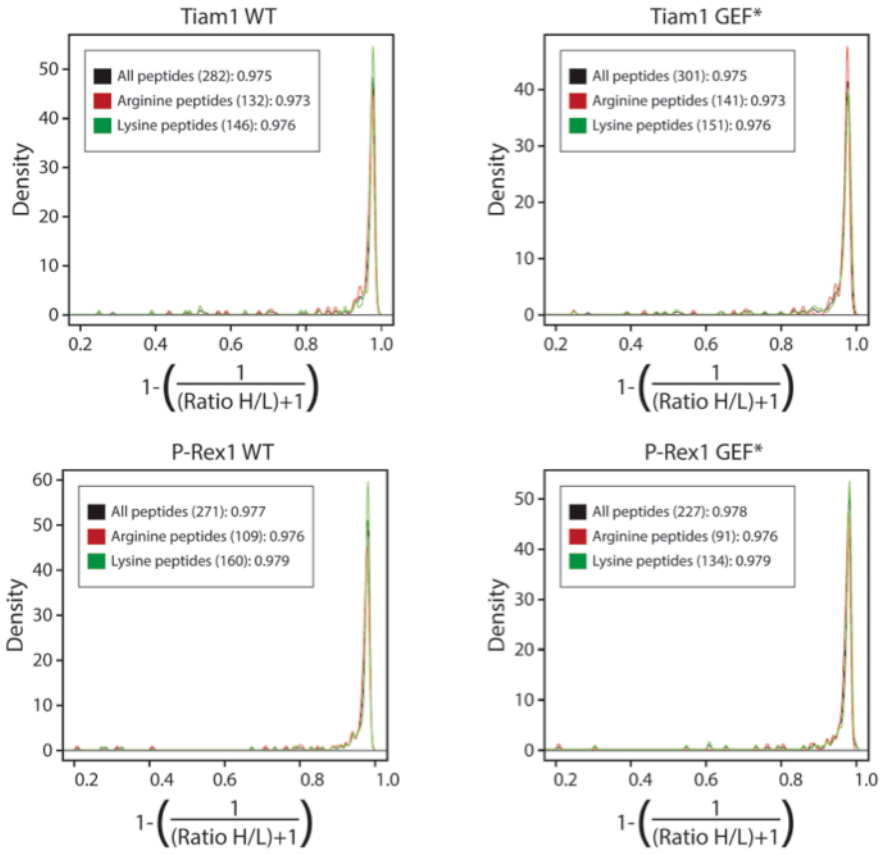

Figure 4.7: SILAC Amino Acid Labelling and Incorporation Check

NIH3T3 cells harbouring the doxycycline (dox) inducible expression system for SF-Rac1 alone (NIH3T3+pRetroX-SF-Rac1 control) or together with Tiam1/P-Rex1 wild type (WT) or GEF-dead mutants (GEF*) were cultured in different isotopically labelled SILAC media ("LIGHT"=K0+R0; "MEDIUM"=K4+R6; "HEAVY"=K8+R10) for 6 doubling rounds. (A) The doubling rate of unlabelled NIH3T3 cells was calculated as 24-36 hours from various experiments. Accordingly the expected cell densities at day3 and day6 (shown in red) were determined for each cell type relative to the initial cell density plated at day1 following SILAC labelling. Cells were counted at various time points and shown are values from day3 and day6. (B) Upon culturing the cells with the isotopically labelled SILAC media, cells were harvested and the efficiency of the dox induced SF-Rac1, Tiam1 WT/GEF* and P-Rex1 WT /GEF* expression was assessed by Western blot analysis using anti-Rac1, anti Tiam1 and anti-P-Rex1 antibodies. (C) The efficiency and rate of amino acid incorporation was assessed by lysing cells after 6 doubling rounds and using mass spectrometry analysis to detect the mass shift in both arginine (R) and lysine (K) protein peptides. Amino acid incorporation rates were calculated using the equation outlined on the x-axis (H=peptides with higher mass shift i.e. labelled; L=peptides with normal masses i.e. unlabelled). Graphs show the amino acid incorporation rates for Tiam1 WT/GEF* and P-Rex1 WT/GEF* using cells treated with 1µg/ml dox (+ dox) for 48 hours.

As shown in Figure 4.7 B upon addition of dox, relatively equal expression of SF-Rac1 was achieved in the different cells and was limited to + dox treated cells. Additionally, co-expression of the different GEF constructs was not affected by culturing cells in the respective labelling media for 6 doubling rounds. Cell lysates were also used to check the amino acid incorporation rate in Tiam1 WT/GEF* and P-Rex1 WT/GEF* expressing cells. Using mass spectrometry, the ratio of K and R labelled protein peptides versus the unlabelled portion was detected. An amino acid incorporation rate was then calculated using the equation outlined in section 2.5.3.2. Figure 4.7 C illustrates the incorporation rates for SILAC labelled cells where the K incorporation profile is presented in green and the R profile in red. As demonstrated from these graphs the incorporation rate for both amino acids exceeded 97 % in all labelled cells indicating successful protein labelling. Similar results were also observed for reverse SILAC labelled cells.

4.2.3.3 The effect of SILAC Labelling on GEF-Rac1-Driven Cellular Effects

As highlighted earlier, in order to label cells using the different SILAC amino acid isotopes, live cells are cultured for 6 doubling rounds in the respective SILAC media to induce the known protein mass shifts upon proteolytic digestion. This is performed in media containing dialysed FBS to avoid contamination of protein samples with naturally occurring amino acids that might be present in normal FBS. As a result of the dialysis process, the FBS lacks certain growth factors and thus some cell lines are affected by culturing in the SILAC media. Therefore it was important to assess the influence of SILAC labelling on the cellular behaviour of NIH3T3 cells, especially upon expression of the different GEFs.

To address this issue, labelled NIH3T3 cells harbouring the dox inducible SF-Rac1/GEF expression system were treated with ethanol (- dox) or 1 μg/ml dox (+ dox) and changes in their morphological phenotypes and migration potential were assessed while culturing in the respective SILAC media. As indicated from Figure 4.8, expression of Tiam1 WT and P-Rex1 WT but not their GEF* mutants, resulted in distinct cellular outcomes. Using the ORIS^{TM} migration assay, Figure 4.8 A and B show that expression of Tiam1 WT in MEDIUM labelled cells was associated with a 17 % and 24 % decrease in cellular migration when compared to control cells labelled in LIGHT SILAC media or to the Tiam1 WT – dox treated cells. In contrast, P-Rex1 WT expressing cells labelled in HEAVY SILAC media exhibited an increased cellular migration rate by 26 % and 20 % when compared to control and P-Rex1 WT – dox treated cells, respectively. These distinct migration abilities were not observed in cells expressing Tiam1 GEF* and P-Rex1 GEF*. These results are in agreement with previous observations outlined in section 4.2.3.3 showing that culturing cells with the different SILAC labels and the use of dialysed FBS did not influence the ability of Tiam1 and P-Rex1 to induce distinct migration abilities.

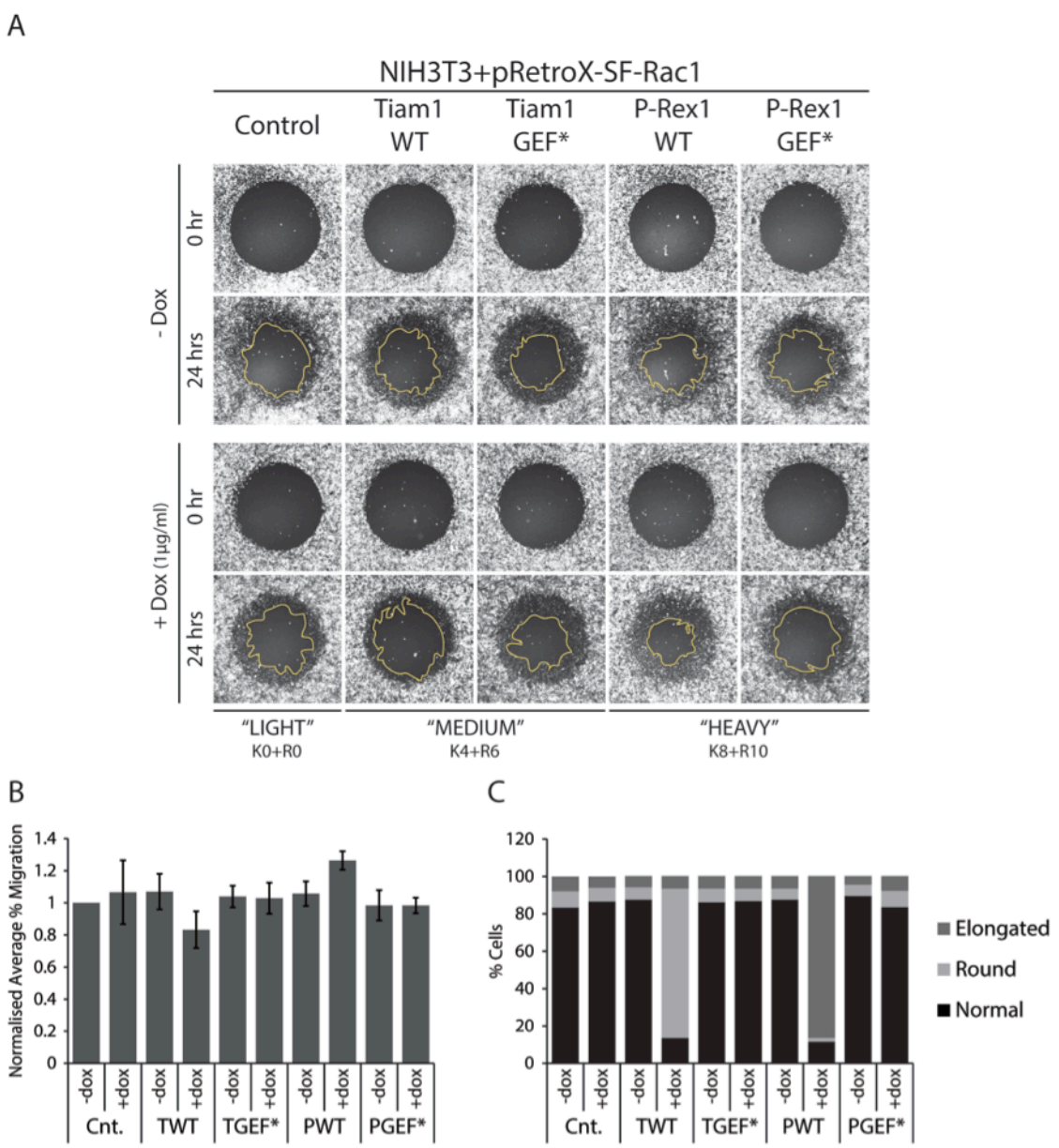

Figure 4.8: The Effect of SILAC Media on GEF-Rac1 Driven Cellular Functions
(A) SILAC labelled NIH3T3 cells harbouring the doxycycline (dox) inducible system for the expression of SF-Rac1 alone (NIH3T3+pRetroX-SF-Rac1 control) or together with wild type (WT) Tiam1 and P-Rex1 or their GEF-dead (GEF*) mutant were treated with ethanol (- dox) or 1 μg/ml dox (+ dox) for 24 hours. Following dox induction the migration potential of these cells was assessed using the Oris™ Migration Assay while cells were still cultured in their designated SILAC media ("LIGHT"=K0+R0; "MEDIUM"=K4+R6; "HEAVY"=K8+R10). Florescence images were taken using the low light microscopy system (5x magnification) at 0 hours and 24 hours post stopper removal. (B) Quantification of cellular migration of – dox and + dox treated cells normalised to control - dox treated cells from one representative experiment. Graphs represent the normalised average % migration ± standard deviation. (C) To see the effect of culturing cells in SILAC media on the GEF induced cellular phenotypes, labelled cells were classified into three groups based on their morphology: normal, round and elongated. Graph represents % cells in each subset from a total of 150 cells/condition from various cell passages and seeding densities.

Similarly, as highlighted in Figure 4.8 C, co-expression of SF-Rac1 together with Tiam1 WT, as expected, results in 80 % of cells falling in the round morphology category with cells showing increased cellular aggregation and increased membrane ruffles as opposed to only 6.6 % in the Tiam1 WT – dox treated cells. P-Rex1 WT expression, on the other hand, resulted in 86.7 % of cells exhibiting a highly polarised cellular structure with increased membrane protrusions and were thus designated the elongated morphology category. Expression of Tiam1 GEF* and P-Rex1 GEF* similar to control (- dox and + dox treated cells) and their respective – dox treated

cells were associated with the majority of cells exhibiting the normal mesenchymal fibroblastic morphology associated with parental NIH3T3 cells. Taken together these results demonstrate that labelling of NIH3T3 cells does not interfere with normal cellular behaviour.

4.2.3.4 Section Summary

In order to overcome the inherent limitations of mass spectrometry, SF-TAP was used in conjunction with SILAC mass spectrometry to quantitatively assess the role of Tiam1 and P-Rex1 in differentially mediating Rac1-effector interactions. As outlined in this section, a five-way SILAC setup was adopted to compare the Rac1 interacting proteins within each set directly, or with the Rac1 interactome identified in the other set, indirectly through the common control LIGHT labelled cells. Two SILAC pairs were conducted in which the SILAC labelling was reversed between Tiam1 WT/GEF* and P-Rex1 WT/GEF* to reduce the number of background proteins identified. Before going forward with the proteomic analysis it was also important to assess the influence of culturing cells in SILAC labelling media on dox induction as well as the cellular behaviour of NIH3T3 cells. Results from this section demonstrate that culturing NIH3T3 cells harbouring the dox inducible SF-Rac1/GEF expression system in SILAC labelling media did not affect the dox induction of SF-Rac1 alone in control cells or together with the different GEF constructs. Additionally, via looking at the GEF-induced morphological changes and migration abilities, results indicate that SILAC labelling does not interfere with normal or GEF-induced cellular functions in these cells, thus highlighting the suitability of this system for proteomic analysis of Rac1-associated proteins upon expression of the different GEF constructs.

4.2.4 Identification of Rac1 Binding Partners Under Different Activating Conditions by SILAC

Given the benefits of utilising SILAC together with the high efficiency of amino acid incorporation detected in NIH3T3 cells and the lack of SILAC labelling interference with the GEF-induced cellular effects, SILAC labelling followed by SF-TAP was used to detect the relative differences in Rac1 protein associations upon expression of the different GEF constructs.

Mass spectrometry samples were prepared as outlined in section 2.5.3.3 and the concentrated proteins were then sent to the Proteome Center at the University of Tuebingen, Germany, headed by Professor Boris Macek for proteolytic digestion followed by mass spectrometry analysis, which was performed by Alejandro Carpy a PhD student in the Macek's group. In total, two SILAC pairs were performed and sent for mass spectrometry analysis, which was conducted simultaneously for all experiments to generate a common list of Rac1 binding partners together with their associated SILAC ratios for each of the submitted samples. For the full list of interactors please refer to Table S.4-S.7 on the supplementary CD accompanying the appendix section.

Prior to sample submission the efficiency of dox induction, SF-Rac1 pulldown and the levels of SF-TAP eluates before mixing were analysed using Western blot analysis. Figure 4.9 outlines the results from a representative SILAC labelling SF-TAP procedure. Using 0.1 % of protein starting material, the dox induction was assessed. As shown from the representative experiment, dox treatment efficiently induced the expression of equal levels of SF-Rac1 alone or together with Tiam1 WT or P-Rex1 WT in set1 and Tiam1 GEF* or P-Rex1 GEF* in set2.

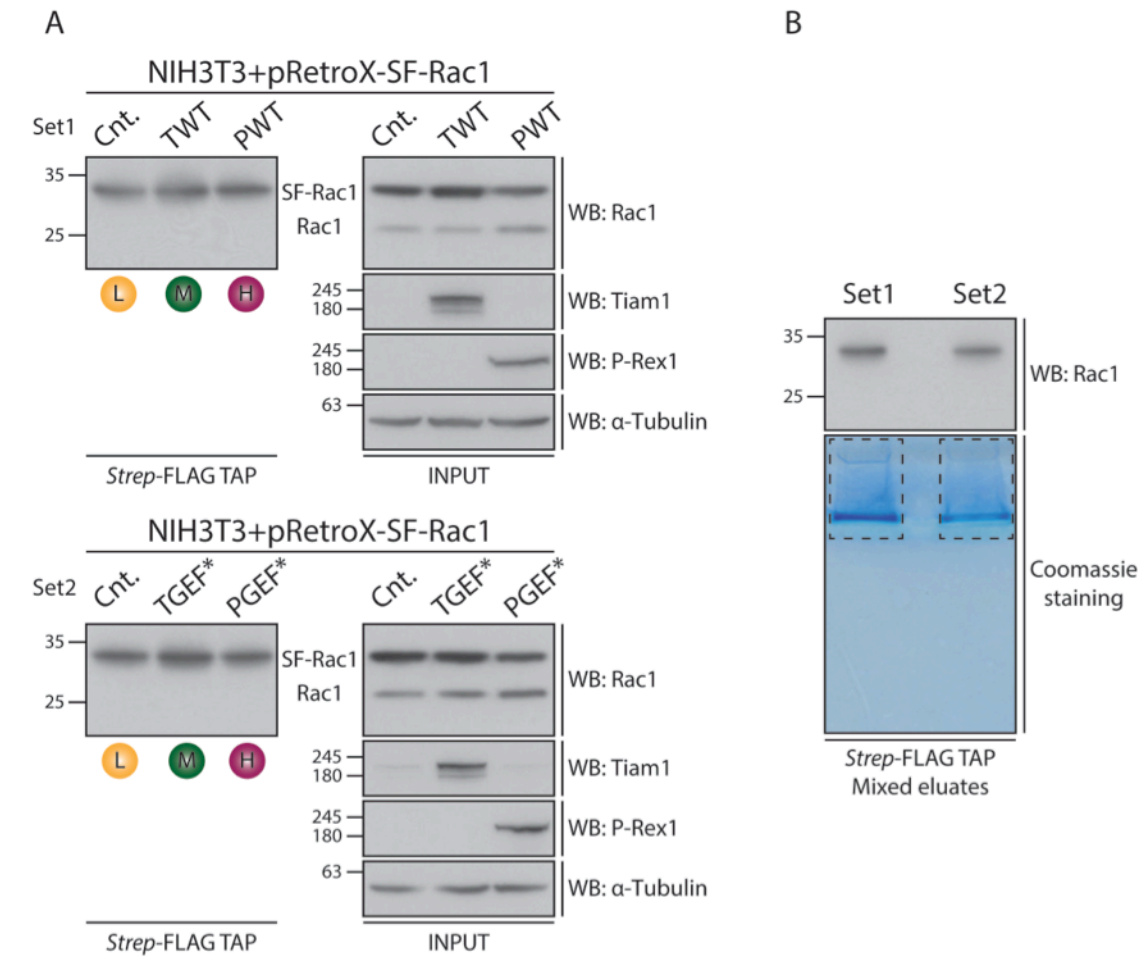

Figure 4.9: Identification of Rac1 Binding Partners Under Different Activating Conditions By SILAC
NIH3T3 cells harbouring the doxycycline (dox) inducible expression system for SF-Rac1 alone (NIH3T3+pRetroX-SF-Rac1 Cnt.) or together with Tiam1/P-Rex1 wild type (WT; Set1) or GEF-dead mutants (GEF*; Set2) were cultured in different isotopically labelled SILAC media (L="LIGHT" K0+R0; M="MEDIUM" K4+R6; H="HEAVY" K8+R10). Cells were harvested and subjected to the SF-TAP technique to pulldown SF-Rac1 and its binding partners. (A) The efficiency of dox induced protein expression and SF-TAP was assessed by Western blot analysis using 0.1% input lysate material and 1% of SF-TAP eluates, respectively. (B) Eluates from each set were mixed and 1% was used for Western blot analysis to ensure equal levels of SF-Rac1 between the two sets. The remainder was sent for mass spectrometry analysis. Samples were prepared by Alejandro Carpy and 1/3 of the concentrated samples were separated for 9 minutes on a 12 % NuPAGE®Novex® Bis-Tris pre-cast gel using SDS-PAGE and stained using Coomassie Blue to visualise the bands. Each lane was cut out as one gel slice and subjected to in-gel digest followed by mass spectrometry analysis to identify Rac1 binding partners upon expression of the different GEF constructs.

To determine the efficiency of SF-TAP and the levels of SF-Rac1 pulldown in each lane, 1 % of SF-TAP eluates, before concentration, were also analysed. As shown in Figure 4.9 A, SF-TAP yielded relatively equal levels of SF-Rac1 from the different GEF expressing cells. Therefore to achieve the equal ratio of mass spectrometry mixtures, equal volumes of the dilute SF-TAP eluates from each set were mixed prior to protein concentration was performed using the 3K Amicon filter units. Following concentration, 1 % of the mixed SF-TAP eluates from each set

were also analysed by Western blot analysis to ensure equal levels of SF-Rac1 between the different sets. As can be seen from Figure 4.9 B (upper panel), using anti-Rac1 antibody detected equal signals for both set1 and set2 indicating that there are equal levels of mixed SF-Rac1 between the two sets. This ensures that differences between the proteomes identified between the two sets are not due to differences in the SF-Rac1 levels analysed. Following sample submission, a third of each sample was run for 9 minutes on a 12 % NuPAGE®Novex® Bis-Tris pre-cast gel, stained with Coomassie Blue to visualise bands for in-gel proteolytic digestion followed by mass spectrometry. The Coomassie staining performed by Alejandro Carpy presented in the lower panel of Figure 4.9 B provides additional confirmation that equal levels of proteins were used for the mass spectrometry protein identification. Similar results were also seen for the other SILAC/reverse SILAC experiments conducted.

4.2.4.1 SILAC Analysis

As mentioned above, in total two SILAC pairs were conducted and analysed together to yield a list of identified Rac1 interactors together with their associated SILAC ratios (Tables S.4; S.7 on the supplementary CD). Combined, 350 proteins were identified from the SILAC experiments. Similar to the analysis conducted on Rac1 interactors identified from the conventional mass spectrometry, the SILAC protein list was also screened for known Rac1 interactors using information from published reports in conjunction with the HPRD and NetPath databases. As illustrated in Table 4.4, as expected the SILAC screen also yielded a number of known Rac1 binding partners in addition to Rac1 (highlighted in bold). This list included known regulators of the Rac1 GDP-GTP cycle (highlighted in green) as well as known Rac1 effectors (highlighted in red). Additionally, predicted Rac1 interactors as indicated by the PIPs database were also identified from the SILAC screen and are outlined in Table 4.5. Through extensive literature research a list of proteins that are implicated in Rac1 signalling was also generated from the SILAC identified protein list and are outlined in Table 4.6. Combined together, this illustrates the efficiency of the SILAC screen in identifying already reported Rac1 binding partners, which suggests that a number of the remaining proteins identified from the screen are specific novel Rac1 interactors.

Out of the proteins identified, 231 proteins had SILAC ratios in ≥ 2 SILAC experiments (Table S.5). SILAC ratios were then used to determine GEF-induced changes in Rac1 binding relative to that seen in control cells. For example, SILAC ratios greater than one indicated that the protein identified was more abundant than in the control LIGHT labelled cells, suggesting that the protein shows increased Rac1 binding. Conversely, SILAC ratios below one, most likely mean that the protein binds less to Rac1 under this condition. However, if the SILAC ratio is unchanged i.e. SILAC ratio around one this demonstrates that the ability of this protein to bind to Rac1 is not affected by the expression of the GEF. Using a cut off of ±1.3 fold-change relative to control cells, proteins identified under each GEF were classified into proteins that show no

change in Rac1 association, proteins that have reduced Rac1 binding and proteins that have increased Rac1 binding when compared to the interaction observed in control LIGHT labelled cells. This cut off was set based on commonly accepted fold change differences that have been previously reported in SILAC studies (Mann, 2006). GEF-induced changes in SILAC ratios were therefore analysed for each experiment individually and then cross-references with one another to assess reproducibility of an observed SILAC pattern and the inferred Rac1 binding capability. Only proteins that exhibited a similar GEF-associated pattern of Rac1 binding in ≥2 SILAC experiments were considered for further analysis, with more weight given to proteins that exhibited an inverted SILAC ratio within a SILAC pair. Figure 4.10 A summaries the number of identified proteins per GEF while categorising them based on their Rac1 binding abilities. Additionally, Alejandro Carpy also employed a commonly used statistical test generated using the MaxQuant software, known as Significance B, which takes into account various factors, such as the number of peptides identified and the associated SILAC ratios to determine whether an observed change in SILAC ratio is significant (Table S.7). It must be noted, however, that Significance B values were not considered for the initial classification of proteins outlined in Figure 4.10 and were instead used as a guide to select proteins for further analysis.

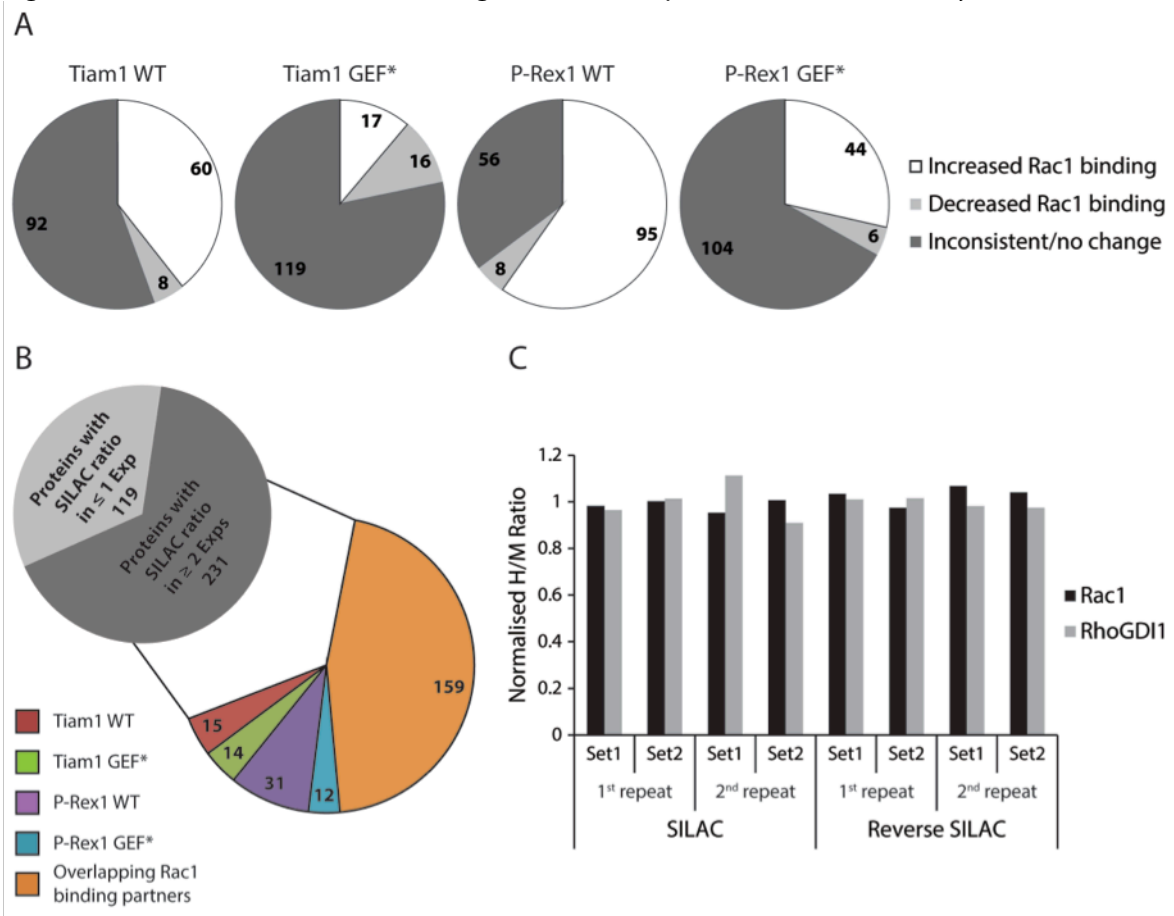

Figure 4.10: SILAC and Reverse SILAC Statistics

(A) Pie chart classifying identified Rac1 binding partners from the SILAC screens into proteins exhibiting unchanged/decreased/increased Rac1 binding upon expression of the indicated GEFs using a SILAC ratio cut off set at ±1.3 fold change relative to control cells. (B) Pie chart of total identified Rac1 binding partners from all four SILAC experiments showing number of proteins that show a specific Rac1 binding pattern only upon expression of the indicated GEFs (cut off set at ±1.3 fold change relative to control cells). (C) Graph showing the normalised heavy (H)/ light (L) ratio (Tiam1/P-Rex1 in SILAC and P-Rex1/Tiam1 in reverse SILAC experiments) for two identified proteins, Rac1 and RhoGDI1 for all four SILAC experiments to demonstrate the effectiveness of using SILAC ratios in assessing Rac1 binding capability.

Table 4.4 List of Known Rac1 Binding Partners Identified From SILAC Experiments

Protein Name	Evidence*
Alpha-actin 1	HPRD
Alpha-tubulin 1	HPRD
Calmodulin	Ref.1
Dedicator of cytokinesis protein 7	Ref.2
Filamin-A	HPRD
Filamin-B	Ref.3
Ras GTPase-activating-like protein IQGAP1	NetPath
Ras GTPase-activating-like protein IQGAP2	HPRD
Ras GTPase-activating-like protein IQGAP3	Ref.4
Ras-related C3 botulinum toxin substrate 1	-
Rho GDP-dissociation inhibitor 1	HPRD
Rho GDP-dissociation inhibitor 2	HPRD
Rho GDP-dissociation inhibitor 3	HPRD

** Data gathered from indicated Pubmed references; the Human Protein Reference Database (HPRD) or the NetPath Database*

Ref.1 (Vidal-Quadras et al., 2011); Ref.2 (Watabe-Uchida et al., 2006); Ref.3 (Jeon et al., 2008); Ref.4 (Wang et al., 2007).

Table 4.5 List of Predicted Rac1 Binding Partners Identified From SILAC Experiments

Protein Name	Interaction Score*
Alpha-actinin 4	0.025
14-3-3 protein gamma	0.152
14-3-3 protein theta	0.028
AP-2 complex subunit mu	0.025
Bifunctional aminoacyl-tRNA synthetase	0.025
Centaurin beta 2	0.104
Coatomer subunit epsilon	0.041
Cofilin-1	3.47
Dynactin subunit 1	0.025
E3 ubiquitin-protein ligase HUWE1	0.028
Heterogeneous nuclear ribonucleoprotein K	0.028
Peptidyl-prolyl cis-trans isomerase A	0.137
S-methyl-5-thioadenosine phosphorylase	0.025
Spectrin alpha 2	0.028
T-complex protein 1 subunit delta	0.025
T-complex protein 1 subunit zeta	0.025

** Data gathered from the Human Protein-Protein Interaction Prediction (PIPs) Database*

Table 4.6 List of Rac1 Binding Partners Involved in Rac1 Signalling Identified From SILAC Experiments

Protein Name	Evidence*
Actin-related protein 2/3 complex subunit 1B	Ref.1
Actin-related protein 2/3 complex subunit 2	Ref.1
Actin-related protein 2/3 complex subunit 3	Ref.1
Actin-related protein 2/3 complex subunit 4	Ref.1
Actin-related protein 3	Ref.1
Alpha-actinin 1	Ref.2
Cell division control protein 42 homolog	Ref.3; 4
Diaphanous-related formin-1	Ref.5
Kinesin-1 heavy chain	Ref.6
Myosin heavy chain 10	Ref.7
Myosin heavy chain 14	Ref.7
Myosin heavy chain 9	Ref.7
Myosin light chain 3	Ref.7
Myosin light polypeptide 6	Ref.7
Myosin regulatory light chain 12B	Ref.7
Myosin-Ic	Ref.7
Myosin-Id	Ref.7
Protein flightless-1 homolog	Ref.8
Ras-related C3 botulinum toxin substrate 3	Ref.9
Zyxin	Ref.10

** Data gathered from indicated Pubmed references*

Ref.1 (Miki et al., 2000); Ref.2 (Kovac et al., 2013); Ref.3 (Price et al., 1998); Ref.4 (Royal et al., 2000); Ref.5 (Lammers et al., 2008); Ref.6 (Takahashi and Suzuki, 2008); Ref.7 (van Leeuwen et al., 1999); Ref.8 (Kopecki et al., 2011); Ref.9 (Vaghi et al., 2014); Ref.10 (Sun et al., 2012).

As mentioned earlier, the main focus of this screen was to identify Rac1 binding partners that exhibit a GEF-induced altered ability to associate with Rac1 that could potentially explain the distinct Rac1 downstream cellular effects observed upon activation with either Tiam1 or P-Rex1. Therefore, proteins that showed differential Rac1 binding upon expression of the WT GEFs were compared to their respective GEF* mutants to eliminate overlapping proteins. These lists were then cross referenced with one another to identify a protein list for each GEF that showed differential Rac1 binding only under the GEF being investigated.

As illustrated in Figure 4.10 B out of the 231 proteins that were associated with a SILAC ratio, 164 proteins showed overlap between the different GEFs. Tiam1 WT expression resulted in specific regulation of 15 proteins, whereas Tiam1 GEF* expression was associated with 14 proteins showing altered Rac1 binding. Analysis of SILAC ratios also revealed that 31 proteins showed differential Rac1 binding upon Rac1 activation by P-Rex1 WT when compared to other GEF expression. Moreover, P-Rex1 GEF* expression specifically regulated Rac1 binding to 12 proteins. Importantly, despite the differential Rac1 association induced by the different GEFs, SILAC ratios for Rac1 showed no change upon expression of the different GEFs. In the forward SILAC experiments the Heavy/Medium (H/M) ratio represents the relative abundance of the protein under P-Rex1 expression over Tiam1 expression and in the reverse SILAC setup this is inverted to present the abundance under Tiam1 expression over P-Rex1 expression. As shown in Figure 4.10 C in all submitted samples the relative abundance of Rac1 relative to the control LIGHT labelled cells showed minimal fluctuations as indicated from the HEAVY (H)/MEDIUM (M) SILAC ratios, which were all around one. This is in agreement with the pre submission analysis showing equal levels of SF-Rac1 purified upon SF-TAP. Interestingly, the known GDI, RhoGDI1, which as highlighted previously binds to both inactive and active Rac1 with equal affinity, showed similar SILAC ratios across the different samples, indicating that the relative abundance of RhoGDI1 protein associated with Rac1 does not change upon expression of the different GEF constructs thus providing an internal control that could be used later for SILAC pattern validation.

4.2.4.2 Section Summary

Analysis presented in this section demonstrates that, similar to the conventional mass spectrometry screens, utilising SF-TAP in conjunction with SILAC as a quantitative mass spectrometry technique allows the identification of Rac1 and its associated binding partners. This is particularly evident from the number of proteins detected that have been shown previously to interact with Rac1. Additionally a number of predicted Rac1 interactors as well as proteins that have been reported to contribute to Rac1 signalling were also identified using SILAC. This adds to the strength of the screen and suggests that a portion of the remaining proteins represents specific novel Rac1 binding partners that have not been yet reported.

Given the quantitative nature of SILAC mass spectrometry, it was also possible to classify the Rac1 binding partners identified upon expression of the different GEFs into proteins that show decreased or increased Rac1 association by setting a ± 1.3 cut off relative to the interaction observed in the control LIGHT labelled cells. As demonstrated in this section, a number of Rac1 binding partners that showed altered Rac1 association were identified upon expression of the different GEFs. By removing overlapping proteins a list of Rac1 binding partners was generated for each GEF highlighting the power of SILAC in detecting changes in the ability of Rac1 to bind to common interactors upon expression of the different GEFs. Additionally, the identified Rac1 and RhoGDI1 SILAC ratios also demonstrate that changes observed with other proteins are specific.

4.2.5 SILAC Follow Up

In order to assess whether the observed GEF-induced differential regulation of Rac1 binding partners contributed to their ability to regulate Rac1 downstream effects, the generated lists outlined above were further analysed to determine their cellular functions.

4.2.5.1 Ingenuity® Analysis for Differentially Regulated Rac1 Binding Partners Upon Expression of Different GEFs

For each GEF the list of proteins that exhibited altered Rac1 binding was further classified into two subsets: increased and decreased Rac1 interactors. These subsets were then further compared against other GEFs to eliminate proteins that showed a similar pattern with the other GEFs. For example, to identify proteins that were specific only to Tiam1 WT expression, proteins under each subset were compared to the list of proteins identified under Tiam1 GEF* and P-Rex1 WT expression. Similarly this was done for Tiam1 GEF*, P-Rex1 WT and P-Rex1 GEF* with the comparisons conducted between the protein lists indicated in the Venn diagrams outlined in Figures 4.12-4.14. Using the Ingenuity® integrated pathway analysis (IPA) core analysis tool these specific proteins were further clustered into functional categories, depending on their documented role in cells from previous reports stored in the Ingenuity® database. Figures 4.11-4.14 list the specifically regulated proteins identified for each GEF as well as the Ingenuity® functional classification. As indicated by the highlighted categories, a number of proteins were identified under each GEF that were associated with cellular functions, including cell morphology, cell signalling, cell-to-cell signalling and interaction, cellular assembly and organisation, as well as cell movement, suggesting that they could be implicated in the GEF-Rac1 signalling that mediates the observed GEF-induced differential Rac1 downstream effects outlined in chapter 3.

A

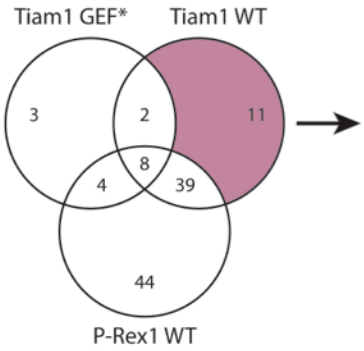

Cellular Function	Proteins
Cell Cycle	DARS,IQGAP3
Cell Death and Survival	HSP90B1,IQGAP1
Cell Morphology	IQGAP1
Cell Signalling	IQGAP3
Cell-To-Cell Signalling and Interaction	HSP90B1,IQGAP1
Cellular Assembly and Organisation	DDX6,MYL6,IQGAP1
Cellular Compromise	HSP90B1
Cellular Development	HSP90B1
Cellular Function and Maintenance	HSP90B1,IQGAP1
Cellular Growth and Proliferation	CCT5,HSP90B1,IPO7,IQGAP1,RPS14
Cellular Movement	IQGAP1
DNA Replication, Recombination, and Repair	CCT5
Gene Expression	DARS,RPS14
Molecular Transport	DDX6,IPO7
Protein Degradation	HSP90B1
Protein Synthesis	HSP90B1,DDX6,DARS,RPS14
RNA Trafficking	DDX6

B

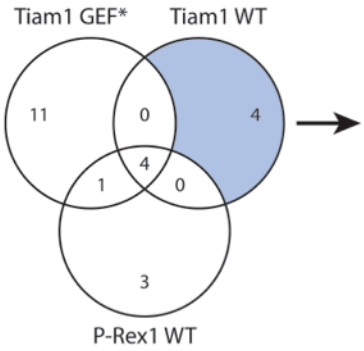

Cellular Function	Proteins
Amino Acid Metabolism	P4HB
Cell Death and Survival	P4HB,EEF2
Cell Morphology	TMOD3
Cell Signalling	RhoGDI2
Cellular Assembly and Organisation	TMOD3
Cellular Movement	TMOD3
Gene Expression	EEF2
Post-Translational Modification	P4HB
Protein Synthesis	EEF2
Small Molecule Biochemistry	P4HB

Figure 4.11: Rac1 Binding Partners Profiles Upon Expression of Wild Type Tiam1
(A) Venn diagram showing number of unique proteins showing increased binding to Rac1 upon expression of wild type (WT) Tiam1 in ≥2 SILAC experiments compared to indicated GEF protein lists. The associated table shows clustering of these unique proteins according to their cellular functions based on analysis using the Ingenuity® Integrated Pathway Analysis software. Highlighted categories represent functions that are directly implicated in the observed GEF-Rac1 driven effects. (B) Venn diagram showing number of unique proteins showing decreased binding to Rac1 upon expression of Tiam1 WT in ≥2 SILAC experiments compared to indicated GEF protein lists. The associated table shows clustering of these unique proteins according to their cellular functions based on analysis using the Ingenuity® Integrated Pathway Analysis software. Highlighted categories represent functions that are directly implicated in the observed GEF-Rac1 driven effects. For full protein names please refer to Tables S.4-S.7 on supplementary CD accompanying the appendix.

A

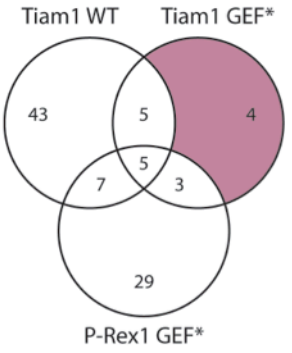

Cellular Function	Proteins
Cell Cycle	RPL11
Cell Death and Survival	RPS3A1,RPLP0
DNA Replication, Recombination, and Repair	DDX1
Gene Expression	RPS24,RPS3A
Protein Synthesis	RPS3A1
RNA Post-Transcriptional Modification	RPL11

B

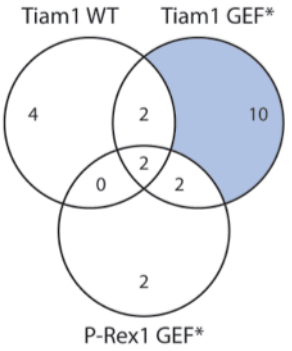

Cellular Function	Proteins
Cell Cycle	CALD1,CLTC,RAN,SFPQ
Cell Death and Survival	HSP90B1,RAN
Cell Morphology	FLNB,ARP3,CALD1,SYNCRIP,CLTC
Cell-To-Cell Signaling and Interaction	FLNB,HSP90B1,CALD1
Cellular Assembly and Organisation	FLNB,ARP3,CALD1,CLTC,RAN,RAP1GDS1
Cellular Compromise	FLNB,HSP90B1,RAN
Cellular Development	FLNB,HSP90B1,ARP3,SFPQ
Cellular Function and Maintenance	FLNB,HSP90B1,ARP3,CALD1,CLTC,RAN,RAP1GDS1
Cellular Growth and Proliferation	HSP90B1
Cellular Movement	FLNB,HSP90B1,ARP3,CALD1
DNA Replication, Recombination, and Repair	RAN
Gene Expression	RAN,SFPQ
Molecular Transport	CLTC,RAN
Protein Degradation	HSP90B1
Protein Synthesis	HSP90B1
Protein Trafficking	CLTC,RAN
RNA Post-Transcriptional Modification	SYNCRIP,RAN,SFPQ
RNA Trafficking	RAN

Figure 4.12: Rac1 Binding Partners Profiles Upon Expression of GEF-Dead Mutant Tiam1
(A) Venn diagram showing number of unique proteins showing increased binding to Rac1 upon expression of GEF-dead mutant (GEF*) Tiam1 in ≥2 SILAC experiments compared to indicated GEF protein lists. The associated table shows clustering of these unique proteins according to their cellular functions based on analysis using the Ingenuity® Integrated Pathway Analysis software. Highlighted categories represent functions that are directly implicated in the observed GEF-Rac1 driven effects. (B) Venn diagram showing number of unique proteins showing decreased binding to Rac1 upon expression of Tiam1 GEF* in ≥2 SILAC experiments compared to indicated GEF protein lists. The associated table shows clustering of these unique proteins according to their cellular functions based on analysis using the Ingenuity® Integrated Pathway Analysis software. Highlighted categories represent functions that are directly implicated in the observed GEF-Rac1 driven effects. For full protein names please refer to Tables S.4-S.7 on supplementary CD accompanying the appendix.

A

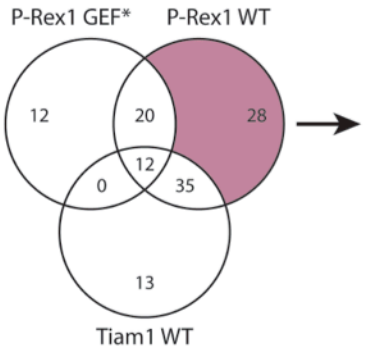

Cellular Function	Proteins
Cell Cycle	YWHAG,DDX3X,RPS6,EIF3E
Cell Death and Survival	ADRM1,YWHAG, ,CCT2,PSMD6,DDX3X,RPS6, ,QARS, RPLP0,HNRNPK,CCT4,RPS3A1,EIF3B,CCT3,Eif5a
Cell Morphology	YWHAG
Cell-To-Cell Signaling and Interaction	YWHAG,EIF3A,PSMC2
Cellular Assembly and Organisation	YWHAG,EEF1B2,EIF3A,FLII,ACTG1,ACTN1
Cellular Compromise	FLII
Cellular Development	EIF3B,CCT2,EIF3A,EEF1B2,RPS6,DDX3X,EIF3E,HNRNPK, ACTG1
Cellular Function and Maintenance	YWHAG,FLII
Cellular Growth and Proliferation	YWHAG,CCT2,EEF1B2,RPS6,DDX3X,EIF3E,HNRNPK, RPS3A,EIF3B,EIF3A,CCT3,PSMC2, ,ACTG1,ACTN1
Cellular Movement	EIF3E,HNRNPK
DNA Replication, Recombination, and Repair	ADRM1,PSMC6,PSMC2
Energy Production	PSMC6,PSMC2
Gene Expression	ADRM1,RPS3A,EIF3B,EEF1B2,EIF3A,DDX3X,EIF3E
Infectious & Metabolic Disease	PSMA3,PSMB6,PSMD1,RPS10
Molecular Transport	EEF1B2
Nucleic Acid Metabolism	PSMC6,EEF1B2,PSMC2
Post-Translational Modification	CCT4
Protein Degradation	ADRM1,PSMC2
Protein Folding	CCT4
Protein Synthesis	ADRM1,EEF1B2,DDX3X,RPS6,EIF3E,HNRNPK,RPS3A1, EIF3B, ,EIF3A,PSMC2
RNA Damage and Repair	EIF3E
RNA Post-Transcriptional Modification	QARS
RNA Trafficking	EIF3A
Small Molecule Biochemistry	PSMC6,EEF1B2,PSMC2

B

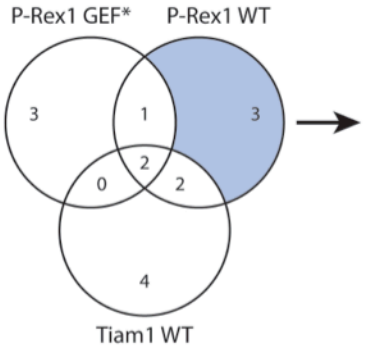

Cellular Function	Proteins
Cell Death and Survival	RAP1GDS1
Cellular Assembly and Organisation	RAP1GDS1,KPNB1
Cellular Development	IPO7
Cellular Function and Maintenance	RAP1GDS1,KPNB1
Cellular Growth and Proliferation	IPO7
Infectious & Metabolic Disease	KPNB1
Molecular Transport	IPO7,KPNB1

Figure 4.13: Rac1 Binding Partners Profiles Upon Expression of Wild Type P-Rex1

(A) Venn diagram showing number of unique proteins showing increased binding to Rac1 upon expression of wild type (WT) P-Rex1 in ≥2 SILAC experiments compared to indicated GEF protein lists. The associated table shows clustering of these unique proteins according to their cellular functions based on analysis using the Ingenuity® Integrated Pathway Analysis software. Highlighted categories represent functions that are directly implicated in the observed GEF-Rac1 driven effects. (B) Venn diagram showing number of unique proteins showing decreased binding to Rac1 upon expression of P-Rex1 WT in ≥2 SILAC experiments compared to indicated GEF protein lists. The associated table shows clustering of these unique proteins according to their cellular functions based on analysis using the Ingenuity® Integrated Pathway Analysis software. Highlighted categories represent functions that are directly implicated in the observed GEF-Rac1 driven effects. For full protein names please refer to Tables S.4-S.7 on supplementary CD accompanying the appendix.

A

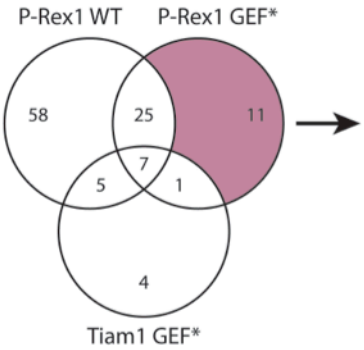

Cellular Function	Proteins
Amino Acid Metabolism	PRMT1
Antigen Presentation	HSP90AB1,HSP90AA1
Cell Cycle	PRMT1
Cell Death and Survival	PSMA6,PSMA7,HSP90AB1,PSMB1,HSP90AA1
Cell Morphology	SERPINH1,HSP90AA1
Cell-To-Cell Signaling and Interaction	PSMD4
Cellular Assembly and Organisation	PRMT1,SERPINH1
Cellular Compromise	HSP90AB1,SERPINH1,HSP90AA1
Cellular Development	PRMT1,HSP90AA1
Cellular Function and Maintenance	HSP90AB1,SERPINH1,HSP90AA1
Cellular Growth and Proliferation	PRMT1,HSP90AB1,SERPINH1
DNA Replication, Recombination, and Repair	PRMT1,HSP90AA1
Drug Metabolism	HSP90AB1
Energy Production	HSP90AA1
Free Radical Scavenging	HSP90AB1
Gene Expression	HSPA9, ,PSMD4,
Infectious & Metabolic Disease	PSMA2,PSMA5,PSMD4,PSMD8
Lipid Metabolism	HSP90AB1
Molecular Transport	HSP90AA1
Nucleic Acid Metabolism	HSP90AA1
Post-Translational Modification	PRMT1,HSP90AB1,HSP90AA1
Protein Folding	HSP90AB1,HSP90AA1
Small Molecule Biochemistry	PRMT1,HSP90AB1,HSP90AA1

B

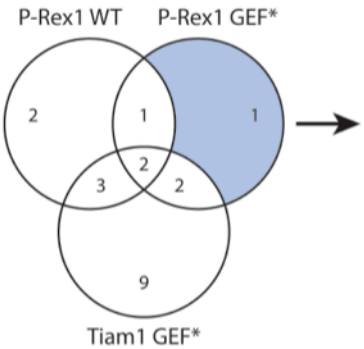

Cellular Function	Proteins
Cellular Function and Maintenance	MDH2
Energy Production	MDH2
Lipid Metabolism	MDH2
Nucleic Acid Metabolism	MDH2
Small Molecule Biochemistry	MDH2

Figure 4.14: Rac1 Binding Partners Profiles Upon Expression of GEF-Dead Mutant P-Rex1
(A) Venn diagram showing number of unique proteins showing increased binding to Rac1 upon expression of GEF-dead mutant (GEF*) P-Rex1 in ≥2 SILAC experiments compared to indicated GEF protein lists. The associated table shows clustering of these unique proteins according to their cellular functions based on analysis using the Ingenuity® Integrated Pathway Analysis software. Highlighted categories represent functions that are directly implicated in the observed GEF-Rac1 driven effects. (B) Venn diagram showing number of unique proteins showing decreased binding to Rac1 upon expression of P-Rex1 GEF* in ≥2 SILAC experiments compared to indicated GEF protein lists. The associated table shows clustering of these unique proteins according to their cellular functions based on analysis using the Ingenuity® Integrated Pathway Analysis software. Highlighted categories represent functions that are directly implicated in the observed GEF-Rac1 driven effects. For full protein names please refer to Tables S.4-S.7 on supplementary CD accompanying the appendix.

To visually compare the SILAC ratios of proteins in these categories, with the help of Hui Sun Leong, the log2 SILAC ratios from a representative SILAC pair were used to generate the heat map outlined in Figure 4.15 using the R Project software. As indicated by the scale bar, increased Rac1 binding was visually represented using a gradient of red shades, with darker shades indicating a more enhanced ability to bind to Rac1; whereas proteins with reduced Rac1 binding, where assigned a blue gradient with dark blue indicating minimal Rac1 interaction or unidentified proteins in this sample. Rac1 and RhoGDI1 were also included in the heat map as a reference. As expected, both Rac1 and RhoGDI proteins had log2 ratios approaching 0 consistent with the no change in their SILAC ratios. Therefore, proteins with similar ratios to Rac1 and RhoGDI1 had a comparable white colour. Importantly, the heat map was generated from the proteins highlighted in Figures 4.11-4.14 and therefore were expected to show a

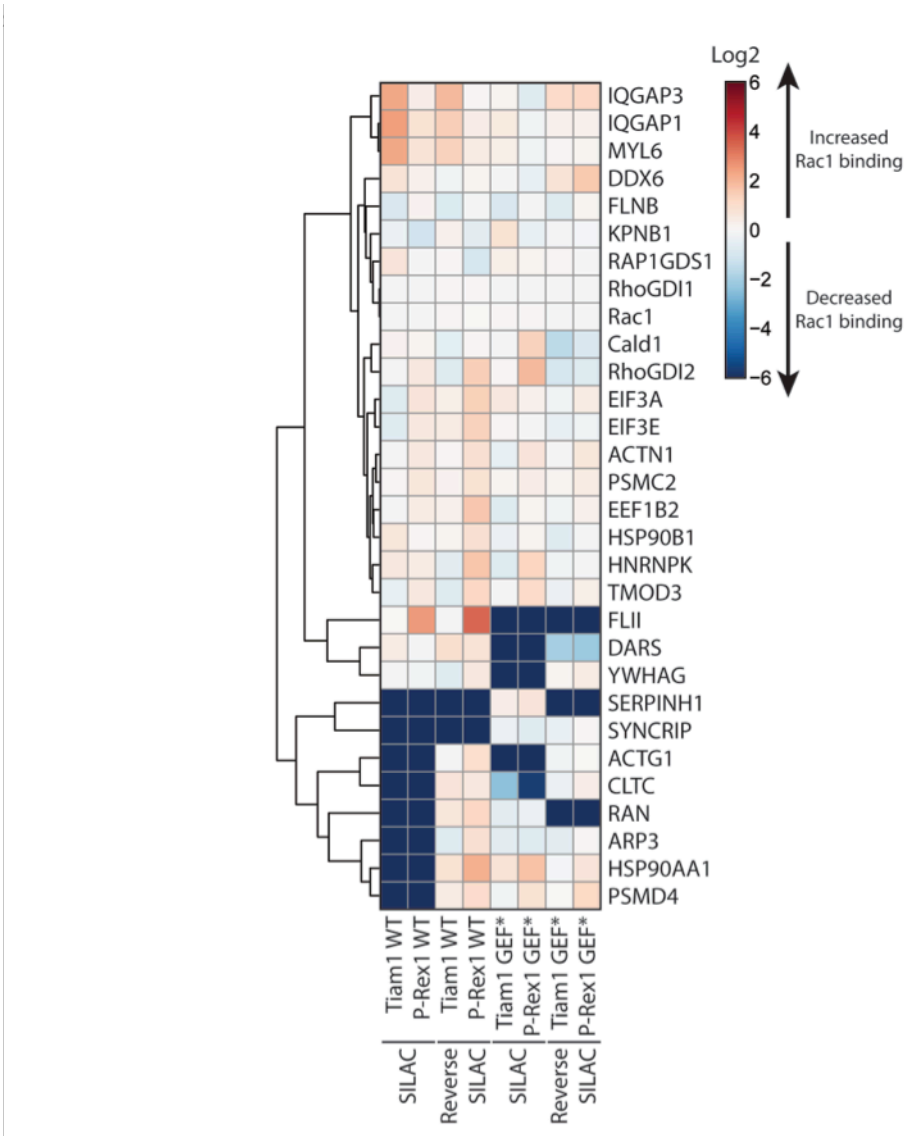

Figure 4.15: Protein Cluster Heat Map

SILAC identified Rac1 binding partners with specific changes in Rac1 binding under expression of each of the GEFs and falling under one of the following Ingenuity® functional groups: cell morphology; cell-to-cell signalling and interaction; cellular assembly and organization; cell movement, cell signalling, were used to generate a heat map using the R Project software. The heat map represents the Log2 of SILAC protein ratios relative to control cells from a representative SILAC pair. Proteins that were not identified or showed reduced Rac1 association compared to control cells were assigned a blue to white gradient; while proteins with increased Rac1 association were assigned a white to red gradient. Hui Sun Leong performed the coding required to generate this heat map.

As can be seen from the heat map presented in Figure 4.15 a number of proteins, including Ras GTPase-activating-like protein 1 (IQGAP1), Ras GTPase-activating-like protein 3 (IQGAP3) and Myosin light polypeptide 6 (MYL6) showed a particularly high increase in their ability to bind to Rac1 upon expression of Tiam1 in both forward and reverse SILAC experiments presented in the heat map. This was not seen upon expression of Tiam1 GEF*, suggesting that these proteins might be involved in the Tiam1-driven Rac1 downstream effects. Additionally, expression of P-Rex1 WT and GEF* was not associated with such increase. Instead a different subset of proteins showing increased Rac1 association was identified for P-Rex1 WT expression. Among these proteins FLII showed the highest change in SILAC ratio when compared to control cells. This interaction was also not detected upon expression of either Tiam1 GEF* or P-Rex1 GEF* suggesting that activation of Rac1 is required for this interaction to occur and that it is mediated specifically through P-Rex1 activation of Rac1 and not Tiam1.

Taken together, these results demonstrate that Tiam1 and P-Rex1 are capable of mediating unique Rac1-protein interactions as well as influencing the level of interaction between Rac1 and proteins that can also bind to Rac1 under normal cellular conditions.

4.2.5.2 SILAC Pattern Validation of Known Rac1 Binding Partners

As indicated above, the purification of SF-Rac1 and its associated protein complexes using SF-TAP followed by quantitative mass spectrometry identified a number of known Rac1 interactors listed in Table 4.6. Interestingly, the interaction of some of these proteins with Rac1 was differentially regulated upon expression of the different GEFs. For example, IQGAP1, as shown in the previous section, exhibited increased Rac1 binding only upon expression of Tiam1 WT. Given its known association with Rac1, examining the Rac1-IQGAP1 interaction upon expression of the different GEFs was used to assess the strength of SILAC in determining GEF-induced changes in Rac1 binding.

To validate the SILAC pattern observed for Rac1-IQGAP1 binding, NIH3T3 cells harbouring the dox inducible SF-Rac1/GEF expression system were treated with 1 μg/ml dox for 48 hours. As a control for non-specific protein binding, ethanol treated NIH3T3 cells harbouring the SF-Rac1 expression system were also used. Cells were harvested, lysed and equal protein levels were used for SF-Rac1 pulldown using the SF-TAP technique. Levels of co-precipitated IQGAP1 were detected by Western blot analysis using anti-IQGAP1 antibody. According to the SILAC ratios outlined in section 4.2.5.1, unlike IQGAP1, RhoGDI1 binds equally to SF-Rac1 upon expression of the different GEFs when compared to control LIGHT labelled cells. Therefore, the levels of co-precipitated RhoGDI1 were also analysed and used as an internal SF-TAP control to assess the efficiency and variation of the SF-Rac1 pulldown between samples. Moreover, anti-Rac1, anti-Tiam1 and anti-P-Rex1 antibodies were used to evaluate the efficiency of dox induction in protein inputs.

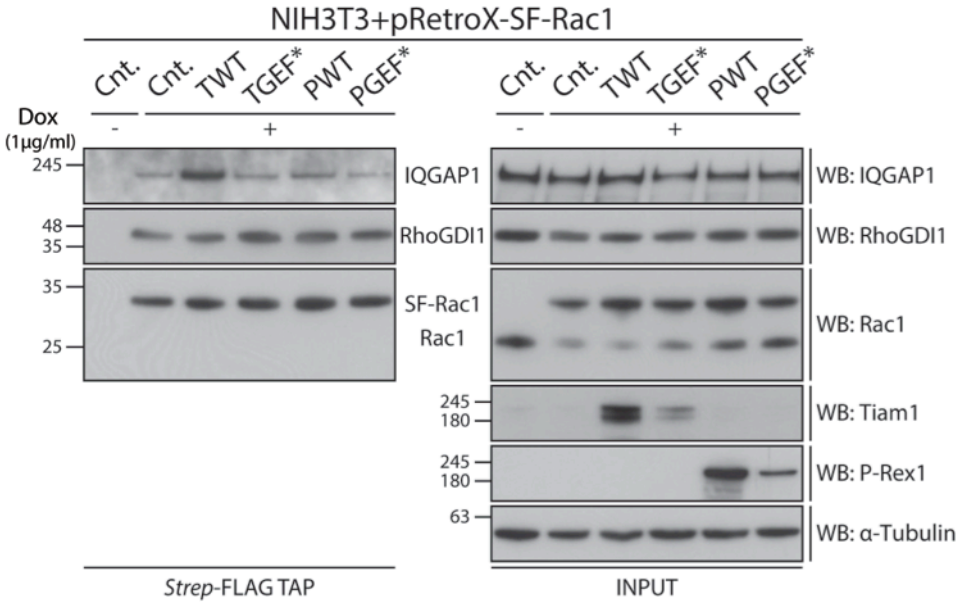

Figure 4.16: Activation of Rac1 by Tiam1 Enhances the Interaction between Exogenous SF-Rac1 and Endogenous IQGAP1 in NIH3T3 Cells

NIH3T3 cells harbouring the doxycycline (dox) inducible system for expression of SF-Rac1 alone (NIH3T3+pRetroX-SF-Rac1 Cnt.) or together with one of the different indicated GEF constructs were treated with ethanol (- dox) or 1μg/ml dox (+ dox) for 48 hours. Cells were harvested and subjected to *Strep*-FLAG Tandem Affinity Purification (TAP) to pulldown SF-Rac1. Co-precipitated IQGAP1 was detected by Western blot analysis using anti-IQGAP1 antibody. Cnt. -dox treated cells were used as a control for non-specific protein binding. Co-precipitated RhoGDI1 was detected by Western blot analysis using anti-RhoGDI1 antibody and was used as an internal control for the efficiency and variation of the SF-Rac1 pulldown between samples. α-Tubulin was used as a loading control. Representative Western blot from three independent experiments.

As illustrated in Figure 4.16 the treatment of cells with dox induced the expression of relatively equal levels of SF-Rac1 alone or together with the indicated GEFs. Similar to previous observations outlined in this chapter, expression of Tiam1 GEF* and P-Rex1 GEF*, relative to their WT counterparts, was reduced when co-expressed with Rac1. However, since this was also seen in samples submitted for SILAC mass spectrometry analysis Tiam1 GEF* and P-Rex1 GEF* were only used as additional controls and conclusions were not drawn based on the interaction levels observed in these lanes. Additionally, endogenous levels of Rac1 appeared higher in Tiam1 GEF* and P-Rex1 GEF* samples. It is important to note that this was not a reproducible observation and thus was interpreted as variation in expression in this particular experiment shown. Analysis of the level of IQGAP1 co-precipitated with SF-Rac1 revealed that, as suggested from the SILAC experiments, ectopic expression of Tiam1 WT, but not P-Rex1 WT resulted in increased Rac1-IQGAP1 binding despite the equal levels of SF-Rac1 purified. In contrast, co-expression of either GEF with SF-Rac1 did not induce any changes in Rac1-RhoGDI1 binding. This is consistent with SILAC ratios described earlier that showed minimal fluctuations in the SILAC ratio when compared to control LIGHT labelled cells. These results provide evidence for the validity of the SILAC screen and show the accuracy of SILAC in detecting GEF-induced differential Rac1 binding to proteins that bind to Rac1 under normal conditions.

4.2.5.3 *SILAC Pattern Validation of Novel Rac1 Binding Partners*

Upon confirming the accuracy of SILAC in revealing GEF-induced changes in protein Rac1 binding abilities, it was interesting to investigate novel Rac1 interactors and validate their associated SILAC patterns.

As mentioned earlier, evidence from the literature together with observations outlined in Chapter 3 demonstrate the ability of P-Rex1, through Rac1 activation, to induce cellular migration. Thus looking at proteins downstream of Rac1 that show increased Rac1 binding upon expression of P-Rex1 WT might help identify key regulators of Rac1-driven cellular migration, thus adding to the existing body of knowledge of how Rac1 promotes cellular migration and invasion in normal and cancer cells. As a result, to identify potential candidates from the SILAC screen for further functional studies, the list of proteins that showed increased Rac1 binding under P-Rex1 WT expression were compared to those proteins with increased Rac1 binding identified upon expression of P-Rex1 GEF*. These proteins were also cross-referenced against proteins that have reduced Rac1 binding upon expression of Tiam1 WT to identify proteins that are differentially regulated upon expression of the two GEFs. As indicated from the Venn diagram presented in Figure 4.17, this comparison identified Tropomodulin-3 (TMOD3) as the only protein that showed increased Rac1 association under P-Rex1 WT while binding less to Rac1 under Tiam1 WT. Increased TMOD3 binding to Rac1 was also seen in P-Rex1 GEF* suggesting that activation of Rac1 is not essential for this interaction to occur. However, given that expression of Tiam1 WT was associated with a specific reduction in the TMOD3 SILAC ratio that was not observed upon expression of Tiam1 GEF*, it was intriguing to examine this interaction further.

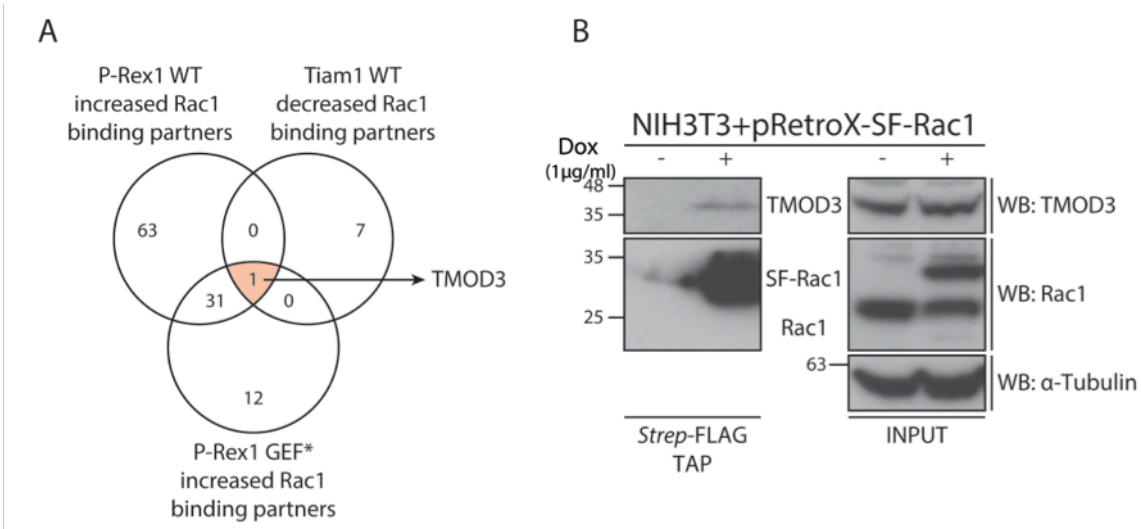

Figure 4.17: TMOD3 is a Novel Rac1 Binding Partner

(A) Venn diagram comparing proteins that show increased Rac1 binding under P-Rex1 wild type (WT) and P-Rex1 GEF-dead mutant (GEF*) together with decreased Rac1 binding under Tiam1 WT expression showing TMOD3 as the only protein that exhibits opposing Rac1 binding under P-Rex1 WT and Tiam1 WT expression. (B) Exogenous SF-Rac1 expressed in NIH3T3 cells was precipitated by two-step *Strep*-FLAG Tandem Affinity Purification (TAP) and co-precipitated endogenous TMOD3 was detected by Western blot analysis using anti-TMOD3 antibody. Lysates from ethanol (- dox) treated NIH3T3 cells harbouring the doxycycline (dox) SF-Rac1 expression system were used as a control for the *Strep*-FLAG TAP to assess non-specific protein binding to the beads. α-Tubulin was used as a loading control. Representative Western blot from three independent experiments.

TMOD3 has not been previously reported to bind to Rac1; therefore it was important to first establish its ability to interact with Rac1. To examine the Rac1-TMOD3 interaction, NIH3T3 cells harbouring the dox inducible SF-Rac1 expression system were treated with ethanol (- dox) or 1 μg/ml dox (+ dox) for 48 hours. Cells were then collected and subjected to SF-TAP to pulldown SF-Rac1. The ability of SF-Rac1 to co-precipitate TMOD3 was evaluated by Western blot analysis using anti-TMOD3 antibody. As demonstrated in Figure 4.17, a band corresponding to endogenous TMOD3 was only detected upon the pulldown of SF-Rac1 in NIH3T3 cells and was not observed in – dox treated cells. This indicates that TMOD3 is indeed capable of binding to Rac1 as suggested from the SILAC experiments.

Following the confirmation that endogenous TMOD3 binds to exogenous SF-Rac1, further analysis was conducted in order to evaluate the role played by GEFs in mediating this interaction. To ensure that TMOD3 binding to Rac1 was not a consequence of increased expression of SF-Rac1 in cells, the interaction between endogenous Rac1 and endogenous TMOD3 was assessed upon expression of Tiam1 WT or P-Rex1 WT in relation to control cells. Additionally, given that NIH3T3 cells do not normally express endogenous P-Rex1 the interaction was assessed in the breast cancer cell line MCF7 instead to eliminate any potential influence that P-Rex1 WT ectopic expression might have in a cellular setting that normally lacks the endogenous protein. The choice of MCF7 cells was based on the screening of a panel of cell lines available in our laboratory, including the cancer cell lines outlined in Figure A.1 in the Appendix section, for high levels of endogenous Tiam1 and P-Rex1. As demonstrated in Figure A.1, MCF7 cells have high levels of both Tiam1 and P-Rex1. Despite these high levels, in order to selectively stimulate GEF-specific Rac1 interactions, the dox inducible GEF expression system was introduced in this cell line and the Rac1-TMOD3 interaction was assessed on an endogenous level using the duolink® In Situ PLA assay upon dox induction. As illustrated in Figure 4.18 A, this assay allowed the detection of *in vivo* protein-protein interactions in fixed cells via the use of mouse anti-Rac1 and rabbit anti-TMOD3 antibodies. Species-specific PLA probes were then applied and based on their proximity (<40 nm apart) a signal was detected by fluorescence microscopy. To account for background duolink® signal, an additional sample was used in which parental MCF7 cells were incubated only with the mouse anti-Rac1 antibody. As expected there was a minimal signal detected in MCF7 parental cells incubated with anti-Rac1 antibody alone. Similarly, a weak signal was detected in parental and Tiam1 WT expressing cells treated with both antibodies, suggesting that Rac1 and TMOD3 do not interact in these cells. Although, SILAC ratios for Tiam1 WT expressing NIH3T3 cells suggest that Tiam1 WT reduces the Rac1-TMOD3 interaction, no additional reduction was seen using the duolink® In Situ PLA assay in MCF7 cells. In sharp contrast, P-Rex1 WT in MCF7 cells resulted in a significant increase in the duolink® signal detected. This indicates that expression of P-Rex1 WT in MCF7 cells results in an increased association between Rac1 and TMOD3. Figure 4.18 B shows representative fluorescence images of the duolink® In Situ PLA. Additionally, phalloidin was used to stain the

actin cytoskeleton and DAPI was used to visualise the nuclei of cells to provide a rough reference as to where the Rac1-TMOD3 interaction occurs. As shown, the P-Rex1 stimulated Rac1-TMOD3 interaction appeared predominantly cytoplasmic.

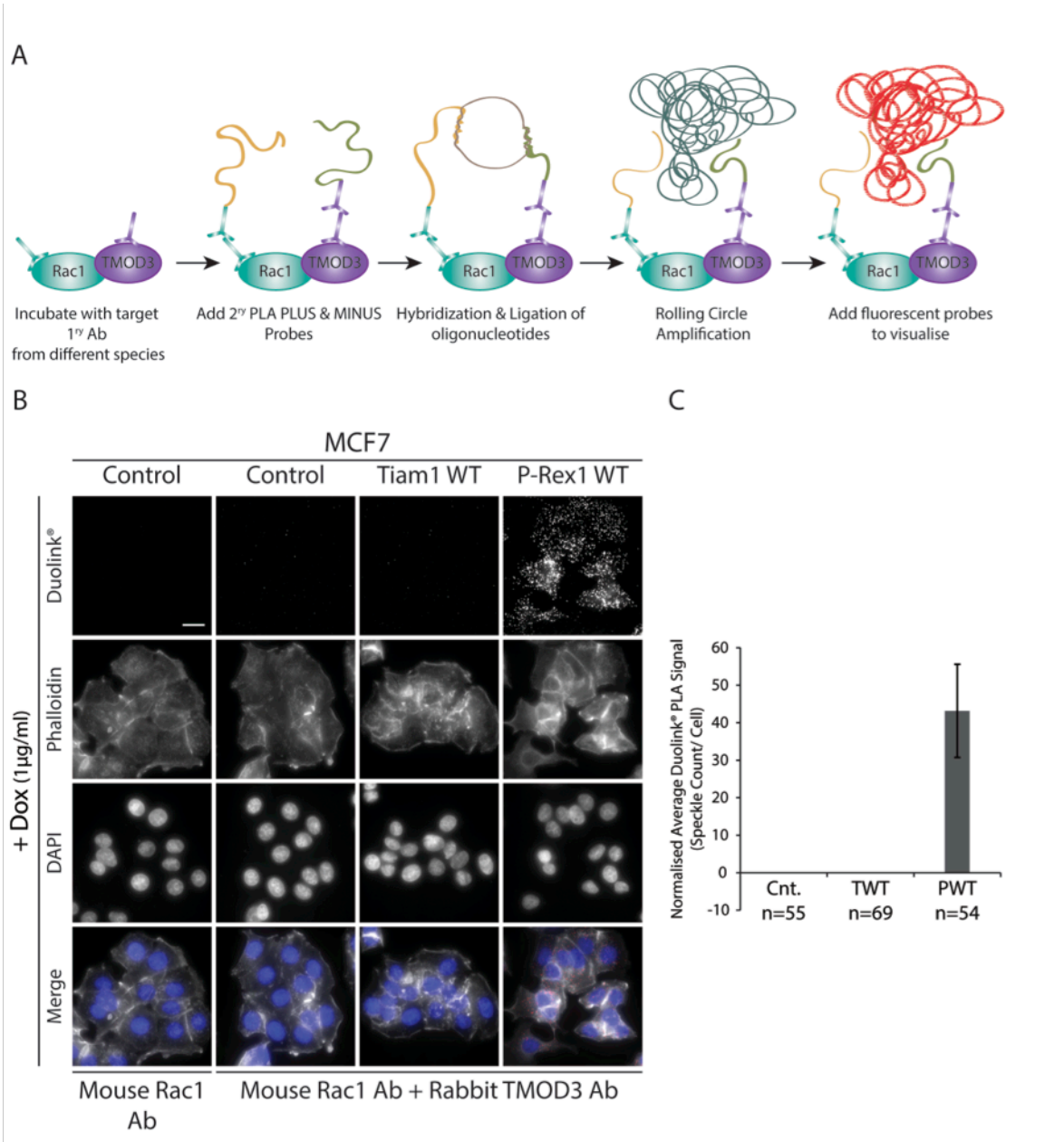

Figure 4.18: Ectopic Expression of P-Rex1 Wild Type Protein Enhances the Endogenous Rac1-TMOD3 Interaction in MCF7 Cells

(A) Schematic representation of duolink® In Situ PLA assay. (B) MCF7 cells harbouring the doxycycline (dox) inducible GEF expression system were treated with 1µg/ml dox for 24 hours. Cells were fixed in 4 % formaldehyde and subjected to the duolink® PLA assay using mouse anti-Rac1 primary antibody (Ab) and rabbit anti-TMOD3 primary Ab. The respective secondary mouse and rabbit PLA probes were used and analysed by fluorescence microscopy using the low light microscope (100x magnification). Phalloidin and DAPI were used to mark different cellular compartments, cell contacts/cytoplasm and nucleus, respectively. Scale bar=20µm. (C) Quantification of average duolink® PLA signal from indicated number of cells in control (Cnt.), Tiam1 WT (TWT) or P-Rex1 WT (PWT) expressing cells using the CellProfiler software. Background duolink® In Situ PLA signal was accounted for by subtracting the average speckle count identified in parental MCF7 cells that were subjected to mouse anti-Rac1 antibody only. Error bars represent ± standard deviation.

The duolink® In Situ PLA assay generated fluorescence dots were also counted as described in section 2.5.5.2. As outlined in Figure 4.18 C, no duolink® signal was detected in parental MCF7 cells or cells expressing Tiam1 WT. On the other hand, expression of P-Rex1 WT

resulted in an average duolink® signal of 43 speckles per cell. Together, these results confirm the SILAC pattern observed in NIH3T3 cells where P-Rex1 WT expression promotes Rac1-TMOD3 binding when compared to control and to Tiam1 WT expressing cells.

Given that the duolink® In Situ PLA did not reveal any Tiam1-induced reduction in the Rac1-TMOD3 interaction and that according to SILAC experiments this interaction was also stimulated by P-Rex1 GEF* this suggested that this interaction might not be essential for the GEF-mediated cellular effects. However, it was speculated that the enhanced association of Rac1 and TMOD3 upon expression of P-Rex1 might help bring other interactors that are important for the P-Rex1-Rac1-driven cellular functions, and that unlike TMOD3 these proteins would require Rac1 activation for binding. To explore this possibility the Ingenuity® IPA software was used to generate protein-protein interaction networks using the total number of proteins showing increased binding to Rac1 upon expression of P-Rex1 WT in ≥ 2 SILAC experiments.

Among the proteins shown to associate with TMOD3 based on the Ingenuity® generated network, the actin-binding protein FLII represented the most promising protein candidate for further functional analysis. However, the interaction suggested by Ingenuity® was only based on a screen that identified both TMOD3 and FLII as CAMKII protein binding partners (Seward et al., 2008), and there was no biochemical evidence present to demonstrate a direct interaction between the two proteins. Therefore, the TMOD3-FLII interaction was first assessed in NIH3T3 cells harbouring the dox inducible P-Rex1 WT expression system in the absence (ethanol - dox treated cells) or presence of P-Rex1 WT (1 μg/ml dox treated cells) to test the hypothesis that TMOD3 might still be involved in P-Rex1 signalling through the recruitment of other Rac1 binding partners. As can be seen from Figure 4.19 immunoprecipitation of endogenous FLII using anti-FLII antibody from – dox treated cells resulted in the co-precipitation of endogenous TMOD3, which was not observed in the Rabbit IgG control. Interestingly, as indicated from the Western blot analysis and the associated densitometric analysis of TMOD3 co-precipitated bands, P-Rex1 ectopic expression resulted in a 2-fold increase in the TMOD3-FLII interaction. This suggests that the modulation of TMOD3-FLII might be important for the P-Rex1-Rac1-driven cellular effects.

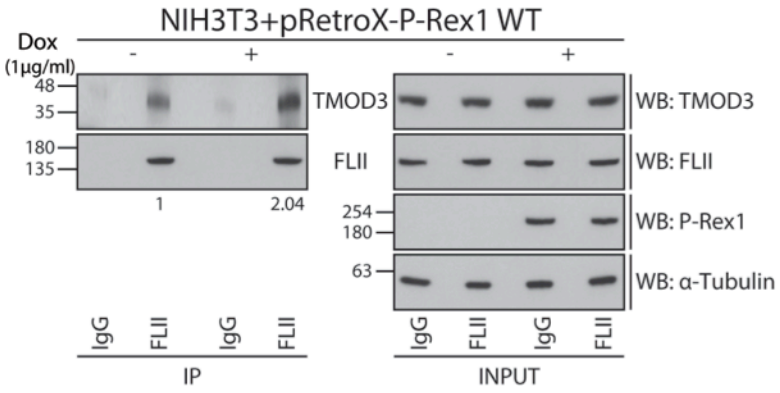

Figure 4.19: Ectopic expression of P-Rex1 Wild Type Protein Enhances the Endogenous TMOD3-FLII Interaction in NIH3T3 Cells

NIH3T3 cells harbouring the doxycycline (dox) inducible system for the expression of wild type P-Rex1 (NIH3T3+pRetroX+P-Rex1 WT) were treated with ethanol (- dox) or 1μg/ml dox (+ dox) for 48 hours. Cells were then harvested and endogenous FLII was immunoprecipitated from the respective lysates using anti-FLII antibody. Co-precipitated TMOD3 was detected by Western blot analysis using anti-TMOD3 antibody. Rabbit IgG was used as a control for immunoprecipitation to determine non-specific protein binding to the beads. α-Tubulin was used as a loading control. The difference in the ability of TMOD3 to bind to FLII in response to P-Rex1 WT expression was assessed using the Image J software to measure the integrated density of the co-precipitated TMOD3 bands. After subtracting background binding to the beads these densities were then normalised to the amount of FLII immunoprecipitated as well as the normalised levels of TMOD3 in the input. The normalised integrated density for this experiment is indicated below the figure.

In addition to its association with TMOD3, FLII showed the biggest differential regulation in Rac1 association upon expression of P-Rex1 WT. As shown from the SILAC experiments and the associated heat map, FLII exhibited a 5-fold and 10-fold increase in its ability to bind to Rac1 upon expression of P-Rex1 WT in one forward and one reverse SILAC experiment, respectively. In contrast, expression of Tiam1 WT in NIH3T3 cells failed to induce any changes in the levels of FLII co-precipitating with SF-Rac1 in the same experiments with SILAC ratios of 1.028 and 0.96 in the forward and reverse SILAC experiments, respectively. Additionally, taking into account the MaxQuant generated Significance B values for FLII SILAC fold changes, there was significant change in the SILAC ratio and hence the abundance of FLII between P-Rex1 WT expressing cells compared to control LIGHT labelled cells ($p=1.46x10^{-6}$) and Tiam1 WT MEDIUM labelled cells ($p=2.43x10^{-6}$) in the forward SILAC experiment. Similarly P-Rex1 WT expression in the reverse SILAC experiment was also associated with a significant increase in the relative levels of FLII associated with SF-Rac1 when compared to control LIGHT labelled cells ($p=7.13x10^{-9}$). Interestingly, as highlighted in subsection 4.2.2.3 using conventional mass spectrometry FLII was also identified as a unique Rac1 binding partner upon expression of P-Rex1 WT in two out of the three conducted mass spectrometry screens thus confirming the SILAC pattern. Moreover, as highlighted in Chapter 1 FLII is a gelsolin family member that has been implicated in regulating cellular migration.

Taken together, this evidence suggests that regulation of the levels of Rac1-FLII binding might play a significant role in driving P-Rex1-Rac1 cellular functions, and that it might be mediated through TMOD3. As a result, the Rac1-FLII interaction was further characterised firstly to examine the ability of FLII to interact with Rac1, then to evaluate the role of P-Rex1 WT

expression on mediating this interaction and finally the functional consequence of such interaction.

4.2.5.4 Section Summary

Using the Ingenuity® IPA software the list of proteins identified showing altered Rac1 binding upon expression of the different GEF constructs was further analysed to generate protein clusters based on their functional roles in cells. From these categories, proteins involved in cell morphology, cell signalling, cell-to-cell signalling and interaction, cellular assembly and organisation, and cellular movement, were of particular interest as they are directly implicated in the differential GEF-Rac1-driven cellular phenotypes outlined in chapter 3. Amongst these proteins, the known Rac1 effector, IQGAP1 showed increased association with Rac1 upon expression of Tiam1 WT, but not Tiam1 GEF*. The Tiam1 WT-mediated increase in the Rac1-IQGAP1 interaction was further confirmed where the pulldown of SF-Rac1 in the presence of Tiam1 WT was associated with more IQGAP1 when compared to parental NIH3T3 cells, or cells expressing the different GEFs. In contrast, activation of Rac1 by P-Rex1 induced an increased Rac1 association with a different subset of proteins. By comparing proteins that show increased Rac1 binding under P-Rex1 WT and P-Rex1 GEF* together with decreased Rac1 binding under Tiam1 WT, TMOD3 was identified as the only protein that exhibits opposing Rac1 binding under P-Rex1 WT and Tiam1 WT expression. Using co-precipitation experiments the interaction between exogenous SF-Rac1 and endogenous TMOD3 was confirmed. Furthermore, via analysing the endogenous interaction between Rac1 and TMOD3 upon expression of the Tiam1 WT or P-Rex1 WT using the duolink® In Situ PLA assay, the SILAC pattern was confirmed in which P-Rex1 WT expression in MCF7 cells resulted in increased association of Rac1 and TMOD3. Based on SILAC ratios obtained from the SILAC experiments, the Rac1-TMOD3 interaction seems to increase also upon expression of P-Rex1 GEF*. This suggests that TMOD3 binding to Rac1 is not restricted to the active form of Rac1 and thus might not be crucial for the P-Rex1-Rac1-driven cellular effects. However, information from the SILAC experiments also shows that Tiam1 WT expression specifically reduces the Rac1-TMOD3 binding and as such it was suggested that TMOD3 binding to Rac1 might be involved in bringing other Rac1 interactors that are important for the GEF-mediated functions. As a result the Ingenuity® IPA software was used to generate protein-protein interaction networks involving TMOD3 together with other proteins from the SILAC screen that show increased Rac1 association upon expression of P-Rex1 WT. Using this network in conjunction with evidence provided from both SILAC and the conventional mass spectrometry, FLII was identified as a promising candidate that might be important in the P-Rex1-Rac1-driven cellular functions.

4.3 Discussion

GEFs play a crucial role in regulating Rac1 signalling through their ability to activate Rac1 in response to upstream signalling (Cote and Vuori, 2007; Rossman et al., 2005). Results outlined in Chapter 3 demonstrate that Tiam1 and P-Rex1 can also mediate distinct cellular functions downstream of Rac1 in different cell lines. Interestingly, Tiam1 and P-Rex1 influenced the role of Rac1 in cellular migration, with Tiam1 impeding cellular migration while P-Rex1 enhancing it. This is particularly important as it helps shed light on a potential regulatory step that could explain the reported dual function of Rac1 in cancer cellular migration and invasion. It was therefore important to further understand and dissect the mechanism by which either GEF dictates Rac1 signalling. As discussed in section 1.5.4.1, several studies have suggested a scaffolding role of GEFs allowing them to dictate GTPase binding to downstream effectors. As a result a proteomic screen was conducted to identify changes in the Rac1 interactome upon expression of Tiam1 or P-Rex1 to investigate whether the GEF-induced differential effects were mediated through the ability of either GEF to influence Rac1 binding to downstream effectors.

4.3.1 *Strep*-FLAG Tandem Affinity Purification and Mass Spectrometry Protein Identification

Due to technical limitations associated with immunoprecipitation of endogenous Rac1 using commercially available anti-Rac1 antibodies, such as high non-specific protein binding to beads, insufficient levels of immunoprecipitated Rac1 to detect associated partners as well as cross reactivity of some of the available antibodies with Cdc42, NIH3T3 cells harbouring the dox inducible SF-Rac1/GEF expression system were generated and used to examine the proteins associated with Rac1 upon expression of the different GEFs.

4.3.1.1 SF-Rac1 Construct Functionality

The SF-tag was generated as an alternative to the original TAP-tag. Via reducing the tag size from 21 KDa to 4.6 KDa, removing the TEV cleavage step as well as replacing the CBP domain, this tag addressed several limitations that were inherent to the original TAP-tag design. Through the size reduction, it was proposed that the SF-tag would reduce the interference of tagging with the functionality of the tagged protein (Gloeckner et al., 2007). This was particularly evident from results outlined in section 4.2.1.2. The first indication that SF-Rac1 and endogenous Rac1 were functionally similar when expressed in cells is that upon dox induction and expression of SF-Rac1, endogenous Rac1 was downregulated. This suggested that the cell recognises both proteins in a similar manner and thus to maintain levels of Rac1 in the cell, the levels of endogenous protein were reduced. It must be noted, however, that the mode of regulating endogenous Rac1 levels has not been investigated further and could be either through reducing the expression of the protein or via promoting its degradation. Consistent with the functional similarity between SF-Rac1 and endogenous Rac1, GST-PAK CRIB active Rac1

pulldown experiments conducted on dox treated cells demonstrated that expression of Tiam1 WT and P-Rex1 WT, but not their GEF* mutants, induced increased levels of active SF-Rac1 in the cells. Additionally, the ability of Tiam1 and P-Rex1 to activate Rac1 was primarily constrained to SF-Rac1 and not endogenous Rac1 indicating that SF-Rac1 is capable of replacing endogenous Rac1 functionally in cells. Moreover, co-expression of Tiam1 WT and P-Rex1 WT with SF-Rac1 in NIH3T3 cells was associated with distinct cellular morphology and migration abilities that were comparable to those seen upon expression of either GEF alone in NIH3T3 cells. Additionally, these differential phenotypes were not observed upon co-expression of Tiam1 GEF* or P-Rex1 GEF* with SF-Rac1. This demonstrates that Tiam1 WT and P-Rex1 WT activation of SF-Rac1 induces distinct Rac1 downstream cellular effects. All together these results provide clear evidence that tagging Rac1 at the N-terminus with SF-tag does not interfere with Rac1 cellular functions.

4.3.1.2 Mass Spectrometry Protein Identification

As indicated in the section above, through removing the TEV cleavage step the SF-TAP technique was considerably shorter than the original TAP procedure (Gloeckner et al., 2007). Thus it was speculated that using this technique could identify transient Rac1 binding partners upon expression of the different GEFs. This was particularly important since Rac1 activation is considered to be a transient process. The efficiency of using the optimised SF-TAP conditions to pulldown of SF-Rac1 and its associated binding partners was thus assessed using mass spectrometry protein identification. Analysis of the protein identified by mass spectrometry revealed a subset of proteins that have been previously reported to bind to Rac1. In addition to Rac1, included in this list were proteins that regulate the GDP-GTP Rac1 cycle, such as the Rac1 GEFs Dedicator of Cytokinesis 7 (DOCK7), Dedicator of cytokinesis protein 1 (DOCK1) and P-Rex1; as well as Engulfment and cell motility protein 1 (ELMO1) all of which have been shown to increase levels of active Rac1 in cells. This could potentially mean that similar to how GTPases cooperate, GEFs also cooperate with other proteins in order to achieve optimal GTPase activation. For example ELMO has been shown to form a ternary complex containing RhoG-ELMO-Dock180 that promotes Rac1 activation (Katoh and Negishi, 2003). Of course, if that is the case this complicates the understanding of the signalling cascades downstream of Rac1 as it introduces other upstream variables that might be important in determining the Rac1-driven cellular effects. Additionally, two members of the GDI family, RhoGDI1 and RhoGDI2, were also identified. Moreover, known Rac1 effectors, including IQGAP1, IQGAP2 and IQGAP3 were also detected by mass spectrometry. The PIPs database also helped identify a number of predicted Rac1 interactors (McDowall et al., 2009). Additionally, literature-curated searches also revealed that SF-TAP followed by mass spectrometry was successful in detecting proteins that are implicated in Rac1 signalling. This demonstrates that as proposed by Gloeckner et al., the SF-tag, due to the shorter purification time, unlike the conventional TAP tag, can be used to detect

transient proteins-protein interactions (Gloeckner et al., 2007; Gloeckner et al., 2009a; Gloeckner et al., 2009b). It also highlights that using this purification method allows the pulldown of substantial amounts of active Rac1. This was particularly evident from the identification of ubiquitin and SUMO-2, which have been shown to preferentially associate with Rac1 in the active form to regulate Rac1 signalling via posttranslational modifications, namely ubiquitylation and SUMOylation, respectively (Castillo-Lluva et al., 2013; Castillo-Lluva et al., 2010; Lynch et al., 2006; Mettouchi and Lemichez, 2012; Torrino et al., 2011; Visvikis et al., 2008). Additionally, this highlights the ability of the technique to maintain Rac1 posttranslational modifications, which might be important in promoting the formation of different protein complexes.

4.3.1.3 Mass Spectrometry and GEF-Mediated Differential Regulation of Rac1 Binding Partners

Via comparing the proteins identified upon expression of the different GEFs a list of unique Rac1 interactors was formulated for each GEF. As outlined in Tables A.1- A.3, Tiam1 WT and P-Rex1 WT were able to influence Rac1 binding to a subset of proteins. However, as highlighted earlier, the extent of overlap and reproducibility between the three mass spectrometry experiments was minimal. This could be due to the varying protein concentrations used as starting material for the SF-TAP technique. In support of this argument both CAND1 and FLII were identified in two experiments with comparable protein inputs, but were lacking from the first experiment, which had a much lower starting material. Another explanation could be that Tiam1 and P-Rex1 do not function mainly through promoting Rac1 binding to unique interactors. Instead, they might influence Rac1 signalling via differentially regulating the ability of common Rac1 interactors to bind to Rac1. In both cases these results called for a more sensitive method to accurately evaluate the potential GEF induced differential regulation of Rac1-effector binding. To tackle this, SF-TAP in conjunction with a quantitative mass spectrometry technique was adopted.

4.3.2 SILAC Protein Identification

There are various methods by which mass spectrometry can be used quantitatively to detect the relative abundance of proteins identified upon expression of the different GEFs. Amongst these is SILAC. As outlined in subsection 4.2.3.1, SILAC involves the labelling of live cells using isotopic variants of amino acids. Due to limitations in the number of isotopic amino acid variations that can be used for SILAC labelling, the same SILAC labels were used for the WT and GEF* versions of Tiam1 and P-Rex1 and they were compared separately (set1 and set2) to a common control. This five-way SILAC setup allowed the direct comparison of Rac1 associated proteins identified within each set and indirectly, through the common control between the two sets.

Prior to SILAC ratio analysis, the validity of the SILAC screens was evaluated via looking at the ability of SILAC to identify known and predicted Rac1 interactors as well as proteins implicated in Rac1 signalling. Similar to the conventional mass spectrometry, SILAC was successful in identifying a number of known Rac1 interactors, all of which were also detected using the conventional mass spectrometry with the exception of RhoGDI3. Some overlap was also observed between conventional and SILAC predicted Rac1 interactors and Rac1 signalling proteins. This confirms that SILAC is suitable for identifying Rac1 binding partners and increases the confidence that other proteins bound to Rac1 are specific novel Rac1 binding partners.

4.3.3 SILAC Screen Validation

Following confirmation of the ability of SILAC to identify Rac1 binding partners, SILAC ratios were used to generate lists of proteins that show altered Rac1 binding upon expression of the different GEFs. There are various ways by which differences in SILAC ratios can be interpreted. The most common method adopted in the proteomics field is to set a SILAC ratio cut off. Acceptable cut offs range from ±1.3-2 fold change differences (Mann, 2006). Therefore, to classify Rac1 interactors into proteins that show unchanged, decreased or increased Rac1 binding a ±1.3 SILAC ratio cut off relative to control LIGHT labelled cells was employed. This helped formulate a list of proteins for each category upon expression of the different GEF constructs, which were then used to identify proteins that show GEF-specific altered Rac1 binding. These lists were further classified into protein clusters according to their functional roles using the Ingenuity® IPA core analysis to narrow the protein lists to Rac1 interactors that are involved in cellular functions that are directly implicated in the GEF-Rac1-driven observed phenotypes. As a result, proteins falling under one of these categories: cell morphology, cell signalling, cell-to-cell signalling and interaction, cellular assembly and organisation and cellular movement, were examined further to identify candidates for SILAC pattern validation.

4.3.3.1 IQGAP1

Among the proteins identified, the known Rac1 effector IQGAP1 exhibited increased Rac1 binding specifically upon expression of Tiam1 WT. This was further confirmed using co-precipitation experiments supporting the accuracy of the SILAC ratios obtained from the screen. Interestingly, these observations are in agreement with a recent study in which the analysis of the IQGAP1 interactome using mass spectrometry, showed that IQGAP1 recruits Rac1 and Tiam1 together with other small GTPases and regulators of GTPases to orchestrate several cellular functions (Jacquemet and Humphries, 2013).

IQGAP1 belongs to the IQGAP family, which in humans consists of three proteins: IQGAP1, IQGAP2 and IQGAP3 (Briggs and Sacks, 2003; White et al., 2009). Due to its structural organisation and domain composition, IQGAP1 has been shown to serve as a scaffolding protein and multiple IQGAP1 binding partners have been identified to date. As a result, IQGAP1 is

implicated in various signalling processes, such as cytoskeleton reorganisation, cell-cell adhesion and proliferation (Johnson et al., 2009). It has also been shown that through its ability to bind to actin, IQGAP1 links Rac1 and Cdc42 to the actin cytoskeleton (Hart et al., 1996a; Hart et al., 1996b). Moreover, IQGAP1 can regulate actin assembly via serving as a calmodulin regulated barbed end actin capping protein (Pelikan-Conchaudron et al., 2011). Given the role of IQGAP1 in regulating the actin cytoskeleton, increased Rac1 binding in response to Tiam1 activation could be important in mediating the extensive membrane ruffling associated with Tiam1 ectopic expression. Intriguingly though, IQGAP1 has been shown to promote migration through its ability to bind to and activate N-WASP thereby stimulating the assembly of the Arp2/3-mediated actin filaments in lamellipodia (Le Clainche et al., 2007). Consistent with this study, IQGAP1 has also been shown to deactivate Rac1 at sites of activated β1-integrin through recruiting the Rac1 GAP, Rac1GAP1, which is important for coordinated directional cellular movement (Jacquemet et al., 2013). These studies seem contradictory to the Tiam1-mediated inhibition of cellular migration in NIH3T3 cells.

In contrast, in a study conducted by Kuroda et al. IQGAP1 was shown to promote migration in E-cadherin expressing mouse L fibroblasts through disrupting the interaction between E-cadherin and its binding partner β-catenin, which in turn mediates the disassembly of cell-cell contacts. Interesting, though these effects were not observed in fibroblasts that do not express E-cadherin (Kuroda et al., 1998). This suggests that cellular context might play a role in determining the role of IQGAP1 in mediating cellular migration. Consistent with this argument, IQGAP1 was implicated in the establishment of vascular endothelial (VE)-cadherin-mediated cell-cell contacts in human endothelial cells (Yamaoka-Tojo et al., 2006). Similarly, IQGAP1 was shown to enhance cell-cell contacts in endocrine cells through its interaction with the tumour suppressor protein Menin (Yan et al., 2009). Taken together, these two studies reveal that, similar to Tiam1-Rac1 signalling, IQGAP1 can potentially lead to opposing cellular effects depending on the cellular context.

Given the reported role of IQGAP1 in both the assembly and disassembly of cell-cell contacts, there are two possible explanations for the Tiam1-enhanced Rac1-IQGAP1 interaction. The first explanation is that increased Rac1 binding is part of a negative feedback loop that is important for maintaining active Rac1 levels or confining it spatially to induce the observed Tiam1 WT-driven cellular effects. This is consistent with previously outlined study showing that IQGAP1 can deactivate Rac1 through promoting its binding to Rac1GAP1 (Jacquemet et al., 2013). An alternative explanation to why Tiam1 promotes the Rac1-IQGAP1 interaction could be that under the cellular context investigated IQGAP1 is important for maintaining cell-cell contacts. Therefore, it might be that through enriching Rac1-IQGAP1 binding above the normal levels, IQGAP1 is stimulated to enhance cell-cell contacts and reduce cellular migration.

In order to determine the functional implications of increased Rac1-IQGAP1 signalling on Tiam1-Rac1-driven cellular effects, the ability of Tiam1 to regulate Rac1 signalling needs to

be assessed in a IQGAP1 null background. This will help elucidate the mechanism by which IQGAP1 might be involved in Tiam1-Rac1 signalling.

4.3.3.2 TMOD3 and FLII

TMOD3 is a family member of TMOD family (Cox and Zoghbi, 2000). Similar to other TMOD proteins, TMOD3 is a pointed end actin capping protein. Members of this family can bind directly to actin or to actin filaments that are associated with tropomyosin, a protein that links the actin cytoskeleton with myosin. The capping activity allows TMODs to block actin filament elongation and depolymerisation (Weber et al., 1994).

As indicated in section 4.2.5.3, TMOD3 was the only protein identified that had opposing Rac1 binding abilities upon expression of Tiam1 WT and P-Rex1 WT. In NIH3T3 cells, P-Rex1 WT and P-Rex1 GEF* expression was associated with increased Rac1-TMOD3 interactions. This suggests that activation of Rac1 is not important for this interaction to occur, and potentially implies that TMOD3 is not implicated in P-Rex1-Rac1 signalling. Consistent with this notion TMOD3 has also been shown to negatively regulate cellular migration in the human microvascular endothelial cells, HMEC-1, where ectopic expression of TMOD3 was associated with reduced cellular migration, loss in cell polarity as well as a loss of the Arp2/3 protein complex in lamellipodia. Depletion of TMOD3, on the other hand, was associated with increased HMEC-1 cellular migration. Together, this demonstrates the negative role of TMOD3 in inhibiting cell motility in endothelial cells through actin filament regulation (Fischer et al., 2003). However, as suggested by the Tiam1 WT associated SILAC ratios, the Rac1-TMOD3 interaction is negatively regulated by Tiam1 WT in cells, hinting at a potential functional role of this interaction in mediating the differential GEF-induced cellular effects. It was therefore speculated that TMOD3 might be a GEF-regulated scaffolding protein that helps bring certain proteins in close proximity for binding once Rac1 is in the active form. Therefore, Ingenuity® IPA generated protein-protein interaction networks were analysed to identify potential Rac1 binding partners that associate with TMOD3. Consistent with its role as a pointed-end actin capping protein, Ingenuity® highlighted the ability of TMOD3 to bind to F-actin as well as actin monomers. Moreover, a relationship was indicated between TMOD3 and FLII through the ability of both proteins to bind CAMKII (Seward et al., 2008). Further biochemical analysis using the NIH3T3 cells harbouring the dox inducible P-Rex1 WT expression system, revealed that TMOD3 and FLII are capable of interacting on an endogenous level. Interestingly, expression of P-Rex1 WT in these cells resulted in an increased association between endogenous TMOD3 and FLII. This suggests that P-Rex1 WT might regulate Rac1-driven cellular functions by promoting the formation of a Rac1-TMOD3-FLII complex that is required for certain functions that are necessary for the P-Rex1-Rac1-driven cellular effects.

In addition to the link between TMOD3 and FLII, results from the SILAC screen also demonstrate that FLII is specifically enriched only upon expression of P-Rex1 WT relative to

control LIGHT labelled cells. This indicates that expression of P-Rex1 WT in cells results in an increased interaction between Rac1-FLII. Although FLII was only identified in two out of the four experiments conducted, the SILAC ratios obtained are from a SILAC pair, in which the SILAC ratio was inverted between the forward and revered SILAC experiments, thus increasing the confidence that this enrichment is true. Moreover, taking into account the Significance B values generated by MaxQuant, the changes in FLII associated SILAC ratios induced by expressing P-Rex1 WT were significant relative to control LIGHT labelled cells in both experiments and Tiam1 WT expressing cells in the forward SILAC experiment. Consistent with these results, FLII was also identified as a unique Rac1 interactor upon expression of P-Rex1 WT in two out of three conducted conventional mass spectrometry screens. This serves as a confirmation for the SILAC pattern described earlier and demonstrates that P-Rex1 WT mediates the Rac1-FLII interaction in cells. All together, this strongly suggests that FLII might play a critical role, either alone or in conjunction with TMOD3 to drive P-Rex1-Rac1 signalling. As a result, the Rac1-FLII interaction was characterised further to validate the interaction and elucidate the functionality of the Rac1-FLII binding as well as its role, if any, in mediating P-Rex1-driven cellular signalling downstream of Rac1.

4.4 Conclusions

The main aim of this part of the PhD project was to elucidate the mechanism by which Tiam1 and P-Rex1 dictate Rac1 downstream effects. Given the evidence from the literature suggesting that GEFs can serve as scaffolding proteins thereby influencing the binding of GTPases to specific effectors, it was interesting to investigate whether Tiam1 and P-Rex1 induce differential Rac1 downstream effects as a consequence of their ability to mediate specific Rac1-protein complexes. To test this hypothesis, the Rac1 interactome upon expression of the different GEF constructs was analysed. Results obtained from conventional mass spectrometry reveal that Tiam1 and P-Rex1 activation of Rac1 is associated with the formation of unique Rac1-protein complexes, such as Rac1-CAND1 under Tiam1 WT and Rac1-FLII under P-Rex1 WT expression. However, the low number of consistently identified unique Rac1 interactors upon activation by either GEF suggests that they might also regulate the levels of commonly bound Rac1 partners. Indeed, SILAC ratios obtained from the two SILAC pairs indicate that Tiam1 and P-Rex1 can also regulate the level of Rac1 binding to a subset of proteins that also interact with Rac1 under normal conditions. Upon confirming the SILAC pattern associated with IQGAP1, RhoGDI1 and TMOD3 the SILAC generated protein lists were screened for potential novel Rac1 effectors that might play a role in mediating the different GEF-induced Rac1 signalling, thus identifying FLII as a promising candidate that shows increased interaction with Rac1 and TMOD3 upon expression of P-Rex1. This called for a better understanding of this interaction. As a result, the Rac1-FLII interaction was further investigated to determine the role of FLII in P-Rex1-Rac1 signalling. The next chapter focuses on addressing this interaction further.

Chapter 5 : P-Rex1, Rac1 and FLII in Cellular Migration

5.1 Introduction

Rac1 signalling is involved in various cellular processes that become aberrant during cancer formation and progression. However, due to the seemingly opposing role of Rac1 in certain cellular functions, such as migration and invasion, understanding the exact role played by Rac1 in cancer progression is hindered. Results outlined in Chapter 3 demonstrate that Tiam1 and P-Rex1, in addition to activating Rac1, can also induce distinct cellular outcomes downstream of Rac1. Through the analysis of the Rac1 interactome upon expression of either GEF, presented in Chapter 4, it became evident that Tiam1 and P-Rex1 can also influence the ability of Rac1 to bind to different interactors. Combined with evidence from the literature it was, therefore, hypothesised that Tiam1 and P-Rex1 mediate specific downstream effects via modulating Rac1-protein interactions, potentially through acting as scaffolding proteins. To test this hypothesis, the SILAC generated protein list was filtered to identify Rac1 interactors that might play a role in specific GEF-Rac1 signalling. Utilising different selection criteria, outlined in Chapter 4, the actin capping protein FLII was identified as a novel Rac1 binding partner that shows specific P-Rex1-induced Rac1 interaction. FLII is a member of the gelsolin protein superfamily and similar to Rac1 is implicated in cytoskeleton rearrangements and has been shown to regulate cellular migration. As a result, the Rac1-FLII interaction was selected for further characterisation to explore the role of FLII in P-Rex1-Rac1 signalling. To better understand how it might regulate P-Rex1-Rac1 signalling a literature review was performed. The following section presents an overview of FLII associated cellular functions that could implicate it in Rac1 signalling.

5.1.1 Protein Flightless-1 Homolog (FLII)

The *FLII* gene was first identified from a screen for mutations involved in reducing flight ability in *Drosophila melanogaster* (*D. melanogaster*) (Homyk and Sheppard, 1977). Characterisation of flight defective flies revealed that mutations in the *FLII* gene locus were associated with developmental defects in the indirect flight muscles as a consequence of abnormal myofibril arrangements (Deak et al., 1982). In more severe cases, mutations in the *FLII* gene were embryonic lethal due to irregularities in actin association with cellularisation membranes that led to abnormal embryonic gastrulation (Miklos and De Couet, 1990; Perrimon et al., 1989; Straub et al., 1996). The cDNA of the *FLII* locus was later cloned and characterised by Campbell et al. in 1993 with the *FLII* gene encoding a 1256 amino acid protein. Bioinformatics analysis the *FLII gene* of *D. melanogaster* revealed a significantly similar coding region in *Caenorhabditis elegans* (*C. elegans*) that encoded a 1257 amino acid protein with a 49 % sequence identity and a 69 % similarity after the consideration of amino acid conservative

substitutions. Alignment of the two homologous protein sequences identified stretches of highly conserved regions, which were then utilized to identify the human *FLII* homologue. The human protein consists of 1269 amino acids and has a 58 % identify when compared to the *D. melanogaster* FLII protein and a 74 % similarity (Campbell et al., 1993). The murine homologue of *FLII* was later identified encoding a 1271 amino acids long protein with 95 % sequence identity to the human FLII protein, which subsequently enabled the functional characterisation of FLII in an animal model (Campbell et al., 2000). Although heterozygous FLII mutant mice are viable and develop normally, homozygous mutations of the murine FLII homologue is embryonic lethal, highlighting the importance of FLII in early mammalian embryonic development (Campbell et al., 2002).

Further database searches revealed sequence similarity between FLII and members of the gelsolin protein superfamily, with FLII proteins containing six characteristic GEL domains. Interestingly, the N-terminus of FLII consists of 16 LRR domain repeats, that are known to modulate protein-protein interactions, further classifying FLII as a member of the LRR protein superfamily (Campbell et al., 1993) (Claudianos and Campbell, 1995). As a result of its domain structure, FLII has been implicated in various cellular processes that could be attributed to characteristics inherent to both superfamilies. Figure 5.1 outlines some of the FLII-mediated cellular processes identified to date.

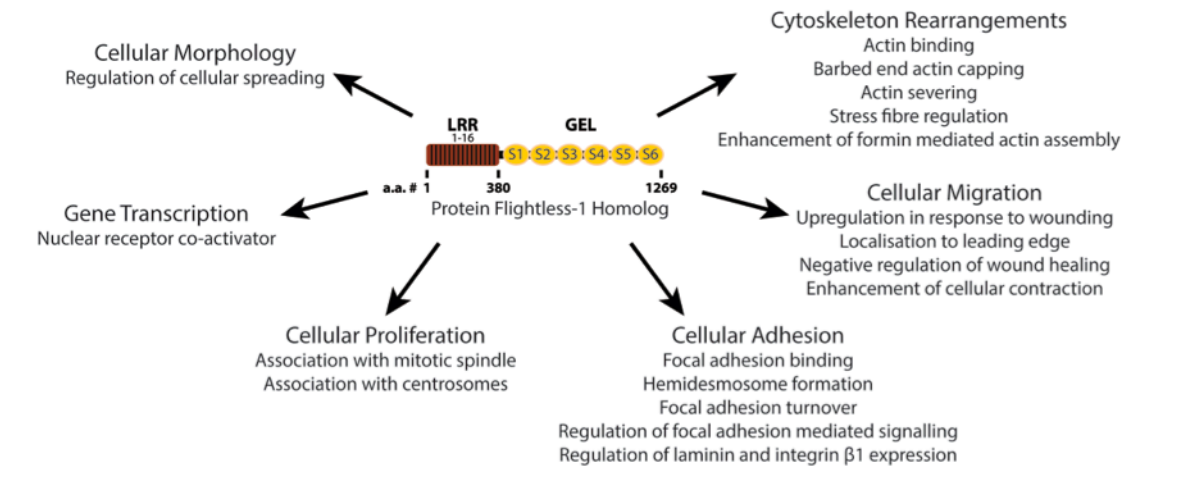

Figure 5.1: Schematic Representation of FLII Regulated Cellular Processes
A simplified schematic representation of key cellular processes that FLII has been shown to regulate based on evidence presented in the literature review outlined in this chapter. LRR= Leucine Rich Repeat; GEL= Gelsolin-like domain; a.a= Amino acid. Figure formulated based on the literature review described in section 5.1.1

5.1.1.1 Role of FLII in Actin Cytoskeleton Rearrangements

Similar to other gelsolin protein superfamily members, FLII is an actin binding protein. In a study conducted by Goshima et al. the *C. elegans* FLII homologue was found to bind to both actin monomers and actin filaments; however, unlike gelsolin, FLII binding to monomeric actin was not calcium dependent (Goshima et al., 1999). This is consistent with the lack of conservation between the *C. elegans* FLII homologue and gelsolin in key residues involved in calcium binding (McLaughlin et al., 1993). Additionally, through co-sedimentation experiments,

the *C. elegans* FLII homologue was shown to act as an actin severing protein (Goshima et al., 1999). The murine homologue was also reported to bind both G-actin and F-actin. However, unlike gelsolin and the *C. elegans* FLII homologue, the murine homologue exhibits minimal actin filaments severing. Additionally, in contrast to gelsolin, the murine homologue of FLII was found to reduce actin polymerisation. Nevertheless, similar to gelsolin, mouse FLII was shown to serve as an actin capping protein of the barbed end of actin filaments (Mohammad et al., 2012).

Despite the evidence suggesting that FLII inhibits actin polymerisation, in a study conducted by Higashi et al. FLII was found to enhance actin assembly, indirectly, via promoting the activity of Daam1 and mDia1 (Higashi et al., 2010). Binding of activated small GTPases, including GTP bound RhoA, RhoB and RhoC but not Rac1 or Cdc42, to the GTPase binding domain (GBD) located adjacent to the DID domain present in both Daam1 and mDia1, has been demonstrated to partially disrupt the DID-DAD interaction unleashing the autoinhibition and stimulating DRFs-mediated actin assembly (Higashi et al., 2008). However, *in vitro* studies show that binding of active RhoA alone is not sufficient to fully stimulate mDia1 actin assembly (Li and Higgs, 2003, 2005). FLII was identified as a protein that binds to both Daam1 and mDia1 through its GEL domain. Further characterisation of the FLII-Daam1 and FLII-mDia1 interactions revealed that FLII binds to the DAD domain in both proteins. As a consequence, FLII competes with DID for DAD interaction and upon binding of activated RhoA to the GBD domain, FLII cooperates with RhoA to enhance the autoinhibition release thus further promoting the full activation of the DRFs-mediated actin assembly (Higashi et al., 2010).

Taken together evidence from the literature demonstrates that FLII is an actin binding protein that regulates actin dynamics through barbed end actin capping, partial actin severing and regulation of other actin binding proteins, such as DRFs to promote actin assembly.

Consistent with its role as an actin binding protein, FLII also localises to actin-based structures during embryonic development. FLII was found to colocalise with actin in parasympathetic neurons harvested from chick embryos particularly in the main body of growth cones as well as the tip of the extending filopodia. Similarly, enrichment of actin and FLII at the hexagonal array that mark the sites of membrane invaginations at early stages preceding cellularisation was reported in *D. melanogaster* embryos of varying stages. Additionally, in the cellularising blastoderm, FLII and actin localise mainly to the cortex as well as the invagination furrows, with increased localisation at furrows in embryos that have almost completed cellularisation (Davy et al., 2000). This is in agreement with the reported role of FLII in ensuring accurate actin localisation to the cellularisation membranes (Straub et al., 1996). FLII was also reported to localise to the actin arc and actin based structures at the leading edge of motile NIH3T3 cells stimulated with 10 % FCS (Davy et al., 2001).

In addition to its role as an actin binding protein, FLII has also been shown to associate to other components of the cytoskeleton. For example, Davy et al. demonstrated the colocalisation of FLII with the microtubule network extending into the leading edge of the

migrating NIH3T3 cells. In quiescent NIH3T3 cells, FLII predominantly localises to the nuclear and perinuclear region with a filamentous FLII network extending into the cytoplasm, and under these conditions FLII showed a better overlap with microtubules than actin filaments in these regions. Furthermore, FLII was reported to localise to other β-tubulin based structures, such as the mitotic spindle particularly at centrosomes, which are structures involved in cellular division. Interestingly, in telophase, FLII was found to localise together with microtubules at the midbody of cells; however it was absent from the actin contractile ring (Davy et al., 2001).

5.1.1.2 Role of FLII in GTPase Signalling

As a result of its domain structure, FLII presents a unique gelsolin protein superfamily member linking the actin cytoskeleton dynamics to other signalling pathways mediated through its ability to bind various protein complexes through the LRR domain (Campbell et al., 1997; Claudianos and Campbell, 1995). This is of particular interest, since comparison of the FLII LRR domain with other members within the LRR structurally related subgroup suggested that the LRR domain in FLII might mediate interaction with Ras proteins and potentially other related small GTPases (Claudianos and Campbell, 1995). For example, the FLII LRR domain shows high homology to the LRR domains present in the *S. cerevisiae* adenylyl cyclase, the *C. elegans SUR-8*, and the mammalian RSP-1. All three proteins have been previously reported to mediate Ras signalling (Cutler et al., 1992; Kataoka et al., 1985; Sieburth et al., 1998; Toda et al., 1985). Moreover, adenylyl cyclase, the closest relative to the FLII LRR domain is among the best-characterised Ras effectors and has been shown to bind to Ras through a Ras-associating domain within its LRR domain (Kido et al., 2002). The link between FLII and Ras signalling was further confirmed upon establishing that the *C. elegans* FLII homologue binds directly to Ras, but not to the small GTPases Rac1, RhoA, Cdc42 and RalA (Goshima et al., 1999).

Additional evidence suggesting the involvement of FLII in Ras and small GTPase signalling include localisation studies in motile NIH3T3 cells. Serum stimulation and induction of cellular migration in NIH3T3 cells was associated with FLII translocation from the nuclear and perinuclear regions to the cytoplasm. In addition to the FLII localisation at actin-rich regions at the periphery of the cell including membrane ruffles and the leading edge of the cell, colocalisation between FLII, Ras and Cdc42 as well as RhoA upon stimulation of cellular migration was also observed at these sites (Davy et al., 2001). More interestingly, increased FLII expression was also found to negatively regulate levels of active Rac1 and active Cdc42. Moreover, expression of constitutively active Rac1 in fibroblasts derived from transgenic FLII overexpressing mice ($FLII^{Tg/Tg}$) rescued some of the spreading defects that were observed in these cells, thus demonstrating that Rac1 and FLII cooperate to regulate actin and focal adhesion dynamics (Kopecki et al., 2011). Taken together this evidence suggests that FLII might be involved in the Ras and small GTPase-mediated cellular migration in NIH3T3 cells.

5.1.1.3 Role of FLII in Cellular Migration

Given the association of FLII with the actin and microtubule cytoskeleton network and its colocalisation with actin cytoskeleton regulators, such as Ras, small GTPases and formins, it is not surprising that FLII is implicated in regulating cellular migration. The first indication that FLII is involved in regulating cellular migration came from the observation that FLII is upregulated in keratinocytes at the wound edge as well as in fibroblasts within the wound bed in mice with WT FLII. Additionally, comparison of wound closure in WT, FLII deficient heterozygous mice ($FLII^{+/-}$) and transgenic mice overexpressing FLII (Tg1) revealed that FLII levels influence the rate of wound repair. Compared to WT mice, $FLII^{+/-}$ mice showed an increased rate of wound closure. Similar observations were also observed *in vitro* in scratched confluent monolayers of skin fibroblasts and keratinocytes extracted from WT and Tg1 mice. Interestingly, increased FLII expression was also shown to reduce proliferation both *in vivo* and *in vitro*. Additionally, an increase in α-smooth muscle actin, a myofibroblast marker involved in scarring, was observed in $FLII^{+/-}$ providing an additional explanation to the enhanced wound healing observed in these mice, since myofibroblasts have been documented to regulate wound contraction. FLII deficiency was also associated with reduced collagen I staining around wounded areas 14 days post wounding, while increased staining was observed in Tg1 wounds. Taken together, this provided substantial evidence of the involvement of FLII in cellular motility potentially via its role in regulating proliferation and ECM remodelling (Cowin et al., 2007). FLII was also reported to negatively regulate scar-free wound healing in early gestation. However, FLII did not localise to actin filaments at that stage, suggesting that FLII can regulate wound healing in an actin independent manner (Lin et al., 2011).

In addition to its role in regulating migration through proliferation and ECM remodelling, FLII has been shown to modulate keratinocyte migration through regulating hemidesmosome formation and integrin-mediated cellular adhesions. Consistent with previous reports, cellular migration of keratinocytes derived from FLII transgenic mice ($FLII^{Tg/Tg}$) was reduced when compared to WT mice, while $FLII^{+/-}$ keratinocytes exhibited increased cellular migration on three different ECM substrates. Interestingly, differential FLII levels were also associated with differences in the ability of derived keratinocytes and fibroblasts to adhere to laminin, collagen I and fibronectin. In both keratinocytes and fibroblasts, increased FLII expression resulted in weaker cell-ECM adhesions and cells exhibited a rounded morphology with impaired cell spreading. On the other hand, $FLII^{+/-}$ derived cells were associated with a significant increase in cellular adhesion. It was also demonstrated that FLII levels regulate expression of laminin and laminin-binding integrin receptors with $FLII^{+/-}$ wounds having elevated levels of both laminin and β1 integrin. This suggested that FLII might regulate cellular migration through modulation of integrin-mediated cellular signalling. This was further corroborated upon confirming that FLII interacts with cytoskeletal proteins known to bind to integrin β1, such as talin, paxillin and vinculin at sites of focal contacts (Kopecki et al., 2009).

Evidence supporting the role of FLII in regulating cellular migration through cellular adhesion was also provided through a study conducted by Mohammed et al. in which they demonstrated that FLII was present in focal adhesion associated cellular fractions prepared using collagen coated beads. Moreover, FLII was shown to colocalise with vinculin at focal adhesions in NIH3T3 cells. Similar to previous observations, FLII depletion using siRNA and shRNA in NIH3T3 cells was associated with enhanced cellular migration while FLII overexpressing cells resulted in reduced cellular migration and cellular adhesion. Additionally, FLII depletion in NIH3T3 cells caused a reduction in the total and activated levels of β1 integrin in non-migrating cells. Total internal reflection fluorescence (TIRF) analysis also revealed that FLII knockdown also reduced the number of focal adhesions with activated vinculin. These results indicated that FLII deficiency reduces the number of focal adhesions (Mohammad et al., 2012). Despite these conflicting reports regarding the role of FLII in regulating cellular adhesion, both studies conducted by Kopecki et al. and Mohammad et al. clearly demonstrated the association of FLII with focal adhesions and with cytoskeletal proteins that are involved in mediating integrin signalling at focal contacts (Kopecki et al., 2009; Mohammad et al., 2012). In another study, FLII was shown to regulate focal adhesion turnover. Fibroblasts from $FLII^{+/-}$, WT and $FLII^{Tg/Tg}$ mice were examined to assess the role of FLII on actin and focal adhesion dynamics. FLII overexpression was associated with increased actin staining with prominent stress fibre formation together with a significant increase in the number and size of focal adhesions. $FLII^{Tg/Tg}$ cells showed decreased staining of p-paxillin, a marker of adhesion-mediated signalling at focal adhesions. Moreover, FLII expression was associated with elevated levels of α-actinin expression compared to WT and $FLII^{+/-}$ derived cells. These results indicated that FLII expression impairs focal adhesion turnover since increased α-actinin expression is a marker of less dynamic focal adhesions with impaired turnover. Consistent with the reduced focal adhesion turnover observed in $FLII^{Tg/Tg}$ cells, an elevated number of fibrillar adhesions were observed with cells exhibiting reduced cellular spreading (Kopecki et al., 2011).

Another mode by which FLII can influence cellular migration is through its role in regulating cellular contraction. Interestingly, fibroblasts derived from $FLII^{+/-}$ mice exhibited a reduced ability to contract the collagen gels in a collagen contraction assay. This suggests that FLII might indirectly promote migration given its requirement for optimal cellular contraction (Kopecki et al., 2011).

Given the importance of FLII as an actin binding protein and a regulator of actin dynamics, together with its involvement in cellular migration, focal adhesion turnover and most importantly its implication in small GTPase signalling, it was intriguing to understand the basis and function of the P-Rex1-mediated Rac1-FLII interaction proposed from the proteomic analysis outlined in Chapter 4.

Evidence from the literature supports a negative role of FLII in cellular migration; however P-Rex1 promotes migration through Rac1 activation. It was therefore interesting to

try and identify a potential link between Rac1 and FLII that can help explain the P-Rex1 associated increased cellular migration. For example, Rac1 has been shown to indirectly regulate chemotaxis in response to EGF stimulation through its downstream effector PAK1, which plays a crucial role in the phosphorylation myosin II-B and its localisation at the leading edge (Even-Faitelson et al., 2005). As indicated earlier in chapter 1, myosin II phosphorylation is key for optimal cellular contraction (Lauffenburger and Horwitz, 1996). Given that FLII deficiency impedes cellular contraction (Kopecki et al., 2011), this might be the potential link between both proteins in inducing P-Rex1-mediated enhanced cellular migration. It was therefore hypothesised that P-Rex1 expression in cells might promote a specific signalling cascade in which FLII exhibits a novel role in promoting cellular migration. Thus, a better understanding of the functional rational behind this P-Rex1-mediated Rac1-FLII interaction was essential in order to determine whether FLII is an important regulator of the P-Rex1-Rac1-mediated cellular effects. This chapter highlights experiments conducted to further characterise the FLII-Rac1 interaction and to assess its functional relevance in relation to the P-Rex1-mediated cellular phenotypes.

5.2 Results

5.2.1 Validation and Characterization of Rac1-FLII Interaction

As indicated in the previous section, compelling evidence suggests that FLII is involved in Ras and small GTPase signalling. However, unlike Ras, a direct interaction between FLII and Rac1 has not been reported to date. As a result, it was important to first examine the ability of FLII to bind to Rac1 before exploring its potential functional role in P-Rex1-mediated Rac1 signalling.

5.2.1.1 Validation of the Rac1-FLII Interaction

In order to validate the Rac1-FLII interaction identified by both conventional and SILAC mass spectrometry experiments, the ability of exogenous SF-Rac1 to co-precipitate endogenous FLII was assessed. HEK293T cells were transiently transfected with a construct expressing SF-Rac1. Next, parental and SF-Rac1 expressing HEK293T cells were subjected to a *Strep* pulldown to precipitate exogenous SF-Rac1. Co-precipitated endogenous FLII was detected by Western blot analysis using an anti-FLII antibody. As indicated in Figure 5.2A, an interaction between exogenous SF-Rac1 and endogenous FLII was seen only in SF-Rac1 expressing cells confirming the specificity of the SF-Rac1- FLII interaction. Due to the high expression levels obtained as a result of transient transfection of HEK293T cells, the interaction was also assessed in NIH3T3 cells harbouring the dox inducible system for the expression of SF-Rac1.

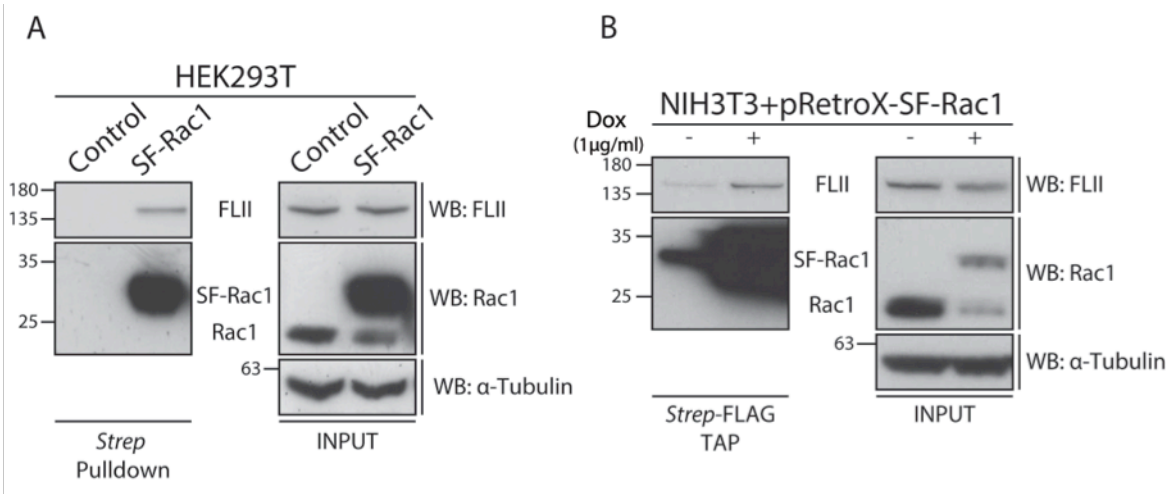

Figure 5.2: FLII is a Novel Rac1 Binding Partner
(A) Exogenous SF-Rac1 expressed in HEK293T cells was precipitated by *Strep* pulldown using *Strep*-Tactin® superflow and co-precipitated endogenous FLII was detected by western blot analysis using anti-FLII antibody. α-Tubulin was used as a loading control. Representative western blot from three independent experiments. (B) Exogenous SF-Rac1 expressed in NIH3T3 cells was precipitated by *Strep*-FLAG Tandem Affinity Purification (TAP) and co-precipitated endogenous FLII was detected by western blot analysis using anti-FLII antibody. Lysates from ethanol (- dox) treated NIH3T3 cells harbouring the doxycycline (dox) SF-Rac1 expression system were used as a control for the *Strep*-FLAG TAP to assess non-specific protein binding to the beads. α-Tubulin was used as a loading control. Representative western blot from three independent experiments.

As shown in Figure 5.2 B in the input lanes, as expected SF-Rac1 expression was only detected in cells that were subjected to dox treatment. Additionally, as observed previously, expression of SF-Rac1 was associated with a reduction in endogenous Rac1 levels, which addressed any potential FLII non-specific binding that might be due to the substantial increase in Rac1 levels seen with transient transfection in HEK293T cells. After 48 hours of ethanol (- dox) or 1 μg/ml dox (+ dox) treatment cells were harvested and subjected to SF-TAP to pulldown exogenous SF-Rac1 and its associated proteins. As indicated by the Western blot analysis outlined in Figure 5.2 B, SF-Rac1 pulldown was only observed in dox treated cells and FLII was also detected in this lane. Despite the non-specific binding of FLII to the beads used in the SF-TAP technique as indicated by the faint band observed in the – dox treated lane, the amount of FLII detected in + dox treated cells was significantly higher, especially given the slightly lower protein FLII input in these cells. Together both pulldown experiments clearly demonstrate the ability of Rac1 and FLII to interact in cells confirming the proteomic analysis described in Chapter 4.

5.2.1.2 Characterisation of the Rac1-FLII Interaction

FLII is a unique member of the gelsolin protein superfamily due to possessing an N-terminal LRR domain and a C-terminal GEL domain. The two domains in FLII have very distinct functions with the GEL domain mediating the actin regulation functions of FLII while the LRR domain promoting protein-protein interactions (Claudianos and Campbell, 1995). Thus to gain functional insight into the Rac1-FLII interaction, it was important to determine the domain to which Rac1 binds to in FLII. FLAG-tagged full length FLII (FLII FL), a GEL truncation mutant (FLII GEL) and a LRR truncation mutant (FLII LRR), previously described by Lee et al. (Lee et al., 2004) were provided as a kind gift from the Stallcup group and used to identify the region to which Rac1 binds to FLII. Figure 5.3 A outlines the mutants used for this analysis. The FLII constructs were introduced separately in HEK293T cells using transient transfection and together with parental HEK293T cells were subjected to a FLAG immunoprecipitation and assessed by Western blotting. As demonstrated in Figure 5.3 B, as expected Rac1 was detected upon immunoprecipitation of FLII FL. Interestingly, increased levels of Rac1 were detected in cells expressing FLII LRR compared to FLII FL despite the even Rac1 levels observed in the input lanes. In contrast, FLII GEL immunoprecipitation was associated with minimal levels of co-precipitated Rac1, suggesting that Rac1 binds preferentially to the LRR domain of FLII. This was further confirmed by conducting the reciprocal experiment in which SF-Rac1 was co-transfected with the different FLII mutants in HEK293T cells. Lysates from the respective cells were then subjected to a *Strep* pulldown to precipitate exogenous SF-Rac1. Differences in the levels of FLII constructs co-precipitated were detected by Western blot analysis using an anti-FLAG® M2 antibody. Consistent with the FLAG immunoprecipitation outlined above, there was an increased association between SF-Rac1 and FLII LRR compared to FLII FL and FLII GEL. The FLII

constructs were also expressed individually in the absence of SF-Rac1 to control for non-specific binding. As shown in Figure 5.3 C, there was minimal non-specific binding upon expression of the FLII FL construct; however, the level detected upon expression of SF-Rac1 was greater than the basal non-specific binding to beads. Collectively, both experiments show that Rac1 preferentially binds to the LRR domain of FLII with no/minimal interaction detected with the GEL domain.

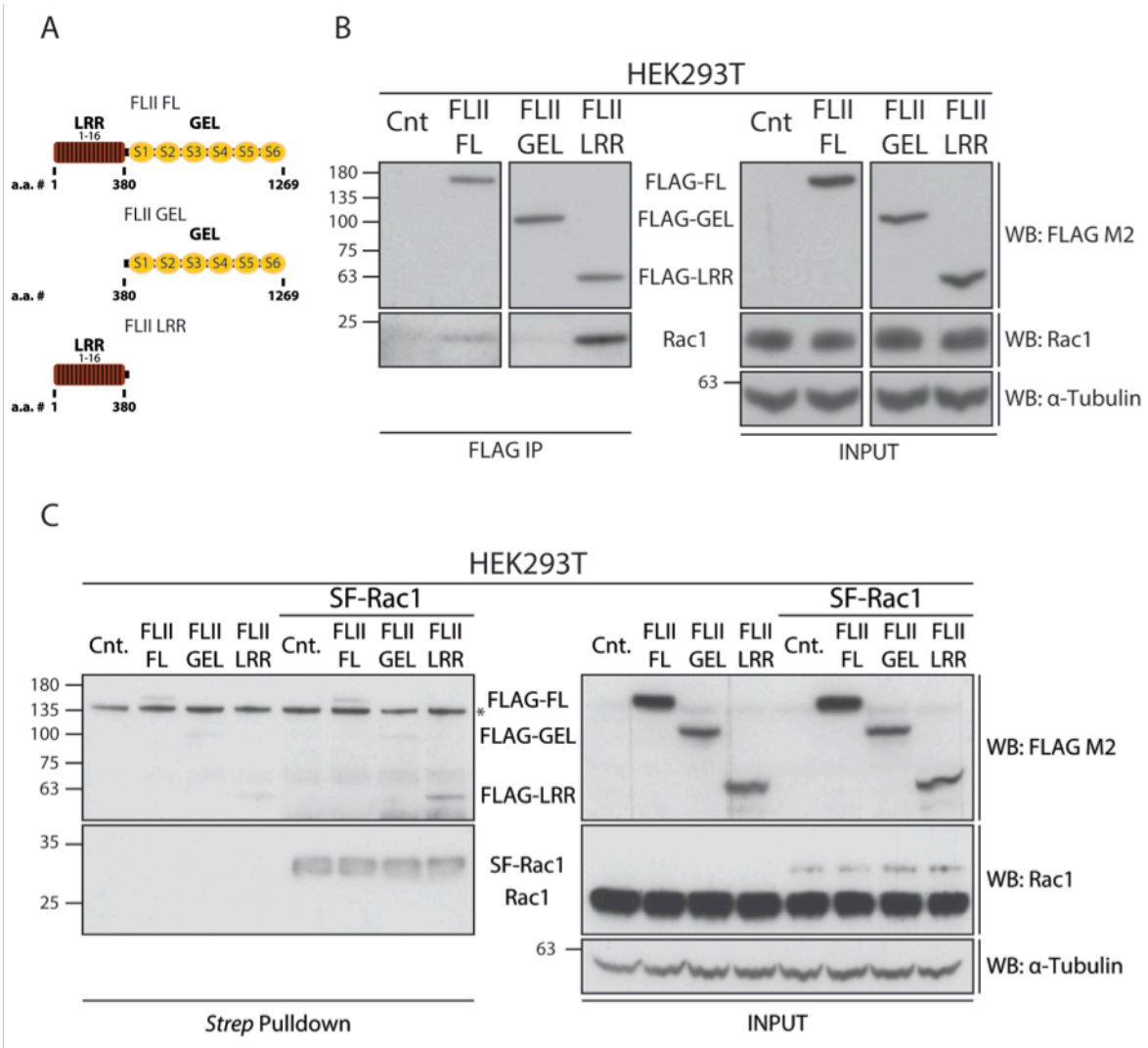

Figure 5.3: Rac1 Binds to the LRR Domain of FLII

(A) Schematic representation of FLII domain structure modified from Liu et al. showing 16 leucine rich repeats (LRR) comprising the N-terminal LRR domain and 6 gelsolin-Like repeats (S1-S6) representing the GEL domain together with the amino acid number (a.a. #) range for each domain (Liu and Yin, 1998). FLII FL represents the full length FL protein; FLII GEL and FLII LRR represent the GEL and LRR truncation mutants, respectively. (B) Exogenous FLAG-tagged FLII FL, FLII GEL or FLII LRR were expressed separately in HEK293T cells and were immunoprecipitated using anti-FLAG® M2 antibody. Co-precipitated endogenous Rac1 was detected in each sample by western blot analysis using anti-Rac1 antibody. α-Tubulin was used as a loading control. Representative western blot from three independent experiments. (C) Exogenous FLAG-tagged FLII FL, FLII GEL or FLII LRR were expressed separately in HEK293T or together with SF-Rac1. Cells where subjected to *Strep* pulldown using Strep®-Tactin superflow to pulldown SF-Rac1. The ability of FLAG-tagged FLII FL, FLII GEL and FLII LRR to bind to SF-Rac1 was assessed in each sample by western blot analysis using anti-FLAG® M2 antibody. α-Tubulin was used as a loading control. * = non-specific band. Representative western blot from three independent experiments.

5.2.1.3 Rac1-FLII SILAC Pattern Validation

Results highlighted in Chapter 4 indicated that the interaction between Rac1 and FLII was GEF mediated, specifically through P-Rex1 activation of Rac1. Upon confirming that FLII interacts with Rac1 under normal cellular conditions it was important to determine whether this interaction is mediated by P-Rex1.

As described earlier in Tables A.2-A.3 in the appendix section, FLII was identified as a unique Rac1 interactor upon P-Rex1 activation of Rac1 in two SF-TAP experiments followed by mass spectrometry analysis, demonstrating that in NIH3T3 cells, P-Rex1 enhances the Rac1-FLII interaction above that detected in parental, Tiam1 WT, Tiam1 GEF* and P-Rex1 GEF* expressing NIH3T3 cells. To further corroborate this result, it was important to examine the suggested SILAC pattern on an endogenous level. Therefore the duolink® In Situ PLA assay was used to examine the ability of endogenous Rac1 and endogenous FLII to interact upon expression of the different GEF constructs. Using NIH3T3 cells harbouring the dox inducible GEF expression system cells were treated with 1 μg/ml dox, fixed in 4 % formaldehyde and subjected to the duolink® In Situ PLA assay using mouse anti-Rac1 and rabbit anti-FLII primary antibodies. Phalloidin and DAPI were also used to stain the actin cytoskeleton and the nuclei. Figure 5.4 A shows representative fluorescence images from the duolink® In Situ PLA assay. As indicated by the increased fluorescence duolink® signal, expression of P-Rex1 WT was found to promote the Rac1-FLII interaction compared to parental and other GEF expressing NIH3T3 cells. Quantification of the average duolink® fluorescence signal per cell using the CellProfiler software, as outlined in 2.5.5.2, revealed a 6-fold increase upon expression of P-Rex1 WT compared to parental NIH3T3 cells. Statistically the increase induced by P-Rex1 WT expression was significantly different than the signal detected in parental ($p=0.004$), Tiam1 WT expressing cells ($p=0.015$) and P-Rex1 GEF* expressing cells ($p=0.006$). In contrast, Tiam1 WT, Tiam1 GEF* and P-Rex1 GEF* expression did not induce a significant increase in the level of signal detected compared to parental cells ($p=0.32$, $p=0.51$, $p=0.32$, respectively). These findings clearly demonstrate that P-Rex1 activation of Rac1 enhances the ability of Rac1 to bind to FLII on an endogenous level in NIH3T3 cells.

Given that NIH3T3 cells do not normally express P-Rex1 and thus this enhanced Rac1-FLII interaction could potentially be an artefact of increased P-Rex1 WT signalling in cells that do not normally contain the protein, MCF7 cells were also used to assess the influence of GEF expression on the Rac1-FLII interaction. MCF7 cells harbouring the dox inducible SF-Rac1/GEF expression system in addition to cells with an empty vector control (EV) were treated with 1 μg/ml dox for 48 hours. Cells were harvested and equal levels of protein inputs were subjected to the SF-TAP technique. Co-precipitated endogenous FLII was detected by Western blot analysis using an anti-FLII antibody. Differences in levels of Rac1-bound endogenous FLII were compared between cells expressing the different GEF constructs using densitometric analysis.

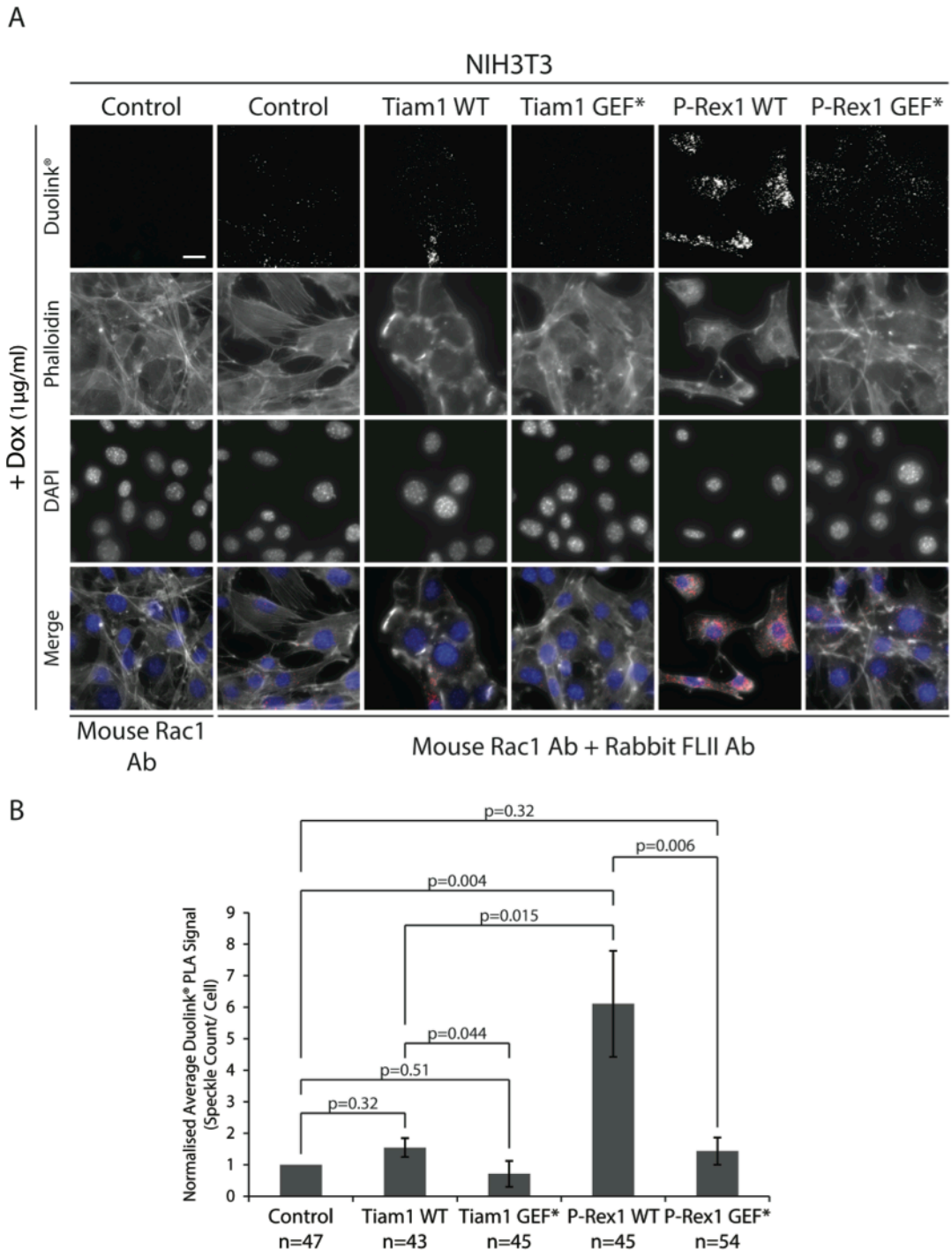

Figure 5.4: Activation of Rac1 by P-Rex1 Enhances the Endogenous Rac1-FLII Interaction in NIH3T3 Cells
(A) NIH3T3 cells harbouring the doxycycline (dox) inducible GEF expression system were fixed in 4 % formaldehyde following 24 hours of dox induction. Cells were then subjected to the duolink® In Situ PLA assay using mouse anti-Rac1 and rabbit anti-FLII primary antibodies. The respective secondary mouse and rabbit PLA probes were used and analysed by fluorescence microscopy using the low light microscope (100x magnification). Phalloidin and DAPI were used to visualise the actin cytoskeleton and nuclei, respectively. Scale bar=20µm. (B) Quantification of average duolink® In Situ PLA signal from indicated number of cells per condition from two independent experiments using the CellProfiler software. Background duolink® In Situ PLA signal was accounted for by subtracting the average speckle count identified in control cells that were subjected to only mouse anti-Rac1 antibody. Error bars represent ± standard error. Student's t-test was performed to determine statistical significance and p-value are shown on graph. p-values ≤ 0.05 are considered significant; ≤0.01 are considered highly significant.

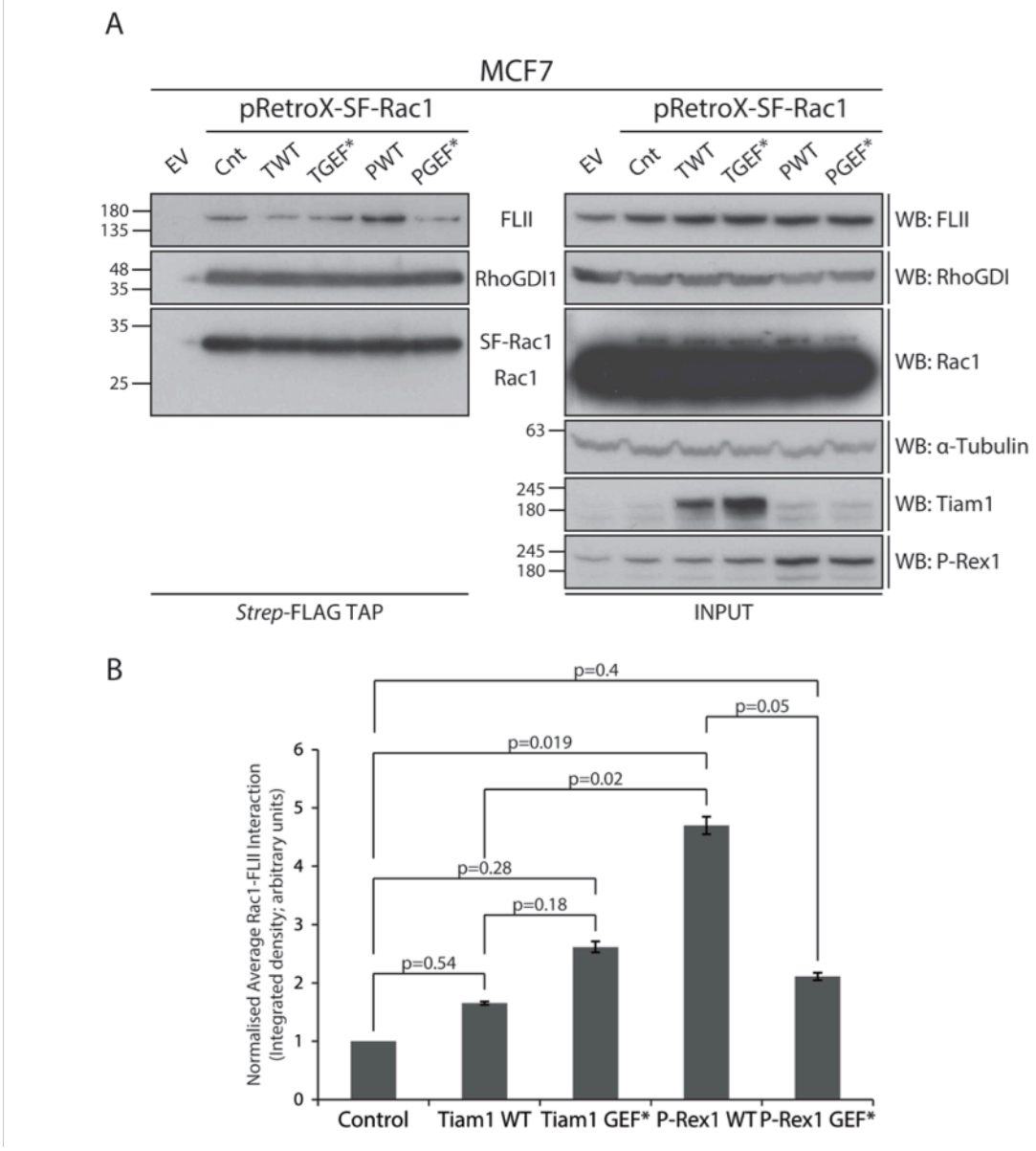

Figure 5.5: Activation of Rac1 by P-Rex1 Enhances the Interaction between Exogenous SF-Rac1 and Endogenous FLII in MCF7 Cells

(A) MCF7 cells harbouring the doxycycline (dox) inducible system for expressing SF-Rac1 together with the different GEF constructs were treated with dox for 48 hours. Cells lysates were then subjected to the *Strep*-FLAG Tandem Affinity Purification (TAP) to pulldown SF-Rac1. Co-precipitated FLII was detected by western blot analysis using anti-FLII antibody. MCF7 cells expressing an empty pRetroX-Tight-Pur vector (EV) were used as a control for non-specific binding. Co-precipitated RhoGDI1 was also detected by western blot analysis using anti-RhoGDI1 antibody and was used as an internal control for the efficiency and variation of the SF-Rac1 pulldown between samples. α-Tubulin was used as a loading control. Representative western blot from three independent experiments. (B) Quantification of average Rac1-FLII interaction from three independent experiments using Image J software to calculate the integrated density from each western blot analysis. Integrated density values from the EV lane were used to subtract the background density levels in each experiment and remaining values were normalised to the control lane. Error bars represent ± standard error. Student's t-test was performed to determine statistical significance and p-value are shown on graph. p-values ≤ 0.05 are considered significant; ≤0.01 are considered highly significant.

As demonstrated in Figure 5.5 A, endogenous FLII was detected in all cells expressing SF-Rac1, regardless of the GEF expression confirming that Rac1 and FLII interact under normal conditions. However, the Rac1-FLII interaction was markedly increased in response to P-Rex1 WT expression. Interestingly this increase was not observed with P-Rex1 GEF* expression,

despite the even expression level of both WT and GEF* mutant P-Rex1. This indicates that activation of Rac1 is required for P-Rex1 to promote the Rac1-FLII interaction. In contrast, both Tiam1 WT and GEF* mutant did not induce an increase in the level of FLII bound to Rac1. Importantly, expression of the different GEFs did not influence the association of Rac1 with RhoGDI1, which as indicated in Chapter 4 was found to have an equal SILAC ratio. This demonstrates that there is selectivity in the P-Rex1 WT-mediated Rac1-FLII interaction. The graph in Figure 5.5 B outlines the integrated density of detected FLII after normalising to the level of SF-Rac1 precipitated in each sample and the respective FLII protein input. Taking into account any non-specific binding to beads detected in the EV control lanes, as demonstrated, P-Rex1 WT expression induces a 4-fold increase in the level of FLII protein detected in the pulldown. Despite the modest increase observed in the integrated density of cells expressing Tiam1 WT, Tiam1 GEF* and P-Rex1 GEF* only P-Rex1 WT induced a significant increase as indicated by the Student's t-test compared to the cells with just SF-Rac1 expression ($p=0.019$).

Additionaly, MCF7 cells were also used to assess the effect of expressing the different GEF constructs on the Rac1-FLII interaction on the endogenous level using the duolink® In Situ PLA. Similar to NIH3T3 cells, expression of P-Rex1 WT in MCF7 cells was also associated with increased duolink® fluorescence signal, indicating an increased Rac1-FLII binding in these cells as demonstrated from the representative images presented in Figure 5.6 A. However, unlike NIH3T3 cells in which a detectable signal was observed in control and cells expressing Tiam1 WT, Tiam1 GEF* and P-Rex1 GEF*, the MCF7 counterparts showed a much reduced signal, which in some cells was even below that detected in cells treated only with mouse anti-Rac1 antibody. This is clearly reflected from the CellProfiler normalised average duolink® fluorescence signal detected per cell outlined in Figure 5.6 B. On average P-Rex1 WT expression induced an eight-fold increase in the duolink® signal detected per cell when compared to parental MCF7 cells. It is important to note, though, that as illustrated by the large error bars, variation was observed between the cells analysed. This could potentially be due to differential P-Rex1 WT expression across the analysed pool since P-Rex1 WT expression was not simultaneously visualised for each cell used for the quantification. An alternative explanation is that this is a true representation of variations in the ability of Rac1 and TMOD3 to bind in cells. However this increase was statistically significant as indicated by the Student's t-test p-value compared to parental cells ($p=0.07$), and highly significant when compared to Tiam1 WT expressing cells ($p=0.0015$) and P-Rex1 GEF* expressing cells ($p=0.01$). In contrast, expression of Tiam1 WT, Tiam1 GEF* and P-Rex1 GEF* failed to induce any significant change in Rac1-FLII detected duolink® signal when compared to the basal signal detected in the parental cells ($p=0.08$, $p=0.07$, $p=0.07$, respectively).

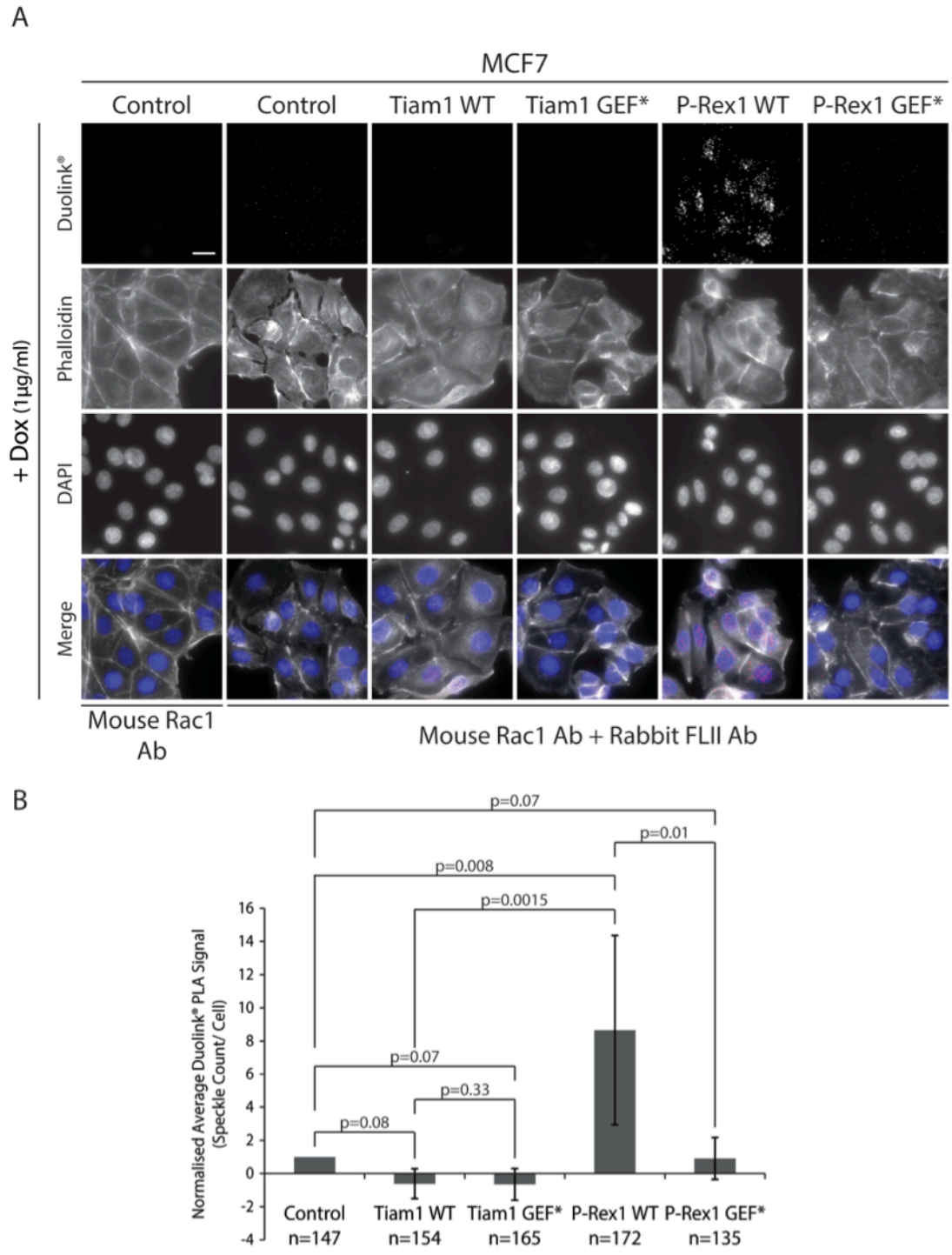

Figure 5.6: Activation of Rac1 by P-Rex1 Enhances the Endogenous Rac1-FLII Interaction in MCF7 Cells
(A) MCF7 cells harbouring the doxycycline (dox) inducible GEF expression system were fixed in 4 % formaldehyde following 24 hours of dox induction. Cells were then subjected to the duolink® In Situ PLA assay using mouse anti-Rac1 and rabbit anti-FLII primary antibodies. The respective secondary mouse and rabbit PLA probes were used and analysed by fluorescence using the low light microscope (100x magnification). Phalloidin and DAPI were used to visualise the actin cytoskeleton and nuclei, respectively. Scale bar=20µm. (B) Quantification of average duolink® PLA signal from indicated number of cells per condition from two independent experiments using the CellProfiler software. Background duolink® In Situ PLA signal was accounted for by subtracting the average speckle count identified in control cells that were subjected to mouse anti-Rac1 antibody. Error bars represent ± standard error. Student's t-test was performed to determine statistical significance and p-value are shown on graph. p-values ≤ 0.05 are considered significant; ≤0.01 are considered highly significant.

5.2.1.4 Section Summary

Results outlined in this section clearly demonstrate that FLII is a novel Rac1 binding partner. Additionally, as demonstrated by the SILAC experiments, FLII is capable of binding to Rac1 under normal cellular conditions; however this interaction is significantly enhanced upon expression of P-Rex1 WT. Interestingly, these observations were seen in different cell lines that have varying levels of endogenous P-Rex1 expression. Moreover, both biochemical and fluorescence based interaction assays conducted in MCF7 cells demonstrate that expression of P-Rex1 GEF*, despite the equal expression levels of P-Rex1 WT and P-Rex1 GEF*, did not enhance the Rac1-FLII interaction, suggesting that activation of Rac1 is critical for the interaction to occur. Consistent with this, Tiam1 GEF* expression also failed to influence the Rac1-FLII interaction compared to the basal levels detected in control cells. However, Tiam1 WT associated activation of Rac1 did not have a stimulatory effect on the Rac1-FLII interaction demonstrating that activation of Rac1, on its own is not sufficient to promote FLII binding. All together, evidence presented in this section support the conducted proteomic analysis and serves as a validation for the FLII SILAC pattern described in Chapter 4.

5.2.2 Investigation of GEF Scaffolding Ability

Having confirmed that the Rac1-FLII is GEF-dependent, it was interesting to investigate the mechanistic role of P-Rex1 in mediating the Rac1-FLII interaction. As highlighted earlier in Chapter 1, GEFs have been proposed to regulate GTPase signalling via serving as scaffolding proteins. It was therefore hypothesised that P-Rex1 enhances the Rac1-FLII interaction above the basal level through binding to FLII itself and serving as a scaffolding protein to bring Rac1 and FLII in close proximity to promote their interaction once Rac1 is in the active form.

5.2.2.1 Characterisation of the GEF-FLII Interaction

In order to investigate whether the P-Rex1-mediated Rac1-FLII interaction was a result of P-Rex1 scaffolding ability, it was important to first establish whether FLII is capable of binding either GEF. HEK293T cells were transiently transfected with constructs expressing FLAG-FLII, Myc-Tiam1 WT or Myc-P-Rex1 WT individually or in the combinations indicated in Figure 5.7. Cells were harvested 48 hours post transfection and equal protein levels were used to immunoprecipitate FLAG-FLII or Myc-GEFs. The ability of FLII and GEFs to co-precipitate was then assessed by Western blot analysis using indicated antibodies. As demonstrated in Figure 5.7 in the input lanes, relatively equal expression levels of FLAG-FLII and Myc-GEFs was achieved upon transfection of HEK293T cells. Interestingly, as detected by the anti-Myc and anti-P-Rex1 antibodies shown in Figure 5.7 A, Myc-P-Rex1 WT was found to co-precipitate with immunoprecipitated FLAG-FLII. In contrast, anti-Myc and anti-Tiam1 antibodies were associated with a non-specific band.

The P-Rex1-FLII specific interaction was further confirmed by conducting the reciprocal experiment in which Myc-GEFs were immunoprecipitated. As shown in Figure 5.7 B, FLAG-FLII was only detected in cells co-transfected with both FLAG-FLII and Myc-P-Rex1 WT, whereas only a faint non-specific FLII band was detected in cells expressing Myc-Tiam1 WT together with FLAG-FLII that was similar in intensity to the band associated with non-specific binding to the beads in cells expressing FLAG-FLII individually. Together both experiments demonstrate that FLII binds preferentially to P-Rex1 but not Tiam1 supporting the hypothesis that the Rac1-FLII interaction is mediated through the ability of P-Rex1 to act as a scaffolding protein.

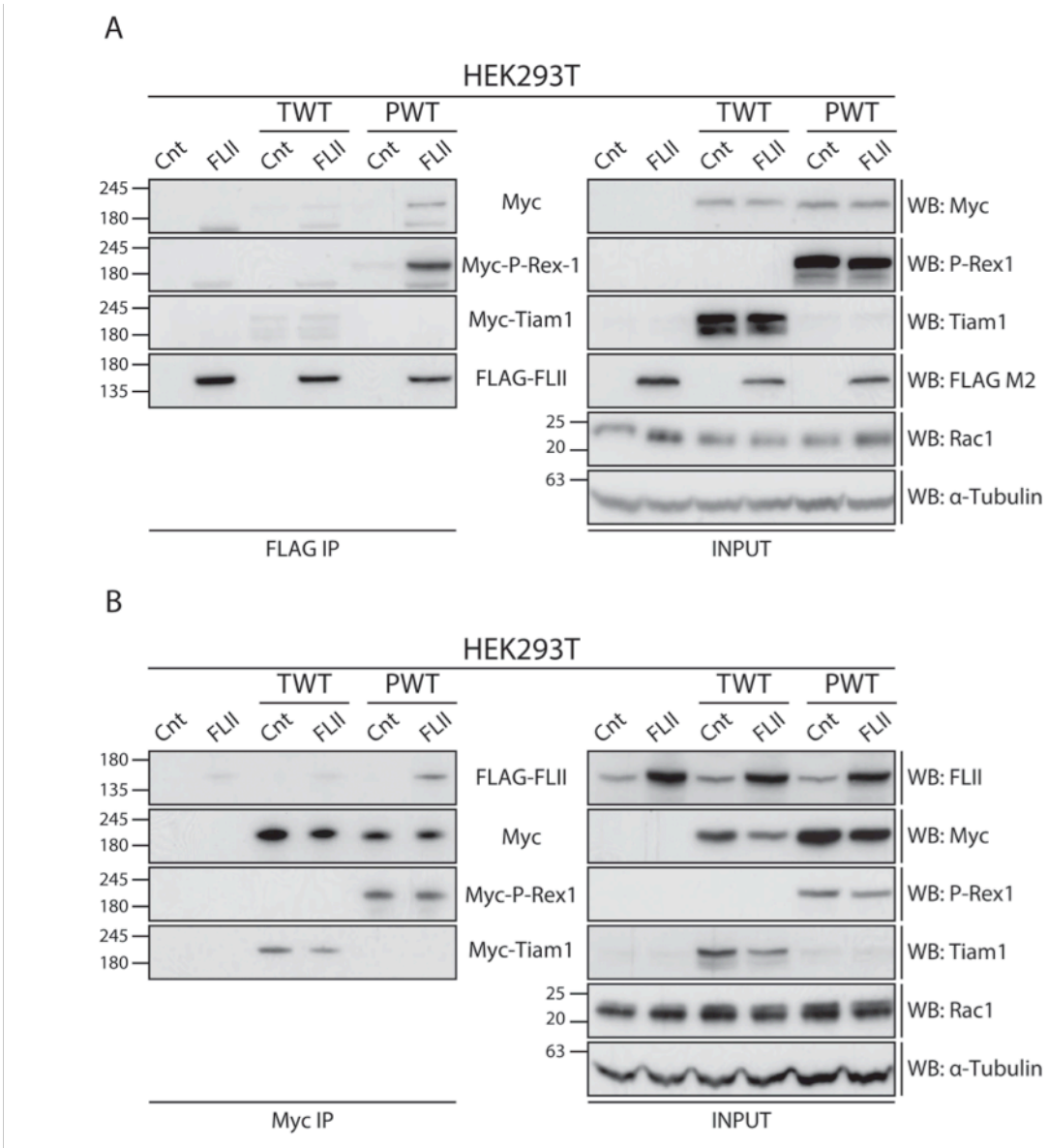

Figure 5.7: Exogenous FLAG-FLII Binds Preferentially to Exogenous Myc-P-Rex1 but not Myc-Tiam1
Exogenous Myc-Tiam1 wild type (TWT) or Myc-P-Rex1 WT (PWT) were expressed in HEK293T cells alone (TWT/ Cnt and PWT/Cnt, respectively) or together with FLAG-FLII (TWT/FLII and PWT/FLII, respectively). (A) FLAG-FLII was immunoprecipitated using anti-FLAG® M2 agarose beads and co-precipitated Myc-Tiam1 WT or Myc P-Rex1 WT was detected by western blot analysis using anti-Myc antibody as well as anti-Tiam1 and anti-P-Rex1 antibodies. α-Tubulin was used as a loading control. Representative western blot from three independent experiments. (B) Myc-Tiam1 and Myc-P-Rex1 were immunoprecipitated using anti-Myc antibody conjugated protein G sepharose® beads and co-precipitated FLII was detected by western blot analysis using anti-FLII antibody. α-Tubulin was used as a loading control. Representative western blot from three independent experiments.

5.2.2.2 Characterisation of the P-Rex1-FLII Interaction

Having established that exogenous FLII binds preferentially to exogenous P-Rex1 WT but not exogenous Tiam1 WT, the P-Rex1-FLII interaction was subjected to further characterisation to gain mechanistic insight into how P-Rex1 might be promoting the Rac1-FLII interaction. To explore the P-Rex1-FLII interaction on an endogenous level, MCF7 cells were utilised to confirm this interaction biochemically. As demonstrated in Figure 5.8 A, immunoprecipitation of endogenous P-Rex1 resulted in the co-precipitation of endogenous FLII. Importantly, this interaction was not seen in lysates incubated with rabbit IgG conjugated beads. In agreement with these results, endogenous FLII was also found to associate with endogenous P-Rex1 in the reciprocal experiment in which endogenous FLII was immunoprecipitated. Similarly, P-Rex1 was not detected in the IgG control lane further confirming that the interaction between endogenous P-Rex1 and endogenous FLII is highly specific.

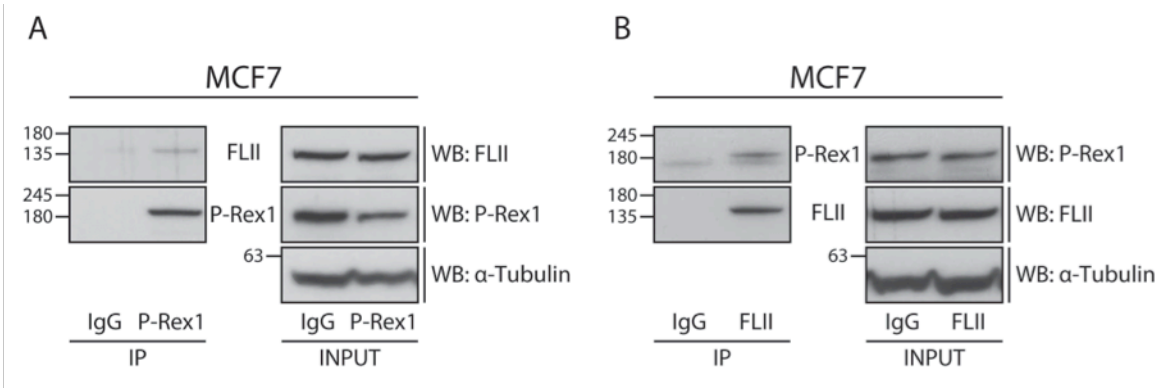

Figure 5.8: FLII is a Novel P-Rex1 Binding Partner
(A) Endogenous P-Rex1 was immunoprecipitated from MCF7 lysates using anti-P-Rex1 antibody conjugated protein G sepharose® beads. Co-precipitated endogenous FLII was detected by western blot analysis using anti-FLII antibody. Representative western blot from three independent experiments. (B) Endogenous FLII was immunoprecipitated from MCF7 lysates using anti-FLII antibody conjugated protein G sepharose® beads. Co-precipitated endogenous P-Rex1 was detected by western blot analysis using anti-P-Rex1 antibody. Rabbit IgG was used as a control for immunoprecipitation to determine non-specific binding to the beads. α-Tubulin was used as a loading control. Representative western blot from three independent experiments.

Next, through examining the ability of P-Rex1 GEF* to bind to FLII, the dependency of this interaction on Rac1 activation was tested. P-Rex1 WT or P-Rex1 GEF* were expressed individually or together with FLAG-FLII in HEK293T cells. Cells were collected 48 hours post transfection and FLAG-FLII was immunoprecipitated. As shown in Figure 5.9, both P-Rex1 WT and P-Rex1 GEF* were found to bind to immunoprecipitated FLAG-FLII in relatively equal levels. This indicates that the P-Rex1-FLII interaction is not dependent on the ability of P-Rex1 to activate Rac1; thus supporting the hypothesis that P-Rex1 binds to FLII upstream of Rac1.

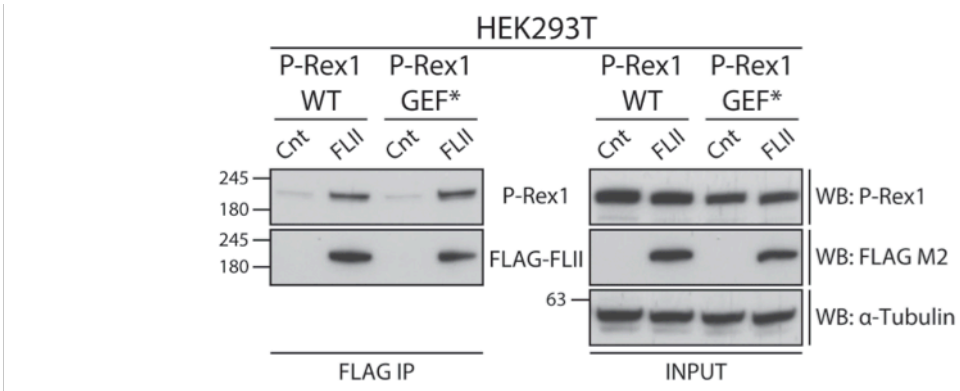

Figure 5.9: P-Rex1 Binds to FLII in an Active Rac1 Independent Manner
Exogenous Myc-tagged P-Rex1 wild type (WT) or GEF-dead mutant (GEF*) were expressed individually or co-expressed with FLAG-tagged FLII (FLAG-FLII) in HEK293T cells. Exogenous FLII was immunoprecipitated using anti-FLAG® M2 agarose beads. Co-precipitated Myc-P-Rex1 WT or GEF* was detected in each sample by western blot analysis using anti-P-Rex1 antibody. α-Tubulin was used as a loading control. Representative western blot from three independent experiments.

Upon confirming the P-Rex1-FLII interaction, FLII truncation mutants shown in Figure 5.3 A were used to determine the FLII domain to which P-Rex1 binds. FLAG-tagged FLII truncation mutants were transiently expressed in HEK293T cells individually or together with P-Rex1 WT. Cells were harvested 48 hours post transfection and equal protein levels were used to immunoprecipitate the different FLII truncation mutants. Co-precipitated P-Rex1 was detected by Western blot analysis using anti-P-Rex1 antibody. As illustrated in Figure 5.10, and consistent with previous observations, P-Rex1 was found to associate with immunoprecipitated FLII FL. Interestingly, unlike Rac1, P-Rex1 was found to bind preferentially to the FLII GEL domain as opposed to the LRR domain as indicated by the more intense P-Rex1 band detected in P-Rex1 expressing cells co-transfected with FLII GEL compared to FLII LRR co-transfected cells.

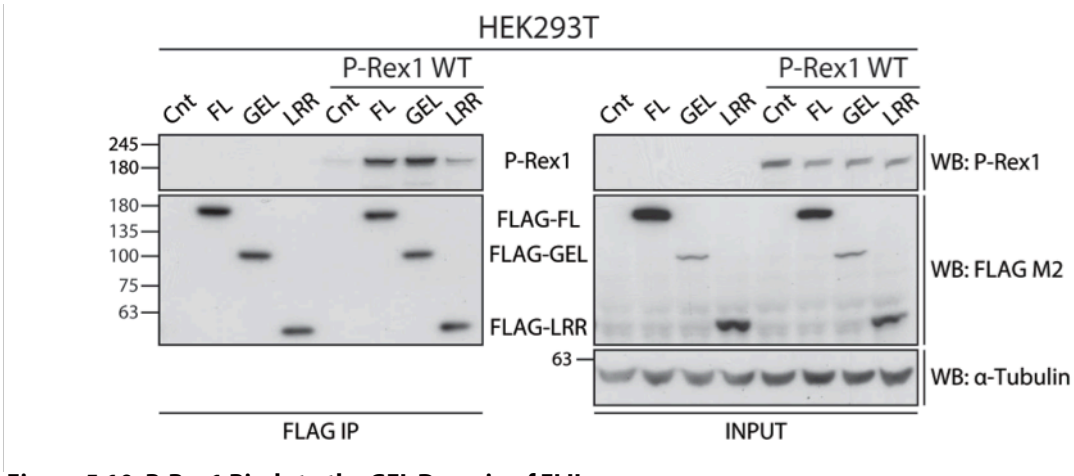

Figure 5.10: P-Rex1 Binds to the GEL Domain of FLII
Exogenous FLAG-tagged FLII full length (FL), FLII Gelsolin truncation mutant (GEL) or FLII leucine rich repeat truncation mutant (LRR) were expressed individually or co-expressed with Myc-P-Rex1 WT in HEK293T cells. The different FLII mutants were immunoprecipitated using anti-FLAG® M2 agarose beads. Co-precipitated Myc-P-Rex1 was detected in each sample by western blot analysis using anti-P-Rex1 antibody. Parental HEK293T cells, cells expressing the different FLAG-FLII mutants on their own and cells expressing Myc-P-Rex1 WT on its own were used as a control for the FLAG IP to determine the non-specific binding to the beads. α-Tubulin was used as a loading control. Representative western blot from three independent experiments.

5.2.2.3 *P-Rex1-Rac1-FLII Interaction*

The finding that P-Rex1 binds preferentially to the GEL domain of FLII, whereas Rac1 binds to the LRR domain supported the idea that both proteins can bind to FLII simultaneously. To test this, MCF7 cells were harvested and cell lysates were prepared under non-denaturing conditions to preserve protein complexes. Proteins were then resolved on a NativePAGE™ Novex® 3–12% Bis-Tris gel followed by Western blot analysis using anti-FLII, ant-P-Rex1, anti-Rac1 and anti-Tiam1 antibodies. The NativeMARK™ Unstained Protein Standard was then used to align the bands detected by each of the different antibodies used. As demonstrated in Figure 5.11 A, a protein band was detected at a similar molecular weight for FLII and P-Rex1. It was more difficult to ascertain whether Rac1 was also present in the same complex since it was detected as a smear. Given that the smear was observed around the same molecular weight in which P-Rex1 and FLII were detected this might suggest that all three proteins could potentially exist in one complex. A schematic representation of the proposed P-Rex1-Rac1-FLII complex is depicted in Figure 5.11 B. However, it is important to note that this is only a preliminary observation and as such should be interpreted with caution. Additionally, in order to accurately determine whether all three proteins exist in the same complex more experiments, such as 2D gel electrophoresis is required.

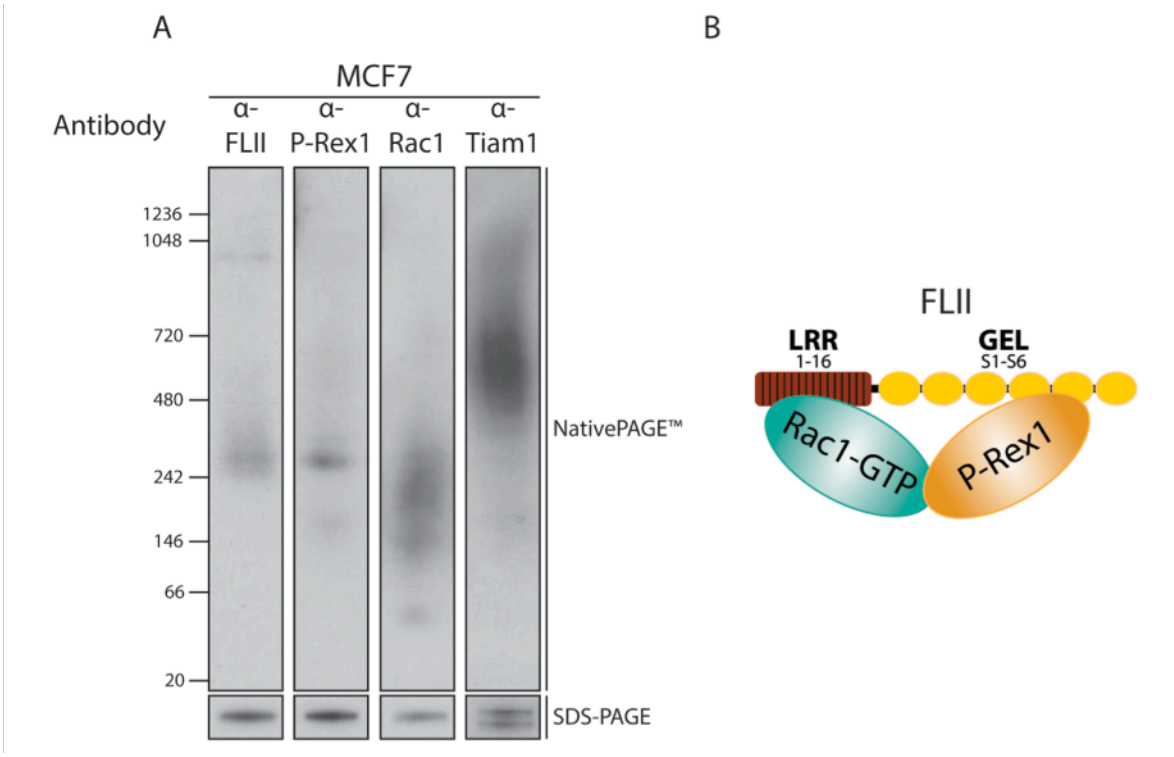

Figure 5.11: Analysis of P-Rex1, Rac1 and FLII Ternary Protein Complex under Denaturing Conditions in MCF7 Cells

(A) NativePAGE™ Bis-Tris gel system was used to analyse lysates from MCF7 cells prepared under non-denaturing conditions. Lysates were resolved on a NativePAGE™ Novex® 3–12% Bis-Tris gel and the ability of endogenous FLII, Rac1, P-Rex1 and Tiam1 to form protein complexes with each other was assessed by western blot analysis using anti-FLII, anti-Rac1, anti-P-Rex1 and anti Tiam1 antibodies, respectively. Western blot strips were aligned using the NativeMark™ Unstained Protein Standard. To ensure that the antibodies were detecting their respective proteins lysates were also run on a parallel SDS-PAGE™ GEL. Representative western blot from two independent experiments. (B) Schematic representation of potential P-Rex1-Rac1-FLII complex based on FLII domain interaction studies outlined in Figure 5.3 and 5.10.

5.2.2.4 Section Summary

Experiments outlined in this section were aimed at investigating the mechanism behind the P-Rex1-mediated Rac1-FLII interaction. Evidence presented demonstrates that FLII binds preferentially to P-Rex1 but not Tiam1. Moreover, through the use of FLII truncation mutants, P-Rex1 was shown to interact through the GEL domain of FLII and that this interaction is not dependent on the ability of P-Rex1 to activate Rac1. Together these findings support a P-Rex1 scaffolding role to bring Rac1 and FLII in close proximity to promote their interaction. It also stresses the importance of the P-Rex1 GEF function, since P-Rex1 GEF* expression does not induce Rac1-FLII binding, despite the ability of the mutant to bind to FLII.

5.2.3 Functional Characterisation of the P-Rex1-Rac1-FLII Interaction

Given the evidence described above, a series of experiments were conducted to try and explore the functional relevance behind the P-Rex1-Rac1-FLII interaction in the P-Rex1-mediated Rac1 signalling highlighted in Chapter 3.

5.2.3.1 Requirement of FLII in P-Rex1-Rac1 Mediated Cellular Migration

As indicated in Chapter 3, P-Rex1 activation of Rac1 was associated with distinct morphological and cellular phenotypes that promote cellular migration. Given the discrepancy in the literature outlined in section 1.5.2 regarding the role of Rac1 in regulating cellular migration and invasion, the identification of signalling pathways implicated in influencing the Rac1 effect on cellular motility is of utmost importance. This together with the evidence presented in the previous sections called for the investigation of the role that FLII plays in the P-Rex1-Rac1-mediated cellular migration.

The first indication that FLII is involved in the P-Rex1-Rac1-mediated cellular migration was from preliminary biochemical studies showing that the interaction between FLII and P-Rex1 and FLII and Rac1 was enhanced upon stimulation of cellular migration in cells. The interaction between endogenous P-Rex1 and endogenous FLII was investigated in stationary and migratory MCF7 cells as outlined in Figure 5.12 A. As shown in Figure 5.12 B there was a six-fold increase in the amount of FLII associated with immunoprecipitated endogenous P-Rex1 in migrating cells when compared to unstimulated cells.

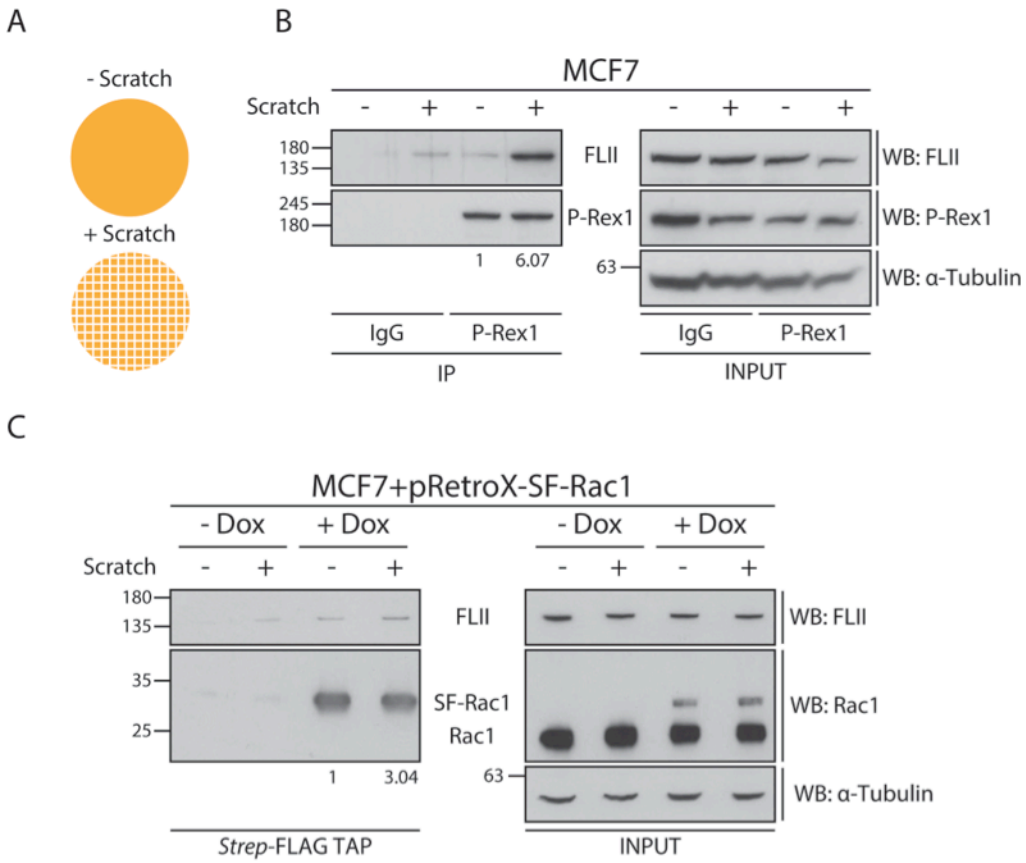

Figure 5.12: Cellular Migration Enhances the P-Rex1-FLII and SF-Rac1-FLII Interactions in MCF7 Cells
(A) Schematic representation of experimental setup. MCF7 cells were plated in a confluent monolayer for 24 hours. Cells were then either left untreated (- scratch) or were subjected to a series of horizontal and vertical scratches (+ scratch) to induce cellular migration. (B) Cells were harvested 24 hours post migration induction and endogenous P-Rex1 was immunoprecipitated from the respective lysates using anti-P-Rex1 antibody conjugated G Sepharose beads. Co-precipitated FLII was detected by western blot analysis using anti-FLII antibody. Rabbit IgG was used as a control for immunoprecipitation to determine non-specific binding to beads. α-Tubulin was used as a loading control. The difference in the ability of P-Rex1 to bind to FLII in response to migration stimulation was assessed using the Image J software to measure the integrated density of the FLII bands of the co-precipitated protein. After subtracting background binding to the beads these densities were then normalised to the amount of P-Rex1 immunoprecipitated as well as the normalised levels of FLII in the input. The normalised integrated density for this experiment is indicated below the figure. (C) MCF7 cells harbouring the doxycycline (dox) inducible SF-Rac1 expression system were treated with ethanol (- dox) or 1μg/ml dox (+ dox) for 24 hours prior to scratching as outlined in (A). Cells were harvested two hours post migration induction and SF-Rac1 was precipitated from the respective lysates using the *Strep*-FLAG Tandem Affinity Purification (TAP) technique. Co-precipitated FLII was detected by western blot analysis using anti-FLII antibody. Lysates from - dox treated cells were used as a control for the *Strep*-FLAG TAP to determine non-specific binding to beads. α-Tubulin was used as a loading control. The difference in the ability of SF-Rac1 to bind to FLII in response to migration stimulation was assessed as outlined above and is indicated below the figure.

An increase in the Rac1-FLII interaction levels was also observed in response to monolayer scratching of MCF7 cells harbouring the dox inducible SF-Rac1 expression system. In this experiment, cells were treated with either ethanol (- dox) or 1 μg/ml dox (+ dox) for 24 hours prior to -/+ scratching of confluent monolayers. Cells were then harvested two hours post migration induction and lysates were subjected to SF-TAP pulldown. Figure 5.12 C highlights the increase in the interaction between SF-Rac1 and endogenous FLII in migrating cells. Densitometric analysis indicated that stimulating cellular migration was associated with a three-fold increase in the amount of FLII bound to precipitated SF-Rac1.

The increase in P-Rex1-FLII and Rac1-FLII interactions even as early as two hours post monolayer scratching suggested that promotion of these interactions might be important for

the role of P-Rex1 and Rac1 in promoting cellular migration. To test this further, parental NIH3T3 and cells harbouring the dox inducible P-Rex1 WT expression system (NIH3T3+pRetroX-P-Rex1 WT) were transiently transfected with two different siRNAs (FLII siRNA1 and FLII siRNA2) to knockdown endogenous FLII. Cells were then treated with ethanol (- dox) or 1 μg/ml dox (+ dox) and the migration potential was assessed using the ORIS™ migration assay. As additional controls, cells treated with the transfection reagent alone (mock) or with a non-targeting siRNA (NT) were used to ensure that any observed changes in migration were due to FLII knockdown and not the transfection protocol. Additionally, prior to cell plating for the ORIS™ migration assay, a small portion of cells were lysed and the efficiency of FLII knockdown was assessed by Western blot analysis. As shown in Figure 5.13 A and B, Western blot analysis confirmed that treatment of cells with the two FLII targeting siRNAs but not with the transfection reagent or the non-targeting siRNA, reduced the level of endogenous FLII.

Fluorescence images from the same representative ORIS™ migration assay at 0 hours and 24 hours post stopper removal are shown in Figure 5.13 C for parental NIH3T3 cells and in Figure 5.13 D for P-Rex1 WT expressing cells. Interestingly, FLII depletion by siRNA in both – dox and + dox treated parental NIH3T3 cells was associated with a modest yet significant reduction in the ability of cells to migrate. Quantification of normalised average percent migration from three independent experiments indicated that in relation to – dox mock treated parental NIH3T3 cells, there was no significant difference in the migration potential of + dox mock ($p=0.43$), as well as - dox and + dox NT ($p=0.83$ and $p=0.99$, respectively) treated cells. In contrast, both FLII siRNA1 and FLII siRNA2 – dox and + dox treated cells exhibited a significant reduction in cellular migration compared to – dox mock treated parental NIH3T3 cells.

The effect of FLII knockdown on P-Rex1 induced cellular migration was also evaluated. As outlined in Figure 5.13 D and F, there was no significant difference between the rate of cellular migration observed in - dox mock and NT treated cells. Additionally, when compared to their parental NIH3T3 counterparts, variations observed in the migration rates in - dox mock and NT treated NIH3T3+pRetroX-P-Rex1 WT were not statistically significant. In contrast, P-Rex1 WT expression in response to dox treatment in both mock and NT treated cells resulted in a significant increase in cellular migration compared to their – dox counterparts by 16.7 % ($p=0.02$) and 19 % ($p=0.019$), respectively. As expected, when compared to the parental counterparts, P-Rex1 WT expression was also associated with a significant increase in migration by 23 % ($p=0.02$) in mock treated cells and 26 % ($p=0.013$) in NT treated cells. Interestingly, as observed with parental NIH3T3 cells, FLII siRNA1 and FLII siRNA2 – dox treated NIH3T3+pRetroX-P-Rex1 WT cells had a significantly reduced ability to migrate compared to – dox mock treated parental and NIH3T3+pRetroX-P-Rex1 WT cells. More importantly, in contrast to mock and NT + dox treated NIH3T3+pRetroX-P-Rex1 WT cells, P-Rex1 WT expression in FLII depleted cells was not associated with an increase in cellular migration. In contrast, knockdown of FLII using FLII siRNA1 and FLII siRNA2 in P-Rex1 WT expressing cells resulted in a significant

decrease in cellular migration by 15 % (p=0.01) and 10 % (p=0.02), respectively, when compared to the – dox mock treated cells and 32 % (p=0.002) and 34.5 % (p=0.004), respectively, when compared to + dox P-Rex1 WT expressing mock treated cells. Additionally, there was no significant difference in the migration observed between – dox and + dox cells treated with FLII siRNA1 (p=0.37) and FLII siRNA2 (p=0.40). This highlights the requirement of FLII in P-Rex1-Rac1-driven cellular migration.

The role of FLII in regulating cellular migration was also examined in NIH3T3 cells harbouring the dox inducible system for Tiam1 WT, Tiam1 GEF* and P-Rex1 GEF* (Figure A.2 in appendix section). Similar to parental NIH3T3 cells, FLII knockdown was associated with a modest yet significant reduction in cellular migration. Interestingly, though, the knockdown of FLII in Tiam1 WT expressing cells did not augment the Tiam1 WT associated reduced cellular migration. This suggests that the observed decrease in cellular migration associated with FLII depletion is not dependent on the role of FLII in regulating proliferation.

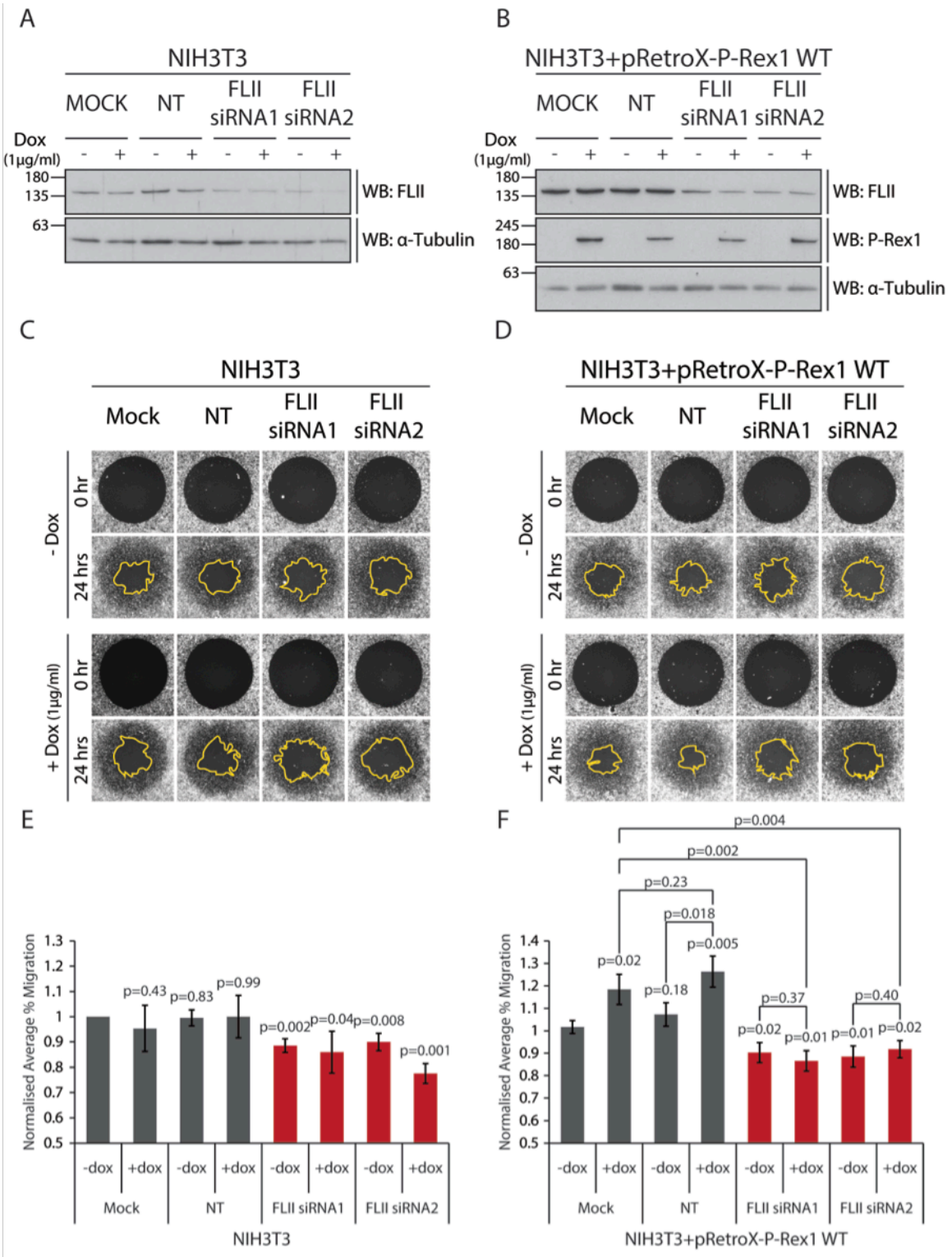

Figure 5.13: FLII is Required for the P-Rex1-Rac1 Driven Cellular Migration in NIH3T3 Cells

Parental and NIH3T3 cells harbouring the doxycycline (dox) inducible system for P-Rex1 wild type expression (NIH3T3+pRetroX-P-Rex1 WT) were treated with mock, non-targeting (NT) or two different siRNAs against FLII (FLLI siRNA1 and FLII siRNA2) for 48 hours. Cells were then re-transfected with the different siRNA constructs and treated with ethanol (- dox) or dox (+ dox) for 24 hours. (A, B) Levels of FLII knockdown were assessed by western blot analysis using anti-FLII antibody in parental (A) and NIH3T3+pRetroX-P-Rex1 WT (B) cells. α-Tubulin was used as a loading control. (C, D) The migration potential of parental (C) and NIH3T3+pRetroX-P-Rex1 WT (D) cells was assessed using the Oris™ Migration Assay. Florescence images were taken using the low light microscopy system (5x magnification) at 0 hours and 24 hours post stopper removal. (E, F) Quantification of cellular migration of – dox and + dox treated parental (E) or NIH3T3+pRetroX-P-Rex1 WT (F) cells normalised to parental - dox mock treated cells. Graphs represent the normalised average % migration ± standard error from three independent experiments. Student's t-test was used to assess significance between migration abilities within the different cells as indicated on the graph. p-values above each bar refer to significance values relative to NIH3T3+pRetroX-P-Rex1 WT - dox mock treated cells. Other values shown in (E) show significance values between indicated pairs. p-values ≤ 0.05 are considered significant; ≤0.01 are considered highly significant.

5.2.3.2 Mechanism of P-Rex1-Rac1-FLII-Mediated Cellular Migration

Results outlined in the previous subsection provided evidence that, not only does FLII bind to P-Rex1 and Rac1 in response to migration, but it is also essential for the P-Rex1-Rac1-mediated cellular migration. To further elucidate the role played by FLII in the P-Rex1-Rac1 signalling pathway it was therefore important to explore the mechanism by which FLII is required for the P-Rex1 associated enhanced cellular migration.

As highlighted in section 5.1.1.3 despite negatively regulating cellular migration, FLII was also shown to enhance cellular contraction in fibroblasts (Kopecki et al., 2011). Given the link between cellular contraction and cellular migration, together with the potential involvement of Rac1 in regulating levels of phosphorylated myosin II, it was hypothesised that P-Rex1 might be involved in promoting cellular contraction in a FLII-dependent manner. However, no reports to date have implicated P-Rex1 in cellular contraction, therefore, it was important to first establish whether P-Rex1 activation of Rac1 was associated with increased cellular contraction.

To explore this possibility, primary human fibroblasts were used to generate empty vector, Tiam1 WT or P-Rex1 WT expressing cell lines using the pRteroX-Tight-Pur retroviral system. Upon dox induction the ability of the different GEF expressing fibroblasts to contract collagen was examined using a collagen contraction assay. As shown in Figure 5.14 A, at 0 hours post -/+ dox treatment no contraction was observed in the collagen gels. Moreover, there was no difference in the size of – dox and + dox treated collagen gels, as well as between gels expressing either Tiam1 WT or P-Rex1 WT with all the discs have a similar surface area to that of the well they were incubated in. After 24 hours, however, as expected, collagen gel contraction was evident. With – dox treated cells the associated cellular contraction was similar across the different fibroblast pools. Additionally, as demonstrated in Figure 5.14 B, compared to the EV – dox treated control, there was no significant difference in the normalised average percent collagen gel contraction with Tiam1 WT – dox controls ($p=0.74$) or P-Rex1 WT – dox controls ($p=0.29$). Similarly, addition of dox to EV gels did not induce any significant changes in cellular contraction compared to the EV – dox treated control ($p=0.81$). Tiam1 WT expression, on the other hand, was associated with a decrease in cellular contraction by 14 %; however this was not statistically significant. In contrast, expression of P-Rex1 WT enhanced cellular contraction significantly by 17 % ($p=0.05$) as compared to the EV – dox treated discs and by 21.4 % ($p=0.04$) as compared to P-Rex1 WT – dox treated discs.

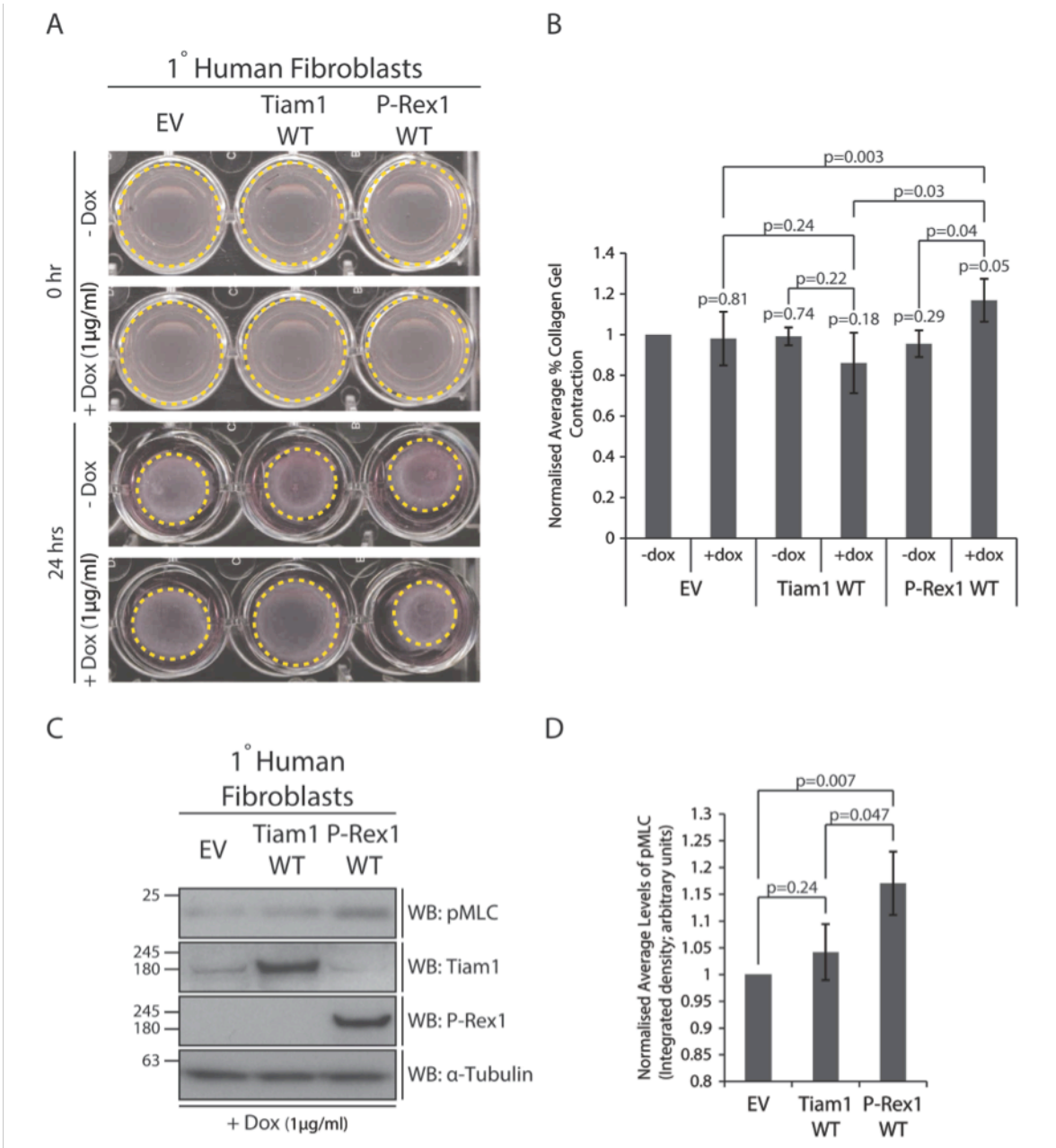

Figure 5.14: Ectopic expression of P-Rex1 Wild Type Induces Cellular Contraction in Primary Human Fibroblasts

(A) The ability of Tiam1 and P-Rex1 to influence cellular contraction was assessed using a collagen gel contraction assay. Primary (1°) human fibroblasts harbouring the doxycycline (dox) inducible system for the expression of empty vector (EV), Tiam1 WT or P-Rex1 WT were mixed with rat-tail collagen I in the absence (- dox) or presence of dox (+ dox) and left for 10 minutes to allow for collagen to set and form circular gel discs. Collagen gels were scanned using an EPSON PERFECTION 3200 PHOTO scanner at 0 hours and 24 hours post -/+ dox treatment. (B) The contraction of collagen gels was calculated as outlined in section 2.7.6. Graph shows the average % collagen gel contraction from three independent experiments normalised to the EV - dox treated cells. Error bars represent ± standard error. Student's t-test was used to assess statistical significance between collagen contraction within the different samples and p-value are indicated on the graph. Values above each bar represent p-value relative to EV – dox treated discs. (C) Biochemical analysis of cellular contraction was conducted on dox inducible 1° human fibroblasts by looking at the levels of phosphorylated myosin light chain (pMLC) 24 hours post dox induction. The levels of pMLC were assessed by western blot analysis using anti-pMLC antibody. The expression of Tiam1 WT or P-Rex1 WT was evaluated using anti-Tiam1 and anti-P-Rex1 antibodies, respectively. α-Tubulin was used as a loading control. Representative western blot from three independent experiments. (D) Levels of pMLC were quantified using Image J software to calculate the integrated density of pMLC bands in each sample. pMLC levels were then normalised to the α-Tubulin loading control. Graph shows the average levels of pMLC in each sample from three independent experiments normalised to the levels in the EV control. Error bars represent ± standard error. Student's t-test was used to assess statistical significance between pMLC levels changes within the different samples and p-value are indicated on the graph.

These observations were further confirmed by biochemical experiments that determined the effect of expressing Tiam1 WT or P-Rex1 WT on the levels of pMLC, a common marker for increased cellular contraction. Using Western blot analysis, lysates from dox treated primary human fibroblasts harbouring the EV, Tiam1 WT, P-Rex1 WT expression system, were evaluated. Consistent with the collagen gel contraction assay, as shown in Figure 5.14 C expression of P-Rex1 WT but not Tiam1 WT was associated with an increase in the levels of pMLC detected in cells relative to the EV control. To quantify this increase Image J software was used to measure the integrated density of the pMLC detected in each sample. Figure 5.14 D shows the normalised average pMLC levels detected in each sample from three independent experiments. Tiam1 WT expression did not induce any significant changes in the level of pMLC in cells relative to the basal level detected in the EV control cells ($p=0.24$). P-Rex1 WT expression, on the other hand, resulted in a highly significant increase in the levels of pMLC by 17 % ($p=0.007$) relative to the EV control. The P-Rex1-mediated pMLC increase was also significantly different compared to Tiam1 WT expressing cells ($p=0.047$). Taken together, these results indicate that P-Rex1 WT is indeed involved in regulating cellular contraction with increased expression of P-Rex1 WT inducing cellular contraction.

Given this newfound role of P-Rex1 in cellular contraction, it was intriguing to explore the role of FLII in P-Rex1-driven cellular contraction. This was done via examining the ability of P-Rex1 to promote cellular contraction, as indicated by pMLC levels, in FLII depleted cells. Primary human fibroblasts harbouring the EV, Tiam1 WT and P-Rex1 WT dox inducible expression systems were, therefore, either left untransfected or were transfected with a siRNA targeting human FLII. As shown in Figure 5.15, as expected in untransfected cells, expression of P-Rex1 WT but not Tiam1 WT resulted in a significant increase in the levels of detected pMLC relative to the EV control cells. Unlike P-Rex1 WT, Tiam1 WT expression, on the other hand, was not associated with a significant change in pMLC levels compared to the basal levels seen in EV cells. Interestingly, the knockdown of FLII in EV cells resulted in a 35 % ($p=0.02$) decrease in the levels of pMLC compared to the basal levels detected in the untransfected EV control. A similar decrease was seen in Tiam1 WT expressing cells transfected with the siRNA against FLII relative to the EV control (43 %, $p=0.02$) and relative to the Tiam1 WT untransfected counterpart (44 %, $p=0.02$). More importantly, a similar effect was seen upon FLII depletion in P-Rex1 WT expressing cells. P-Rex1 WT expression in the absence of FLII was associated with a 42 % ($p=0.005$) decrease in detected pMLC relative to the basal level seen in EV untransfected cells instead of the 29 % increase associated with P-Rex1 WT expression in untransfected cells. These findings indicate that the enhanced cellular contraction observed upon expression of P-Rex1 is mediated through FLII and that in the absence of FLII P-Rex1 is no longer able to stimulate cellular migration.

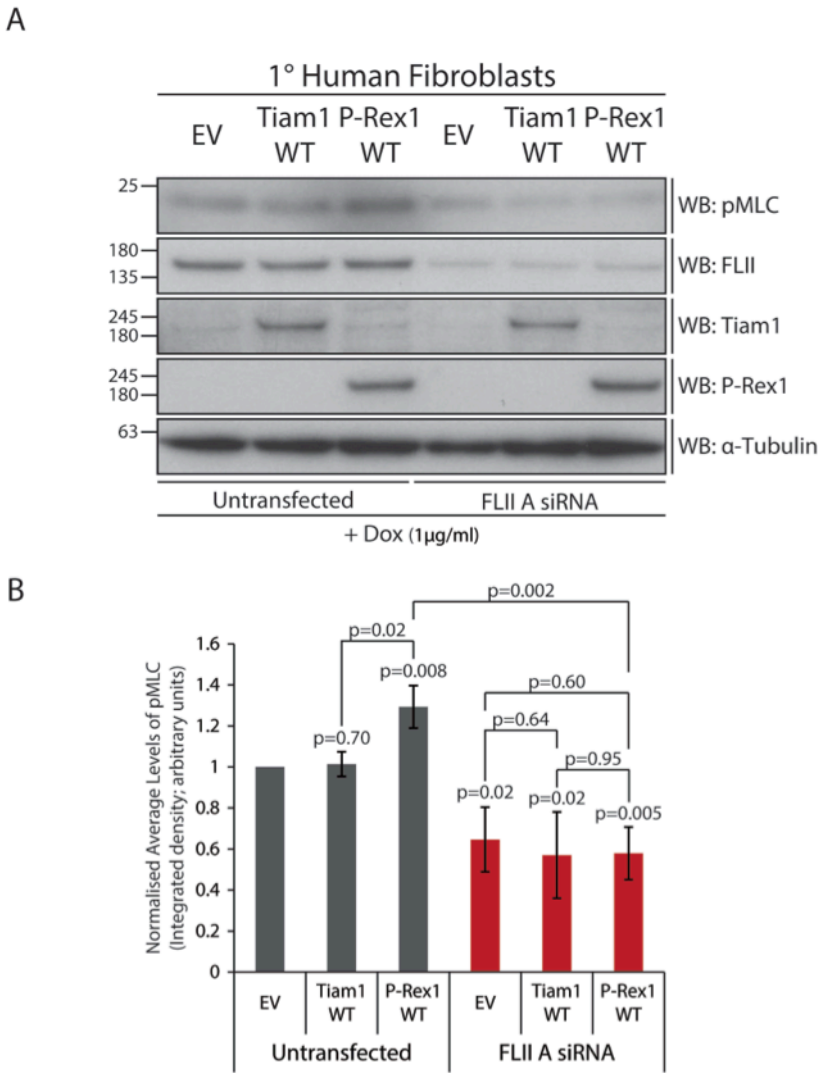

Figure 5.15: FLII is Required for Basal and P-Rex1-Driven Cellular Contraction in Primary Human Fibroblasts

(A) Primary (1°) human fibroblasts harbouring the doxycycline (dox) inducible system for the expression of empty vector (EV), Tiam1 WT or P-Rex1 WT were left untransfected or were treated with siRNA against human FLII (FLII A). After 24 hours post FLII knockdown expression of EV, Tiam1 WT or P-Rex1 was induced by adding dox for an additional 24 hours. Cells were then collected and biochemical analysis of cellular contraction was conducted by looking at the levels of phosphorylated myosin light chain (pMLC). The levels of pMLC were assessed by western blot analysis using anti-pMLC antibody. The efficiency of FLII knockdown was assessed using anti-FLII antibody and the expression of either Tiam1 WT or P-Rex1 WT was evaluated using anti-Tiam1 and anti-P-Rex1 antibodies, respectively. α-Tubulin was used as a loading control. Representative western blot from three independent experiments. (B) Levels of pMLC were quantified using Image J software to calculate the integrated density of pMLC bands in each sample. pMLC levels were then normalised to the α-Tubulin loading control. Graph shows the average levels of pMLC in each sample from three independent experiments normalised to the levels in the EV control. Error bars represent ± standard error. Student's t-test was used to assess statistical significance between the changes in pMLC levels within the different samples. p-values above each bar refer to significance values relative to EV untransfected cells. Other p-values shown represent significance values between indicated pairs. p-values ≤ 0.05 are considered significant; ≤0.01 are considered highly significant.

5.2.3.3 Section Summary

Experiments outlined in this section were aimed at exploring whether FLII is involved in P-Rex1-Rac1-mediated cellular effects with a particular focus on cellular migration. Results from this section demonstrate that there is an increased interaction between P-Rex1 and FLII as well as Rac1 and FLII in response to cellular migration, providing the first indication of the involvement of FLII in P-Rex1-Rac1-mediated cellular migration. The requirement of FLII for this

process was then confirmed by evaluating the ability of P-Rex1 WT to induce cellular migration in cells transfected with two different siRNAs against FLII. Interestingly, results from the ORIS^{TM} migration assay using these cells revealed that P-Rex1 WT expression did not enhance cellular migration in FLII depleted cells, whereas in mock and NT treated cells P-Rex1 WT expression, as observed previously, resulted in increased cellular migration. FLII knockdown was also associated with a modest decrease in cellular migration in parental NIH3T3. This demonstrates that under these conditions FLII is required for optimal cellular migration and highlights the dependency of P-Rex1 WT on FLII to promote cellular migration, supporting the hypothesis that P-Rex1 WT promotes Rac1-FLII binding to facilitate specific P-Rex1-Rac1-mediated effects. In particular, through the use of collagen gel contraction assay in conjunction with biochemical analysis, it was shown that P-Rex1 WT expression enhances cellular contraction. More importantly, FLII knockdown inhibited the P-Rex1 WT-mediated increase in cellular contraction, demonstrating the dependency of P-Rex1 on FLII to promote cellular contraction. Combined, experiments outlined in this section indicate that the interaction between FLII and Rac1 is mediated by P-Rex1 to direct certain cellular processes, such as cellular contraction, which ultimately translates into increased cellular migration.

5.3 Discussion

5.3.1.1 FLII is a Novel Rac1 Binding Partner

As highlighted earlier in section 5.1.1.2, the LRR domain of FLII is closely related to the LRR domain of the well-characterised Ras effector *S. cerevisiae* adenylyl cyclase (Claudianos and Campbell, 1995; Kido et al., 2002). Consistently, FLII was shown to interact interacts with Ras *in vitro*, particularly through the LRR domain (Goshima et al., 1999). It has also been demonstrated that FLII translocates from the nuclear and perinuclear regions to the cells' leading edge in motile cells, where it colocalises with other small GTPases at membrane ruffles (Davy et al., 2001). Additionally, functional characterisation of FLII also revealed that the role of FLII in regulating focal adhesion turnover is mediated through Rac1 signalling (Kopecki et al., 2011). Given this evidence it was not surprising that FLII was identified as a novel Rac1 binding partner from the proteomic analysis outlined in Chapter 4. However, despite the compelling evidence suggesting the involvement of FLII in small GTPases signalling there was no biochemical evidence supporting an interaction between Rac1 and FLII. In fact, in a study conducted by Goshima et al. the *C. elegans* FLII homologue was reported to interact with Ras but not with the small GTPases Rac1, RhoA, Cdc42 and RalA (Goshima et al., 1999). Despite this report, evidence presented in section 5.2.1.1 and 5.2.1.2 demonstrate that FLII is capable of interacting with Rac1 through its LRR domain under normal cellular conditions. This is consistent with the sequence homology of the LRR domain of FLII with other proteins that are known to bind Ras and other small GTPases (Claudianos and Campbell, 1995). It must be noted, however, that there is a possibility that FLII might be binding to Rac1 through an intermediate protein. Although, given the stringent nature of the SF-TAP technique it is more likely that FLII binds directly to Rac1. Nevertheless, future work will focus on examining this interaction in an *in vitro* setting using purified Rac1 and FLII proteins.

5.3.1.2 P-Rex1 Activation of Rac1 Promotes the Rac1-FLII Interaction

Proteomic analysis associated with the SILAC experiments outlined in Chapter 4 indicated that the ability of FLII to bind to Rac1 is enhanced upon activation of Rac1 by P-Rex1. Additionally, FLII was identified as a unique binding partner of Rac1 only upon expression of P-Rex1 WT in the conventional mass spectrometry experiments. These experiments already hinted at a novel role of P-Rex1 in regulating Rac1 signalling; however, due to the variation in the expression of P-Rex1 WT and GEF* in these experiments it was important to confirm these results by alternative methods. Indeed, using the duolink® In Situ PLA assay in NIH3T3 cells harbouring the dox inducible GEF expression system, in which WT and GEF* expression was shown to be even in Chapter 3, the FLII associated SILAC pattern was confirmed. Similar results were also seen in MCF7 cells on both the endogenous and exogenous levels. Importantly, despite their similar expression levels, P-Rex1 WT and not P-Rex1 GEF* was found to enhance

Rac1-FLII binding demonstrating the importance of Rac1 activation in FLII binding. Together results outlined in this chapter provide evidence supporting the role of P-Rex1 in mediating specific Rac1-effector complexes in cells.

5.3.1.3 P-Rex1 Promotes the Rac1-FLII Interaction Through Its Scaffolding Abilities

Various GEFs have been proposed to regulate GTPase signalling through serving as scaffolding proteins. Outlined in section 1.5.4.1 are examples of GEFs that have been reported to induce the interaction of Rac1 with specific effectors including Tiam1, and members of the PIX family of GEFs. Despite the accumulating evidence in the literature supporting the scaffolding role of GEFs in dictating GTPase signalling, there is no direct evidence showing that two different GEFs induce distinct effects, under the same cellular conditions, through their scaffolding abilities. Additionally, to date no study has suggested a scaffolding role for P-Rex1 in Rac1 signalling. It was therefore intriguing to investigate whether the P-Rex1-mediated Rac1-FLII interaction was due to its scaffolding ability.

Through a series of co-immunoprecipitation experimental results outlined in section 5.2.2.1 clearly demonstrate that FLII binds preferentially to P-Rex1 and not Tiam1. Confirming the interaction on an endogenous level also added more confidence that this is a true interaction. However, as is the case with the Rac1-FLII interaction, it is still important to establish whether the proteins are capable of binding directly to one another in an *in vitro* setting. Interestingly, though, both P-Rex1 WT and GEF* were capable of binding to FLII, suggesting that the P-Rex1-FLII interaction is not dependent on Rac1 activation. Moreover, through domain truncation mutants, P-Rex1 was found to interact to the GEL domain of FLII, whereas Rac1 binds to the LRR domain. This suggests that both P-Rex1 and Rac1 could potentially bind to FLII simultaneously supporting the hypothesis that P-Rex1 might function through bringing FLII in close proximity allowing active Rac1 to bind to the LRR domain of FLII and thus inducing specific downstream effects required to promote cellular migration. However in order to further support this hypothesis the preliminary evidence conducted on MCF7 lysates prepared under non-denaturing conditions, which suggest that P-Rex1, FLII and Rac1 might exist in one complex in cells need to be further validated. Moreover, additional experiments, such as 2D gel electrophoresis or far-Western blotting, are necessary to confirm the actual components of the complexes in which P-Rex1, Rac1 and FLII are detected in cells. This will also highlight any additional binding partners that might play a role in P-Rex1-Rac1 signalling.

The P-Rex1 GEL interaction was also quite interesting from another prospective as it is normally the LRR domain of FLII that is thought to promote protein-protein interactions while the GEL domain facilitates the actin regulation properties of FLII (Claudianos and Campbell, 1995). However, FLII has been shown to bind to several proteins, including the DRFs Daam1 and mDia1 through its GEL domain. This interaction has been shown to enhance the activation of

Daam1 and mDia1 and subsequently promote formin related actin assembly (Higashi et al., 2010). Given that P-Rex1 also binds to the GEL domain, this interaction might be an indication that FLII is involved in regulating the activity of P-Rex1 in cells, however additional experiments are required to assess if this is indeed the case. Defining the P-Rex1 domain to which FLII binds might also help in determining whether FLII is important in regulating P-Rex1 activity.

5.3.1.4 FLII is Required for P-Rex1-Mediated Cellular Signalling Implicated in Promoting Cellular Migration

Upon its discovery FLII was found to localise to membrane ruffles and lamellipodia at the leading edge of motile cells. It was also found to colocalise with Ras and small GTPases at these sites. Additionally, given its role in regulating actin dynamics, it was proposed that FLII is an important regulator of cellular migration (Davy et al., 2001). Further characterisation of FLII cellular functions identified it as a negative regulator of wound healing and cellular migration through its role in cellular proliferation and cellular adhesion (Adams et al., 2008; Cowin et al., 2007; Kopecki et al., 2009; Kopecki et al., 2011; Lin et al., 2011; Mohammad et al., 2012). However, given the role of FLII in regulating cellular contraction, it was proposed that under the conditions in which P-Rex1 is the primary GEF for Rac1 activation, the enhanced interaction between Rac1-FLII dictates a pro-migratory role of FLII in cells.

Consistent with the proposed hypothesis that FLII is important for the P-Rex1-Rac1-driven cellular migration, results outlined in section 5.2.3 demonstrate that indeed, FLII is required for the ability of P-Rex1 to promote cellular migration. Interestingly, FLII knockdown was also found to suppress cellular migration in parental NIH3T3 cells, suggesting that under the conditions examined FLII is required for optimal cellular migration. This clearly contradicts reports found in the literature regarding the role of FLII in cellular migration. This discrepancy might be due to differences in the experimental techniques involved in assessing cellular migration. In the highlighted reports the role of FLII in cellular migration was mainly assessed using *in vitro* wound healing assays and animal wounding in *in vivo* experiments, which is associated with the disruption of the ECM. FLII has been shown to regulate expression of important components of the ECM, such as collagen I and laminin. Moreover, it has been proposed that FLII can regulate ECM remodelling (Cowin et al., 2007; Kopecki et al., 2009). Therefore, in these studies, it could be that the role of FLII in ECM remodelling overrides its other cellular functions and therefore dictates a negative role of FLII in cellular migration. It would be therefore, interesting to examine whether using the ORIS^{TM} migration assay there is no disruption of the ECM and thus other cellular process that FLII regulate might be more important, such as its role in mediating cellular contraction.

Given the potential involvement of Rac1 in regulating cellular contraction indirectly through the role of PAK1 in the phosphorylation and localisation of myosin II B (Even-Faitelson et al., 2005), results from the collagen contraction assays are extremely promising. Firstly, they

revealed that P-Rex1 is involved in regulating cellular contraction. More importantly, these results also highlighted the requirement of FLII for P-Rex1-mediated cellular contraction. Consistently, P-Rex1 expression, but not Tiam1 was associated with increased pMLC that was also FLII dependent. Activation of myosin II through the phosphorylation of MLC has been directly implicated in cellular migration through its role in promoting stress fibre formation and focal adhesion assembly in the cell centre of migrating cells, which are important for the actomyosin contractility required for cellular movement. However, increased pMLC at the cell centre and rear is mediated through RhoA-ROCK signalling (Totsukawa et al., 2000), which is known to negatively regulate the activity of Rac1 (Leeuwen et al., 1997). However, work conducted by Matsumara et al., demonstrates that the presence of two pMLC pools in migrating cells, one at the leading edge near membrane ruffles and one at the cell rear towards the nucleus (Matsumura et al., 1998). Additionally, myosin II activity was shown to regulate contraction in the lamella, which is important for generating the force required for forward cellular movement (Giannone et al., 2007). Therefore, it is possible that the interaction of P-Rex1-Rac1-FLII induces increased levels pMLC at the leading edge. This is consistent with both FLII and Rac1 localising at the leading edge of cells in migrating cells (Davy et al., 2001; Machacek et al., 2009). Examining the localisation of pMLC upon expression of P-Rex1 in migrating cells, might help determine the pool that P-Rex1-Rac1-FLII are regulating in cells to promote migration. Additionally, it would be interesting to examine if MLCK is also involved in the P-Rex1-Rac1-FLII induced cellular migration, since MLC phosphorylation at the leading edge is mediated through the activity of MLCK (Totsukawa et al., 2000). Thus it could be that FLII is important in activating MLCK, which in turn phosphorylates MLC and promotes contraction at the leading edge. It would be interesting to examine the ability of MLCK to phosphorylate MLC in FLII depleted cells, as well as to examine the ability of FLII to bind to MLCK or MLC.

In addition to its role in regulating cellular contraction FLII has also been reported to regulate the activity of Daam1 and mDia1, both of which are regulated by small GTPases and are involved in cellular migration. Interestingly, mDia1 is a Rho effector, however it has been linked to Rac1 activation and membrane ruffle formation and is implicated in focal adhesion remodelling and migration of cancer cells (Narumiya et al., 2009). Formins have also known to regulate filopodia formation, structures that motile cells use to sense their environment (Machaidze et al., 2010). Therefore, FLII binding to Rac1 could also be important in enhancing DRF activity to promote cellular migration. It would be informative to look at the ability of FLII to bind to and activate DRFs, such as mDia1 and Daam1, in response to P-Rex1 expression or deletion. Additionally, it is also vital to further dissect the amino acids in the LRR and the GEL domain that are important for mediating the Rac1 and P-Rex1 interactions, respectively. This will allow the generation of mutants that have impaired Rac1 and P-Rex1 binding, which could then be used to further assess the role of this interaction on the P-Rex1-Rac1-mediated cellular migration.

5.4 Conclusions

Results outlined in this chapter highlight a novel P-Rex1-mediated signalling pathway implicated in promoting cellular migration. This pathway involves the novel Rac1 and P-Rex1 binding partner FLII. Through this previously unreported ability of P-Rex1 to bind to FLII, P-Rex1 enhances the otherwise minimal Rac1-FLII interaction in cells, firstly via bringing the two proteins in close proximity and secondly through activating Rac1 to allow the interaction to occur. Interestingly, FLII was found to promote cellular migration in parental and P-Rex1 WT expressing NIH3T3 cells, demonstrating the importance of FLII for optimal cellular migration in these cells, but more importantly highlighting the dependency of P-Rex1 on FLII for promoting the Rac1-driven cellular migration. Further characterisation of the functional role of FLII revealed that FLII through an unknown mechanism that involves the phosphorylation of MLC is required for the P-Rex1-mediated cellular contraction to occur, which in turn could explain the dependency of P-Rex1 on FLII for promoting cellular migration through Rac1. Figure 5.16 represents a schematic representation of a working model depicting a potential mechanism for the P-Rex1-Rac1-FLII-mediated cellular migration.

In the proposed model activation of Rac1 by P-Rex1 promotes the binding of FLII to Rac1 through the LRR domain of FLII. This interaction is potentially mediated via the ability of P-Rex1 to bind to FLII coupled with its ability to activate Rac1, thus exposing the LRR domain of FLII to the activated proteins and enhancing this interaction. In turn, through FLII, P-Rex1 and Rac1 are able to increase the phosphorylation of MLC, which enhances cellular contraction, ultimately resulting in an increased ability of cells to migrate.

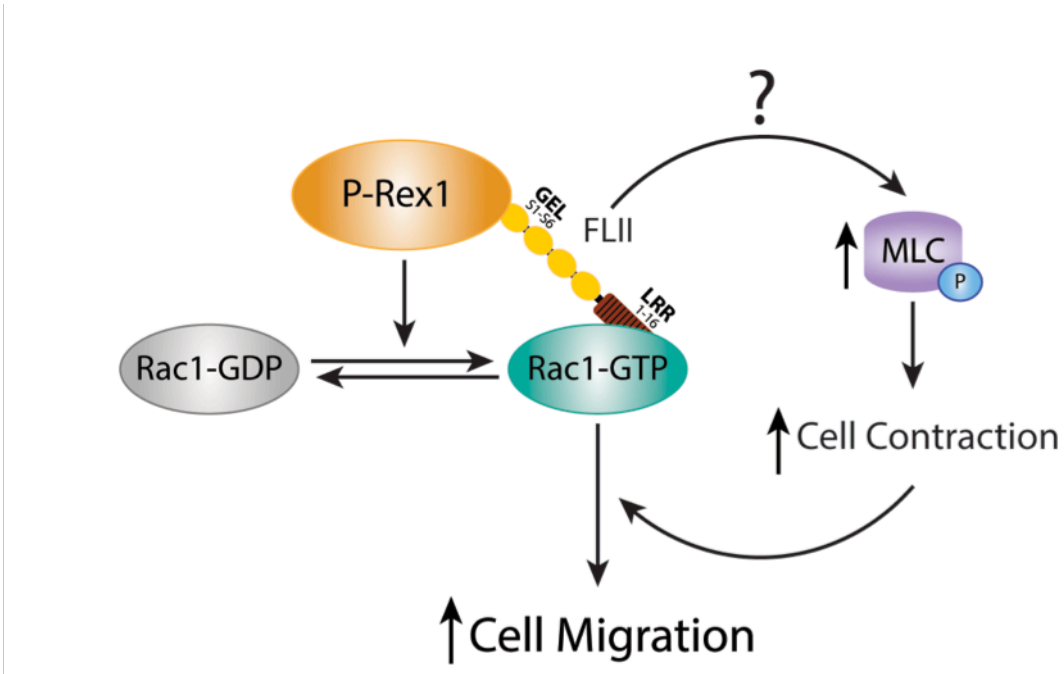

Figure 5.16: Schematic Representation of P-Rex1-Driven Cellular Migration Through Active Rac1 and FLII

Activation of Rac1 by P-Rex1 results in Rac1 binding to a set of downstream effectors, including FLII. Via its scaffolding ability, P-Rex1 binds to FLII and brings it in close proximity to active Rac1 thus promoting the Rac1-FLII binding. Through FLII, P-Rex1 and Rac1 are then able to increase the levels of pMLC, which is reflected in increased cellular contraction. This increase is then able to mediate cellular movement and as a result cells acquire a more migratory phenotype. GEL=Gelsolin-like domain; LRR=Leucine Rich Repeat domain; P=Phosphorylation

Chapter 6 : General Discussion and Future Directions

Rac1 is involved in various cellular processes that are important for normal cellular functioning and are also implicated in cancer initiation and progression (Etienne-Manneville and Hall, 2002; Mack et al., 2011; Sahai and Marshall, 2002). Although representing an important regulator of carcinogenesis, activation of Rac1 and the associated downstream signalling cascades are still poorly understood due to their diversity and complexity (Jaffe and Hall, 2005; Mack et al., 2011). Identifying such mechanisms can assist in elucidating the controversial role of Rac1 in mediating cellular signalling. To date various factors have been implicated in influencing Rac1 downstream signalling, including the cell type in which Rac1 is activated, the localisation of active Rac1 and substrate specificity that dictates signalling from the ECM (Etienne-Manneville and Hall, 2002; Sander et al., 1998). However, this project is focused on identifying key regulators of Rac1 signalling that could dictate cellular functions downstream of Rac1 in spite of extracellular signalling, particularly to try and gain a better understanding of the signalling pathways directly downstream of Rac1 that are involved in either inhibiting or promoting cellular migration and invasion.

6.1 The Role of GEFs in Dictating Rac1 Downstream Effects

Results outlined in this thesis provide clear evidence for the role of Tiam1 and P-Rex1 in dictating Rac1 signalling. Through the use of a controlled cellular system in which GEF expression was the only variable, it was shown that expression of Tiam1 and P-Rex1 induces distinct cellular phenotypes in three different cell lines. Additionally, via assessing the role of GEF* mutants of both proteins, these effects are found to be directly linked to their ability to activate Rac1, thus demonstrating that Tiam1 and P-Rex1 dictate Rac1 downstream effects. Through quantitative proteomics, Tiam1 and P-Rex1 were also found to influence the Rac1 interactome. Consistent with these observations, Tiam1 is reported to serve as a scaffolding protein thus promoting Rac1 binding to IB2/JIP2 to selectively trigger the MKK3 and P38 signalling cascade over the JNK signalling cascade, as well as spinophilin to induce the activation of p70 S6 kinase over PAK (Buchsbaum et al., 2002, 2003). These findings together with supporting evidence from the literature strongly indicate that Tiam1 and P-Rex1 influence Rac1 signalling firstly through activating Rac1 and secondly through influencing its ability to bind to specific downstream effectors. Interestingly, results from the quantitative proteomic screen also suggest that Tiam1 and P-Rex1 function mainly through altering the Rac1 binding ability of proteins that interact with Rac1 under normal cellular conditions. This potentially implicates GEFs, not only in influencing Rac1 binding, but also in the spatiotemporal regulation of Rac1 effectors. However, additional experiments are required to determine if the latter proposed function is true.

6.1.1 Tiam1 Differential Regulation of Rac1 Signalling

Results also demonstrate that Tiam1 activation of Rac1 stimulates cellular aggregation and enhances cell-cell contacts. In MDCKII and A431 cells Tiam1 is also shown to impede HGF/EGF-induced cellular scattering. This is in agreement with the reported role of Tiam1 in reducing HGF-induced cellular scattering in MDCKII cells via enhancing E-cadherin-mediated cell-cell contacts (Hordijk et al., 1997). Results obtained from the NIH3T3 GEF expression system are of particular interest. NIH3T3 cells are mesenchymal in nature and form very weak cell-cell contacts, thus it is intriguing to see that expression of Tiam1 in these cells induced an epithelial-like morphology and is associated with reduced migration. A similar phenotypic switch is seen in metastatic melanoma cells, in which Tiam1 is shown to impede cellular migration through regulating the actin cytoskeleton to promote cell-cell contacts and induce an epithelial-like morphology (Uhlenbrock et al., 2004). Together these results suggest that Tiam1 activation of Rac1, in the absence of external stimuli, is associated with reduced cellular migration potentially through its ability to increase actin and cadherin deposition at cell-cell contacts.

Interestingly, members of the IQGAP family, namely IQGAP1 and IQGAP3 exhibited increased Rac1 binding upon expression of Tiam1. IQGAP1, similar to Rac1 signalling, is implicated in mediating the assembly and disassembly of cell-cell contacts. Therefore, it could be argued that under the cellular conditions tested, IQGAP1 plays an important role in mediating cell-cell contacts. Further analysis of the Rac1-IQGAP1 interaction is therefore needed to determine the functional significance of this Tiam1-mediated interaction.

6.1.2 P-Rex1 Differential Regulation of Rac1 Signalling

In contrast to Tiam1, P-Rex1 activation of Rac1 promotes the dissociation of cells from one another, which was more visually clear in the epithelial MDCKII and A431 cell lines. P-Rex1 has a well-established role in promoting cellular migration as detailed in section 1.6.2.1. Thus it is reassuring to see that in all cell lines P-Rex1 activation of Rac1 promotes cellular migration and cellular scattering. Results from scattering experiments conducted in MDCKII and A431 cells suggest that similar to Tiam1, P-Rex1 might be regulating cell-cell contacts to mediate the observed cellular phenotypes. Additionally, P-Rex1 expressing cells are associated with the formation of thin extended membrane protrusions. Rac1 has been shown to contribute to lamellipodia formation through activating the Arp2/3 protein complex (Miki et al., 2000). Thus, P-Rex1 might also be utilising this machinery to promote migration. Consistent with this notion, four subunits of the Arp2/3 protein complex, namely the Arpc1b, Arpc 2, Arpc3 and Arp3, were identified as increased Rac1 binding partners under P-Rex1 WT but not P-Rex1 GEF* in a single SILAC experiment (highlighted in Table S.4). More interestingly, these components show decreased Rac1 binding upon expression of Tiam1 WT. Therefore, although they are only identified in one experiment it would be interesting to further examine whether P-Rex1

enhances cellular migration through promoting Rac1 interaction to the Arp2/3 protein complex and whether this is important in the activation of the complex to stimulate the formation of the branched actin filaments necessary for the P-Rex1-mediated membrane protrusions.

6.1.2.1 P-Rex1-Rac1-FLII Signalling Cascade

Through the analysis of changes in the Rac1 interactome induced by Tiam1 and P-Rex1, FLII was identified as a novel Rac1 binding partner that shows increased interaction with Rac1 upon expression of P-Rex1. This finding was initially surprising, given that FLII is an important negative regulator of wound healing (Adams et al., 2008; Cowin et al., 2007; Jackson et al., 2012). However, further analysis of the Rac1-FLII interaction helped uncover a novel role of FLII in regulating cellular migration. Through its ability to regulate cellular contraction, FLII is able to promote P-Rex1-Rac1-mediated cellular migration, thus identifying a new signalling pathway that is involved in promoting cellular migration upon Rac1 activation. Results outlined thus far demonstrate a dependency of P-Rex1-Rac1 signalling on FLII to promote migration. It would be interesting to investigate whether this dependency is reciprocal, by examining the ability of FLII to promote cellular contraction in P-Rex1 or Rac1 depleted cells.

Future work will focus on further identifying components of this pathway to determine the mechanism by which FLII is able to regulate the levels of pMLC and influence contraction. Expression of P-Rex1 was also found to mediate the interaction between FLII and TMOD3. Although TMOD3 has been shown to reduce cellular migration (Fischer et al., 2003), it is also known to interact with tropomysoin (Weber et al., 1994). This could thus be the potential link between FLII and increased MLC phosphorylation, since tropomysoin is implicated in regulating cellular contraction through its ability to bind to myosin, among other proteins (El-Mezgueldi, 2014). It is, therefore important to explore the implications of this interaction further. Moreover, to identify additional components involved in this pathway it might be useful to conduct a proteomic screen with FLII as the bait protein in cells with differential P-Rex1 expression levels. This could help identify overlapping proteins identified in both Rac1 and FLII interactomes that could play a role in the signalling cascade described in chapter 5.

6.2 Implications in Cancer Progression

Results presented in this thesis highlight a novel role of Tiam1 and P-Rex1 in manipulating Rac1 signalling to either reduce or promote cellular migration, respectively. Upregulation of P-Rex1 has been implicated in promoting metastasis in prostate cancer as well as in melanoma (Lindsay et al., 2011; Qin et al., 2009). Additionally, P-Rex1 has also been identified as an important mediator of ErbB receptor signalling, which promotes Rac1-driven migration and proliferation in breast cancer (Sosa et al., 2010). Moreover, high P-Rex1 expression has been associated with poor patient outcome in breast cancer (Montero et al.,

2011). Given the observed P-Rex1 cellular effects using the dox inducible system outlined in this study, it could be argued that this mimics the upregulation observed in cancer. The P-Rex1-associated phenotype observed in A431 cells further supports this idea. Therefore, in order to better understand the signalling cascade associated with P-Rex1 upregulation in cancer, it is imperative to utilise the A431 system to examine the differential regulation of Rac1 *in vivo*. Future work will focus on establishing xenograft models in both zebrafish and in mice using A431 cells as well as melanoma and prostate cancer cell lines to examine whether the differential Rac1-driven effects observed with Tiam1 and P-Rex1 *in vitro* are also reproducible *in vivo*. Additionally, this will be combined with FLII depletion to verify if P-Rex1-Rac1-FLII signalling plays a role in tumour progression. It would also be interesting to utilise the already existing FLII heterozygous and transgenic mouse models combined with P-Rex1 overexpression to explore the role of FLII in mediating P-Rex1-Rac1-driven cellular migration *in vivo*. Together these experiments will help link work presented in this thesis with the role of Rac1 in cancer metastasis allowing for a better understanding of the role of Rac1 in this process. Additionally, it will provide insight as to whether FLII could present a good candidate for drug targeting to help minimise cancer metastasis in tumours with P-Rex1 upregulation.

6.3 Conclusions

Work presented in this thesis identifies Tiam1 and P-Rex1 as important nodes in Rac1 signalling. Through their ability to influence the composition of the Rac1 interactome, they dictate Rac1 cellular effects, including cellular migration. Given this role, they help decipher a very complex and tightly regulated cellular process that is implicated not only in cancer progression but also in fundamental processes that involve normal cells, such as migration of cells during embryonic development and also upon wounding (Lauffenburger and Horwitz, 1996). In addition to FLII, other proteins identified from the quantitative proteomic screen, if studied further, could also provide useful insights into Rac1 signalling in cellular migration and cancer metastasis.

Based on work presented in this thesis together with evidence from the literature a model was proposed for how Tiam1 and P-Rex1 regulate Rac1 signalling in cells. As shown in Figure 6.1 Tiam1 and P-Rex1, similar to other GEFs, increase levels of active Rac1 in cells by facilitating the exchange of GDP with GTP. In addition, Tiam1 and P-Rex1 can differentially direct Rac1 signalling through modulating the Rac1 interactome. They can then either promote the formation of unique Rac1-protein interactions, or differentially regulate the Rac1 binding ability of proteins that interact with Rac1 under normal conditions, potentially through serving as scaffolding proteins. This in turn induces distinct signalling cascades that are implicated in inhibiting cellular migration in the case of Tiam1 or promoting cellular migration in the case of P-Rex1.

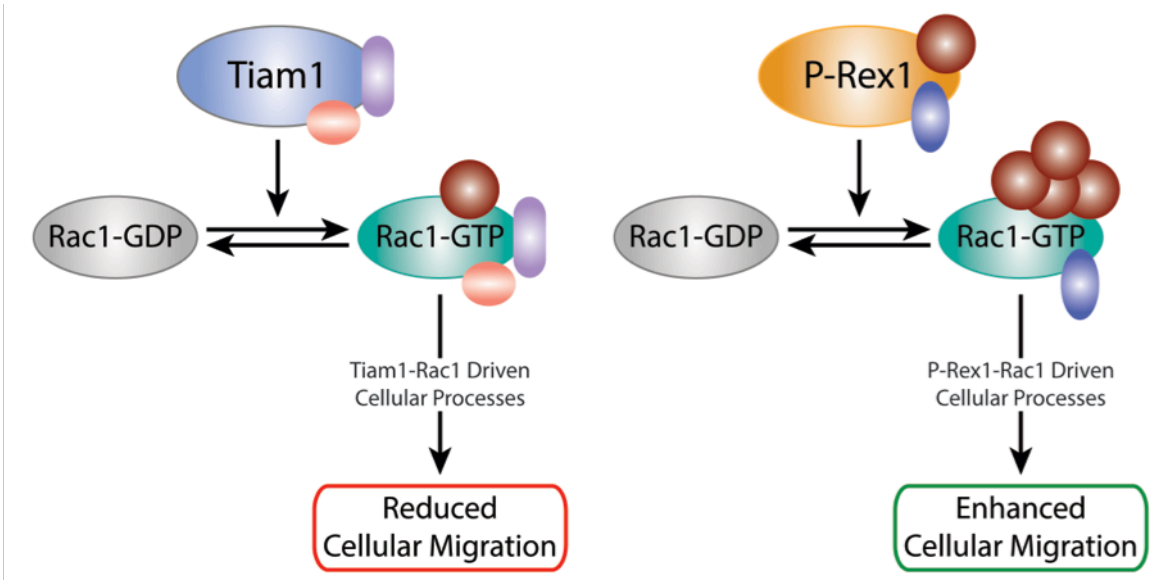

Figure 6.1: Schematic Representation of GEF-Induced Rac1 Downstream Effects Model
Tiam1 and P-Rex1 activate Rac1 by facilitating the exchange of GDP with GTP. Active Rac1 is then able to bind to downstream effectors and thereby elicit various downstream cellular functions. In addition to acting as Rac1 activators, Tiam1 and P-Rex1 can serve as scaffolding proteins bringing certain Rac1 effectors in close proximity to activated Rac1. As a result, activation of Rac1 by either GEF mediates the formation of a number of unique Rac1-protein complexes as well as altered association levels of commonly bound Rac1 interactors. In this model activation of Rac1 by Tiam1 results in Rac1 binding to a set of downstream effectors, which induce a series of cellular changes that lead to an inhibitory migratory effect. P-Rex1 activation of Rac1, on the other hand, results in Rac1 binding to a different set of effectors involved in enhancing cellular migration.

Appendix

Table A.1 list of Unique Rac1 Binding Partners Upon Expression of Tiam1 WT and P-Rex1 WT Indentified From Mass Spectrometry Experiments: BR1

Tiam1 WT	P-Rex1 WT
1700018F24Rik protein	40S ribosomal protein SA
26S protease regulatory subunit 4	Anoctamin-1
26S proteasome non-ATPase regulatory subunit 14	Beta-actin-like protein 2
Armadillo repeat containing, X-linked 4	C2 domain-containing protein 3
BC002199 protein	DENN domain-containing protein 2C
cDNA sequence BC031441	Dock10 protein
Complement decay-accelerating factor, GPI-anchored	GTP-binding protein Rhes
Elongation factor 1-delta	Kelch-like protein 23
Fd	Klra19 protein
FERM and PDZ domain-containing protein 4	MHC I-like leukocyte 2
FERM domain containing 5	Nebulin
Glyceraldehyde-3-phosphate dehydrogenase, testis-specific	O-phosphoseryl-tRNA(Sec) selenium transferase
Histone deacetylase 2	Olfactory receptor 958
IgE-binding protein	Phosphatidylinositol-3,4,5-trisphosphate 5-phosphatase 1
Insulin receptor substrate 1	Protein regulator of cytokinesis 1
Interleukin 15 receptor alpha chain	R3H domain-containing protein 2
Lysyl oxidase homolog 4	Receptor-type tyrosine-protein phosphatase beta
Mas-related G-protein coupled receptor member A8	Schlafen 10
Mediator complex subunit 24	Tubulin, beta 2B
Metastasis-associated protein MTA2	Ubiquitin carboxyl-terminal hydrolase Yap1 protein
Monoglyceride lipase	
Natural cytotoxicity triggering receptor 1	
Novel preferentially expressed antigen in melanoma (Prame) protein	
Odorant receptor S50	
p21 (CDKN1A)-activated kinase 7	

PAB-dependent poly(A)-specific ribonuclease subunit 2	
Poly(rC)-binding protein 3	
Prolow-density lipoprotein receptor-related protein 1	
Protease (Prosome, macropain) 26S subunit, ATPase 5	
Proteasome (Prosome, macropain) 26S subunit ATPase 3	
Protein C20orf103	
Protein Daple	
Protein ERGIC-53-like	
Protein numb homolog	
Protein phosphatase 1A	
Protein QN1 homolog	
Protocadherin Fat 3	
Psmc6 protein	
Putative ribosomal RNA methyltransferase NOP2	
Recombination-activating gene 1	
Rho-associated protein kinase 2	
Septin-4	
T-complex protein 1 subunit alpha B	
Transcription factor jun-B	
Transglutaminase 3, E polypeptide	
Translocon-associated protein subunit alpha	
Ubiquitin carboxyl-terminal hydrolase	
Ubiquitin-associated protein 1	
Vascular endothelial growth factor receptor 3	
WD repeat domain 81	
WD repeat-containing protein 7	
Zinc finger protein 503	

Table A.2 list of Unique Rac1 Binding Partners Upon Expression of Tiam1 WT and P-Rex1 WT Indentified From Mass Spectrometry Experiments: BR2

Tiam1 WT	P-Rex1 WT
2610507B11Rik protein	4933409K07Rik protein
5-hydroxytryptamine receptor 7	Alpha-1-antitrypsin 1-6
Acyl-CoA dehydrogenase family member 11	Anaphase promoting complex subunit 2
Apoptosis-inducing factor 3	Ankrd13a protein
Arf-GAP with SH3 domain, ANK repeat and PH domain-containing protein 2	ATP-binding cassette, sub-family B (MDR/TAP), member 7
Aspartyl aminopeptidase	Brca1
Calsequestrin-1	Cancer susceptibility candidate 5
Cell division cycle protein 27 homolog	Citrate lyase subunit beta-like protein, mitochondrial
Clathrin heavy chain 1	Eukaryotic translation initiation factor 4 gamma 1
Copine VIII	Fibronectin
Cullin-associated NEDD8-dissociated protein 1	G protein-coupled receptor 64
D630002G06Rik protein	Gasdermin-D
DnaJ homolog subfamily A member 2	Heparan sulfate (Glucosamine) 3-O-sulfotransferase 6
Engulfment and cell motility protein 1	Hyaluronidase-4
Fam179b protein	Junction plakoglobin
Fragilis	KH domain-containing, RNA-binding, signal transduction-associated protein 1
Insulin receptor-related protein	Kinetochore-associated protein KNL-2 homolog
Kank1 protein	Left-right dynein
Limkain-b1	Ly9
M-phase inducer phosphatase 1	Methyl-CpG binding domain protein 5
Microtubule-associated protein 4	Microtubule-associated protein RP/EB family member 1
Multiple PDZ domain protein	Myosin-10
Myosin-7B	Novel KRAB box and zinc finger, C2H2 type domain containing protein
Nuclear autoantigenic sperm protein	Nucleolysin TIAR
Nuclear receptor coactivator 5	Nucleoside diphosphate-linked moiety X motif 19, mitochondrial
Olfactory receptor Olfr714	Olfactory receptor 353

Origin recognition complex subunit 3-like (S. cerevisiae)	Olfr703 protein
Pard3 protein	Phosphatase and actin regulator 3
Protein Hook homolog 3	Plasma serine protease inhibitor
Protein kinase N3	Procollagen-lysine,2-oxoglutarate 5-dioxygenase 2
Putative skeletal muscle ryanodine receptor	Protein ARMCX6
Rootletin	Protein flightless-1 homolog
Scm-like with four MBT domains protein 1	Rab proteins geranylgeranyltransferase component A 1
Septin-11	Regulation of nuclear pre-mRNA domain-containing protein 2
Serpin H1	Seryl-tRNA synthetase, cytoplasmic
Small ubiquitin-related modifier 2	Synaptic vesicle glycoprotein 2B
Tankyrase 1 binding protein 1	Titin
Telomeric repeat-binding factor 2-interacting protein 1	Transcription factor AP-2 delta
Thiosulfate sulfurtransferase	Transcription intermediary factor 1-alpha
URB2 ribosome biogenesis 2 homolog (S. cerevisiae)	Transient receptor potential cation channel subfamily M member 8
WD repeat domain 81	Ubiquitin carboxyl-terminal hydrolase
	UTP14, U3 small nucleolar ribonucleoprotein, homolog B (Yeast)
	Ventral anterior homeobox 1

Table A.3 list of Unique Rac1 Binding Partners Upon Expression of Tiam1 WT and P-Rex1 WT Indentified From Mass Spectrometry Experiments: BR3

Tiam1 WT	P-Rex1 WT
1-acyl-sn-glycerol-3-phosphate acyltransferase alpha	6-phosphofructo-2-kinase/fructose-2, 6-biphosphatase 2, isoform CRA_a
28S ribosomal protein S21, mitochondrial	Activating transcription factor 7-interacting protein 2
Aldehyde oxidase	Adenylosuccinate synthetase isozyme 1
Anoctamin-6	Alpha-1-antitrypsin 1-6
ATP synthase subunit alpha, mitochondrial	Ankyrin repeat domain 6
ATP-binding cassette protein	AP-2 complex subunit beta
ATPase, class II, type 9A	ATP-dependent RNA helicase DDX3X
Basic leucine zipper and W2 domain-containing protein 2	Autophagy-related protein 101
Beta-globin	Cleavage stimulation factor, 3' pre-RNA, subunit 3
Calcium/calmodulin-dependent protein kinase type II beta chain	Col1a1 protein
Calnexin	COP9 signalosome complex subunit 7a
Carcinoembryonic antigen-related cell adhesion molecule 5	Coronin-7
Centrosomal protein of 290 kDa	Cryptochrome-1
Chymase 2	Cytokine-dependent hematopoietic cell linker
Ciliary rootlet coiled-coil, rootletin	Family with sequence similarity 171, member A1
Coiled-coil domain containing 73	Granzyme E
Cullin-associated NEDD8-dissociated protein 1	Harmonin
Cullin-associated NEDD8-dissociated protein 2	Heat shock protein 105 kDa
Cyclin G-associated kinase	Heterogeneous nuclear ribonucleoprotein M
Cysteine and tyrosine-rich protein 1	Inosine-5'-monophosphate dehydrogenase 1
Dynamin-binding protein	Integrin alpha-2
Enpp3 protein	Isoleucine-tRNA synthetase
Ephrin receptor	Kelch repeat and BTB domain-containing protein 5
Eukaryotic translation initiation factor 3 subunit E	Kif20b protein
Exocyst complex component 1	Kinesin-1 heavy chain
Exocyst complex component 4	Kinesin-like protein KIFC2

GCN1 general control of amino-acid synthesis 1-like 1 (Yeast)	Leucine-rich repeat-containing G protein-coupled receptor 4
Genetic suppressor element 1	LIM homeobox protein 3
Glycogen [starch] synthase, muscle	Lutropin-choriogonadotropic hormone receptor
GTP-binding protein GUF1 homolog	MCG6542, isoform CRA_f
Heterogeneous nuclear ribonucleoprotein U	Methionine synthase
Hydroxymethylglutaryl-CoA synthase, mitochondrial	Microtubule-associated protein 1B
Integrin-linked protein kinase	Myosin binding protein C, cardiac
Kelch-like protein 35	Nub1 protein
Malignant fibrous histiocytoma-amplified sequence 1 homolog	Nuclear autoantigenic sperm protein
Mc5 VLCL	Odorant receptor S19
Melanophilin	OTTMUSG00000018782 protein
Methionyl-tRNA synthetase, cytoplasmic	Phosphatidylinositol 3,4,5-trisphosphate-dependent Rac exchanger 1 protein
Microtubule-associated protein 4	Phosphoinositide-3-kinase, regulatory subunit 5, p101
Mitochondrial folate transporter/carrier	Pre-mRNA-processing-splicing factor 8
Multifunctional protein ADE2	Protein flightless-1 homolog
Myosin heavy chain	Protocadherin Fat 3
Nebulin	Ribosomal protein L14
Nucleophosmin	RNA polymerase 1-2
Olfactomedin 2	Serine/threonine-protein phosphatase 6 regulatory ankyrin repeat subunit B
Olfactory receptor 353	Snrk protein
Olfactory receptor Olfr213	Sulfated glycoprotein 1
Oxygen-regulated protein 1	SUMO-1-specific protease
Pentatricopeptide repeat-containing protein 3, mitochondrial	Synaptic vesicle membrane protein VAT-1 homolog
Peroxisomal 2,4-dienoyl-CoA reductase	Transmembrane channel-like gene family 6
Phospholipid transfer protein	Ubiquitin carboxyl-terminal hydrolase
Plectin-1	Vasohibin 1
Potassium channel subfamily U member 1	Voltage-dependent P/Q-type calcium channel subunit alpha-1A

Potassium voltage-gated channel subfamily KQT member 1	Zfp219 protein
Protein phosphatase 1G	Zinc finger protein with KRAB and SCAN domains 1
Protein Wnt	
Putative pheromone receptor	
Renalase	
Replication protein A 70 kDa DNA-binding subunit	
Rho guanine nucleotide exchange factor 2	
SAFB-like transcription modulator	
SECIS-binding protein 2-like	
Secreted frizzled-related protein 2	
Septin-2	
Serine/threonine-protein kinase PINK1, mitochondrial	
Serine/threonine-protein kinase SMG1	
Serpin B10	
Spermatogenesis-associated protein 1	
Strn3 protein	
Sulfide:quinone oxidoreductase, mitochondrial	
Translation initiation factor eIF-2B subunit epsilon	
Tripartite motif protein 25	
Tripartite motif-containing protein 42	
Uridine-cytidine kinase-like 1	
UTP11-like, U3 small nucleolar ribonucleoprotein, (Yeast)	
von Willebrand factor A domain-containing protein 5A	
WD repeat-containing protein mio	
Zinc finger and BTB domain containing 32	
Zinc finger protein 532	

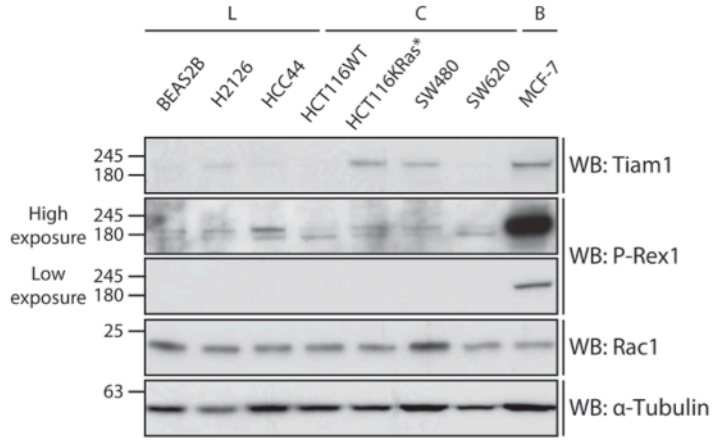

Figure A.1: Screening of Panel of Cancer Cell lines for Endogenous Levels of Tiam1, P-Rex1 and Rac1
A panel of Lung (L), Colon (C) and Breast (B) Cancer cell lines were screened by Western blotting for endogenous levels of Tiam1, P-Rex1 and Rac1 using anti-Tiam1, anti-P-Rex1 and anti-Rac1 antibodies, respectively. α-Tubulin was used as a loading control.

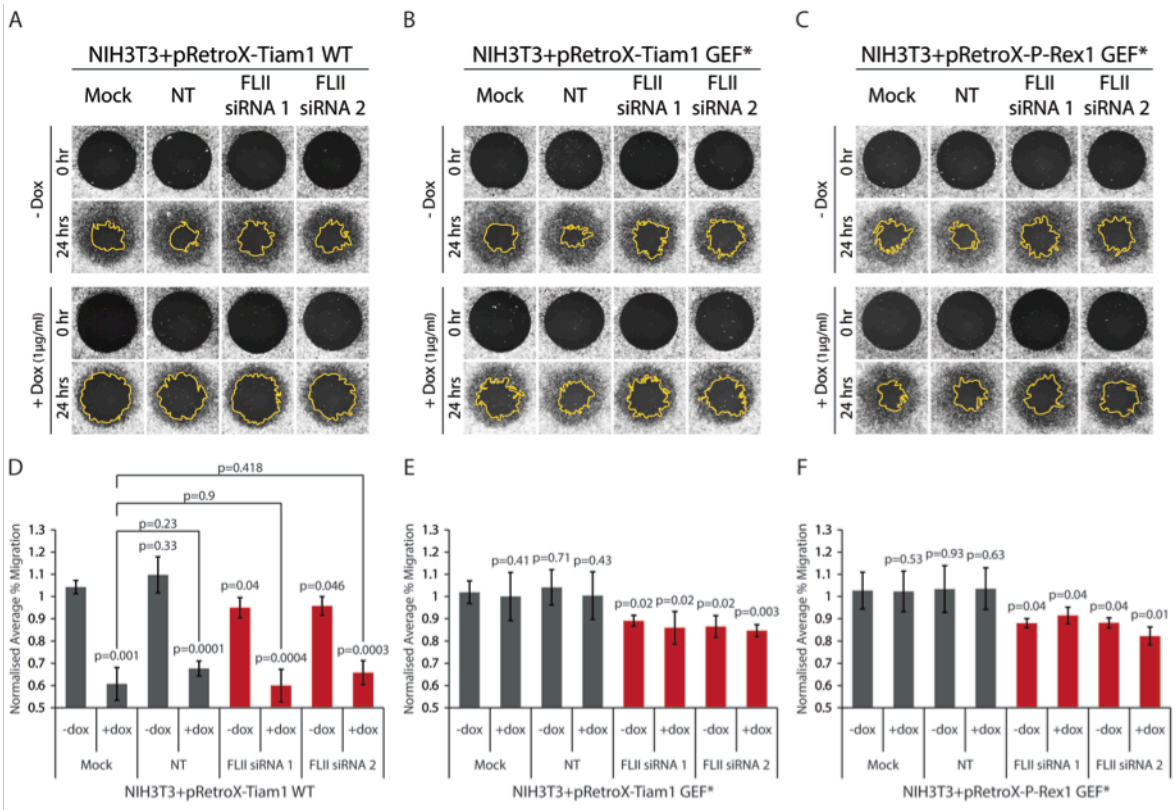

Figure A.2: The Effect of FLII Knock Down on Cellular Migration in NIH3T3 Cells
NIH3T3 cells harbouring the doxycycline (dox) inducible system for expression of Tiam1 wild type, Tiam1 GEF-dead mutant and P-Rex1 GEF-dead mutant (NIH3T3+pRetroX-Tiam1 WT/Tiam1 GEF*/P-Rex1 GEF*) were treated with mock, non-targeting (NT) or two different siRNAs against FLII (FLII siRNA1 and FLII siRNA2) for 48 hours. Cells were then reinfected with the different siRNA constructs and treated with ethanol (-dox) or dox (+dox) for 24 hours. (A, B, C) The migration potential of cells expressing Tiam1 WT (A), Tiam1 GEF* (B) and P-Rex1 GEF* (C) was assessed using the Oris™ Migration Assay. Florescence images were taken using the low light microscopy system (5x magnification) at 0 hours and 24 hours post stopper removal. Representative images from one out of three independent experiments. (D, E, F) Quantification of cellular migration of –dox and +dox treated cells expressing Tiam1 WT (D) Tiam1 GEF* (E) and P-Rex1 GEF* (F) normalised to parental -dox mock treated cells (see figure 5.12). Graphs represent the normalised average % migration ± standard error from three independent experiments. Student's t-test was used to assess significance between migration abilities within the different cells as indicated on the graph. p-values above each bar refer to significance values relative to the internal -dox mock treated cells. Other values shown in (D) show significance values between indicated pairs. p-values ≤ 0.05 are considered significant; ≤0.01 are considered highly significant.

List of Files on Supplementary CD

There are two Excel files on the CD, named Tables S.1-S.3 Mass Spec HM and Tables S.4-S.7 SILAC HM.

Tables S.1-S.3 outline the total list of proteins identified from the three BR of conventional mass spectrometry. The table titles are as follows:

Table S.1 List of Total Proteins Identified From Mass Spectrometry Experiment BR1
Table S.2 List of Total Proteins Identified From Mass Spectrometry Experiment BR2
Table S.3 List of Total Proteins Identified From Mass Spectrometry Experiment BR3

Tables S.4-S.7 outline the total list of proteins identified from two SILAC pairs together with their SILAC ratios. Table S.7 represents the original MaxQuant generated file provided by Alejandro Carpy. The table titles are as follows:

Table S.4 List of Total Proteins Identified From SILAC Experiments
Table S.5 List of Protein with SILAC Ratios in ≥ 2 SILAC Experiments
Table S.6 List of Protein with SILAC Ratios in ≤ 1 SILAC Experiments
Table S.7 MaxQuant Generated Protein List From SILAC Experiments

I have also uploaded an electronic version of my thesis for your reference if needed.

References

Abercrombie, M., Heaysman, J.E., and Pegrum, S.M. (1970). The locomotion of fibroblasts in culture. I. Movements of the leading edge. Exp Cell Res *59*, 393-398.

Abercrombie, M., Heaysman, J.E., and Pegrum, S.M. (1971). The locomotion of fibroblasts in culture. IV. Electron microscopy of the leading lamella. Exp Cell Res *67*, 359-367.

Adams, D.H., Strudwick, X.L., Kopecki, Z., Hooper-Jones, J.A., Matthaei, K.I., Campbell, H.D., Powell, B.C., and Cowin, A.J. (2008). Gender specific effects on the actin-remodelling protein Flightless I and TGF-beta1 contribute to impaired wound healing in aged skin. Int J Biochem Cell Biol *40*, 1555-1569.

Aebersold, R., and Mann, M. (2003). Mass spectrometry-based proteomics. Nature *422*, 198-207.

Agell, N., Bachs, O., Rocamora, N., and Villalonga, P. (2002). Modulation of the Ras/Raf/MEK/ERK pathway by Ca(2+), and calmodulin. Cell Signal *14*, 649-654.

Aguirre-Ghiso, J.A. (2007). Models, mechanisms and clinical evidence for cancer dormancy. Nat Rev Cancer *7*, 834-846.

Ahmed, S., Goh, W.I., and Bu, W. (2010). I-BAR domains, IRSp53 and filopodium formation. Semin Cell Dev Biol *21*, 350-356.

Ahuja, R., Pinyol, R., Reichenbach, N., Custer, L., Klingensmith, J., Kessels, M.M., and Qualmann, B. (2007). Cordon-bleu is an actin nucleation factor and controls neuronal morphology. Cell *131*, 337-350.

Akin, O., and Mullins, R.D. (2008). Capping protein increases the rate of actin-based motility by promoting filament nucleation by the Arp2/3 complex. Cell *133*, 841-851.

Alan, J.K., and Lundquist, E.A. (2013). Mutationally activated Rho GTPases in cancer. Small GTPases *4*, 159-163.

Alberts, A.S. (2001). Identification of a carboxyl-terminal diaphanous-related formin homology protein autoregulatory domain. J Biol Chem *276*, 2824-2830.

Andreasen, P.A., Kjoller, L., Christensen, L., and Duffy, M.J. (1997). The urokinase-type plasminogen activator system in cancer metastasis: a review. Int J Cancer *72*, 1-22.

Angrand, P.O., Segura, I., Volkel, P., Ghidelli, S., Terry, R., Brajenovic, M., Vintersten, K., Klein, R., Superti-Furga, G., Drewes, G., *et al.* (2006). Transgenic mouse proteomics identifies new 14-3-3-associated proteins involved in cytoskeletal rearrangements and cell signaling. Mol Cell Proteomics *5*, 2211-2227.

Archer, S.K., Behm, C.A., Claudianos, C., and Campbell, H.D. (2004). The flightless I protein and the gelsolin family in nuclear hormone receptor-mediated signalling. Biochem Soc Trans *32*, 940-942.

Archer, S.K., Claudianos, C., and Campbell, H.D. (2005). Evolution of the gelsolin family of actin-binding proteins as novel transcriptional coactivators. Bioessays *27*, 388-396.

Arora, P.D., Janmey, P.A., and McCulloch, C.A. (1999). A role for gelsolin in stress fiber-dependent cell contraction. Exp Cell Res *250*, 155-167.

Arora, P.D., and McCulloch, C.A. (1996). Dependence of fibroblast migration on actin severing activity of gelsolin. J Biol Chem *271*, 20516-20523.

Ayala, I., Giacchetti, G., Caldieri, G., Attanasio, F., Mariggio, S., Tete, S., Polishchuk, R., Castronovo, V., and Buccione, R. (2009). Faciogenital dysplasia protein Fgd1 regulates invadopodia biogenesis and extracellular matrix degradation and is up-regulated in prostate and breast cancer. Cancer Res *69*, 747-752.

Aznar, S., Fernandez-Valeron, P., Espina, C., and Lacal, J.C. (2004). Rho GTPases: potential candidates for anticancer therapy. Cancer Lett *206*, 181-191.

Bear, J.E., and Gertler, F.B. (2009). Ena/VASP: towards resolving a pointed controversy at the barbed end. J Cell Sci *122*, 1947-1953.

Benitah, S.A., Valeron, P.F., van Aelst, L., Marshall, C.J., and Lacal, J.C. (2004). Rho GTPases in human cancer: an unresolved link to upstream and downstream transcriptional regulation. Biochim Biophys Acta *1705*, 121-132.

Benzinger, A., Muster, N., Koch, H.B., Yates, J.R., 3rd, and Hermeking, H. (2005). Targeted proteomic analysis of 14-3-3 sigma, a p53 effector commonly silenced in cancer. Mol Cell Proteomics *4*, 785-795.

Bernards, A. (2003). GAPs galore! A survey of putative Ras superfamily GTPase activating proteins in man and Drosophila. Biochim Biophys Acta *1603*, 47-82.

Betson, M., Lozano, E., Zhang, J., and Braga, V.M. (2002). Rac activation upon cell-cell contact formation is dependent on signaling from the epidermal growth factor receptor. J Biol Chem *277*, 36962-36969.

Bhat, H.F., Baba, R.A., Adams, M.E., and Khanday, F.A. (2014). Role of SNTA1 in Rac1 activation, modulation of ROS generation, and migratory potential of human breast cancer cells. Br J Cancer *110*, 706-714.

Bolis, A., Corbetta, S., Cioce, A., and de Curtis, I. (2003). Differential distribution of Rac1 and Rac3 GTPases in the developing mouse brain: implications for a role of Rac3 in Purkinje cell differentiation. Eur J Neurosci *18*, 2417-2424.

Borths, E.L., and Welch, M.D. (2002). Turning on the Arp2/3 complex at atomic resolution. Structure *10*, 131-135.

Bosco, E.E., Mulloy, J.C., and Zheng, Y. (2009). Rac1 GTPase: a "Rac" of all trades. Cell Mol Life Sci *66*, 370-374.

Boureux, A., Vignal, E., Faure, S., and Fort, P. (2007). Evolution of the Rho family of ras-like GTPases in eukaryotes. Mol Biol Evol *24*, 203-216.

Bourguignon, L.Y., Zhu, H., Shao, L., and Chen, Y.W. (2000). Ankyrin-Tiam1 interaction promotes Rac1 signaling and metastatic breast tumor cell invasion and migration. J Cell Biol *150*, 177-191.

Bourne, H.R., Sanders, D.A., and McCormick, F. (1991). The GTPase superfamily: conserved structure and molecular mechanism. Nature *349*, 117-127.

Bouwmeester, T., Bauch, A., Ruffner, H., Angrand, P.O., Bergamini, G., Croughton, K., Cruciat, C., Eberhard, D., Gagneur, J., Ghidelli, S.*, et al.* (2004). A physical and functional map of the human TNF-alpha/NF-kappa B signal transduction pathway. Nat Cell Biol *6*, 97-105.

Brandt, D.T., Marion, S., Griffiths, G., Watanabe, T., Kaibuchi, K., and Grosse, R. (2007). Dia1 and IQGAP1 interact in cell migration and phagocytic cup formation. J Cell Biol *178*, 193-200.

Braun, A., Dang, K., Buslig, F., Baird, M.A., Davidson, M.W., Waterman, C.M., and Myers, K.A. (2014). Rac1 and Aurora A regulate MCAK to polarize microtubule growth in migrating endothelial cells. J Cell Biol *206*, 97-112.

Breitsprecher, D., Kiesewetter, A.K., Linkner, J., Urbanke, C., Resch, G.P., Small, J.V., and Faix, J. (2008). Clustering of VASP actively drives processive, WH2 domain-mediated actin filament elongation. EMBO J *27*, 2943-2954.

Briggs, M.W., and Sacks, D.B. (2003). IQGAP1 as signal integrator: Ca2+, calmodulin, Cdc42 and the cytoskeleton. FEBS Lett *542*, 7-11.

Buccione, R., Caldieri, G., and Ayala, I. (2009). Invadopodia: specialized tumor cell structures for the focal degradation of the extracellular matrix. Cancer metastasis reviews *28*, 137-149.

Buchsbaum, R.J., Connolly, B.A., and Feig, L.A. (2002). Interaction of Rac exchange factors Tiam1 and Ras-GRF1 with a scaffold for the p38 mitogen-activated protein kinase cascade. Mol Cell Biol *22*, 4073-4085.

Buchsbaum, R.J., Connolly, B.A., and Feig, L.A. (2003). Regulation of p70 S6 kinase by complex formation between the Rac guanine nucleotide exchange factor (Rac-GEF) Tiam1 and the scaffold spinophilin. J Biol Chem *278*, 18833-18841.

Burridge, K., and Wennerberg, K. (2004). Rho and Rac Take Center Stage. Cell *116*, 167-179.

Buss, J.E., Kudlow, J.E., Lazar, C.S., and Gill, G.N. (1982). Altered epidermal growth factor (EGF)-stimulated protein kinase activity in variant A431 cells with altered growth responses to EGF. Proc Natl Acad Sci U S A *79*, 2574-2578.

Bustelo, X.R., Sauzeau, V., and Berenjeno, I.M. (2007). GTP-binding proteins of the Rho/Rac family: regulation, effectors and functions in vivo. Bioessays *29*, 356-370.

Campbell, A.D., Lawn, S., McGarry, L.C., Welch, H.C., Ozanne, B.W., and Norman, J.C. (2013). P-Rex1 cooperates with PDGFRbeta to drive cellular migration in 3D microenvironments. PLoS One *8*, e53982.

Campbell, H.D., Fountain, S., McLennan, I.S., Berven, L.A., Crouch, M.F., Davy, D.A., Hooper, J.A., Waterford, K., Chen, K.S., Lupski, J.R., *et al.* (2002). Fliih, a gelsolin-related cytoskeletal regulator essential for early mammalian embryonic development. Mol Cell Biol *22*, 3518-3526.

Campbell, H.D., Fountain, S., Young, I.G., Claudianos, C., Hoheisel, J.D., Chen, K.S., and Lupski, J.R. (1997). Genomic structure, evolution, and expression of human FLII, a gelsolin and leucine-rich-repeat family member: overlap with LLGL. Genomics *42*, 46-54.

Campbell, H.D., Fountain, S., Young, I.G., Weitz, S., Lichter, P., and Hoheisel, J.D. (2000). Fliih, the murine homologue of the Drosophila melanogaster flightless I gene: nucleotide sequence, chromosomal mapping and overlap with Llglh. DNA sequence : the journal of DNA sequencing and mapping *11*, 29-40.

Campbell, H.D., Schimansky, T., Claudianos, C., Ozsarac, N., Kasprzak, A.B., Cotsell, J.N., Young, I.G., de Couet, H.G., and Miklos, G.L. (1993). The Drosophila melanogaster flightless-I gene involved in gastrulation and muscle degeneration encodes gelsolin-like and leucine-rich repeat domains and is conserved in Caenorhabditis elegans and humans. Proc Natl Acad Sci U S A *90*, 11386-11390.

Carpy, A., Krug, K., Graf, S., Koch, A., Popic, S., Hauf, S., and Macek, B. (2014). Absolute proteome and phosphoproteome dynamics during the cell cycle of fission yeast. Mol Cell Proteomics.

Castillo-Lluva, S., Tan, C.T., Daugaard, M., Sorensen, P.H., and Malliri, A. (2013). The tumour suppressor HACE1 controls cell migration by regulating Rac1 degradation. Oncogene *32*, 1735-1742.

Castillo-Lluva, S., Tatham, M.H., Jones, R.C., Jaffray, E.G., Edmondson, R.D., Hay, R.T., and Malliri, A. (2010). SUMOylation of the GTPase Rac1 is required for optimal cell migration. Nat Cell Biol *12*, 1078-1085.

Chambers, A.F., Groom, A.C., and MacDonald, I.C. (2002). Dissemination and growth of cancer cells in metastatic sites. Nat Rev Cancer *2*, 563-572.

Chan, A.Y., Coniglio, S.J., Chuang, Y.Y., Michaelson, D., Knaus, U.G., Philips, M.R., and Symons, M. (2005). Roles of the Rac1 and Rac3 GTPases in human tumor cell invasion. Oncogene *24*, 7821-7829.

Chellaiah, M., Kizer, N., Silva, M., Alvarez, U., Kwiatkowski, D., and Hruska, K.A. (2000). Gelsolin deficiency blocks podosome assembly and produces increased bone mass and strength. J Cell Biol *148*, 665-678.

Chen, W.T. (1981). Mechanism of retraction of the trailing edge during fibroblast movement. J Cell Biol *90*, 187-200.

Chesarone, M.A., DuPage, A.G., and Goode, B.L. (2010). Unleashing formins to remodel the actin and microtubule cytoskeletons. Nat Rev Mol Cell Biol *11*, 62-74.

Chinkers, M., McKanna, J.A., and Cohen, S. (1979). Rapid induction of morphological changes in human carcinoma cells A-431 by epidermal growth factors. J Cell Biol *83*, 260-265.

Cho, Y.J., Zhang, B., Kaartinen, V., Haataja, L., de Curtis, I., Groffen, J., and Heisterkamp, N. (2005). Generation of rac3 null mutant mice: role of Rac3 in Bcr/Abl-caused lymphoblastic leukemia. Mol Cell Biol *25*, 5777-5785.

Choi, C.K., Vicente-Manzanares, M., Zareno, J., Whitmore, L.A., Mogilner, A., and Horwitz, A.R. (2008). Actin and alpha-actinin orchestrate the assembly and maturation of nascent adhesions in a myosin II motor-independent manner. Nat Cell Biol *10*, 1039-1050.

Choi, Y., Kim, H., Chung, H., Hwang, J.S., Shin, J.A., Han, I.O., and Oh, E.S. (2010). Syndecan-2 regulates cell migration in colon cancer cells through Tiam1-mediated Rac activation. Biochem Biophys Res Commun *391*, 921-925.

Christofori, G. (2006). New signals from the invasive front. Nature *441*, 444-450.

Chuang, T.H., Xu, X., Knaus, U.G., Hart, M.J., and Bokoch, G.M. (1993). GDP dissociation inhibitor prevents intrinsic and GTPase activating protein-stimulated GTP hydrolysis by the Rac GTP-binding protein. J Biol Chem *268*, 775-778.

Claudianos, C., and Campbell, H.D. (1995). The novel flightless-I gene brings together two gene families, actin-binding proteins related to gelsolin and leucine-rich-repeat proteins involved in Ras signal transduction. Mol Biol Evol *12*, 405-414.

Connolly, B.A., Rice, J., Feig, L.A., and Buchsbaum, R.J. (2005). Tiam1-IRSp53 complex formation directs specificity of rac-mediated actin cytoskeleton regulation. Mol Cell Biol *25*, 4602-4614.

Cook-Mills, J.M., Johnson, J.D., Deem, T.L., Ochi, A., Wang, L., and Zheng, Y. (2004). Calcium mobilization and Rac1 activation are required for VCAM-1 (vascular cell adhesion molecule-1) stimulation of NADPH oxidase activity. The Biochemical journal *378*, 539-547.

Cote, J.F., and Vuori, K. (2007). GEF what? Dock180 and related proteins help Rac to polarize cells in new ways. Trends Cell Biol *17*, 383-393.

Cowin, A.J., Adams, D.H., Strudwick, X.L., Chan, H., Hooper, J.A., Sander, G.R., Rayner, T.E., Matthaei, K.I., Powell, B.C., and Campbell, H.D. (2007). Flightless I deficiency enhances wound repair by increasing cell migration and proliferation. J Pathol *211*, 572-581.

Cox, E.A., and Huttenlocher, A. (1998). Regulation of integrin-mediated adhesion during cell migration. Microscopy research and technique *43*, 412-419.

Cox, P.R., and Zoghbi, H.Y. (2000). Sequencing, expression analysis, and mapping of three unique human tropomodulin genes and their mouse orthologs. Genomics *63*, 97-107.

Cunningham, C.C., Stossel, T.P., and Kwiatkowski, D.J. (1991). Enhanced motility in NIH 3T3 fibroblasts that overexpress gelsolin. Science *251*, 1233-1236.

Cutler, M.L., Bassin, R.H., Zanoni, L., and Talbot, N. (1992). Isolation of rsp-1, a novel cDNA capable of suppressing v-Ras transformation. Mol Cell Biol *12*, 3750-3756.

Damoulakis, G., Gambardella, L., Rossman, K.L., Lawson, C.D., Anderson, K.E., Fukui, Y., Welch, H.C., Der, C.J., Stephens, L.R., and Hawkins, P.T. (2014). P-Rex1 directly activates RhoG to regulate GPCR-driven Rac signalling and actin polarity in neutrophils. J Cell Sci *127*, 2589-2600.

Davy, D.A., Ball, E.E., Matthaei, K.I., Campbell, H.D., and Crouch, M.F. (2000). The flightless I protein localizes to actin-based structures during embryonic development. Immunol Cell Biol *78*, 423-429.

Davy, D.A., Campbell, H.D., Fountain, S., de Jong, D., and Crouch, M.F. (2001). The flightless I protein colocalizes with actin- and microtubule-based structures in motile Swiss 3T3 fibroblasts: evidence for the involvement of PI 3-kinase and Ras-related small GTPases. J Cell Sci *114*, 549-562.

Dawson, J.C., Bruche, S., Spence, H.J., Braga, V.M., and Machesky, L.M. (2012). Mtss1 promotes cell-cell junction assembly and stability through the small GTPase Rac1. PLoS One *7*, e31141.

De Wever, O., Nguyen, Q.D., Van Hoorde, L., Bracke, M., Bruyneel, E., Gespach, C., and Mareel, M. (2004). Tenascin-C and SF/HGF produced by myofibroblasts in vitro provide convergent pro-invasive signals to human colon cancer cells through RhoA and Rac. FASEB J *18*, 1016-1018.

Deak, II, Bellamy, P.R., Bienz, M., Dubuis, Y., Fenner, E., Gollin, M., Rahmi, A., Ramp, T., Reinhardt, C.A., and Cotton, B. (1982). Mutations affecting the indirect flight muscles of Drosophila melanogaster. Journal of embryology and experimental morphology *69*, 61-81.

Dechow, T.N., Pedranzini, L., Leitch, A., Leslie, K., Gerald, W.L., Linkov, I., and Bromberg, J.F. (2004). Requirement of matrix metalloproteinase-9 for the transformation of human mammary epithelial cells by Stat3-C. Proc Natl Acad Sci U S A *101*, 10602-10607.

Derksen, P.W., Liu, X., Saridin, F., van der Gulden, H., Zevenhoven, J., Evers, B., van Beijnum, J.R., Griffioen, A.W., Vink, J., Krimpenfort, P.*, et al.* (2006). Somatic inactivation of E-cadherin and p53 in mice leads to metastatic lobular mammary carcinoma through induction of anoikis resistance and angiogenesis. Cancer cell *10*, 437-449.

DerMardirossian, C., and Bokoch, G.M. (2005). GDIs: central regulatory molecules in Rho GTPase activation. Trends in Cell Biology *15*, 356-363.

Dong, X., Mo, Z., Bokoch, G., Guo, C., Li, Z., and Wu, D. (2005). P-Rex1 is a primary Rac2 guanine nucleotide exchange factor in mouse neutrophils. Curr Biol *15*, 1874-1879.

Du, D., Pedersen, E., Wang, Z., Karlsson, R., Chen, Z., Wu, X., and Brakebusch, C. (2009). Cdc42 is crucial for the maturation of primordial cell junctions in keratinocytes independent of Rac1. Exp Cell Res *315*, 1480-1489.

Ehler, E., van Leeuwen, F., Collard, J.G., and Salinas, P.C. (1997). Expression of Tiam-1 in the developing brain suggests a role for the Tiam-1-Rac signaling pathway in cell migration and neurite outgrowth. Mol Cell Neurosci *9*, 1-12.

Ehrlich, J.S., Hansen, M.D., and Nelson, W.J. (2002). Spatio-temporal regulation of Rac1 localization and lamellipodia dynamics during epithelial cell-cell adhesion. Dev Cell *3*, 259-270.

El-Mezgueldi, M. (2014). Tropomyosin dynamics. Journal of muscle research and cell motility.

Engers, R., Springer, E., Michiels, F., Collard, J.G., and Gabbert, H.E. (2001). Rac affects invasion of human renal cell carcinomas by up-regulating tissue inhibitor of metalloproteinases (TIMP)-1 and TIMP-2 expression. J Biol Chem *276*, 41889-41897.

Etienne-Manneville, S., and Hall, A. (2001). Integrin-Mediated Activation of Cdc42 Controls Cell Polarity in Migrating Astrocytes through PKCζ. Cell *106*, 489-498.

Etienne-Manneville, S., and Hall, A. (2002). Rho GTPases in cell biology. Nature *420*, 629-635.

Evans, C.A., Tonge, R., Blinco, D., Pierce, A., Shaw, J., Lu, Y., Hamzah, H.G., Gray, A., Downes, C.P., Gaskell, S.J., *et al.* (2004). Comparative proteomics of primitive hematopoietic cell populations reveals differences in expression of proteins regulating motility. Blood *103*, 3751-3759.

Even-Faitelson, L., Rosenberg, M., and Ravid, S. (2005). PAK1 regulates myosin II-B phosphorylation, filament assembly, localization and cell chemotaxis. Cell Signal *17*, 1137-1148.

Felding-Habermann, B., O'Toole, T.E., Smith, J.W., Fransvea, E., Ruggeri, Z.M., Ginsberg, M.H., Hughes, P.E., Pampori, N., Shattil, S.J., Saven, A., *et al.* (2001). Integrin activation controls metastasis in human breast cancer. Proc Natl Acad Sci U S A *98*, 1853-1858.

Fischer, R.S., Fritz-Six, K.L., and Fowler, V.M. (2003). Pointed-end capping by tropomodulin3 negatively regulates endothelial cell motility. J Cell Biol *161*, 371-380.

Frasa, M.A., Maximiano, F.C., Smolarczyk, K., Francis, R.E., Betson, M.E., Lozano, E., Goldenring, J., Seabra, M.C., Rak, A., Ahmadian, M.R., *et al.* (2010). Armus is a Rac1 effector that inactivates Rab7 and regulates E-cadherin degradation. Curr Biol *20*, 198-208.

Friedl, P. (2004). Prespecification and plasticity: shifting mechanisms of cell migration. Curr Opin Cell Biol *16*, 14-23.

Friedl, P., Hegerfeldt, Y., and Tusch, M. (2004). Collective cell migration in morphogenesis and cancer. Int J Dev Biol *48*, 441-449.

Friedl, P., and Wolf, K. (2003). Tumour-cell invasion and migration: diversity and escape mechanisms. Nat Rev Cancer *3*, 362-374.

Friedl, P., and Wolf, K. (2008). Tube travel: the role of proteases in individual and collective cancer cell invasion. Cancer Res *68*, 7247-7249.

Friedl, P., and Wolf, K. (2010). Plasticity of cell migration: a multiscale tuning model. J Cell Biol *188*, 11-19.

Frisch, S.M., and Francis, H. (1994). Disruption of epithelial cell-matrix interactions induces apoptosis. J Cell Biol *124*, 619-626.

Fujii, M., Kawai, K., Egami, Y., and Araki, N. (2013). Dissecting the roles of Rac1 activation and deactivation in macropinocytosis using microscopic photo-manipulation. Scientific reports *3*, 2385.

Fujita, Y., Hogan, C., and Braga, V.M. (2006). Regulation of cell-cell adhesion by Rap1. Methods Enzymol *407*, 359-372.

Fujita, Y., Krause, G., Scheffner, M., Zechner, D., Leddy, H.E., Behrens, J., Sommer, T., and Birchmeier, W. (2002). Hakai, a c-Cbl-like protein, ubiquitinates and induces endocytosis of the E-cadherin complex. Nat Cell Biol *4*, 222-231.

Fukuhara, A., Shimizu, K., Kawakatsu, T., Fukuhara, T., and Takai, Y. (2003). Involvement of nectin-activated Cdc42 small G protein in organization of adherens and tight junctions in Madin-Darby canine kidney cells. J Biol Chem *278*, 51885-51893.

Fukuhara, T., Shimizu, K., Kawakatsu, T., Fukuyama, T., Minami, Y., Honda, T., Hoshino, T., Yamada, T., Ogita, H., Okada, M., *et al.* (2004). Activation of Cdc42 by trans interactions of the cell adhesion molecules nectins through c-Src and Cdc42-GEF FRG. J Cell Biol *166*, 393-405.

Gadea, G., Sanz-Moreno, V., Self, A., Godi, A., and Marshall, C.J. (2008). DOCK10-mediated Cdc42 activation is necessary for amoeboid invasion of melanoma cells. Curr Biol *18*, 1456-1465.

Gardel, M.L., Schneider, I.C., Aratyn-Schaus, Y., and Waterman, C.M. (2010). Mechanical integration of actin and adhesion dynamics in cell migration. Annu Rev Cell Dev Biol *26*, 315-333.

Geiger, T.R., and Peeper, D.S. (2005). The neurotrophic receptor TrkB in anoikis resistance and metastasis: a perspective. Cancer Res *65*, 7033-7036.

Geiger, T.R., and Peeper, D.S. (2009). Metastasis mechanisms. Biochim Biophys Acta *1796*, 293-308.

Giannone, G., Dubin-Thaler, B.J., Rossier, O., Cai, Y., Chaga, O., Jiang, G., Beaver, W., Dobereiner, H.G., Freund, Y., Borisy, G., *et al.* (2007). Lamellipodial actin mechanically links myosin activity with adhesion-site formation. Cell *128*, 561-575.

Gimbrone, M.A., Jr., Leapman, S.B., Cotran, R.S., and Folkman, J. (1972). Tumor dormancy in vivo by prevention of neovascularization. J Exp Med *136*, 261-276.

Gingras, A.C., Aebersold, R., and Raught, B. (2005). Advances in protein complex analysis using mass spectrometry. J Physiol *563*, 11-21.

Glenney, J.R., Jr., Geisler, N., Kaulfus, P., and Weber, K. (1981). Demonstration of at least two different actin-binding sites in villin, a calcium-regulated modulator of F-actin organization. J Biol Chem *256*, 8156-8161.

Gloeckner, C.J., Boldt, K., Schumacher, A., Roepman, R., and Ueffing, M. (2007). A novel tandem affinity purification strategy for the efficient isolation and characterisation of native protein complexes. Proteomics *7*, 4228-4234.

Gloeckner, C.J., Boldt, K., Schumacher, A., and Ueffing, M. (2009a). Tandem affinity purification of protein complexes from mammalian cells by the Strep/FLAG (SF)-TAP tag. Methods Mol Biol *564*, 359-372.

Gloeckner, C.J., Boldt, K., and Ueffing, M. (2009b). Strep/FLAG tandem affinity purification (SF-TAP) to study protein interactions. Current protocols in protein science / editorial board, John E. Coligan ... [et al.] *Chapter 19*, Unit19 20.

Goley, E.D., Rodenbusch, S.E., Martin, A.C., and Welch, M.D. (2004). Critical conformational changes in the Arp2/3 complex are induced by nucleotide and nucleation promoting factor. Mol Cell *16*, 269-279.

Gomez del Pulgar, T., Benitah, S.A., Valeron, P.F., Espina, C., and Lacal, J.C. (2005). Rho GTPase expression in tumourigenesis: evidence for a significant link. Bioessays *27*, 602-613.

Goode, B.L., and Eck, M.J. (2007). Mechanism and function of formins in the control of actin assembly. Annu Rev Biochem *76*, 593-627.

Goshima, M., Kariya, K., Yamawaki-Kataoka, Y., Okada, T., Shibatohge, M., Shima, F., Fujimoto, E., and Kataoka, T. (1999). Characterization of a novel Ras-binding protein Ce-FLI-1 comprising leucine-rich repeats and gelsolin-like domains. Biochem Biophys Res Commun *257*, 111-116.

Gumienny, T.L., Brugnera, E., Tosello-Trampont, A.C., Kinchen, J.M., Haney, L.B., Nishiwaki, K., Walk, S.F., Nemergut, M.E., Macara, I.G., Francis, R., *et al.* (2001). CED-12/ELMO, a novel member of the CrkII/Dock180/Rac pathway, is required for phagocytosis and cell migration. Cell *107*, 27-41.

Haataja, L., Groffen, J., and Heisterkamp, N. (1997). Characterization of RAC3, a novel member of the Rho family. J Biol Chem *272*, 20384-20388.

Habets, G.G., van der Kammen, R.A., Stam, J.C., Michiels, F., and Collard, J.G. (1995). Sequence of the human invasion-inducing TIAM1 gene, its conservation in evolution and its expression in tumor cell lines of different tissue origin. Oncogene *10*, 1371-1376.

Hage, B., Meinel, K., Baum, I., Giehl, K., and Menke, A. (2009). Rac1 activation inhibits E-cadherin-mediated adherens junctions via binding to IQGAP1 in pancreatic carcinoma cells. Cell Commun Signal *7*, 23.

Hansen, M.D., Ehrlich, J.S., and Nelson, W.J. (2002). Molecular mechanism for orienting membrane and actin dynamics to nascent cell-cell contacts in epithelial cells. J Biol Chem *277*, 45371-45376.

Harris, H. (2008). Concerning the origin of malignant tumours by Theodor Boveri. Translated and annotated by Henry Harris. Preface. J Cell Sci *121 Suppl 1*, v-vi.

Hart, M.J., Callow, M.G., Souza, B., and Polakis, P. (1996a). IQGAP1, a calmodulin-binding protein with a rasGAP-related domain, is a potential effector for cdc42Hs. EMBO J *15*, 2997-3005.

Hart, M.J., Sharma, S., elMasry, N., Qiu, R.G., McCabe, P., Polakis, P., and Bollag, G. (1996b). Identification of a novel guanine nucleotide exchange factor for the Rho GTPase. J Biol Chem *271*, 25452-25458.

Hatanaka, H., Ogura, K., Moriyama, K., Ichikawa, S., Yahara, I., and Inagaki, F. (1996). Tertiary structure of destrin and structural similarity between two actin-regulating protein families. Cell *85*, 1047-1055.

Hazan, R.B., Phillips, G.R., Qiao, R.F., Norton, L., and Aaronson, S.A. (2000). Exogenous expression of N-cadherin in breast cancer cells induces cell migration, invasion, and metastasis. J Cell Biol *148*, 779-790.

Heasman, S.J., and Ridley, A.J. (2008). Mammalian Rho GTPases: new insights into their functions from in vivo studies. Nat Rev Mol Cell Biol *9*, 690-701.

Higashi, T., Ikeda, T., Murakami, T., Shirakawa, R., Kawato, M., Okawa, K., Furuse, M., Kimura, T., Kita, T., and Horiuchi, H. (2010). Flightless-I (Fli-I) regulates the actin assembly activity of diaphanous-related formins (DRFs) Daam1 and mDia1 in cooperation with active Rho GTPase. J Biol Chem *285*, 16231-16238.

Higashi, T., Ikeda, T., Shirakawa, R., Kondo, H., Kawato, M., Horiguchi, M., Okuda, T., Okawa, K., Fukai, S., Nureki, O., *et al.* (2008). Biochemical characterization of the Rho GTPase-regulated actin assembly by diaphanous-related formins, mDia1 and Daam1, in platelets. J Biol Chem *283*, 8746-8755.

Hodis, E., Watson, I.R., Kryukov, G.V., Arold, S.T., Imielinski, M., Theurillat, J.P., Nickerson, E., Auclair, D., Li, L., Place, C., *et al.* (2012). A landscape of driver mutations in melanoma. Cell *150*, 251-263.

Homyk, T., and Sheppard, D.E. (1977). Behavioral Mutants of DROSOPHILA MELANOGASTER. I. Isolation and Mapping of Mutations Which Decrease Flight Ability. Genetics *87*, 95-104.

Hordijk, P.L., ten Klooster, J.P., van der Kammen, R.A., Michiels, F., Oomen, L.C., and Collard, J.G. (1997). Inhibition of invasion of epithelial cells by Tiam1-Rac signaling. Science *278*, 1464-1466.

Hotulainen, P., Llano, O., Smirnov, S., Tanhuanpaa, K., Faix, J., Rivera, C., and Lappalainen, P. (2009). Defining mechanisms of actin polymerization and depolymerization during dendritic spine morphogenesis. J Cell Biol *185*, 323-339.

Hou, M., Tan, L., Wang, X., and Zhu, Y.S. (2004). Antisense Tiam1 down-regulates the invasiveness of 95D cells in vitro. Acta biochimica et biophysica Sinica *36*, 537-540.

Itoh, M., Murata, T., Suzuki, T., Shindoh, M., Nakajima, K., Imai, K., and Yoshida, K. (2006). Requirement of STAT3 activation for maximal collagenase-1 (MMP-1) induction by epidermal growth factor and malignant characteristics in T24 bladder cancer cells. Oncogene *25*, 1195-1204.

Jackson, J.E., Kopecki, Z., Adams, D.H., and Cowin, A.J. (2012). Flii neutralizing antibodies improve wound healing in porcine preclinical studies. Wound Repair Regen *20*, 523-536.

Jacquemet, G., and Humphries, M.J. (2013). IQGAP1 is a key node within the small GTPase network. Small GTPases *4*, 199-207.

Jacquemet, G., Morgan, M.R., Byron, A., Humphries, J.D., Choi, C.K., Chen, C.S., Caswell, P.T., and Humphries, M.J. (2013). Rac1 is deactivated at integrin activation sites through an IQGAP1-filamin-A-RacGAP1 pathway. J Cell Sci *126*, 4121-4135.

Jaffe, A.B., and Hall, A. (2005). Rho GTPases: biochemistry and biology. Annu Rev Cell Dev Biol *21*, 247-269.

Jechlinger, M., Grunert, S., Tamir, I.H., Janda, E., Ludemann, S., Waerner, T., Seither, P., Weith, A., Beug, H., and Kraut, N. (2003). Expression profiling of epithelial plasticity in tumor progression. Oncogene *22*, 7155-7169.

Jeon, Y.J., Choi, J.S., Lee, J.Y., Yu, K.R., Ka, S.H., Cho, Y., Choi, E.J., Baek, S.H., Seol, J.H., Park, D., *et al.* (2008). Filamin B serves as a molecular scaffold for type I interferon-induced c-Jun NH2-terminal kinase signaling pathway. Mol Biol Cell *19*, 5116-5130.

Jin, G., Sah, R.L., Li, Y.S., Lotz, M., Shyy, J.Y., and Chien, S. (2000). Biomechanical regulation of matrix metalloproteinase-9 in cultured chondrocytes. J Orthop Res *18*, 899-908.

Johnson, M., Sharma, M., and Henderson, B.R. (2009). IQGAP1 regulation and roles in cancer. Cell Signal *21*, 1471-1478.

Johnston, S.A., Bramble, J.P., Yeung, C.L., Mendes, P.M., and Machesky, L.M. (2008). Arp2/3 complex activity in filopodia of spreading cells. BMC cell biology *9*, 65.

Jordan, P., Brazao, R., Boavida, M.G., Gespach, C., and Chastre, E. (1999). Cloning of a novel human Rac1b splice variant with increased expression in colorectal tumors. Oncogene *18*, 6835-6839.

Kakiuchi, M., Nishizawa, T., Ueda, H., Gotoh, K., Tanaka, A., Hayashi, A., Yamamoto, S., Tatsuno, K., Katoh, H., Watanabe, Y.*, et al.* (2014). Recurrent gain-of-function mutations of RHOA in diffuse-type gastric carcinoma. Nature genetics *46*, 583-587.

Kamai, T., Yamanishi, T., Shirataki, H., Takagi, K., Asami, H., Ito, Y., and Yoshida, K. (2004). Overexpression of RhoA, Rac1, and Cdc42 GTPases is associated with progression in testicular cancer. Clin Cancer Res *10*, 4799-4805.

Kandasamy, K., Mohan, S.S., Raju, R., Keerthikumar, S., Kumar, G.S., Venugopal, A.K., Telikicherla, D., Navarro, J.D., Mathivanan, S., Pecquet, C.*, et al.* (2010). NetPath: a public resource of curated signal transduction pathways. Genome Biol *11*, R3.

Kataoka, T., Broek, D., and Wigler, M. (1985). DNA sequence and characterization of the S. cerevisiae gene encoding adenylate cyclase. Cell *43*, 493-505.

Katoh, H., and Negishi, M. (2003). RhoG activates Rac1 by direct interaction with the Dock180-binding protein Elmo. Nature *424*, 461-464.

Kawakatsu, T., Shimizu, K., Honda, T., Fukuhara, T., Hoshino, T., and Takai, Y. (2002). Trans-interactions of nectins induce formation of filopodia and Lamellipodia through the respective activation of Cdc42 and Rac small G proteins. J Biol Chem *277*, 50749-50755.

Kawazu, M., Ueno, T., Kontani, K., Ogita, Y., Ando, M., Fukumura, K., Yamato, A., Soda, M., Takeuchi, K., Miki, Y.*, et al.* (2013). Transforming mutations of RAC guanosine triphosphatases in human cancers. Proc Natl Acad Sci U S A *110*, 3029-3034.

Keely, P.J., Westwick, J.K., Whitehead, I.P., Der, C.J., and Parise, L.V. (1997). Cdc42 and Rac1 induce integrin-mediated cell motility and invasiveness through PI(3)K. Nature *390*, 632-636.

Khanna, C., Wan, X., Bose, S., Cassaday, R., Olomu, O., Mendoza, A., Yeung, C., Gorlick, R., Hewitt, S.M., and Helman, L.J. (2004). The membrane-cytoskeleton linker ezrin is necessary for osteosarcoma metastasis. Nat Med *10*, 182-186.

Kheradmand, F., Werner, E., Tremble, P., Symons, M., and Werb, Z. (1998). Role of Rac1 and oxygen radicals in collagenase-1 expression induced by cell shape change. Science *280*, 898-902.

Khosravi-Far, R., Solski, P.A., Clark, G.J., Kinch, M.S., and Der, C.J. (1995). Activation of Rac1, RhoA, and mitogen-activated protein kinases is required for Ras transformation. Mol Cell Biol *15*, 6443-6453.

Kido, M., Shima, F., Satoh, T., Asato, T., Kariya, K., and Kataoka, T. (2002). Critical function of the Ras-associating domain as a primary Ras-binding site for regulation of Saccharomyces cerevisiae adenylyl cyclase. J Biol Chem *277*, 3117-3123.

Kimura, K., Kawamoto, K., Teranishi, S., and Nishida, T. (2006). Role of Rac1 in fibronectin-induced adhesion and motility of human corneal epithelial cells. Invest Ophthalmol Vis Sci *47*, 4323-4329.

Kissil, J.L., Walmsley, M.J., Hanlon, L., Haigis, K.M., Bender Kim, C.F., Sweet-Cordero, A., Eckman, M.S., Tuveson, D.A., Capobianco, A.J., Tybulewicz, V.L.*, et al.* (2007). Requirement for Rac1 in a K-ras induced lung cancer in the mouse. Cancer Res *67*, 8089-8094.

Kobe, B., and Deisenhofer, J. (1995). Proteins with leucine-rich repeats. Current opinion in structural biology *5*, 409-416.

Kobe, B., and Kajava, A.V. (2001). The leucine-rich repeat as a protein recognition motif. Current opinion in structural biology *11*, 725-732.

Kopecki, Z., Arkell, R., Powell, B.C., and Cowin, A.J. (2009). Flightless I regulates hemidesmosome formation and integrin-mediated cellular adhesion and migration during wound repair. J Invest Dermatol *129*, 2031-2045.

Kopecki, Z., O'Neill, G.M., Arkell, R.M., and Cowin, A.J. (2011). Regulation of focal adhesions by flightless i involves inhibition of paxillin phosphorylation via a Rac1-dependent pathway. J Invest Dermatol *131*, 1450-1459.

Kovac, B., Teo, J.L., Makela, T.P., and Vallenius, T. (2013). Assembly of non-contractile dorsal stress fibers requires alpha-actinin-1 and Rac1 in migrating and spreading cells. J Cell Sci *126*, 263-273.

Krause, S.A., Cundell, M.J., Poon, P.P., McGhie, J., Johnston, G.C., Price, C., and Gray, J.V. (2012). Functional specialisation of yeast Rho1 GTP exchange factors. J Cell Sci *125*, 2721-2731.

Krauthammer, M., Kong, Y., Ha, B.H., Evans, P., Bacchiocchi, A., McCusker, J.P., Cheng, E., Davis, M.J., Goh, G., Choi, M.*, et al.* (2012). Exome sequencing identifies recurrent somatic RAC1 mutations in melanoma. Nature genetics *44*, 1006-1014.

Kreishman-Deitrick, M., Goley, E.D., Burdine, L., Denison, C., Egile, C., Li, R., Murali, N., Kodadek, T.J., Welch, M.D., and Rosen, M.K. (2005). NMR analyses of the activation of the Arp2/3 complex by neuronal Wiskott-Aldrich syndrome protein. Biochemistry *44*, 15247-15256.

Krug, K., Carpy, A., Behrends, G., Matic, K., Soares, N.C., and Macek, B. (2013). Deep coverage of the Escherichia coli proteome enables the assessment of false discovery rates in simple proteogenomic experiments. Mol Cell Proteomics *12*, 3420-3430.

Kuroda, S., Fukata, M., Nakagawa, M., Fujii, K., Nakamura, T., Ookubo, T., Izawa, I., Nagase, T., Nomura, N., Tani, H.*, et al.* (1998). Role of IQGAP1, a target of the small GTPases Cdc42 and Rac1, in regulation of E-cadherin- mediated cell-cell adhesion. Science *281*, 832-835.

Kwiatkowski, D.J. (1999). Functions of gelsolin: motility, signaling, apoptosis, cancer. Curr Opin Cell Biol *11*, 103-108.

Kwiatkowski, D.J., Stossel, T.P., Orkin, S.H., Mole, J.E., Colten, H.R., and Yin, H.L. (1986). Plasma and cytoplasmic gelsolins are encoded by a single gene and contain a duplicated actin-binding domain. Nature *323*, 455-458.

Kwon, T., Kwon, D.Y., Chun, J., Kim, J.H., and Kang, S.S. (2000). Akt protein kinase inhibits Rac1-GTP binding through phosphorylation at serine 71 of Rac1. J Biol Chem *275*, 423-428.

Lai, F.P., Szczodrak, M., Block, J., Faix, J., Breitsprecher, D., Mannherz, H.G., Stradal, T.E., Dunn, G.A., Small, J.V., and Rottner, K. (2008). Arp2/3 complex interactions and actin network turnover in lamellipodia. EMBO J *27*, 982-992.

Lambert, J.M., Lambert, Q.T., Reuther, G.W., Malliri, A., Siderovski, D.P., Sondek, J., Collard, J.G., and Der, C.J. (2002). Tiam1 mediates Ras activation of Rac by a PI(3)K-independent mechanism. Nat Cell Biol *4*, 621-625.

Lammers, M., Meyer, S., Kuhlmann, D., and Wittinghofer, A. (2008). Specificity of interactions between mDia isoforms and Rho proteins. J Biol Chem *283*, 35236-35246.

Lauffenburger, D.A., and Horwitz, A.F. (1996). Cell Migration: A Physically Integrated Molecular Process. Cell *84*, 359-369.

Laukaitis, C.M., Webb, D.J., Donais, K., and Horwitz, A.F. (2001). Differential dynamics of alpha 5 integrin, paxillin, and alpha-actinin during formation and disassembly of adhesions in migrating cells. J Cell Biol *153*, 1427-1440.

Lawson, M.A., and Maxfield, F.R. (1995). Ca(2+)- and calcineurin-dependent recycling of an integrin to the front of migrating neutrophils. Nature *377*, 75-79.

Le Clainche, C., Schlaepfer, D., Ferrari, A., Klingauf, M., Grohmanova, K., Veligodskiy, A., Didry, D., Le, D., Egile, C., Carlier, M.F.*, et al.* (2007). IQGAP1 stimulates actin assembly through the N-WASP-Arp2/3 pathway. J Biol Chem *282*, 426-435.

Lee, Y.H., Campbell, H.D., and Stallcup, M.R. (2004). Developmentally essential protein flightless I is a nuclear receptor coactivator with actin binding activity. Mol Cell Biol *24*, 2103-2117.

Leeuwen, F.N., Kain, H.E., Kammen, R.A., Michiels, F., Kranenburg, O.W., and Collard, J.G. (1997). The guanine nucleotide exchange factor Tiam1 affects neuronal morphology; opposing roles for the small GTPases Rac and Rho. J Cell Biol *139*, 797-807.

Li, F., and Higgs, H.N. (2003). The mouse Formin mDia1 is a potent actin nucleation factor regulated by autoinhibition. Curr Biol *13*, 1335-1340.

Li, F., and Higgs, H.N. (2005). Dissecting requirements for auto-inhibition of actin nucleation by the formin, mDia1. J Biol Chem *280*, 6986-6992.

Lin, C.H., Waters, J.M., Powell, B.C., Arkell, R.M., and Cowin, A.J. (2011). Decreased expression of Flightless I, a gelsolin family member and developmental regulator, in early-gestation fetal wounds improves healing. Mamm Genome *22*, 341-352.

Lindqvist, M., Horn, Z., Bryja, V., Schulte, G., Papachristou, P., Ajima, R., Dyberg, C., Arenas, E., Yamaguchi, T.P., Lagercrantz, H., *et al.* (2010). Vang-like protein 2 and Rac1 interact to regulate adherens junctions. J Cell Sci *123*, 472-483.

Lindsay, C.R., Lawn, S., Campbell, A.D., Faller, W.J., Rambow, F., Mort, R.L., Timpson, P., Li, A., Cammareri, P., Ridgway, R.A., *et al.* (2011). P-Rex1 is required for efficient melanoblast migration and melanoma metastasis. Nat Commun *2*, 555.

Liotta, L.A., and Kohn, E. (2004). Anoikis: cancer and the homeless cell. Nature *430*, 973-974.

Liu, Y.T., and Yin, H.L. (1998). Identification of the binding partners for flightless I, A novel protein bridging the leucine-rich repeat and the gelsolin superfamilies. J Biol Chem *273*, 7920-7927.

Lizarraga, F., Poincloux, R., Romao, M., Montagnac, G., Le Dez, G., Bonne, I., Rigaill, G., Raposo, G., and Chavrier, P. (2009). Diaphanous-related formins are required for invadopodia formation and invasion of breast tumor cells. Cancer Res *69*, 2792-2800.

Lozano, E., Betson, M., and Braga, V.M. (2003). Tumor progression: Small GTPases and loss of cell-cell adhesion. Bioessays *25*, 452-463.

Lozano, E., Frasa, M.A., Smolarczyk, K., Knaus, U.G., and Braga, V.M. (2008). PAK is required for the disruption of E-cadherin adhesion by the small GTPase Rac. J Cell Sci *121*, 933-938.

Lu, M., Witke, W., Kwiatkowski, D.J., and Kosik, K.S. (1997). Delayed retraction of filopodia in gelsolin null mice. J Cell Biol *138*, 1279-1287.

Lynch, E.A., Stall, J., Schmidt, G., Chavrier, P., and D'Souza-Schorey, C. (2006). Proteasome-mediated degradation of Rac1-GTP during epithelial cell scattering. Mol Biol Cell *17*, 2236-2242.

Machacek, M., Hodgson, L., Welch, C., Elliott, H., Pertz, O., Nalbant, P., Abell, A., Johnson, G.L., Hahn, K.M., and Danuser, G. (2009). Coordination of Rho GTPase activities during cell protrusion. Nature *461*, 99-103.

Machaidze, G., Sokoll, A., Shimada, A., Lustig, A., Mazur, A., Wittinghofer, A., Aebi, U., and Mannherz, H.G. (2010). Actin filament bundling and different nucleating effects of mouse Diaphanous-related formin FH2 domains on actin/ADF and actin/cofilin complexes. J Mol Biol *403*, 529-545.

Machesky, L.M., and Li, A. (2010). Fascin: Invasive filopodia promoting metastasis. Communicative & integrative biology *3*, 263-270.

Mack, N.A., Porter, A.P., Whalley, H.J., Schwarz, J.P., Jones, R.C., Khaja, A.S., Bjartell, A., Anderson, K.I., and Malliri, A. (2012). beta2-syntrophin and Par-3 promote an apicobasal Rac activity gradient at cell-cell junctions by differentially regulating Tiam1 activity. Nat Cell Biol *14*, 1169-1180.

Mack, N.A., Whalley, H.J., Castillo-Lluva, S., and Malliri, A. (2011). The diverse roles of Rac signaling in tumorigenesis. Cell Cycle *10*, 1571-1581.

Mallavarapu, A., and Mitchison, T. (1999). Regulated actin cytoskeleton assembly at filopodium tips controls their extension and retraction. J Cell Biol *146*, 1097-1106.

Malliri, A., and Collard, J.G. (2003). Role of Rho-family proteins in cell adhesion and cancer. Curr Opin Cell Biol *15*, 583-589.

Malliri, A., Rygiel, T.P., van der Kammen, R.A., Song, J.Y., Engers, R., Hurlstone, A.F., Clevers, H., and Collard, J.G. (2006). The rac activator Tiam1 is a Wnt-responsive gene that modifies intestinal tumor development. J Biol Chem *281*, 543-548.

Malliri, A., van der Kammen, R.A., Clark, K., van der Valk, M., Michiels, F., and Collard, J.G. (2002). Mice deficient in the Rac activator Tiam1 are resistant to Ras-induced skin tumours. Nature *417*, 867-871.

Malliri, A., van Es, S., Huveneers, S., and Collard, J.G. (2004). The Rac exchange factor Tiam1 is required for the establishment and maintenance of cadherin-based adhesions. J Biol Chem *279*, 30092-30098.

Mann, M. (2006). Functional and quantitative proteomics using SILAC. Nat Rev Mol Cell Biol *7*, 952-958.

Manser, E., Loo, T.H., Koh, C.G., Zhao, Z.S., Chen, X.Q., Tan, L., Tan, I., Leung, T., and Lim, L. (1998). PAK kinases are directly coupled to the PIX family of nucleotide exchange factors. Mol Cell *1*, 183-192.

Matos, P., and Jordan, P. (2006). Rac1, but not Rac1B, stimulates RelB-mediated gene transcription in colorectal cancer cells. J Biol Chem *281*, 13724-13732.

Matsumura, F., Ono, S., Yamakita, Y., Totsukawa, G., and Yamashiro, S. (1998). Specific localization of serine 19 phosphorylated myosin II during cell locomotion and mitosis of cultured cells. J Cell Biol *140*, 119-129.

Matter, K., and Balda, M.S. (2003). Signalling to and from tight junctions. Nat Rev Mol Cell Biol *4*, 225-236.

McCawley, L.J., O'Brien, P., and Hudson, L.G. (1997). Overexpression of the epidermal growth factor receptor contributes to enhanced ligand-mediated motility in keratinocyte cell lines. Endocrinology *138*, 121-127.

McDowall, M.D., Scott, M.S., and Barton, G.J. (2009). PIPs: human protein-protein interaction prediction database. Nucleic Acids Res *37*, D651-656.

McGough, A.M., Staiger, C.J., Min, J.K., and Simonetti, K.D. (2003). The gelsolin family of actin regulatory proteins: modular structures, versatile functions. FEBS Lett *552*, 75-81.

McKinnell, R.G. (2006). The biological basis of cancer, 2nd edn (Cambridge ; New York: Cambridge University Press).

McLaughlin, P.J., Gooch, J.T., Mannherz, H.G., and Weeds, A.G. (1993). Structure of gelsolin segment 1-actin complex and the mechanism of filament severing. Nature *364*, 685-692.

Meller, J., Vidali, L., and Schwartz, M.A. (2008). Endogenous RhoG is dispensable for integrin-mediated cell spreading but contributes to Rac-independent migration. J Cell Sci *121*, 1981-1989.

Mellor, H. (2010). The role of formins in filopodia formation. Biochim Biophys Acta *1803*, 191-200.

Merajver, S.D., and Usmani, S.Z. (2005). Multifaceted role of Rho proteins in angiogenesis. J Mammary Gland Biol Neoplasia *10*, 291-298.

Meredith, J.E., Jr., Fazeli, B., and Schwartz, M.A. (1993). The extracellular matrix as a cell survival factor. Mol Biol Cell *4*, 953-961.

Mertens, A.E., Roovers, R.C., and Collard, J.G. (2003). Regulation of Tiam1-Rac signalling. FEBS Lett *546*, 11-16.

Mettouchi, A., and Lemichez, E. (2012). Ubiquitylation of active Rac1 by the E3 ubiquitin-ligase HACE1. Small GTPases *3*, 102-106.

Meyer, D.K., Olenik, C., Hofmann, F., Barth, H., Leemhuis, J., Brunig, I., Aktories, K., and Norenberg, W. (2000). Regulation of somatodendritic GABAA receptor channels in rat hippocampal neurons: evidence for a role of the small GTPase Rac1. J Neurosci *20*, 6743-6751.

Michiels, F., Habets, G.G., Stam, J.C., van der Kammen, R.A., and Collard, J.G. (1995). A role for Rac in Tiam1-induced membrane ruffling and invasion. Nature *375*, 338-340.

Miki, H., Yamaguchi, H., Suetsugu, S., and Takenawa, T. (2000). IRSp53 is an essential intermediate between Rac and WAVE in the regulation of membrane ruffling. Nature *408*, 732-735.

Miklos, G.L., and De Couet, H.G. (1990). The mutations previously designated as flightless-I3, flightless-O2 and standby are members of the W-2 lethal complementation group at the base of the X-chromosome of Drosophila melanogaster. Journal of neurogenetics *6*, 133-151.

Minard, M.E., Herynk, M.H., Collard, J.G., and Gallick, G.E. (2005). The guanine nucleotide exchange factor Tiam1 increases colon carcinoma growth at metastatic sites in an orthotopic nude mouse model. Oncogene *24*, 2568-2573.

Minard, M.E., Kim, L.S., Price, J.E., and Gallick, G.E. (2004). The role of the guanine nucleotide exchange factor Tiam1 in cellular migration, invasion, adhesion and tumor progression. Breast Cancer Res Treat *84*, 21-32.

Mishra, V.S., Henske, E.P., Kwiatkowski, D.J., and Southwick, F.S. (1994). The human actin-regulatory protein cap G: gene structure and chromosome location. Genomics *23*, 560-565.

Mohammad, I., Arora, P.D., Naghibzadeh, Y., Wang, Y., Li, J., Mascarenhas, W., Janmey, P.A., Dawson, J.F., and McCulloch, C.A. (2012). Flightless I is a focal adhesion-associated actin-capping protein that regulates cell migration. FASEB J *26*, 3260-3272.

Montero, J.C., Seoane, S., Ocana, A., and Pandiella, A. (2011). P-Rex1 participates in Neuregulin-ErbB signal transduction and its expression correlates with patient outcome in breast cancer. Oncogene *30*, 1059-1071.

Moon, S.Y., and Zheng, Y. (2003). Rho GTPase-activating proteins in cell regulation. Trends Cell Biol *13*, 13-22.

Morimura, S., and Takahashi, K. (2011). Rac1 and Stathmin but Not EB1 Are Required for Invasion of Breast Cancer Cells in Response to IGF-I. International journal of cell biology *2011*, 615912.

Moriyama, T., Kataoka, H., Hamasuna, R., Yoshida, E., Sameshima, T., Iseda, T., Yokogami, K., Nakano, S., Koono, M., and Wakisaka, S. (1999). Simultaneous up-regulation of urokinase-type plasminogen activator (uPA) and uPA receptor by hepatocyte growth factor/scatter factor in human glioma cells. Clin Exp Metastasis *17*, 873-879.

Mullins, R.D., Heuser, J.A., and Pollard, T.D. (1998). The interaction of Arp2/3 complex with actin: nucleation, high affinity pointed end capping, and formation of branching networks of filaments. Proc Natl Acad Sci U S A *95*, 6181-6186.

Nabeshima, K., Inoue, T., Shimao, Y., and Sameshima, T. (2002). Matrix metalloproteinases in tumor invasion: role for cell migration. Pathology international *52*, 255-264.

Nakagawa, M., Fukata, M., Yamaga, M., Itoh, N., and Kaibuchi, K. (2001). Recruitment and activation of Rac1 by the formation of E-cadherin-mediated cell-cell adhesion sites. J Cell Sci *114*, 1829-1838.

Narumiya, S., Tanji, M., and Ishizaki, T. (2009). Rho signaling, ROCK and mDia1, in transformation, metastasis and invasion. Cancer metastasis reviews *28*, 65-76.

Nie, B., Cheng, N., Dinauer, M.C., and Ye, R.D. (2010). Characterization of P-Rex1 for its role in fMet-Leu-Phe-induced superoxide production in reconstituted COS(phox) cells. Cell Signal *22*, 770-782.

Nieman, M.T., Prudoff, R.S., Johnson, K.R., and Wheelock, M.J. (1999). N-cadherin promotes motility in human breast cancer cells regardless of their E-cadherin expression. J Cell Biol *147*, 631-644.

Nishimura, K., Matsumiya, K., Miura, H., Tsujimura, A., Nonomura, N., Matsumoto, K., Nakamura, T., and Okuyama, A. (2003a). Effects of hepatocyte growth factor on urokinase-type plasminogen activator (uPA) and uPA receptor in DU145 prostate cancer cells. International journal of andrology *26*, 175-179.

Nishimura, K., Ting, H.J., Harada, Y., Tokizane, T., Nonomura, N., Kang, H.Y., Chang, H.C., Yeh, S., Miyamoto, H., Shin, M.*, et al.* (2003b). Modulation of androgen receptor transactivation by gelsolin: a newly identified androgen receptor coregulator. Cancer Res *63*, 4888-4894.

Nobes, C.D., and Hall, A. (1995). Rho, rac, and cdc42 GTPases regulate the assembly of multimolecular focal complexes associated with actin stress fibers, lamellipodia, and filopodia. Cell *81*, 53-62.

Nobes, C.D., and Hall, A. (1999). Rho GTPases control polarity, protrusion, and adhesion during cell movement. J Cell Biol *144*, 1235-1244.

Nola, S., Daigaku, R., Smolarczyk, K., Carstens, M., Martin-Martin, B., Longmore, G., Bailly, M., and Braga, V.M. (2011). Ajuba is required for Rac activation and maintenance of E-cadherin adhesion. J Cell Biol *195*, 855-871.

Nomanbhoy, T.K., and Cerione, R. (1996). Characterization of the interaction between RhoGDI and Cdc42Hs using fluorescence spectroscopy. J Biol Chem *271*, 10004-10009.

Oak, S.A., Zhou, Y.W., and Jarrett, H.W. (2003). Skeletal muscle signaling pathway through the dystrophin glycoprotein complex and Rac1. J Biol Chem *278*, 39287-39295.

Olofsson, B. (1999). Rho guanine dissociation inhibitors: pivotal molecules in cellular signalling. Cell Signal *11*, 545-554.

Onder, T.T., Gupta, P.B., Mani, S.A., Yang, J., Lander, E.S., and Weinberg, R.A. (2008). Loss of E-cadherin promotes metastasis via multiple downstream transcriptional pathways. Cancer Res *68*, 3645-3654.

Ong, S.E., Blagoev, B., Kratchmarova, I., Kristensen, D.B., Steen, H., Pandey, A., and Mann, M. (2002). Stable isotope labeling by amino acids in cell culture, SILAC, as a simple and accurate approach to expression proteomics. Mol Cell Proteomics *1*, 376-386.

Ong, S.E., and Mann, M. (2005). Mass spectrometry-based proteomics turns quantitative. Nature chemical biology *1*, 252-262.

Onoda, K., Yu, F.X., and Yin, H.L. (1993). gCap39 is a nuclear and cytoplasmic protein. Cell Motil Cytoskeleton *26*, 227-238.

Oser, M., Yamaguchi, H., Mader, C.C., Bravo-Cordero, J.J., Arias, M., Chen, X., Desmarais, V., van Rheenen, J., Koleske, A.J., and Condeelis, J. (2009). Cortactin regulates cofilin and N-WASp activities to control the stages of invadopodium assembly and maturation. J Cell Biol *186*, 571-587.

Palecek, S.P., Huttenlocher, A., Horwitz, A.F., and Lauffenburger, D.A. (1998). Physical and biochemical regulation of integrin release during rear detachment of migrating cells. J Cell Sci *111 (Pt 7)*, 929-940.

Pan, Y., Bi, F., Liu, N., Xue, Y., Yao, X., Zheng, Y., and Fan, D. (2004). Expression of seven main Rho family members in gastric carcinoma. Biochem Biophys Res Commun *315*, 686-691.

Park, M., Dean, M., Cooper, C.S., Schmidt, M., O'Brien, S.J., Blair, D.G., and Vande Woude, G.F. (1986). Mechanism of met oncogene activation. Cell *45*, 895-904.

Parri, M., and Chiarugi, P. (2010). Rac and Rho GTPases in cancer cell motility control. Cell Communication and Signaling *8*.

Pechlivanis, M., and Kuhlmann, J. (2006). Hydrophobic modifications of Ras proteins by isoprenoid groups and fatty acids--More than just membrane anchoring. Biochim Biophys Acta *1764*, 1914-1931.

Pelikan-Conchaudron, A., Le Clainche, C., Didry, D., and Carlier, M.F. (2011). The IQGAP1 protein is a calmodulin-regulated barbed end capper of actin filaments: possible implications in its function in cell migration. J Biol Chem *286*, 35119-35128.

Pellieux, C., Desgeorges, A., Pigeon, C.H., Chambaz, C., Yin, H., Hayoz, D., and Silacci, P. (2003). Cap G, a gelsolin family protein modulating protective effects of unidirectional shear stress. J Biol Chem *278*, 29136-29144.

Perl, A.K., Wilgenbus, P., Dahl, U., Semb, H., and Christofori, G. (1998). A causal role for E-cadherin in the transition from adenoma to carcinoma. Nature *392*, 190-193.

Perrimon, N., Smouse, D., and Miklos, G.L. (1989). Developmental genetics of loci at the base of the X chromosome of Drosophila melanogaster. Genetics *121*, 313-331.

Pertz, O. (2010). Spatio-temporal Rho GTPase signaling - where are we now? J Cell Sci *123*, 1841-1850.

Pertz, O., Hodgson, L., Klemke, R.L., and Hahn, K.M. (2006). Spatiotemporal dynamics of RhoA activity in migrating cells. Nature *440*, 1069-1072.

Pescatore, L.A., Bonatto, D., Forti, F.L., Sadok, A., Kovacic, H., and Laurindo, F.R. (2012). Protein disulfide isomerase is required for platelet-derived growth factor-induced vascular smooth muscle cell migration, Nox1 NADPH oxidase expression, and RhoGTPase activation. J Biol Chem *287*, 29290-29300.

Pestonjamasp, K.N., Pope, R.K., Wulfkuhle, J.D., and Luna, E.J. (1997). Supervillin (p205): A novel membrane-associated, F-actin-binding protein in the villin/gelsolin superfamily. J Cell Biol *139*, 1255-1269.

Pollard, T.D., Blanchoin, L., and Mullins, R.D. (2000). Molecular mechanisms controlling actin filament dynamics in nonmuscle cells. Annu Rev Biophys Biomol Struct *29*, 545-576.

Pollard, T.D., and Cooper, J.A. (2009). Actin, a central player in cell shape and movement. Science *326*, 1208-1212.

Potter, D.A., Tirnauer, J.S., Janssen, R., Croall, D.E., Hughes, C.N., Fiacco, K.A., Mier, J.W., Maki, M., and Herman, I.M. (1998). Calpain regulates actin remodeling during cell spreading. J Cell Biol *141*, 647-662.

Prasad, T.S., Kandasamy, K., and Pandey, A. (2009). Human Protein Reference Database and Human Proteinpedia as discovery tools for systems biology. Methods Mol Biol *577*, 67-79.

Prendergast, G.C., and Ziff, E.B. (1991). Mbh 1: a novel gelsolin/severin-related protein which binds actin in vitro and exhibits nuclear localization in vivo. EMBO J *10*, 757-766.

Preudhomme, C., Roumier, C., Hildebrand, M.P., Dallery-Prudhomme, E., Lantoine, D., Lai, J.L., Daudignon, A., Adenis, C., Bauters, F., Fenaux, P., *et al.* (2000). Nonrandom 4p13 rearrangements of the RhoH/TTF gene, encoding a GTP-binding protein, in non-Hodgkin's lymphoma and multiple myeloma. Oncogene *19*, 2023-2032.

Price, L.S., Leng, J., Schwartz, M.A., and Bokoch, G.M. (1998). Activation of Rac and Cdc42 by integrins mediates cell spreading. Mol Biol Cell *9*, 1863-1871.

Pruyne, D., Evangelista, M., Yang, C., Bi, E., Zigmond, S., Bretscher, A., and Boone, C. (2002). Role of formins in actin assembly: nucleation and barbed-end association. Science *297*, 612-615.

Qin, J., Xie, Y., Wang, B., Hoshino, M., Wolff, D.W., Zhao, J., Scofield, M.A., Dowd, F.J., Lin, M.F., and Tu, Y. (2009). Upregulation of PIP3-dependent Rac exchanger 1 (P-Rex1) promotes prostate cancer metastasis. Oncogene *28*, 1853-1863.

Rajagopal, S., Ji, Y., Xu, K., Li, Y., Wicks, K., Liu, J., Wong, K.W., Herman, I.M., Isberg, R.R., and Buchsbaum, R.J. (2010). Scaffold proteins IRSp53 and spinophilin regulate localized Rac activation by T-lymphocyte invasion and metastasis protein 1 (TIAM1). J Biol Chem *285*, 18060-18071.

Rechsteiner, M. (1990). PEST sequences are signals for rapid intracellular proteolysis. Seminars in cell biology *1*, 433-440.

Regen, C.M., and Horwitz, A.F. (1992). Dynamics of beta 1 integrin-mediated adhesive contacts in motile fibroblasts. J Cell Biol *119*, 1347-1359.

Ren, G., Crampton, M.S., and Yap, A.S. (2009). Cortactin: Coordinating adhesion and the actin cytoskeleton at cellular protrusions. Cell Motil Cytoskeleton *66*, 865-873.

Ridley, A.J. (2001). Rho family proteins: coordinating cell responses. Trends in Cell Biology *11*, 471-477.

Ridley, A.J. (2011). Life at the leading edge. Cell *145*, 1012-1022.

Ridley, A.J., Comoglio, P.M., and Hall, A. (1995). Regulation of scatter factor/hepatocyte growth factor responses by Ras, Rac, and Rho in MDCK cells. Mol Cell Biol *15*, 1110-1122.

Ridley, A.J., Schwartz, M.A., Burridge, K., Firtel, R.A., Ginsberg, M.H., Borisy, G., Parsons, J.T., and Horwitz, A.R. (2003). Cell migration: integrating signals from front to back. Science *302*, 1704-1709.

Rigaut, G., Shevchenko, A., Rutz, B., Wilm, M., Mann, M., and Seraphin, B. (1999). A generic protein purification method for protein complex characterization and proteome exploration. Nat Biotechnol *17*, 1030-1032.

Rijken, P.J., Hage, W.J., van Bergen en Henegouwen, P.M., Verkleij, A.J., and Boonstra, J. (1991). Epidermal growth factor induces rapid reorganization of the actin microfilament system in human A431 cells. J Cell Sci *100 (Pt 3)*, 491-499.

Roberts, A.W., Kim, C., Zhen, L., Lowe, J.B., Kapur, R., Petryniak, B., Spaetti, A., Pollock, J.D., Borneo, J.B., Bradford, G.B., *et al.* (1999). Deficiency of the hematopoietic cell-specific Rho family GTPase Rac2 is characterized by abnormalities in neutrophil function and host defense. Immunity *10*, 183-196.

Rodal, A.A., Sokolova, O., Robins, D.B., Daugherty, K.M., Hippenmeyer, S., Riezman, H., Grigorieff, N., and Goode, B.L. (2005). Conformational changes in the Arp2/3 complex leading to actin nucleation. Nature structural & molecular biology *12*, 26-31.

Rossman, K.L., Der, C.J., and Sondek, J. (2005). GEF means go: turning on RHO GTPases with guanine nucleotide-exchange factors. Nat Rev Mol Cell Biol *6*, 167-180.

Rottner, K., Hall, A., and Small, J.V. (1999). Interplay between Rac and Rho in the control of substrate contact dynamics. Curr Biol *9*, 640-648.

Roy, B.C., Kakinuma, N., and Kiyama, R. (2009). Kank attenuates actin remodeling by preventing interaction between IRSp53 and Rac1. J Cell Biol *184*, 253-267.

Royal, I., Lamarche-Vane, N., Lamorte, L., Kaibuchi, K., and Park, M. (2000). Activation of cdc42, rac, PAK, and rho-kinase in response to hepatocyte growth factor differentially regulates epithelial cell colony spreading and dissociation. Mol Biol Cell *11*, 1709-1725.

Sagot, I., Rodal, A.A., Moseley, J., Goode, B.L., and Pellman, D. (2002). An actin nucleation mechanism mediated by Bni1 and profilin. Nat Cell Biol *4*, 626-631.

Sahai, E. (2007). Illuminating the metastatic process. Nat Rev Cancer *7*, 737-749.

Sahai, E., and Marshall, C.J. (2002). RHO-GTPases and cancer. Nat Rev Cancer *2*, 133-142.

Sahai, E., and Marshall, C.J. (2003). Differing modes of tumour cell invasion have distinct requirements for Rho/ROCK signalling and extracellular proteolysis. Nature Cell Biology *5*, 711-719.

Sampson, E.R., Yeh, S.Y., Chang, H.C., Tsai, M.Y., Wang, X., Ting, H.J., and Chang, C. (2001). Identification and characterization of androgen receptor associated coregulators in prostate cancer cells. Journal of biological regulators and homeostatic agents *15*, 123-129.

Sander, E.E., ten Klooster, J.P., van Delft, S., van der Kammen, R.A., and Collard, J.G. (1999). Rac downregulates Rho activity: reciprocal balance between both GTPases determines cellular morphology and migratory behavior. J Cell Biol *147*, 1009-1022.

Sander, E.E., van Delft, S., ten Klooster, J.P., Reid, T., van der Kammen, R.A., Michiels, F., and Collard, J.G. (1998). Matrix-dependent Tiam1/Rac signaling in epithelial cells promotes either cell-cell adhesion or cell migration and is regulated by phosphatidylinositol 3-kinase. J Cell Biol *143*, 1385-1398.

Sarmiento, C., Wang, W., Dovas, A., Yamaguchi, H., Sidani, M., El-Sibai, M., Desmarais, V., Holman, H.A., Kitchen, S., Backer, J.M., *et al.* (2008). WASP family members and formin proteins coordinate regulation of cell protrusions in carcinoma cells. J Cell Biol *180*, 1245-1260.

Schmidt, A., and Hall, A. (2002). Guanine nucleotide exchange factors for Rho GTPases: turning on the switch. Genes Dev *16*, 1587-1609.

Schmidt, C.E., Horwitz, A.F., Lauffenburger, D.A., and Sheetz, M.P. (1993). Integrin-cytoskeletal interactions in migrating fibroblasts are dynamic, asymmetric, and regulated. J Cell Biol *123*, 977-991.

Schnelzer, A., Prechtel, D., Knaus, U., Dehne, K., Gerhard, M., Graeff, H., Harbeck, N., Schmitt, M., and Lengyel, E. (2000). Rac1 in human breast cancer: overexpression, mutation analysis, and characterization of a new isoform, Rac1b. Oncogene *19*, 3013-3020.

Schoumacher, M., Goldman, R.D., Louvard, D., and Vignjevic, D.M. (2010). Actin, microtubules, and vimentin intermediate filaments cooperate for elongation of invadopodia. J Cell Biol *189*, 541-556.

Schulze, W.X., and Mann, M. (2004). A novel proteomic screen for peptide-protein interactions. J Biol Chem *279*, 10756-10764.

Scott, L.A., Vass, J.K., Parkinson, E.K., Gillespie, D.A., Winnie, J.N., and Ozanne, B.W. (2004). Invasion of normal human fibroblasts induced by v-Fos is independent of proliferation, immortalization, and the tumor suppressors p16INK4a and p53. Mol Cell Biol *24*, 1540-1559.

Scott, M.S., and Barton, G.J. (2007). Probabilistic prediction and ranking of human protein-protein interactions. BMC bioinformatics *8*, 239.

Seward, M.E., Easley, C.A.t., McLeod, J.J., Myers, A.L., and Tombes, R.M. (2008). Flightless-I, a gelsolin family member and transcriptional regulator, preferentially binds directly to activated cytosolic CaMK-II. FEBS Lett *582*, 2489-2495.

Shan, L., Li, J., Wei, M., Ma, J., Wan, L., Zhu, W., Li, Y., Zhu, H., Arnold, J.M., and Peng, T. (2010). Disruption of Rac1 signaling reduces ischemia-reperfusion injury in the diabetic heart by inhibiting calpain. Free Radic Biol Med *49*, 1804-1814.

Shirsat, N.V., Pignolo, R.J., Kreider, B.L., and Rovera, G. (1990). A member of the ras gene superfamily is expressed specifically in T, B and myeloid hemopoietic cells. Oncogene *5*, 769-772.

Sieburth, D.S., Sun, Q., and Han, M. (1998). SUR-8, a conserved Ras-binding protein with leucine-rich repeats, positively regulates Ras-mediated signaling in C. elegans. Cell *94*, 119-130.

Silacci, P., Mazzolai, L., Gauci, C., Stergiopulos, N., Yin, H.L., and Hayoz, D. (2004). Gelsolin superfamily proteins: key regulators of cellular functions. Cell Mol Life Sci *61*, 2614-2623.

Sosa, M.S., Lopez-Haber, C., Yang, C., Wang, H., Lemmon, M.A., Busillo, J.M., Luo, J., Benovic, J.L., Klein-Szanto, A., Yagi, H., *et al.* (2010). Identification of the Rac-GEF P-Rex1 as an essential mediator of ErbB signaling in breast cancer. Mol Cell *40*, 877-892.

Stam, J.C., Sander, E.E., Michiels, F., van Leeuwen, F.N., Kain, H.E., van der Kammen, R.A., and Collard, J.G. (1997). Targeting of Tiam1 to the plasma membrane requires the cooperative function of the N-terminal pleckstrin homology domain and an adjacent protein interaction domain. J Biol Chem *272*, 28447-28454.

Stoker, M., Gherardi, E., Perryman, M., and Gray, J. (1987). Scatter factor is a fibroblast-derived modulator of epithelial cell mobility. Nature *327*, 239-242.

Stransky, N., Egloff, A.M., Tward, A.D., Kostic, A.D., Cibulskis, K., Sivachenko, A., Kryukov, G.V., Lawrence, M.S., Sougnez, C., McKenna, A., *et al.* (2011). The mutational landscape of head and neck squamous cell carcinoma. Science *333*, 1157-1160.

Straub, K.L., Stella, M.C., and Leptin, M. (1996). The gelsolin-related flightless I protein is required for actin distribution during cellularisation in Drosophila. J Cell Sci *109 (Pt 1)*, 263-270.

Sudhakar, A. (2009). History of Cancer, Ancient and Modern Treatment Methods. Journal of cancer science & therapy *1*, 1-4.

Sullivan, S.J., Daukas, G., and Zigmond, S.H. (1984). Asymmetric distribution of the chemotactic peptide receptor on polymorphonuclear leukocytes. J Cell Biol *99*, 1461-1467.

Sun, H.Q., Kwiatkowska, K., Wooten, D.C., and Yin, H.L. (1995). Effects of CapG overexpression on agonist-induced motility and second messenger generation. J Cell Biol *129*, 147-156.

Sun, Z., Huang, S., Li, Z., and Meininger, G.A. (2012). Zyxin is involved in regulation of mechanotransduction in arteriole smooth muscle cells. Front Physiol *3*, 472.

Svitkina, T.M., and Borisy, G.G. (1999). Arp2/3 complex and actin depolymerizing factor/cofilin in dendritic organization and treadmilling of actin filament array in lamellipodia. J Cell Biol *145*, 1009-1026.

Syed, Z.A., Yin, W., Hughes, K., Gill, J.N., Shi, R., and Clifford, J.L. (2011). HGF/c-met/Stat3 signaling during skin tumor cell invasion: indications for a positive feedback loop. BMC cancer *11*, 180.

Takahashi, K., and Suzuki, K. (2008). Requirement of kinesin-mediated membrane transport of WAVE2 along microtubules for lamellipodia formation promoted by hepatocyte growth factor. Exp Cell Res *314*, 2313-2322.

Takenawa, T., and Miki, H. (2001). WASP and WAVE family proteins: key molecules for rapid rearrangement of cortical actin filaments and cell movement. J Cell Sci *114*, 1801-1809.

Takenawa, T., and Suetsugu, S. (2007). The WASP-WAVE protein network: connecting the membrane to the cytoskeleton. Nat Rev Mol Cell Biol *8*, 37-48.

Tarin, D., Thompson, E.W., and Newgreen, D.F. (2005). The fallacy of epithelial mesenchymal transition in neoplasia. Cancer Res *65*, 5996-6000; discussion 6000-5991.

Teng, T.S., Lin, B., Manser, E., Ng, D.C., and Cao, X. (2009). Stat3 promotes directional cell migration by regulating Rac1 activity via its activator betaPIX. J Cell Sci *122*, 4150-4159.

Thiery, J.P. (2002). Epithelial-mesenchymal transitions in tumour progression. Nat Rev Cancer *2*, 442-454.

Thiery, J.P., and Sleeman, J.P. (2006). Complex networks orchestrate epithelial-mesenchymal transitions. Nat Rev Mol Cell Biol *7*, 131-142.

Thompson, E.W., Newgreen, D.F., and Tarin, D. (2005). Carcinoma invasion and metastasis: a role for epithelial-mesenchymal transition? Cancer Res *65*, 5991-5995; discussion 5995.

Ting, H.J., Yeh, S., Nishimura, K., and Chang, C. (2002). Supervillin associates with androgen receptor and modulates its transcriptional activity. Proc Natl Acad Sci U S A *99*, 661-666.

Toda, T., Uno, I., Ishikawa, T., Powers, S., Kataoka, T., Broek, D., Cameron, S., Broach, J., Matsumoto, K., and Wigler, M. (1985). In yeast, RAS proteins are controlling elements of adenylate cyclase. Cell *40*, 27-36.

Tolias, K.F., Bikoff, J.B., Burette, A., Paradis, S., Harrar, D., Tavazoie, S., Weinberg, R.J., and Greenberg, M.E. (2005). The Rac1-GEF Tiam1 couples the NMDA receptor to the activity-dependent development of dendritic arbors and spines. Neuron *45*, 525-538.

Torrino, S., Visvikis, O., Doye, A., Boyer, L., Stefani, C., Munro, P., Bertoglio, J., Gacon, G., Mettouchi, A., and Lemichez, E. (2011). The E3 ubiquitin-ligase HACE1 catalyzes the ubiquitylation of active Rac1. Dev Cell *21*, 959-965.

Totsukawa, G., Yamakita, Y., Yamashiro, S., Hartshorne, D.J., Sasaki, Y., and Matsumura, F. (2000). Distinct roles of ROCK (Rho-kinase) and MLCK in spatial regulation of MLC phosphorylation for assembly of stress fibers and focal adhesions in 3T3 fibroblasts. J Cell Biol *150*, 797-806.

Twombly, R. (2003). New carcinogen list includes estrogen, UV radiation. J Natl Cancer Inst *95*, 185-186.

Uhlenbrock, K., Eberth, A., Herbrand, U., Daryab, N., Stege, P., Meier, F., Friedl, P., Collard, J.G., and Ahmadian, M.R. (2004). The RacGEF Tiam1 inhibits migration and invasion of metastatic melanoma via a novel adhesive mechanism. J Cell Sci *117*, 4863-4871.

Urban, E., Jacob, S., Nemethova, M., Resch, G.P., and Small, J.V. (2010). Electron tomography reveals unbranched networks of actin filaments in lamellipodia. Nat Cell Biol *12*, 429-435.

Vaghi, V., Pennucci, R., Talpo, F., Corbetta, S., Montinaro, V., Barone, C., Croci, L., Spaiardi, P., Consalez, G.G., Biella, G., *et al.* (2014). Rac1 and rac3 GTPases control synergistically the development of cortical and hippocampal GABAergic interneurons. Cerebral cortex *24*, 1247-1258.

Valencia, A., Chardin, P., Wittinghofer, A., and Sander, C. (1991). The ras protein family: evolutionary tree and role of conserved amino acids. Biochemistry *30*, 4637-4648.

van Leeuwen, F.N., van Delft, S., Kain, H.E., van der Kammen, R.A., and Collard, J.G. (1999). Rac regulates phosphorylation of the myosin-II heavy chain, actinomyosin disassembly and cell spreading. Nat Cell Biol *1*, 242-248.

van Rheenen, J., Condeelis, J., and Glogauer, M. (2009). A common cofilin activity cycle in invasive tumor cells and inflammatory cells. J Cell Sci *122*, 305-311.

Vaughan, L., Tan, C.T., Chapman, A., Nonaka, D., Mack, N.A., Smith, D., Booton, R., Hurlstone, A.F., and Malliri, A. (2015). HUWE1 Ubiquitylates and Degrades the RAC Activator TIAM1 Promoting Cell-Cell Adhesion Disassembly, Migration, and Invasion. Cell reports *10*, 88-102.

Vidal-Quadras, M., Gelabert-Baldrich, M., Soriano-Castell, D., Llado, A., Rentero, C., Calvo, M., Pol, A., Enrich, C., and Tebar, F. (2011). Rac1 and calmodulin interactions modulate dynamics of ARF6-dependent endocytosis. Traffic *12*, 1879-1896.

Villace, P., Marion, R.M., and Ortin, J. (2004). The composition of Staufen-containing RNA granules from human cells indicates their role in the regulated transport and translation of messenger RNAs. Nucleic Acids Res *32*, 2411-2420.

Vincent, S., Jeanteur, P., and Fort, P. (1992). Growth-regulated expression of rhoG, a new member of the ras homolog gene family. Mol Cell Biol *12*, 3138-3148.

Visvikis, O., Lores, P., Boyer, L., Chardin, P., Lemichez, E., and Gacon, G. (2008). Activated Rac1, but not the tumorigenic variant Rac1b, is ubiquitinated on Lys 147 through a JNK-regulated process. FEBS J *275*, 386-396.

Voulgari, A., and Pintzas, A. (2009). Epithelial-mesenchymal transition in cancer metastasis: mechanisms, markers and strategies to overcome drug resistance in the clinic. Biochim Biophys Acta *1796*, 75-90.

Wang, G., Yan, Q., Woods, A., Aubrey, L.A., Feng, Q., and Beier, F. (2011). Inducible nitric oxide synthase-nitric oxide signaling mediates the mitogenic activity of Rac1 during endochondral bone growth. J Cell Sci *124*, 3405-3413.

Wang, J., Dai, J.M., Che, Y.L., Gao, Y.M., Peng, H.J., Liu, B., Wang, H., and Linghu, H. (2014). Elmo1 helps dock180 to regulate Rac1 activity and cell migration of ovarian cancer. International journal of gynecological cancer : official journal of the International Gynecological Cancer Society *24*, 844-850.

Wang, S., Watanabe, T., Noritake, J., Fukata, M., Yoshimura, T., Itoh, N., Harada, T., Nakagawa, M., Matsuura, Y., Arimura, N., *et al.* (2007). IQGAP3, a novel effector of Rac1 and Cdc42, regulates neurite outgrowth. J Cell Sci *120*, 567-577.

Watabe-Uchida, M., John, K.A., Janas, J.A., Newey, S.E., and Van Aelst, L. (2006). The Rac activator DOCK7 regulates neuronal polarity through local phosphorylation of stathmin/Op18. Neuron *51*, 727-739.

Webb, D.J., Donais, K., Whitmore, L.A., Thomas, S.M., Turner, C.E., Parsons, J.T., and Horwitz, A.F. (2004). FAK-Src signalling through paxillin, ERK and MLCK regulates adhesion disassembly. Nat Cell Biol *6*, 154-161.

Weber, A., Pennise, C.R., Babcock, G.G., and Fowler, V.M. (1994). Tropomodulin caps the pointed ends of actin filaments. J Cell Biol *127*, 1627-1635.

Wehrle-Haller, B., and Imhof, B.A. (2003). Actin, microtubules and focal adhesion dynamics during cell migration. Int J Biochem Cell Biol *35*, 39-50.

Weinberg, R.A. (2007). The biology of cancer (New York ; Abingdon: Garland Science).

Welch, H.C., Coadwell, W.J., Ellson, C.D., Ferguson, G.J., Andrews, S.R., Erdjument-Bromage, H., Tempst, P., Hawkins, P.T., and Stephens, L.R. (2002). P-Rex1, a PtdIns(3,4,5)P3- and Gbetagamma-regulated guanine-nucleotide exchange factor for Rac. Cell *108*, 809-821.

Welch, H.C., Condliffe, A.M., Milne, L.J., Ferguson, G.J., Hill, K., Webb, L.M., Okkenhaug, K., Coadwell, W.J., Andrews, S.R., Thelen, M., *et al.* (2005). P-Rex1 regulates neutrophil function. Curr Biol *15*, 1867-1873.

Welch, M.D., and Mullins, R.D. (2002). Cellular control of actin nucleation. Annu Rev Cell Dev Biol *18*, 247-288.

Westermarck, J., and Kahari, V.M. (1999). Regulation of matrix metalloproteinase expression in tumor invasion. FASEB J *13*, 781-792.

White, C.D., Brown, M.D., and Sacks, D.B. (2009). IQGAPs in cancer: a family of scaffold proteins underlying tumorigenesis. FEBS Lett *583*, 1817-1824.

Wicki, A., Lehembre, F., Wick, N., Hantusch, B., Kerjaschki, D., and Christofori, G. (2006). Tumor invasion in the absence of epithelial-mesenchymal transition: podoplanin-mediated remodeling of the actin cytoskeleton. Cancer cell *9*, 261-272.

Wilson, C.A., Tsuchida, M.A., Allen, G.M., Barnhart, E.L., Applegate, K.T., Yam, P.T., Ji, L., Keren, K., Danuser, G., and Theriot, J.A. (2010). Myosin II contributes to cell-scale actin network treadmilling through network disassembly. Nature *465*, 373-377.

Witke, W., Li, W., Kwiatkowski, D.J., and Southwick, F.S. (2001). Comparisons of CapG and gelsolin-null macrophages: demonstration of a unique role for CapG in receptor-mediated ruffling, phagocytosis, and vesicle rocketing. J Cell Biol *154*, 775-784.

Wolf, K., Mazo, I., Leung, H., Engelke, K., von Andrian, U.H., Deryugina, E.I., Strongin, A.Y., Brocker, E.B., and Friedl, P. (2003). Compensation mechanism in tumor cell migration: mesenchymal-amoeboid transition after blocking of pericellular proteolysis. Journal of Cell Biology *160*, 267-277.

Wolf, K., Wu, Y.I., Liu, Y., Geiger, J., Tam, E., Overall, C., Stack, M.S., and Friedl, P. (2007). Multi-step pericellular proteolysis controls the transition from individual to collective cancer cell invasion. Nat Cell Biol *9*, 893-904.

Worthylake, D.K., Rossman, K.L., and Sondek, J. (2000). Crystal structure of Rac1 in complex with the guanine nucleotide exchange region of Tiam1. Nature *408*, 682-688.

Wu, Y.I., Frey, D., Lungu, O.I., Jaehrig, A., Schlichting, I., Kuhlman, B., and Hahn, K.M. (2009). A genetically encoded photoactivatable Rac controls the motility of living cells. Nature *461*, 104-108.

Wulfkuhle, J.D., Donina, I.E., Stark, N.H., Pope, R.K., Pestonjamasp, K.N., Niswonger, M.L., and Luna, E.J. (1999). Domain analysis of supervillin, an F-actin bundling plasma membrane protein with functional nuclear localization signals. J Cell Sci *112 (Pt 13)*, 2125-2136.

Wyckoff, J., Wang, W., Lin, E.Y., Wang, Y., Pixley, F., Stanley, E.R., Graf, T., Pollard, J.W., Segall, J., and Condeelis, J. (2004). A paracrine loop between tumor cells and macrophages is required for tumor cell migration in mammary tumors. Cancer Res *64*, 7022-7029.

Wyckoff, J.B., Jones, J.G., Condeelis, J.S., and Segall, J.E. (2000). A critical step in metastasis: in vivo analysis of intravasation at the primary tumor. Cancer Res *60*, 2504-2511.

Wyckoff, J.B., Wang, Y., Lin, E.Y., Li, J.F., Goswami, S., Stanley, E.R., Segall, J.E., Pollard, J.W., and Condeelis, J. (2007). Direct visualization of macrophage-assisted tumor cell intravasation in mammary tumors. Cancer Res *67*, 2649-2656.

Xie, T.X., Wei, D., Liu, M., Gao, A.C., Ali-Osman, F., Sawaya, R., and Huang, S. (2004). Stat3 activation regulates the expression of matrix metalloproteinase-2 and tumor invasion and metastasis. Oncogene *23*, 3550-3560.

Xu, J., Rodriguez, D., Petitclerc, E., Kim, J.J., Hangai, M., Moon, Y.S., Davis, G.E., and Brooks, P.C. (2001). Proteolytic exposure of a cryptic site within collagen type IV is required for angiogenesis and tumor growth in vivo. J Cell Biol *154*, 1069-1079.

Xu, Y., Moseley, J.B., Sagot, I., Poy, F., Pellman, D., Goode, B.L., and Eck, M.J. (2004). Crystal structures of a Formin Homology-2 domain reveal a tethered dimer architecture. Cell *116*, 711-723.

Yamaoka-Tojo, M., Tojo, T., Kim, H.W., Hilenski, L., Patrushev, N.A., Zhang, L., Fukai, T., and Ushio-Fukai, M. (2006). IQGAP1 mediates VE-cadherin-based cell-cell contacts and VEGF signaling at adherence junctions linked to angiogenesis. Arteriosclerosis, thrombosis, and vascular biology *26*, 1991-1997.

Yan, J., Yang, Y., Zhang, H., King, C., Kan, H.M., Cai, Y., Yuan, C.X., Bloom, G.S., and Hua, X. (2009). Menin interacts with IQGAP1 to enhance intercellular adhesion of beta-cells. Oncogene *28*, 973-982.

Yang, C., Czech, L., Gerboth, S., Kojima, S., Scita, G., and Svitkina, T. (2007). Novel roles of formin mDia2 in lamellipodia and filopodia formation in motile cells. PLoS Biol *5*, e317.

Yilmaz, M., and Christofori, G. (2010). Mechanisms of Motility in Metastasizing Cells. Molecular Cancer Research *8*, 629-642.

Yin, H.L., and Stossel, T.P. (1979). Control of cytoplasmic actin gel-sol transformation by gelsolin, a calcium-dependent regulatory protein. Nature *281*, 583-586.

Yoon, C.H., Hyun, K.H., Kim, R.K., Lee, H., Lim, E.J., Chung, H.Y., An, S., Park, M.J., Suh, Y., Kim, M.J., *et al.* (2011). The small GTPase Rac1 is involved in the maintenance of stemness and malignancies in glioma stem-like cells. FEBS Lett *585*, 2331-2338.

Yoshizawa, M., Kawauchi, T., Sone, M., Nishimura, Y.V., Terao, M., Chihama, K., Nabeshima, Y., and Hoshino, M. (2005). Involvement of a Rac activator,P-Rex1, in neurotrophin-derived signaling and neuronal migration. J Neurosci *25*, 4406-4419.

Yu, W., Datta, A., Leroy, P., O'Brien, L.E., Mak, G., Jou, T.S., Matlin, K.S., Mostov, K.E., and Zegers, M.M. (2005). Beta1-integrin orients epithelial polarity via Rac1 and laminin. Mol Biol Cell *16*, 433-445.

Yukinaga, H., Shionyu, C., Hirata, E., Ui-Tei, K., Nagashima, T., Kondo, S., Okada-Hatakeyama, M., Naoki, H., and Matsuda, M. (2014). Fluctuation of Rac1 activity is associated with the phenotypic and transcriptional heterogeneity of glioma cells. J Cell Sci *127*, 1805-1815.

Zaidel-Bar, R., Milo, R., Kam, Z., and Geiger, B. (2007). A paxillin tyrosine phosphorylation switch regulates the assembly and form of cell-matrix adhesions. J Cell Sci *120*, 137-148.

Zamir, E., and Geiger, B. (2001). Molecular complexity and dynamics of cell-matrix adhesions. J Cell Sci *114*, 3583-3590.

Zamir, E., Katz, M., Posen, Y., Erez, N., Yamada, K.M., Katz, B.Z., Lin, S., Lin, D.C., Bershadsky, A., Kam, Z., *et al.* (2000). Dynamics and segregation of cell-matrix adhesions in cultured fibroblasts. Nat Cell Biol *2*, 191-196.

Zhao, H., Pykalainen, A., and Lappalainen, P. (2011). I-BAR domain proteins: linking actin and plasma membrane dynamics. Curr Opin Cell Biol *23*, 14-21.

Zhou, K., Wang, Y., Gorski, J.L., Nomura, N., Collard, J., and Bokoch, G.M. (1998). Guanine nucleotide exchange factors regulate specificity of downstream signaling from Rac and Cdc42. J Biol Chem *273*, 16782-16786.

Zhu, Z., Sanchez-Sweatman, O., Huang, X., Wiltrout, R., Khokha, R., Zhao, Q., and Gorelik, E. (2001). Anoikis and metastatic potential of cloudman S91 melanoma cells. Cancer Res *61*, 1707-1716.

Zuchero, J.B., Coutts, A.S., Quinlan, M.E., Thangue, N.B., and Mullins, R.D. (2009). p53-cofactor JMY is a multifunctional actin nucleation factor. Nat Cell Biol *11*, 451-459.